

# THE JOURNAL OF PHYSICAL CHEMISTRY

Volume 74, Number 19 September 17, 1970

- Radical Reactions in an Electron Spin Resonance Cavity Homogeneous Reactor . . . . . A. A. Westenberg, N. deHaas, and J. M. Roscoe 3431
- Electron Spin Resonance Spectra of Radical Anions of Styrene and Related Compounds . . . . . A. R. Buick, T. J. Kemp, and T. J. Stone 3439
- Thermal Decomposition of the Acetate Ion in Potassium Halide Matrices . . . . . I. C. Hisatsune, E. C. Beahm, and R. J. Kempf 3444
- Electrical Mobilities of Lithium-6, Calcium-45, and Nitrate Ions in Liquid Mixtures of Lithium Nitrate and Calcium Nitrate . . . . . Jan C. T. Kwak, J. A. A. Ketelaar, P. P. E. Maenaut, and A. J. H. Boerboom 3449
- Chemiluminescence from the Reaction of Oxygen Atoms with Dicyanoacetylene . . . . . J. A. Meyer and D. W. Setser 3452
- The Reactions of Energetic Fluorine-18 Atoms with Tetrafluoroethylene . . . . . Thomas Smail, George E. Miller, and F. S. Rowland 3464
- Optical Filter Effect in the Photolysis of Solid Potassium Trisoxalatocobaltate(III) Trihydrate . . . . . H. E. Spencer and M. W. Schmidt 3472
- The Radiation Chemistry of Tetramethylsilane. I. Vapor Phase . . . . . Gilbert J. Mains and Jonas Dedinas 3476
- The Radiation Chemistry of Tetramethylsilane. II. Liquid Phase . . . . . Gilbert J. Mains and Jonas Dedinas 3483
- The Yield of Thermal Hydrogen Atoms from the  $\gamma$  Radiolysis of Liquid 2,2,4-Trimethylpentane . . . . . Krishan M. Bansal and Stefan J. Rząd 3486
- Further Observations on Products Formed in the Radiolysis of Alkali Metal Halates and Perhalates by Cobalt-60  $\gamma$  Rays . . . . . G. E. Boyd and L. C. Brown 3490
- The Crystal and Molecular Structure of Bisbipyridyl- $\mu$ -dihydroxo-dicopper(II) Nitrate . . . . . Richard J. Majeste and Edward A. Meyers 3497
- A Statistical-Thermodynamic Model of Aqueous Solutions of Alcohols . . . . . Nora Laiken and George Némethy 3501
- The Viscous Flow and Glass Transition Temperature of Some Hydrocarbons . . . . . Gerald L. Faerber, Sung Wan Kim, and Henry Eyring 3510
- Mutual and Tracer Diffusion Coefficients and Frictional Coefficients for the Systems Benzene-Chlorobenzene, Benzene-*n*-Hexane, and Benzene-*n*-Heptane at 25° . . . . . Kenneth R. Harris, Claudio K. N. Pua, and Peter J. Dunlop 3518
- Membrane Osmometry of Aqueous Micellar Solutions of Pure Nonionic and Ionic Surfactants . . . . . D. Attwood, P. H. Elworthy, and S. B. Kayne 3529
- Linear Enthalpy-Spectral Shift Correlations for 2,2,2-Trifluoroethanol . . . . . A. D. Sherry and K. F. Purcell 3535
- Dielectric Behavior of the System Benzyl Chloride-Benzene . . . . . E. M. Turner, W. W. Ehrhardt, G. Leone, and W. E. Vaughan 3543

## NOTES

- Behavior of Structure-Making and Structure-Breaking Solutes Near Temperature of Maximum Density of Water . . . . . T. S. Sarma and J. C. Ahluwalia 3547
- Direct Determination of Triplet  $\leftarrow$  Triplet Absorption Extinction Coefficients. II. Quinoline, Isoquinoline, and Quinoxaline . . . . . Steven G. Hadley 3551
- Chemiluminescence and Thermoluminescence from a  $\gamma$ -Irradiated Silica-Alumina Gel . . . . . Robert R. Hentz and S. B. Ziemecki 3552

## AUTHOR INDEX

- |                                                                                                                                                                                                                                                                                           |                                                                                                                                                                                                                                                              |                                                                                                                                                                                                                                                                                      |                                                                                                                                                                                                                                   |                                                                                                                                                                                                                                        |
|-------------------------------------------------------------------------------------------------------------------------------------------------------------------------------------------------------------------------------------------------------------------------------------------|--------------------------------------------------------------------------------------------------------------------------------------------------------------------------------------------------------------------------------------------------------------|--------------------------------------------------------------------------------------------------------------------------------------------------------------------------------------------------------------------------------------------------------------------------------------|-----------------------------------------------------------------------------------------------------------------------------------------------------------------------------------------------------------------------------------|----------------------------------------------------------------------------------------------------------------------------------------------------------------------------------------------------------------------------------------|
| <p>Ahluwalia, J. C., 3547<br/>Attwood, D., 3529</p> <p>Bansal, K. M., 3486<br/>Beahm, E. C., 3444<br/>Boerboom, A. J. H.,<br/>3449</p> <p>Boyd, G. E., 3490<br/>Brown, L. C., 3490<br/>Buick, A. R., 3439</p> <p>Dedinas, J., 3476, 3483<br/>deHaas, N., 3431<br/>Dunlop, P. J., 3518</p> | <p>Ehrhardt, W. W., 3543<br/>Elworthy, P. H., 3529<br/>Eyring, H., 3510</p> <p>Faerber, G. L., 3510</p> <p>Hadley, S. G., 3551<br/>Harris, K. R., 3518<br/>Hentz, R. R., 3552<br/>Hisatsune, I. C., 3444</p> <p>Kayne, S. B., 3529<br/>Kemp, T. J., 3439</p> | <p>Kempf, R. J., 3444<br/>Ketelaar, J. A. A., 3449<br/>Kim, S. W., 3510<br/>Kwak, J. C. T., 3449</p> <p>Laiken, N., 3501<br/>Leone, G., 3543</p> <p>Maenaut, P. P. E., 3449<br/>Mains, G. J., 3476, 3483<br/>Majeste, R. J., 3497<br/>Meyer, J. A., 3452<br/>Meyers, E. A., 3497</p> | <p>Miller, G. E., 3464<br/>Némethy, G., 3501</p> <p>Pua, C. K. N., 3518<br/>Purcell, K. F., 3535</p> <p>Roscoe, J. M., 3431<br/>Rowland, F. S., 3464<br/>Rzad, S. J., 3486</p> <p>Sarma, T. S., 3547<br/>Schmidt, M. W., 3472</p> | <p>Setser, D. W., 3452<br/>Sherry, A. D., 3535<br/>Smail, T., 3464<br/>Spencer, H. E., 3472<br/>Stone, T. J., 3439</p> <p>Turner, E. M., 3543</p> <p>Vaughan, W. E., 3543</p> <p>Westenberg, A. A., 3431<br/>Ziamecki, S. B., 3552</p> |
|-------------------------------------------------------------------------------------------------------------------------------------------------------------------------------------------------------------------------------------------------------------------------------------------|--------------------------------------------------------------------------------------------------------------------------------------------------------------------------------------------------------------------------------------------------------------|--------------------------------------------------------------------------------------------------------------------------------------------------------------------------------------------------------------------------------------------------------------------------------------|-----------------------------------------------------------------------------------------------------------------------------------------------------------------------------------------------------------------------------------|----------------------------------------------------------------------------------------------------------------------------------------------------------------------------------------------------------------------------------------|

# THE JOURNAL OF PHYSICAL CHEMISTRY

Registered in U. S. Patent Office © Copyright, 1970, by the American Chemical Society

VOLUME 74, NUMBER 19 SEPTEMBER 17, 1970

## Radical Reactions in an Electron Spin Resonance

### Cavity Homogeneous Reactor

by A. A. Westenberg,\* N. deHaas, and J. M. Roscoe

*Applied Physics Laboratory, The Johns Hopkins University, Silver Spring, Maryland 20910 (Received May 7, 1970)*

Experiments are described using a homogeneous reactor entirely contained within the detection cavity of an esr spectrometer. This permits atom and radical concentrations in the homogeneous reaction zone to be directly measured. The effective reactor volume was calibrated using the room temperature  $O + C_2H_2$  reaction as a known "standard" rate constant, and the volume obtained was very close to the geometric volume. Direct measurements on the reaction  $O + OH \rightarrow O_2 + H$  ( $k_4$ ) were then carried out with the reactor operated at temperatures in the range 228–340°K. The results gave  $k_4 = 2.0 \pm 0.3 \times 10^{13} \text{ cm}^3 \text{ mol}^{-1} \text{ sec}^{-1}$  independent of temperature, in good agreement with previously reported values. Attempts to measure  $OH + OH \rightarrow H_2O + O$  were unsuccessful, for reasons which are discussed.

### Introduction

The idea of a homogeneous ("well-stirred") reactor was apparently first developed by Denbigh<sup>1</sup> as a means of measuring reaction rates in liquids, and the basic principles were later summarized by Denbigh and Page.<sup>2</sup> After a number of engineering applications of this concept to the determination of overall rates in combustion reactions,<sup>3</sup> the well-known work of Kistiakowsky and Volpi<sup>4</sup> appears to be the first use of a homogeneous reactor for the determination of rate coefficients of elementary gas reactions. A few other studies by this technique have been reported subsequently.<sup>5,6</sup>

Electron spin resonance (esr) spectroscopy has now been developed into a practical and rather versatile method for the quantitative measurement of gas-phase atom and radical concentrations, and a number of applications to kinetics have been made.<sup>7–10</sup> All of these studies utilized esr as a detector in a linear (one-dimensional) fast-flow system. The work of Mulcahy, *et al.*,<sup>6</sup> is the only previous report of the use of esr with a homogeneous reactor, where esr was used to monitor inlet and outlet atom concentrations in a double cavity arrangement. All previous esr work in both linear and

homogeneous reactors has been concerned with measurements of atom-molecule reaction rates, except for the study of  $OH + OH \rightarrow H_2O + O$  in this laboratory.<sup>11</sup> It seemed that the use of a homogeneous reactor *entirely contained within an esr detection cavity* might offer

\* To whom correspondence should be addressed.

- (1) K. G. Denbigh, *Trans. Faraday Soc.*, **40**, 352 (1944).
- (2) K. G. Denbigh and F. M. Page, *Discuss. Faraday Soc.*, **17**, 145 (1954).
- (3) J. P. Longwell and M. A. Weiss, *Ind. Eng. Chem.*, **47**, 1634 (1955).
- (4) G. B. Kistiakowsky and G. G. Volpi, *J. Chem. Phys.*, **27**, 1141 (1957).
- (5) E. L. Wong and A. E. Potter, *ibid.*, **43**, 3371 (1965); *Can. J. Chem.*, **45**, 367 (1967).
- (6) M. F. R. Mulcahy, J. R. Steven, and J. C. Ward, *J. Phys. Chem.*, **71**, 2124 (1967).
- (7) A. A. Westenberg and N. deHaas, *J. Chem. Phys.*, **50**, 707 (1969), and preceding papers.
- (8) J. M. Brown and B. A. Thrush, *Trans. Faraday Soc.*, **63**, 630 (1967).
- (9) K. Hoyermann, H. G. Wagner, and J. Wolfrum, *Ber. Bunsenges. Phys. Chem.*, **71**, 599 (1967).
- (10) M. J. Kurylo and R. B. Timmons, *J. Chem. Phys.*, **50**, 5076 (1969).
- (11) G. Dixon-Lewis, W. E. Wilson, and A. A. Westenberg, *ibid.*, **44**, 2877 (1966).

some possibilities in the difficult area of atom-radical and radical-radical rate measurements.

The work on the OH + OH reaction<sup>11</sup> was done in a linear reactor with movement of the entire esr cavity (and associated magnet) to establish the time (spatial) dependence of the OH decay. This was not only tedious and difficult, but would be practically impossible at other than room temperature. Another important consideration when attempting to deal with extremely fast atom-radical reactions ( $k > 10^{13} \text{ cm}^3 \text{ mol}^{-1} \text{ sec}^{-1}$ ) is the difficulty of separating mixing time from reaction time in a linear flow system before concentrations drop too low for adequate measurement, a particularly vexing problem using esr, where spatial resolution ( $\sim 2 \text{ cm}$ ) is not especially good. The present paper outlines the principles for operating an esr cavity as a homogeneous reactor and gives some results with such a system.

### Reactor Theory

The basic idea of the homogeneous reactor is very simple and may be briefly reviewed. Assume that two reactants A and B are separately introduced to a reactor of volume  $V$  where they react with a rate constant  $k$ . Mixing is assumed to be so rapid that the concentrations of all species (as well as temperature and pressure) are uniform everywhere in the volume—hence the name homogeneous reactor. The inlet flows of A and B are steady, and they are diluted with a large excess of inert gas so that the total volumetric flow rate  $\dot{V}$  in and out of the reactor is essentially constant. (The latter is not an essential requirement but makes the interpretation somewhat easier.) The concentrations (A) and (B) in the reactor are the same as those leaving it, so that the governing equation is easily derived by equating the difference between inlet and outlet flow rates of a given species to the rate at which it is being consumed by reaction in the volume  $V$ , *i.e.*

$$[(A)_0 - (A)]\dot{V} = k(A)(B)V \quad (1)$$

where  $\dot{V}$  and the molar concentrations are evaluated at the pressure and temperature existing in the reactor. Measurement of the ratio  $(A)_0/(A)$  and the absolute (B) allows  $k$  to be determined. The ratio  $(A)_0/(A)$  is determined in this technique by the relative esr signal due to A with the reactant B turned off and on. This has the advantage of measuring A as it actually exists inside the reactor, but it has the distinct disadvantage (compared to a movable source linear reactor) that loss of A on the walls of the reactor is not canceled out, since with any wall loss the measurement of  $(A)_0$  with  $(B) = 0$  is not the concentration entering the reactor. If independent knowledge of the  $(A)_0$  entering the reactor is available, then a measure of A with and without B would allow a first-order wall loss of A to be canceled, but this is not ordinarily feasible. Thus, it is important that

wall losses be negligible compared to the homogeneous gas phase contribution to  $k$ .

The key assumption clearly is that of "instantaneous" mixing which, if valid, allows the condition of homogeneity to obtain in the reactor. As noted in ref 4, this limit may be approached in practice if conditions are such that the average time  $t_D$  required for any species to diffuse to the walls is small compared to its average residence time  $t_R$  in the reactor; *i.e.*, the requirement for homogeneity is

$$t_D/t_R \ll 1 \quad (2)$$

If  $r$  is some characteristic distance to the wall, the average diffusion time  $t_D \sim r^2/2D$ , where  $D$  is the diffusion coefficient of a given species in the mixture. The average residence time may be approximated by  $t_R \sim V/\dot{V}$ , although this is an upper limit since reactants are partially consumed in the reaction. Equation 2 thus becomes

$$r^2\dot{V}/2DV \ll 1$$

or since  $D \propto D_1/P$  and  $\dot{V} \propto \dot{V}_1/P$ , where  $D_1$  and  $\dot{V}_1$  refer to some reference pressure

$$r^2\dot{V}_1/2D_1V \ll 1 \quad (3)$$

The rapid mixing criterion is thus independent of the pressure in the reactor. It is somewhat temperature dependent, however, since  $D_1$  and  $\dot{V}_1$  are different functions of temperature ( $\dot{V}_1 \propto T$ , while  $D_1$  is roughly proportional to  $T^{0.7}$ ). Once the geometry of a reactor has been fixed, eq 3 governs the maximum total flow rate  $\dot{V}_1$  allowable for a given  $D_1$ . The geometry will be determined by a compromise between practical convenience, the size of the esr cavity itself, and the rate of the reaction to be measured *via* a relation like eq 1.

### Experimental Section

The cavity was essentially the same as that used in a previous investigation,<sup>7</sup> being a large access hole cavity modeled after one described by Carrington, *et al.*<sup>12</sup> A diagram of the cavity is shown in Figure 1. This particular version had a modulation section constructed of slotted brass (silver plated) to allow penetration of the 100-kc modulation field. Operation was in the TE<sub>012</sub> mode, and the indicated orientation of the microwave electric and magnetic field vectors allowed both electric and magnetic dipole transitions to be observed when the cavity was placed with its axis perpendicular to the external field. The spectrometer was a Varian Model 4502 with 9-in. magnet.

A reactor was constructed to fit closely within this cavity ( $\sim 1\text{-mm}$  clearance). Figure 2 illustrates the reactor schematically. It was made entirely of quartz, the walls being etched down to about 0.8 mm for minimum cavity loading. Even so, the necessary large

(12) A. Carrington, P. N. Dyer, and D. H. Levy, *J. Chem. Phys.*, **47**, 1756 (1967).

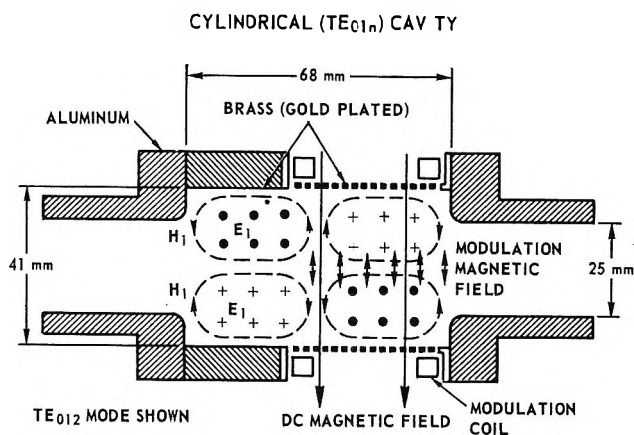


Figure 1. Schematic diagram of cylindrical  $TE_{01n}$  cavity showing orientation of various field vectors.

amount of quartz resulted in a loaded  $Q$  of only about 1500. The geometric reactor volume (excluding the small volume taken up by the injector) was  $67 \text{ cm}^3$  from inlet hole to outlet hole.

Atoms were furnished to the main inlet flow in the usual way by a microwave discharge in a few per cent of the parent diatomic molecule diluted with helium, while various stable reactants could be fed to the simple four-hole injector near the center of the reactor. All metering was done by means of jewelled, critical orifices, except for  $\text{NO}_2$  which was throttled through a Granville-Phillips leak. The  $\text{NO}_2$  was calibrated each time by transferring the flow into a known volume and timing the pressure rise on an oil (Kel-F) manometer. This method is to be preferred over the alternative of metering  $\text{NO}_2$  out of a known volume, since corrections for  $\text{N}_2\text{O}_4$ - $\text{NO}_2$  equilibrium may be avoided entirely by keeping the final calibration pressure very low. All gases used were best commercial grade taken directly from the tanks.

The reactor was provided with a Pyrex-enclosed thermocouple which could be moved along the axis for temperature measurement, or entirely removed from the reactor to a position downstream while esr measurements were being taken. Pressure in the reactor was measured by connecting the injector to a McLeod gauge after transferring the gas flow normally fed through the injector to the main flow upstream of the reactor. In this way, any additional pressure contributed by the stable reactant flow (a small fraction of the total at most) was maintained during pressure measurement.

For operation above or below room temperature, the entire cavity was encapsulated in styrofoam molded in place. A stream of dry nitrogen gas, either cooled by passage through liquid nitrogen or heated by a water bath, was fed to the inside of the cavity (but outside the reactor, of course) and allowed to pass around the main inlet tube for some distance upstream before escaping to the room. The reactor wall temperature was continuously monitored by a thermocouple, while

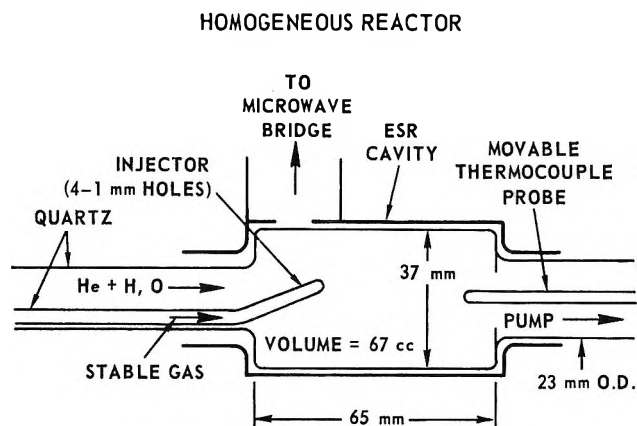


Figure 2. Schematic diagram of homogeneous reactor contained in  $TE_{01n}$  cylindrical cavity.

the actual gas temperature in the reactor was measured with the movable thermocouple mentioned above. The temperature profile from inlet to outlet end of the reactor could be kept fairly uniform by this arrangement (within  $\sim 10^\circ\text{K}$ ), and long term stability after attainment of lowest ( $225^\circ\text{K}$ ) or highest ( $340^\circ\text{K}$ ) temperature was good (within  $\sim 2^\circ\text{K}$ ). For the low activation energy reactions of interest, this degree of spatial homogeneity in the reactor was adequate.

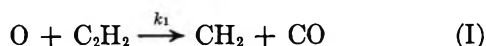
The geometry of the reactor was such that the characteristic dimension  $r$  in eq 3 was about 2 cm. Since rapid mixing is promoted by making  $D_1$  as large as possible, the use of helium as an inert carrier gas was clearly indicated. For most species a binary diffusion coefficient in helium at  $300^\circ\text{K}$  and 1 atm pressure of about  $0.5 \text{ cm}^2/\text{sec}$  is a reasonable estimate (H atoms having a larger  $D_1$ , of course). Thus, for a reactor volume  $V$  of  $67 \text{ cm}^3$ , the homogeneity criterion of eq 3 required that the total flow rate  $\dot{V}_1$  (at  $300^\circ\text{K}$  and 1 atm) be kept less than about  $1.5 \text{ cm}^3/\text{sec}$  ( $r^2\dot{V}_1/2D_1V \leq 0.1$ ).

### Reactor Calibration Results

It is clear that the validity of the homogeneous reactor model needed testing in some way, even though the criterion given by eq 3 is met. A direct check on the homogeneity of the concentrations during reaction would be highly desirable, but this was practically impossible in the present case (nor has it really been done satisfactorily in any previous work, although some evidence has been offered<sup>6</sup>). The esr measurements simply record spatial averages of concentration over a rather ill-defined volume determined by the microwave and modulation fields in the cavity. It is also not exactly obvious what volume should be used in equations like (1), since the influence of inlet and outlet end effects, possible aerodynamic effects, etc., make the geometric volume of the reactor subject to some uncertainty.

Under the circumstances it seemed that the most significant test of the system we could perform would be to compare a rate constant measured in the reactor

with a known value from other independent experiments. While such a comparison would not have been very meaningful a few years ago, we feel that in certain cases kinetic data have now been refined enough to rely on for such a purpose. After examining a number of candidates for the role of "calibrating reaction," it was decided that the reaction



would be the most favorable. Besides being of a suitable magnitude for our reactor at room temperature, it is a fairly simple and clean reaction with rather good references. There have been six recent absolute room temperature measurements of  $k_1$  for the  $\text{O} + \text{C}_2\text{H}_2$  primary reaction. These were all fast-flow, linear reactor experiments using a variety of detection methods and reaction conditions. Five of these studies were discussed in the paper from this laboratory.<sup>13</sup> Our own value<sup>13</sup> obtained under pseudo-first-order conditions, *i.e.*, with  $(\text{C}_2\text{H}_2) \gg (\text{O})$ , was  $k_1 = 8.9 \pm 0.3 \times 10^{10} \text{ cm}^3 \text{ mol}^{-1} \text{ sec}^{-1}$ , using esr detection. The other determinations discussed in that paper gave the values  $9.2 \pm 0.4$ ,<sup>8</sup>  $8.4$ ,<sup>14</sup>  $9.0 \pm 1.8$ ,<sup>15</sup> and  $9.6$ <sup>16</sup> ( $\times 10^{10}$ ). Since then one other measurement has appeared<sup>17</sup> giving  $8.0 \pm 1.2$ . This rather impressive unanimity lends considerable confidence that the value  $k_1 = 8.9 \times 10^{10}$  at room temperature should be reliable at least to  $\pm 10\%$ .

A test of the homogeneous reactor actually requires only the value  $nk_1$ , where  $n$  is the stoichiometric coefficient for the number of O atoms consumed per  $\text{C}_2\text{H}_2$  molecule.  $nk_1$  is the directly determined O-decay rate under excess  $\text{C}_2\text{H}_2$  conditions in our previous experiments,<sup>13</sup> the data giving  $nk_1 = 17.8 \times 10^{10}$ . The value  $n = 2$ , measured by mass spectrometry, then led to the value  $k_1 = 8.9 \times 10^{10}$  quoted above, and this stoichiometry has also been independently verified.<sup>13</sup>

Thus eq 1 was employed with  $\text{B} = \text{C}_2\text{H}_2$ , under large excess  $\text{C}_2\text{H}_2$  conditions so that  $(\text{C}_2\text{H}_2)$  was constant, *i.e.*

$$nk_1V = \frac{\dot{V}}{(\text{C}_2\text{H}_2)} \left[ \frac{(\text{O})_0}{(\text{O})} - 1 \right] \quad (\text{4})$$

$\dot{V}$  and  $(\text{C}_2\text{H}_2)$  were evaluated from the metered flow rates at the pressure in the reactor, and  $(\text{O})_0/(\text{O})$  was a direct esr peak height ratio with the  $\text{C}_2\text{H}_2$  off and on. The reactor walls were uncoated for these experiments.

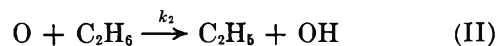
Results of 16 such calibration runs on  $k_1$  are given in Table I. The ranges of pressure, flow rates, and degree of reaction were about as great as could be covered in the apparatus while retaining good precision. The actual O atom concentration entering the reactor was considerably less than indicated by the inlet  $\text{O}_2$  rate (to the discharge) due to incomplete dissociation and losses up to the reactor. The data showed the desired independence of all variables except for a slight variation with the  $\text{C}_2\text{H}_2$  inlet rate (all else being constant),

**Table I:** Summary of Calibration Runs on the Homogeneous Reactor Using the  $\text{O} + \text{C}_2\text{H}_2$  Reaction ( $k_1$ ) at Room Temperature. Helium Carrier. Geometric Volume = 62  $\text{cm}^3$

Pressure, mm	Inlet flow rates, $\text{cm}^3 \text{ atm sec}^{-1}$			$(\text{O})_0/(\text{O})$	$nk_1V$ , $\text{cm}^6 \text{ mol}^{-1} \text{ sec}^{-1}$
	$\text{C}_2\text{H}_2$	$\text{O}_2$	Total		
0.26	0.024	0.009	1.20	2.00	$1.28 \times 10^{13}$
0.26	0.059	0.009	1.24	3.47	1.31
0.26	0.130	0.009	1.31	6.36	1.36
0.35	0.040	0.010	1.38	3.28	1.22
0.35	0.115	0.010	1.45	8.30	1.41
0.37	0.026	0.003	1.32	2.40	0.99
0.37	0.026	0.010	1.33	2.47	1.05
0.37	0.026	0.014	1.33	2.30	0.93
0.38	0.026	0.009	2.35	1.54	1.10
0.38	0.065	0.009	2.38	2.30	1.07
0.38	0.130	0.009	2.45	3.67	1.13
0.54	0.039	0.010	1.38	6.32	1.23
0.54	0.069	0.010	1.41	11.1	1.35
0.59	0.022	0.008	2.14	2.42	1.19
0.59	0.022	0.008	2.86	1.67	1.00
0.72	0.069	0.010	2.10	8.61	1.30
				Av	$1.18 \pm 0.13 \times 10^{13}$

increasing  $\text{C}_2\text{H}_2$  usually giving slightly increasing  $nk_1V$ . The reason for this is not clear, and in any case it was not serious. In some cases the total flow rate was deliberately increased to values somewhat greater than the  $1.5 \text{ cm}^3/\text{sec}$  required by eq 3, which was only a rough upper limit anyway. No variation in the measured result up to  $\dot{V}_1 \sim 2.8$  could be detected. Several runs using an argon carrier (in which the diffusion coefficients would be 3–4 times lower than in helium) did give different results (higher  $nk_1V$ ), however, indicating that the homogeneity criterion was probably not being fulfilled. The average of all the values in Table I is  $\langle nk_1V \rangle = 1.18 \pm 0.13 \times 10^{13} \text{ cm}^6 \text{ mol}^{-1} \text{ sec}^{-1}$ , and using the independent value  $nk_1 = 17.8 \times 10^{10} \text{ cm}^3 \text{ mol}^{-1} \text{ sec}^{-1}$  gives a calibration value for the reactor volume of  $66 \text{ cm}^3$ . This is remarkably close to the measured geometric volume of  $62 \text{ cm}^3$ . (This work was done on an earlier version of the reactor having a slightly smaller volume than the  $67 \text{ cm}^3$  shown in Figure 1.)

Similar calibration runs were made using two other reactions with rather mixed results. Eight runs on



gave  $\langle nk_2V \rangle = 4.4 \pm 0.4 \times 10^{11}$ . These were re-

(13) A. A. Westenberg and N. deHaas, *J. Phys. Chem.*, **73**, 1181 (1969).

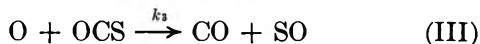
(14) C. A. Arrington, W. Brennen, G. P. Glass, J. V. Michael, and H. Niki, *J. Chem. Phys.*, **43**, 525 (1965).

(15) J. O. Sullivan and P. Warneck, *J. Phys. Chem.*, **69**, 1749 (1965).

(16) K. Hoyermann, H. G. Wagner, and J. Wolfrum, *Z. Phys. Chem. (Frankfurt am Main)*, **55**, 72 (1967).

(17) G. S. James and G. P. Glass, *J. Chem. Phys.*, **50**, 2268 (1969).

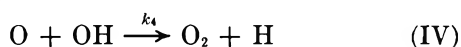
stricted to conditions giving  $(O)_0/(O) < 3$ , since for higher values there was a definite increase in the  $nk_2V$  value measured. This is, of course, a reaction with much more complex stoichiometry ( $n \sim 6$ ), and there is much less information on it than on reaction I. The most recent data obtained in our laboratory<sup>18</sup> give  $nk_2 = 5.1 \times 10^9$ , which yields a volume  $V = 86 \text{ cm}^3$ , or about 30% larger than the  $66 \text{ cm}^3$  derived from the  $O + C_2H_2$  results. Similar measurements on



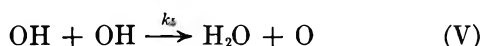
gave  $\langle nk_3V \rangle = 7.9 \pm 0.4 \times 10^{11}$  for six runs, again restricted to  $(O)_0/(O) < 3$  because of an increasing trend beyond this. Using our value<sup>7</sup>  $nk_3 = 8.5 \times 10^9$  one obtains  $V = 93 \text{ cm}^3$ , or about 40% above the  $O + C_2H_2$  result. In the  $O + OCS$  case there may be serious wall losses, since SO is a product of the primary reaction, and there could be loss of O due to  $O + SO$  reaction on the walls of the reactor, which would give too high a measured  $nk_3V$ . Although both  $k_2$  and  $k_3$  results gave values of  $V$  larger than the geometric volume, it is felt that they are less reliable than the very well established reaction I. Therefore, the validity of the homogeneous reactor model and the use of its geometric volume seems at least partially verified.

### Results for Radical-Radical Reactions

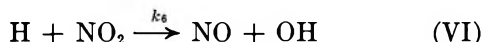
The use of the homogeneous reactor for radical-radical reactions may be illustrated by new results for



There have been three previous fairly direct measurements of  $k_4$  at room temperature. Clyne<sup>19</sup> measured the decay of O atoms generated from



in a linear flow system, the OH radicals being generated by the reaction



The O decay was monitored by its well-known chemiluminescence with NO, absolute (O) being determined by  $NO_2$  titration. Assuming a steady state of (O) at any point between reactions IV and V, Clyne was able to show that the O decay rate was directly related to  $k_4$ , and obtained  $k_4 = 3 \pm 1 \times 10^{13} \text{ cm}^3 \text{ mol}^{-1} \text{ sec}^{-1}$  at 265 and 293°K. Kaufman and Del Greco<sup>20</sup> used a double discharge linear flow system, producing OH from reaction VI in the presence of O from  $N + NO \rightarrow N_2 + O$ . Since (VI) is much faster than the  $O + NO_2$  reaction, it is possible to cause the  $NO_2$  to react nearly exclusively with H even when O is present, a fact utilized in our own experiments to be described shortly. By monitoring OH decays by uv absorption with and without added O, and using a rather complex graphical method of data analysis, Kaufman and Del Greco

estimated  $k_4 \sim 1 \times 10^{13}$  at room temperature. In later work,<sup>21</sup> Kaufman reinvestigated  $k_4$  in the OH decay system without adding extra O, apparently in a manner similar to Clyne's employing steady state (O), but measuring both OH and O decays. Few details were given, but Kaufman's revised value for  $k_4$  is  $3 \pm 1 \times 10^{13}$  at 300°K, in excellent agreement with Clyne's value. Very recently, Breen and Glass<sup>22</sup> have reported a value  $k_4 = 2.6 \pm 0.8 \times 10^{13}$  from a linear reactor with esr detection, using the steady-state assumption for (O). This was an experiment similar to ref 11 on  $k_5$ , but employing a movable  $NO_2$  source for OH and a fixed cavity, while ref 11 used a fixed source and movable cavity. The value of  $k_4$  determined by Breen and Glass relies directly on their measurement of the product  $k_5$  (OH) as well as absolute (O) at steady state, so that it probably is not as reliable, but their reported value agrees well with the others.

The homogeneous reactor offered a particularly simple and direct approach to the measurement of  $k_4$ . Small amounts of both  $H_2$  and  $O_2$  diluted in helium were passed through the discharge so that H and O entered the reactor through the main inlet in low concentration (1–2%). This inlet esr signal for O atom was  $(O)_0$ , with  $(H)_0 > (O)_0$ .  $NO_2$  was then metered into the central injector, and since the rate constant for  $H + NO_2$  is at least 10 times larger than that for  $O + NO_2$ , the former reaction occurred practically to the exclusion of the latter, as was noted earlier. The OH generated in reaction VI then reacted homogeneously with the O present by reaction IV (and with itself to a slight extent by reaction V) giving esr readings (O) and (OH). The governing relation for O loss in the reactor was then

$$[(O)_0 - (O)]\dot{V} = [k_4(O)(OH) - k_5(OH)^2]V$$

so that

$$k_4 = \left[ \frac{(O)_0}{(O)} - 1 \right] \frac{\dot{V}}{(OH)V} + \frac{k_5(OH)}{(O)} \quad (5)$$

In practice the second term above was completely negligible compared to the first, so that  $k_4$  could be determined by relative measurements of the O signal with the  $NO_2$  off and on, and an absolute esr measure of (OH) when the  $NO_2$  was flowing. (The absolute OH required the NO calibration procedure which has been described,<sup>23</sup> and the details for carrying this out at other than room temperature are given in the Appendix.) Knowledge of  $k_5$  was thus not required for

(18) A. A. Westenberg and N. deHaas, *J. Chem. Phys.*, **50**, 2512 (1969).

(19) M. A. A. Clyne, "Ninth Symposium on Combustion," Academic Press, New York, N. Y., 1963, p 211.

(20) F. Kaufman and F. P. Del Greco, *ibid.*, p 659.

(21) F. Kaufman, *Ann. Geophys.*, **20**, 106 (1964).

(22) J. E. Breen and G. P. Glass, *J. Chem. Phys.*, **52**, 1082 (1970).

(23) A. A. Westenberg, *ibid.*, **43**, 1544 (1965).

Table II: Summary of Measurements of  $k_4$  for  $O + OH \rightarrow H_2 + H$  in the Homogeneous Reactor. Helium Carrier.  $V = 67 \text{ cm}^3$

Temp, °K	Pressure, mm	Inlet flow rates, $\text{cm}^3 \text{ atm sec}^{-1}$				(O) <sub>0</sub> /(O)	(OH), mol/cm <sup>3</sup>	$k_4$ , $\text{cm}^3 \text{ mol}^{-1} \text{ sec}^{-1}$
		H <sub>2</sub>	O <sub>2</sub>	NO <sub>2</sub>	Total			
228 ± 2	0.71	0.080	0.024	0.047	1.41	2.12	$0.67 \times 10^{-12}$	$2.9 \times 10^{13}$
	0.70	0.080	0.024	0.062	1.43	9.00	5.88	2.4
	0.70	0.100	0.034	0.094	2.29	8.26	8.88	2.3
	0.70	0.100	0.034	0.094	2.29	12.5	14.2	2.3
298	0.55	0.070	0.014	0.034	1.27	3.30	2.85	2.3
	0.56	0.070	0.021	0.043	1.29	4.29	4.78	1.9
	0.60	0.068	0.025	0.065	1.32	4.29	4.25	2.0
	0.63	0.072	0.020	0.043	1.88	5.42	9.63	1.7
	0.63	0.072	0.020	0.046	1.88	7.58	16.9	1.4
	0.63	0.090	0.029	0.049	1.38	2.92	3.03	1.6
	0.64	0.072	0.020	...	1.37	16.9	20.7	2.0
	0.64	0.072	0.020	...	1.37	6.59	6.96	2.1
	0.68	0.081	0.032	0.045	1.33	2.70	2.08	1.8
	0.76	0.105	0.027	0.055	1.43	6.95	6.01	2.1
	0.88	0.069	0.027	0.051	2.02	11.2	13.5	2.1
	0.88	0.069	0.027	0.044	2.01	3.61	3.45	2.1
	340 ± 4	0.40	0.082	0.023	0.016	1.63	1.88	1.90
0.63		0.082	0.023	0.024	1.64	2.28	2.48	1.7
0.63		0.082	0.023	0.029	1.64	3.72	4.17	2.2
0.70		0.079	0.025	0.038	0.92	6.26	5.68	1.6
0.71		0.079	0.025	0.045	0.93	10.7	10.8	1.6
Av $2.0 \pm 0.3$ $\times 10^{13}$								

the measurement of  $k_4$ , which is a very desirable feature of this method.

A summary of the runs made at three temperatures over a modest range is given in Table II. The range of flow variables and pressure was rather restricted, mostly because of the necessity of retaining sufficient OH signal for a good integrated intensity measurement. But within the accessible ranges, the results for  $k_4$  are rather uniform and show no significant temperature dependence. Averaging the runs at all temperatures together gives  $k_4 = 2.0 \pm 0.3 \times 10^{13}$ , in good agreement with the results of Clyne<sup>19</sup> and Kaufman<sup>21</sup> discussed earlier. The lack of temperature dependence found by Clyne is also verified over a somewhat larger range. An essentially zero activation energy would be expected for such a fast reaction.

The value for  $k_4$  derived<sup>24,25</sup> from the extensively studied reverse reaction and the equilibrium constant is  $1.3 \times 10^{13}$  with zero activation energy. This is not too significant a comparison, however, since the compilation for  $k_{-4}$  itself depends heavily on the data of Clyne and Kaufman for  $k_4$  and the equilibrium constant at the low temperature end. Our present data for  $k_4$  thus confirm that the  $H + O_2$  composite rate constant  $k_{-4} = 2.2 \times 10^{14} \exp(-16,800/RT)$  derived using this low-temperature  $k_4$  anchor is probably valid.

Attempts to measure  $k_5$  and its temperature dependence were not successful. Two different methods were used which should have worked in principle, but

there were difficulties which will be noted. With H<sub>2</sub> in the discharge with helium, the main inlet flow contained only H in this experiment. NO<sub>2</sub> was then metered into the central injector, generating OH by reaction VI, followed by reactions V and IV. Assuming these are the only reactions occurring and that all rates are finite, the homogeneous reactor equation for NO<sub>2</sub> is

$$[(NO_2)_0 - (NO_2)]\dot{V} = [\dot{V}_{NO_2}N/\dot{V} - (NO_2)]\dot{V} = k_6(H)(NO_2)V \quad (6)$$

where  $N = P/RT$  is the total molar concentration. The equation for H atom (with steady-state O atom) is

$$[(H)_0 - (H)]\dot{V} = [k_6(H)(NO_2) - k_5(OH)^2]V \quad (7)$$

Since there is no OH in the inlet flow, its equation is

$$-(OH)\dot{V} = [-k_6(H)(NO_2) + 3k_5(OH)^2]V \quad (8)$$

*Method I.* Addition of eq 6 and 8 gives

$$k_5 = \frac{[\dot{V}_{NO_2}N/\dot{V} - (NO_2) - (OH)]\dot{V}}{3(OH)^2V} \quad (9)$$

which is the correct form when OH generation by (VI) is assumed to be not infinitely fast. When  $k_6$  is as-

(24) R. M. Fristrom and A. A. Westenberg, "Flame Structure," McGraw-Hill Book Co., New York, N. Y., 1965, p 361.

(25) D. L. Baulch, D. D. Drysdale, and A. C. Lloyd, High Temperature Reaction Rate Data Report No. 3, Department of Physical Chemistry, The University of Leeds, England, April 1969.

**Table III:** Summary of Measurements of  $k_5$  for  $\text{OH} + \text{OH} \rightarrow \text{H}_2\text{O} + \text{O}$  at Room Temperature in the Homogeneous Reactor. Helium Carrier.  $V = 67 \text{ cm}^3$ 

Method I							
Pressure, mm	Inlet flow rates, $\text{cm}^3 \text{ atm sec}^{-1}$			$(\text{OH})_0$ , $\text{mol/cm}^3$	$k_5$ , $\text{cm}^3 \text{ mol}^{-1} \text{ sec}^{-1}$		
	$\text{H}_2$	$\text{NO}_2$	Total				
0.26	0.09	0.021	0.61	$52 \times 10^{-12}$	$1.5 \times 10^{12}$		
0.30	0.06	0.039	1.47	59	2.1		
0.30	0.09	0.025	0.61	37	3.9		
0.34	0.08	0.034	1.72	56	2.0		
0.39	0.09	0.078	1.20	115	1.2		
0.56	0.07	0.061	0.68	63	3.3		
0.58	0.07	0.091	1.88	106	1.6		
0.58	0.07	0.099	1.11	93	2.4		
0.63	0.09	0.053	0.84	59	2.4		
0.67	0.09	0.076	0.86	78	2.1		
0.68	0.09	0.098	2.27	118	1.4		
0.70	0.09	0.094	1.23	100	2.0		
0.73	0.07	0.065	1.08	66	3.2		
0.75	0.07	0.088	2.00	107	1.6		
0.75	0.07	0.090	2.75	107	1.6		

Method II							
Pressure, mm	Inlet flow rates, $\text{cm}^3 \text{ atm sec}^{-1}$			$(\text{H})_0$ , $\text{mol/cm}^3$	$(\text{H})/(\text{H})_0$	$(\text{OH})_0$ , $\text{mol/cm}^3$	$k_5$ , $\text{cm}^3 \text{ mol}^{-1} \text{ sec}^{-1}$
	$\text{H}_2$	$\text{NO}_2$	Total				
0.41	0.12	0.048	1.22	$10 \times 10^{-10}$	0.57	$87 \times 10^{-12}$	$0.77 \times 10^{12}$
0.41	0.12	0.063	1.23	17	0.29	86	2.7
0.43	0.10	0.037	1.22	10	0.67	56	1.5
0.55	0.10	0.065	1.23	21	0.32	70	3.5
0.55	0.10	0.065	1.23	33	0.32	93	3.2
0.66	0.11	0.048	1.56	23	0.59	89	1.4
0.67	0.11	0.047	1.55	16	0.56	88	1.0
0.67	0.11	0.068	1.58	11	0.35	90	1.1
0.88	0.11	0.037	1.13	15	0.47	37	4.1

sumed to be infinite,  $(\text{NO}_2) = 0$  (providing it is not added in excess), and the term  $\dot{V}_{\text{NO}_2} N / \dot{V}$  is simply equivalent to an inlet  $(\text{OH})_0$ .

Since it was not possible to measure the residual  $(\text{NO}_2)$  in this experiment, a direct test of this assumption could not be made. A large number of experiments were performed at room temperature with  $(\text{NO}_2)$  taken to be zero, however, so that  $k_5$  could be evaluated simply from the metered flow rate of  $\text{NO}_2$  and  $\dot{V}$ , together with an esr measurement of  $(\text{OH})$ . The results were not very satisfactory, as shown in Table III. The values of  $k_5$  tend to be higher than our earlier value<sup>11</sup> of  $1.5 \times 10^{12}$  and to increase with decreasing  $\dot{V}_{\text{NO}_2}$ . This is the behavior to be expected when neglect of the  $(\text{NO}_2)$  in eq 9 is not justified; *i.e.*, a residual  $(\text{NO}_2)$  would be more significant at low values of  $\dot{V}_{\text{NO}_2}$ , so that its neglect would lead to a relatively larger apparent  $k_5$ . In other words, the effect of finite  $k_6$  combined with appreciable mixing time for the entering  $\text{NO}_2$  means that the frequent practice of computing initial  $(\text{OH})_0$  from the inlet  $\text{NO}_2$  rate may tend to overestimate the effective  $(\text{OH})_0$ . In

the present experiments this leads to a high apparent  $k_5$ , while in linear reactor experiments an overestimate of  $(\text{OH})_0$  would tend to underestimate  $k_5$  for a given measured  $(\text{OH})^{-1}$  slope. The latter point had been noted earlier<sup>11</sup> in attempting to understand the discrepancy between our value of  $k_5$  obtained in a linear reactor and the lower values of Kaufman and Del Greco.<sup>20</sup> The overestimate of  $(\text{OH})_0$  by the  $\text{NO}_2$  rate has also been noted by Breen and Glass.<sup>22</sup>

Another possible cause of the difficulty might be loss of OH on the walls, particularly due to the deposit formation which is known to occur with the  $\text{H} + \text{NO}_2$  system. This deposit (presumably  $\text{NH}_4\text{NO}_3$ ) was noted previously<sup>11</sup> in this laboratory and elsewhere, and was again apparent in the present work. It tended to concentrate around the central injector. Since the deposit is known to accentuate OH loss, it may have been a contributor to the high values of  $k_5$  measured. Breen and Glass<sup>22</sup> have also invoked a wall loss in the analysis of their linear reactor data, which gave a  $k_5$  lower than either ref 20 or 11.

Method II. Addition of eq 7 and 8 gives

$$k_6 = \frac{[(H)_0 - (H) - (OH)]\dot{V}}{2(OH)^2V} \quad (10)$$

which is an alternate form not requiring a value for initial  $(OH)_0$ . The initial  $(H)_0$  was obtained by esr with the  $NO_2$  off, while  $(H)$  and  $(OH)$  were obtained with  $NO_2$  on. No assumption was necessary about the rapidity of reaction VI, since this term cancels out. This method was also unsatisfactory, giving erratic values of  $k_5$  depending on  $\dot{V}_{NO_2}$  (see Table III). It seems most likely that deposit formation and serious wall loss of OH were largely responsible for this behavior.

Thus, the homogeneous reactor is suitable only for radical-radical reactions which are fast enough in the gas phase so that wall losses are negligible. Establishing this in a given case is difficult, and lacking independent evidence, perhaps the best indication that wall losses are not important would be a set of results consistent with an analytical model derived for zero wall loss which are independent of flow variables over as wide a range as possible. In some cases finite wall losses can be canceled out, as noted earlier.

### Appendix

For operation of the reactor at other than room temperature, in the case of reaction IV the temperature dependence of the calibration relation for determining absolute  $(OH)$  is required. The general procedure for calibrating electric dipole species such as OH against NO has been described in detail.<sup>23</sup> The integrated esr intensity is given by

$$\int_0^\infty \chi''_{ij} dH = \frac{(OH)h\nu_0 |(\mu_r)_{ij}|^2 \exp(-E_i/kT)}{k\beta g_{eff} TZ} \quad (11)$$

where the terms have been defined previously.<sup>23</sup> The last factor in eq 11 contains all of the temperature-dependent quantities.

The OH lines best suited for practical intensity measurements are those for the lowest rotational level  $J = 3/2$  of the  ${}^2\pi_{3/2}$  ground state, for which the Boltzmann factor is unity. The total partition function  $Z$  for OH as function of  $T$  was derived from the appropriate thermodynamic tables<sup>26</sup> and is given in Table IV. For present purposes the single OH line  $M_J = 1/2 \rightarrow 3/2$ ,  $M_I = 1/2$ , ( $J = 3/2$ ,  ${}^2\pi_{3/2}$  state) of the  $+ \rightarrow - \Delta$  doubling transition was more convenient than the composite OH lines (lines A and B in the notation of ref 23) used previously. This is the lowest field line (7926

Table IV: Total Partition Functions for OH and NO as Functions of Temperature

Temp. °K	$Z_{OH}$	$Z_{NO}$
100	28.4	292
200	54.2	704
300	82.8	1160
400	113	1632
500	143	2124
600	175	2630
700	206	3154
800	236	3702
900	268	4284
1000	296	5103

$G$  at 8765 Mc) of the set of six  $+ \rightarrow -$  transitions for  $J = 3/2$ ,  ${}^2\pi_{3/2}$ . Let us designate it as line C. For this line  $|(\mu_r)_{ij}|^2 = 0.634$  and  $g_{eff} = 0.935$ , so that eq 11 gives

$$(OH) = 1.47 \left( \frac{k\beta}{h\nu_0} \right) T_{OH} Z_{OH} \int_0^\infty \chi''(OH, \text{line C}) dH \quad (12)$$

In a similar manner, the relation for line "a" of NO may be derived (line "a" is the lowest field line of the nine-line  $J = 3/2$ ,  ${}^2\pi_{3/2}$  set of NO transitions,<sup>23</sup> lying at 7944 G for  $\nu_0 = 8765$  Mc). The Boltzmann factor for the desired level is not unity in this case,<sup>23</sup> so the result is

$$(NO) = 64.5 \left( \frac{k\beta}{h\nu_0} \right) T_{NO} Z_{NO} \exp(-180/T_{NO}) \times \int_0^\infty \chi''(NO, \text{line a}) dH \quad (13)$$

Normally the NO calibration is carried out with pure NO in the reactor at a pressure  $P_{NO}$ , and the calibration temperature  $T_{NO}$  may be different than the temperature  $T_{OH}$  at which OH is measured. Combining eq 12 and 13 gives the working relation

$$(OH) = [0.0228] \left[ \frac{P_{NO}}{RT_{NO}} \right] \left[ \frac{T_{OH}}{T_{NO}} \right] \left[ \frac{Z_{OH}}{Z_{NO}} \right] \times \left[ \exp\left(\frac{-180}{T_{NO}}\right) \right] \frac{\int_0^\infty \chi''(OH, \text{line C}) dH}{\int_0^\infty \chi''(NO, \text{line a}) dH} \quad (14)$$

(26) "JANAF Thermochemical Tables," Dow Chemical Co., Midland, Mich., 1960.

# Electron Spin Resonance Spectra of Radical Anions of Styrene and Related Compounds

by A. R. Buick, T. J. Kemp, and T. J. Stone

*School of Molecular Sciences, University of Warwick, Coventry CV4 7AL, Great Britain (Received April 14, 1970)*

Well resolved electron spin resonance spectra of the radical anions of the following compounds are reported: styrene,  $\alpha$ -methylstyrene, *o*- and *m*-methylstyrene, *o*-, *m*-, and *p*-fluorostyrene, *o*- and *p*-vinylpyridine, cinnamic acid, and phenylacetylene. All were obtained by means of continuous-flow reduction of the parent compound by solutions of electrons in liquid ammonia. Delay between mixing and observation permitted observation of secondary radicals in certain cases. Assignment of coupling constants was achieved in all cases by comparing experimental spin densities with those calculated by the Hückel and McLachlan procedures.

## Introduction

Radical anions of a very large number of aromatic molecules have been examined spectroscopically by both electronic and electron spin resonance (esr) techniques and the resulting spectra have been discussed in terms of molecular orbital (MO) theory of increasing degrees of sophistication. While many radical anions are sufficiently stable to permit leisurely investigation at room temperature, this is not the case for some of those of simple structure which undergo either rapid dimerization or disproportionation, and in these instances spectroscopic identification depends on the application either of fast reaction techniques such as flash photolysis or pulse radiolysis (which afford optical and kinetic data) or of a matrix isolation method,<sup>1</sup> which depends on preparation of the radical anion in a glass or polycrystalline environment, often at low temperature, by allowing the parent molecule to capture a relatively mobile electron generated radiation- or photo-chemically; the immobile radical anion can then be studied optically or by esr. Electrolysis of nonaqueous systems at low temperatures has also proved effective in allowing a steady-state concentration of the radical anions of pyridine<sup>2</sup> and butadiene<sup>3</sup> to be built up permitting unequivocal esr characterization.

We report here the well resolved solution esr spectra of styrene and a number of related compounds. While Hamill<sup>4</sup> has reported optical spectra of the radical anion of styrene ( $\text{sty}^{\cdot -}$ ) following  $\gamma$  irradiation of 0.1 *M* solutions in 2-methyltetrahydrofuran at 77°K, attempts to produce an unambiguous liquid-phase spectrum by pulse radiolysis of liquid styrene and solutions have been unsuccessful.<sup>5,6</sup> Williams and colleagues<sup>7</sup> have obtained the similar optical spectrum of  $\alpha$ -methylstyrene using a technique similar to that of Hamill, but esr examination of these glassy solutions revealed a broad peak showing slight but unresolved structure due to the line-broadening effects associated with solid-state

electron resonance. Special interest is attached to  $\text{sty}^{\cdot -}$  and also the radical anion of *p*-vinylpyridine in view of their intermediacy in anionic polymerization by alkali metals and aromatic hydrocarbon radical ions.<sup>8-10</sup>

## Experimental Section

**Chemicals.** Styrenes and vinylpyridines were obtained from Koch-Light Laboratories Ltd. and were purified by vacuum distillation immediately prior to use. Anhydrous ammonia of a quoted purity of 99.98% was supplied by Imperial Chemical Industries Ltd. Very small pieces of sodium were added until a blue color was obtained.

**Technique.** As previously described,<sup>11</sup> ca.  $10^{-2}$  *M* solutions in ammonia of the substrate and of sodium were conveyed separately from 2-l. flasks surrounded by chips of solid carbon dioxide by applying a pressure of pure nitrogen. The solutions were then mixed in a 15-jet multicapillary mixer of 2-mm internal diameter placed in the resonant cavity of a Decca Radar Ltd. X-1 esr spectrometer incorporating a 7-in. magnet from Newport Instruments Ltd. At the fastest flow rates employed ( $8 \text{ ml sec}^{-1}$ ), mixing is calculated to be com-

(1) W. H. Hamill in "Radical Ions," E. T. Kaiser and L. Kevan, Ed., Interscience, New York, N. Y., 1968, Chapter 9.

(2) C. L. Talcott and R. J. Myers, *Mol. Phys.*, **12**, 549 (1967).

(3) D. H. Levy and R. J. Myers, *J. Chem. Phys.*, **41**, 1062 (1964).

(4) M. R. Ronayne, J. P. Guarino, and W. H. Hamill, *J. Amer. Chem. Soc.*, **84**, 4230 (1962).

(5) J. P. Keene, E. J. Land, and A. J. Swallow, *ibid.*, **87**, 5284 (1965).

(6) K. W. Chambers, E. Collinson, F. S. Dainton, and F. Wilkinson, *Trans. Faraday Soc.*, **63**, 1699 (1967).

(7) J. Lin, K. Tsuji, and F. Williams, *ibid.*, **64**, 2896 (1968).

(8) K. F. O'Driscoll and A. V. Tobolsky, *J. Polym. Sci.*, **31**, 115, 123 (1958).

(9) M. Szwarc, *Prog. Phys. Org. Chem.*, **6**, 323 (1968).

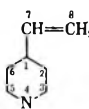
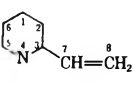
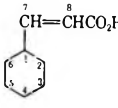
(10) D. Laurin and G. Parravano, *J. Polym. Sci.*, **A6**, 1047 (1968).

(11) A. R. Buick, T. J. Kemp, G. T. Neal, and T. J. Stone, *J. Chem. Soc. A*, 666 (1969).

Table I: Coupling Constants and Experimental and Theoretical Spin Densities

Substrate	Position	Exptl coupling constants, Oe	Exptl spin densities ( $Q_{CH^H} = 26.9$ )	Theor spin densities	
				Hückel	McLachlan
	2	3.82	0.142	0.134	0.142
	3	0.87	0.032	0.008	-0.024
	4	5.51	0.205	0.182	0.204
	5	0.59	0.022	0.042	0.020
	6	2.00	0.074	0.082	0.074
	7	1.51	0.056	0.085	0.044
	8	7.35	0.367	0.307	0.368
		2	3.44	0.128	0.138
3		0.29	0.011	0.008	-0.024
4		5.07	0.188	0.188	0.213
5		0.65	0.024	0.045	0.024
6		2.15	0.080	0.081	0.074
7		1.31	0.047	0.080	0.045
8		6.65	0.333	0.278	0.334
		2	3.77	0.140	0.157
	3	0.37	0.014	0.002	-0.032
	4	4.92	0.183	0.181	0.203
	5	0.89	0.033	0.065	0.049
	6	1.48	0.053	0.062	0.049
	7	2.60	0.097	0.084	0.046
	8	7.68	0.384	0.292	0.350
		2	3.98	0.148	0.145
3		0.64	0.024	0.006	-0.024
4		5.49	0.204	0.176	0.197
5		0.86	0.031	0.045	0.026
6		2.17	0.081	0.075	0.065
7		1.52	0.056	0.085	0.044
8		7.35	0.368	0.307	0.368
		2	5.89	0.118	0.116
	3	0.38	0.014	0.018	-0.011
	4	4.57	0.170	0.188	0.213
	5	0.94	0.035	0.029	0.004
	6	1.84	0.068	0.099	0.097
	7	0.94	0.035	0.087	0.048
	8	7.51	0.376	0.301	0.360
		2	3.98	0.148	0.142
3		1.22	0.024	0.006	-0.034
4		5.23	0.194	0.178	0.200
5		1.00	0.037	0.044	0.024
6		2.43	0.090	0.077	0.068
7		1.53	0.057	0.085	0.044
8		7.66	0.383	0.307	0.368
		2	5.29	0.197	0.142
	3	0.49	0.018	0.004	-0.029
	4	11.17	0.223	0.176	0.196
	5	1.26	0.047	0.035	0.014
	6	2.53	0.094	0.082	0.076
	7	1.41	0.052	0.089	0.050
	8	8.53	0.426	0.304	0.365
		2	4.50	0.167	0.145
3		< line width	0	0.004	-0.029
4		13.34	0.267	0.181	0.204
5		1.09	0.041	0.039	0.017
6		1.80	0.067	0.081	0.075
7		1.70	0.061	0.084	0.050
8		6.34	0.317	0.275	0.330

Table I (Continued)

Substrate	Position	Exptl coupling constants, Oe	Exptl spin densities ( $Q_{\text{CH}^{\text{H}}} = 26.9$ )	Theor spin densities	
				Huckel	McLachlan
	2	2.49	0.092	0.097	0.086
	3	0.47	0.017	0.042	0.028
	4	3.95	0.138	0.153	0.159
	5	2.12	0.079	0.082	0.076
	6	1.02	0.038	0.070	0.051
	7	0.32	0.012	0.061	0.015
	8	8.30	0.415	0.302	0.370
	1	3.44	0.128	0.073	0.066
	2	< line width		0.048	0.025
	3	...		0.195	0.217
	4	3.36	0.118	0.136	0.138
	5	< line width		0.001	-0.026
	6	4.39	0.163	0.148	0.158
	7	0.73	0.027	0.073	0.025
	8	7.72	0.386	0.325	0.397
	1	3.87	0.144	0.128	0.150
	3	1.18	0.043	0.002	-0.028
	4	4.91	0.183	0.143	0.170
	5	0.81	0.030	0.153	-0.011
	6	3.20	0.119	0.104	0.120
	7	8.08	0.300	0.184	0.193
	8	3.02	0.151	0.176	0.177

plete in <5 msec. Spectra were normally run for 300 or 500 sec. The temperature of the cavity was monitored with a thermocouple and was invariably in the range  $-39$  to  $-42^\circ$ . The resolution of the spectra is apparent from the Figures 1 and 2.

Occasionally mixing was performed 6 ft outside the cavity in order to place a 1-sec time interval between reaction and recording and thereby to characterize any fast secondary reactions.

Spectra were analyzed by trial and error until a reasonable fit was obtained, an exact fit being achieved by performing a series of computer simulations. Computation of electron spin densities was performed with a program supplied by Dr. D. M. Hirst on an International Computer Ltd. 4130 system computer.

## Results

Well resolved spectra of the corresponding radical anion were obtained with the following compounds: styrene (Figure 1),  $\alpha$ -methylstyrene (Figure 2), *o*-, *m*-, and *p*-methylstyrenes, *o*-, *m*-, and *p*-fluorostyrenes, *p*-fluoro- $\alpha$ -methylstyrene, *o*- and *p*-vinylpyridines, cinnamic acid, and phenylacetylene (Figure 1). All spectra were analyzed with the exception of that of *p*-methylstyrene. Coupling constants are listed in Table I. Values of  $g$  for the radicals studied are all in the neighborhood of 2.003 (Table II).

The run with phenylacetylene produced, in addition to a major spectrum assigned to phenylacetylene radical anion, a minor spectrum, suggesting incursion by a secondary product or an impurity. When the solutions

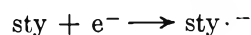
Table II: Values of  $g$  for Radicals

Substrate	$g$ value	Substrate	$g$ value
Styrene	2.0027	<i>p</i> -Fluorostyrene	2.0029
$\alpha$ -Methylstyrene	2.0027	<i>p</i> -Fluoro- $\alpha$ -methylstyrene	2.0029
<i>o</i> -Methylstyrene	2.0027	Cinnamic acid	2.0030
<i>m</i> -Methylstyrene	2.0027	2-Vinylpyridine	2.0029
<i>o</i> -Fluorostyrene	2.0027	4-Vinylpyridine	2.0030
<i>m</i> -Fluorostyrene	2.0027		

of phenylacetylene and sodium were mixed 6 ft outside the cavity, a distance corresponding to a time interval of 1 sec between mixing and recording, the minor component was greatly enhanced at the expense of the phenylacetylene radical anion and proved on inspection to be the spectrum of styrene radical anion. A run with phenylpropionic acid produced, instead of the phenylpropionic acid radical anion, the cinnamic acid radical anion, indicating the initial stages of reduction of the acetylene to be complete in a few milliseconds.

## Discussion

It is clear from the observations that we are witnessing electron attachment in solution to these substrates to give a monomeric radical anion, *e.g.*



In the case of phenylacetylene, a rapid sequence of reduction and protonation steps is taking place to produce ultimately the styrene radical anion.

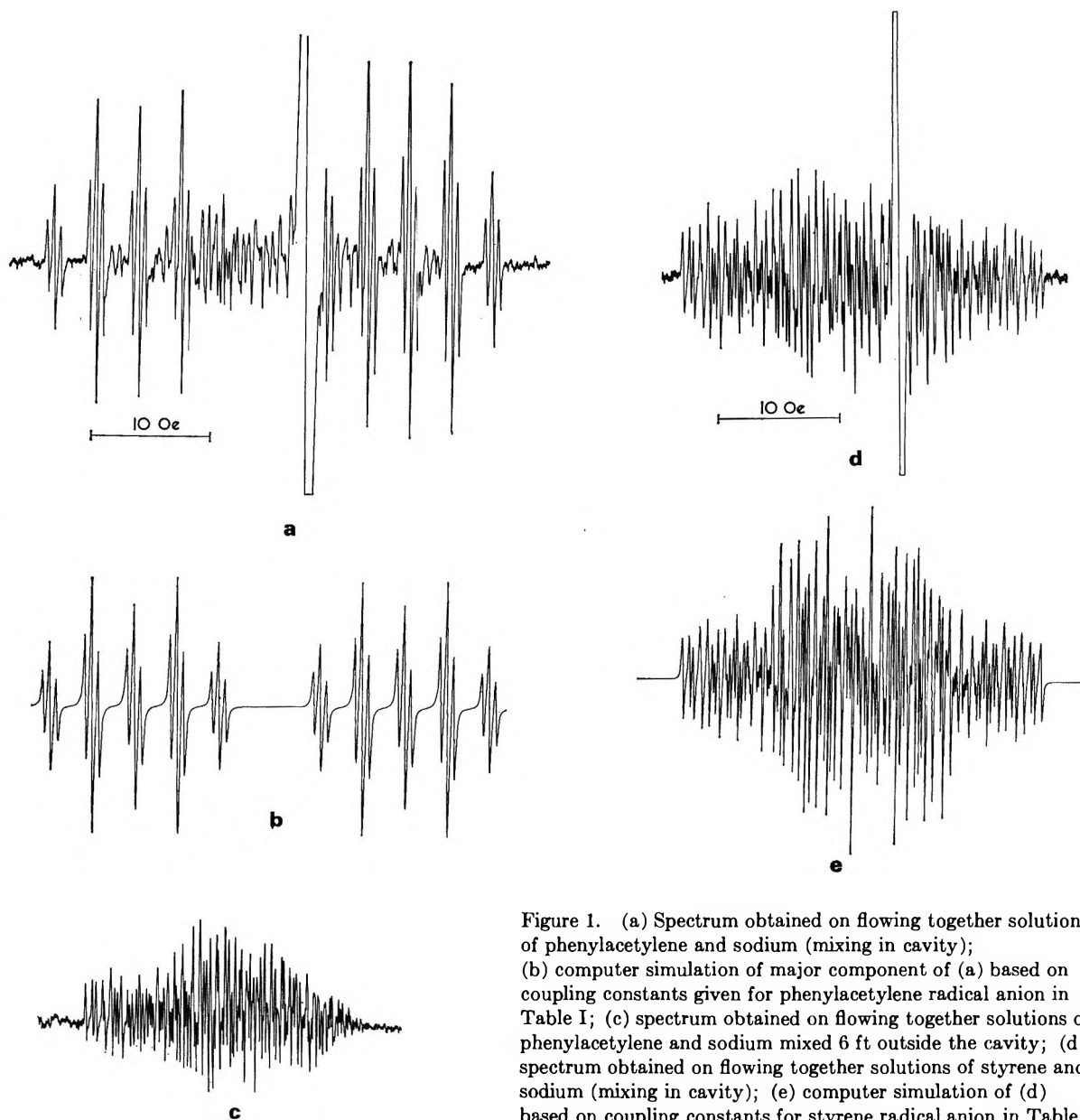


Figure 1. (a) Spectrum obtained on flowing together solutions of phenylacetylene and sodium (mixing in cavity); (b) computer simulation of major component of (a) based on coupling constants given for phenylacetylene radical anion in Table I; (c) spectrum obtained on flowing together solutions of phenylacetylene and sodium mixed 6 ft outside the cavity; (d) spectrum obtained on flowing together solutions of styrene and sodium (mixing in cavity); (e) computer simulation of (d) based on coupling constants for styrene radical anion in Table I.

These are the first reported spectra of monophenylated ethylene and acetylene radical anions (with the exception of our preliminary note<sup>12</sup>), although several accounts exist of spectra of more highly substituted analogs including stilbene,<sup>13,14</sup> tetraphenylethylene,<sup>15-17</sup> 1-phenylpropene,<sup>18</sup> and diphenylacetylene (tolan).<sup>13</sup> The complete absence of alkali metal splitting indicates very loose or negligible ion pairing in the relatively polar solvent employed. The fate of  $\text{sty} \cdot^-$  is presumably dimerization to give distyryl dianion<sup>9</sup> which then participates in anionic polymerization to yield ultimately living polystyrene anion. A similar occurrence has been noted for *p*-vinylpyridine in liquid ammonia.<sup>10</sup>

The production of the cinnamic acid radical anion is not surprising in view of the successful observation of benzoic acid radical anion using the liquid ammonia flow technique.<sup>19</sup>

*Molecular Orbital Calculations.* Assignment of measured coupling constants to definite positions in the compounds examined was effected by making a comparison of experimental electron spin densities, ob-

(12) A. R. Buick, T. J. Kemp, G. T. Neal, and T. J. Stone, *Chem. Commun.*, 282 (1970).

(13) C. S. Johnson, Jr., and R. Chang, *J. Chem. Phys.*, **43**, 3183 (1965).

(14) N. M. Atherton, F. Gerson, and J. N. Ockwell, *J. Chem. Soc. A*, 109 (1966).

(15) J. C. Chippendale, P. S. Gill, and E. Warhurst, *Trans. Faraday Soc.*, 1088 (1967).

(16) A. Cserhegyi, J. Jagur-Grodzinski, and M. Szwarc, *J. Amer. Chem. Soc.*, **91**, 1892 (1969).

(17) B. J. Tabner, *J. Chem. Soc. A*, 2487 (1969).

(18) F. Sundholm and H. Tylli, *Acta Chem. Scand.*, **23**, 1085 (1969).

(19) A. R. Buick, T. J. Kemp, G. T. Neal, and T. J. Stone, *Chem. Commun.*, 1331 (1968).

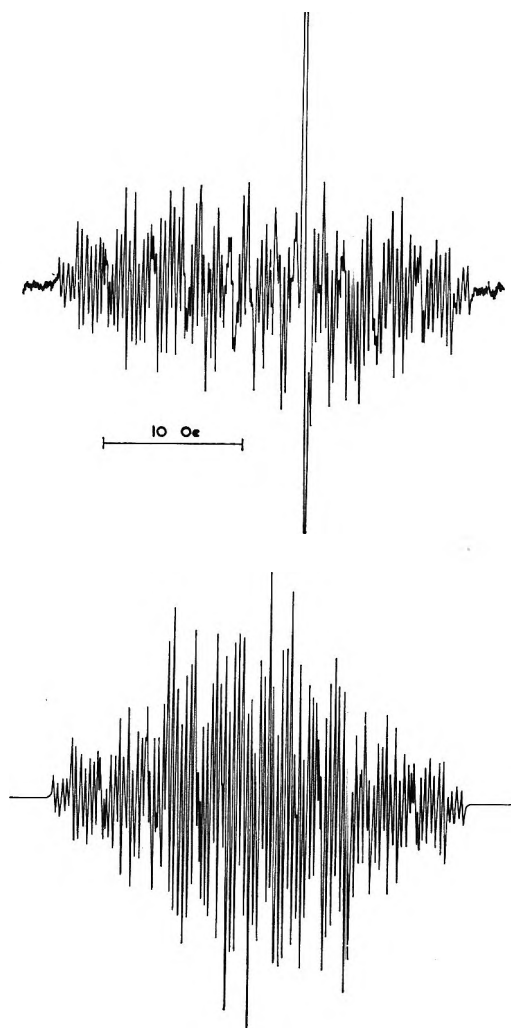
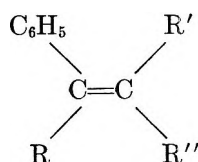


Figure 2. Upper: spectrum obtained on flowing together solutions of  $\alpha$ -methylstyrene and sodium (mixing in cavity). Lower: computer simulation of spectrum of  $\alpha$ -methylstyrene based on coupling constants in Table I.

tained from the McConnell equation, with theoretical spin densities calculated by means of the Hückel<sup>20</sup> and McLachlan<sup>21</sup> procedures.

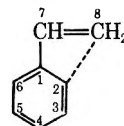
These calculations involve the following variable parameters; the Coulomb integrals ( $h$ ) for each atom, resonance integrals ( $k$ ) for each bond, and  $\lambda$ , the McLachlan configuration interaction parameter. Values of  $h$  for aromatic ring carbon atoms are usually taken as being zero while for the aromatic C-C bond  $k = 1$ . For styrene itself the remaining values required are  $h$  and  $k$  for the side chain and  $\lambda$ .

The general pattern of aromatic coupling constants in compounds of the formula



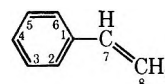
is well known, e.g., in 1-phenylpropene,<sup>18</sup> tetraphenyl-

ethylene,<sup>17</sup> and stilbene.<sup>14</sup> MO calculations have proved either impossible<sup>22</sup> or very difficult<sup>15</sup> due to the inequivalence of all aromatic protons. Coulomb and resonance integrals were in most cases kept equal, while  $\lambda$  was given values of 1.0 and 1.2. Two empirical approaches, denoted the  $\alpha$ <sup>23</sup> and  $\beta$  effects<sup>23,24</sup> have been used successfully to produce inequivalent spin densities at ortho- and meta-aromatic positions. The former considers a repulsion energy, the latter an imaginary bond, to exist between one ortho proton and the pair of ethylenic protons. Reasonable success has

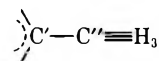


been achieved by both methods, although Johnson and Chang<sup>13</sup> favor the  $\beta$  effect from a comparison of net charges on the  $\alpha$  carbon atoms in terephthaldehyde and stilbene. We have used the easily manipulatable  $\alpha$  effect, giving the carbon atom at the 2-position a Coulomb integral of 0.17; other workers<sup>14,23</sup> have used values of 0.15–0.20 with success.

Our  $h$ ,  $k$ , and  $\lambda$  parameters for styrene were varied in a manner similar to that utilized for pyridines<sup>25</sup> and aromatic carboxylic acids<sup>26</sup> until the ratios of the spin densities at the 2- and 4- positions and the 6- and 4- positions compared well with the corresponding ratios of the coupling constants. The following values  $h_2 = 0.17$ ,  $k_{17} = 1.3$ ,  $\lambda = 0.6$ , and,  $k_{78} = 1.3$



produced McLachlan theoretical spin density ratios of 0.694 and 0.364 which are identical with the experimental coupling constant ratios. The McConnell parameter,  $Q_{\text{CH}^{\text{H}}}$ , was evaluated from positions of high spin density (ortho and para rather than the less reliable meta) to be 26.9 Oe. Consideration of several styrenes gave  $Q_{=\text{CH}_2^{\text{H}}} = 20$  Oe. The values of  $h$ ,  $k$ ,  $\lambda$ , and  $Q$  obtained in this way were then used to assign coupling constants of various substituted styrenes with the following supplementary parameters,<sup>25,26</sup> for methyl:  $h_{\text{C}} = -0.2$ ,



(20) A. Streitwieser, "Molecular Orbital Theory for Organic Chemists," Wiley, New York, N. Y., 1961.

(21) A. D. McLachlan, *Mol. Phys.*, **3**, 233 (1960).

(22) C. Corvaja and G. Giacometti, ref 9 of our ref 14.

(23) P. H. Reiger and G. K. Fraenkel, *J. Chem. Phys.*, **37**, 2811 (1962).

(24) E. W. Stone and A. H. Maki, *ibid.*, **38**, 1999 (1963).

(25) A. R. Buick, T. J. Kemp, G. T. Neal, and T. J. Stone, *J. Chem. Soc. A*, 1609 (1969).

(26) A. R. Buick, T. J. Kemp, G. T. Neal, and T. J. Stone, *ibid.*, in press.

$k_{C'-C''} = 0.76$ ,  $h_{C''} = -0.1$ ,  $k_{C''=H_3} = 2.0$ ,  $h_{H_3} = -0.5$ , and  $Q_{C-CH_3^H} = 28.0$  Oe.

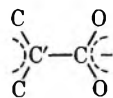
For fluorine:  $h_C = 0.1$ ,  $k_{C-F} = 0.7$ ,  $h_F = 1.6$ , and  $Q_{CF^F} = 50$  Oe



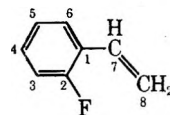
For vinylpyridine:  $h_N = 0.8$ ,  $k_{CN} = 1.1$ , and,  $Q_{N^N} = 28.5$  Oe



For cinnamic acid:  $h_O = 2.0$ ,  $k_{C'-C} = 1.2$ , and,  $k_{C-O} = 1.6$



A choice arises for *o*-fluorostyrene as to whether F is in the 2- or 6- positions



and MO calculations favor the 2- position, assuming that the spin density distribution in sty. - itself is as shown in Table I. Similarly, *m*-fluorine is placed in the 3-position while ortho- and meta-methyl groups are placed in 6- or 5- positions, respectively. It was possible to alter parameters to give slightly better correlation between  $a_H$  and  $\rho$  in some cases, but in an exercise to assign coupling constants this is of limited value.

*Acknowledgments.* We thank the Science Research Council for a grant to purchase a Decca esr spectrometer. Imperial Chemical Industries Ltd. provided a grant for the purchase of chemicals. Mr. I. Elson helped in a number of the flow experiments.

## Thermal Decomposition of the Acetate Ion in Potassium

### Halide Matrices<sup>1a</sup>

by I. C. Hisatsune,<sup>1b</sup> E. C. Beahm, and R. J. Kempf

Department of Chemistry, Whitmore Laboratory, The Pennsylvania State University, University Park, Pennsylvania 16802  
(Received April 27, 1970)

The thermal decomposition of the acetate ion isolated in a KI matrix followed a first-order mechanism and gave the formate ion as the major ionic product. In the temperature range 480–574°, the decomposition rate constant determined from an infrared band of the acetate ion or the formate ion was  $6.3 \times 10^8 \exp[-(46.7 \pm 0.2 \text{ kcal})/RT]$  sec<sup>-1</sup>. In KCl and KBr matrices, the solubility of the acetate ion was small, and the decomposition, which appeared to be diffusion controlled, produced the formate and carbonate ions.  $\gamma$  Irradiation of the acetate ion in a KBr matrix gave methane and ethane as well as trapped carbon dioxide anion free radical.

### Introduction

Oakwood and Miller<sup>2</sup> reported in 1950 that, contrary to what is stated in many organic chemistry textbooks, the fusion reaction



in the temperature range of 350–380° gives in addition to the expected hydrocarbon other gaseous products. In the decomposition of sodium salts of propionate, butyrate, and caproate, these authors found hydrogen and methane as major products. Only the pyrolysis of

sodium acetate, among the four salts they examined, appeared to obey this reaction stoichiometry.

According to the pyrolysis studies of simple organic salts that we have carried out in recent years, the complexities reported for reaction 1 may be due in part to

(1) (a) This work was supported by PHS Grant EC-97 from the Environmental Control Administration and by Grant AFOSR-907-67 from the AFOSR(SRC)-OAR, USAF. (b) To whom correspondence should be addressed.

(2) T. S. Oakwood and M. R. Miller, *J. Amer. Chem. Soc.*, **72**, 1849 (1950).

the formate ion.<sup>3</sup> Not only have we observed this ubiquitous formate ion in the decompositions of the oxalate ion,<sup>4</sup> the fumarate ion,<sup>5</sup> and even the bicarbonate ion,<sup>6</sup> but we have also found that the formate itself decomposes by second-order kinetics into hydrogen, carbon monoxide, and carbonate.<sup>7</sup>

In this paper we report the kinetics of the formate ion production from the thermal decomposition of the acetate ion dispersed in potassium halide matrices. Some results from the acetate decomposition induced by  $\gamma$  irradiation are also presented.

### Experimental Section

Fisher reagent grade sodium acetate was used directly as the solute, and the potassium halides for the matrices were infrared optical grade salts from the Harshaw Co. The isotopic compounds  $\text{CH}_3^{13}\text{CO}_2\text{Na}$  (56.5 atom %) and  $\text{CD}_3\text{CO}_2\text{Na}$  (99 atom %) came from Merck Sharp and Dohme of Canada, Ltd., while the sources of  $^{13}\text{CH}_3\text{CO}_2\text{Na}$  (58.1 atom %) and  $\text{CH}_3\text{C}^{18}\text{O}_2\text{Na}$  (90 atom %) were, respectively, the Volk Radiochemical Co. and the Bio-Rad Laboratories.

The technique of disk fabrication and the experimental procedure for kinetic studies with the pressed disks have been described before.<sup>3,7</sup> The decomposition reactions were followed by infrared spectroscopy with a Perkin-Elmer Model 21 ( $\text{NaCl}$  and  $\text{CaF}_2$  prisms) spectrometer and occasionally with a Perkin-Elmer Model 521 grating instrument. The kinetic results from both instruments were the same within experimental uncertainties. The Varian spectrometer employed for esr measurements and the various cobalt-60  $\gamma$ -ray sources used to irradiate the pressed disks have also been described before.<sup>3,8</sup>

### Results

Whether sodium acetate was dispersed in a KI matrix by the freeze-dry method or by grinding, the strongest infrared band in the initial spectrum of the pressed disk was a broad peak at  $1581\text{ cm}^{-1}$  corresponding to the CO-antisymmetric stretch fundamental. Heating of such a disk at  $120^\circ$  for as long as 4 weeks produced practically no reaction, but there was much decomposition of the acetate accompanied by a carbonate formation if the solute and matrix mixture was heated as a powder at the same temperature. When a disk was heated at about  $350$  to  $400^\circ$  for 1 to 2 hr or at  $500^\circ$  for 3 to 4 min, the broad band at  $1581\text{ cm}^{-1}$  disappeared and in its place a sharp peak due to the matrix isolated acetate ion appeared at  $1595\text{ cm}^{-1}$ . Traces of  $\text{HCO}_2^-$ ,  $\text{HCO}_3^-$ , and  $\text{CO}_3^{2-}$  were produced during this heating process, but these ions did not appear to come from the decomposition of the acetate ion. Continued heating of a disk at a temperature of about  $500^\circ$  caused the  $1595\text{ cm}^{-1}$  acetate band to decay smoothly and the absorption bands of matrix isolated  $\text{HCO}_2^-$  to grow. Also, during this process the disk developed a dark color due

to carbon formation. Within the limits of experimental errors, the rate of growth of the  $1615\text{ cm}^{-1}$  formate band was the same as the decay rate of the  $1595\text{ cm}^{-1}$  acetate band, and both were first order in the acetate concentration over 85 to 95% of the reaction. The first-order rate constants obtained from the KI disks with 0.2 to 0.4 mg/g of solute are summarized in Figure 1 as an Arrhenius plot for the temperature range  $480$ – $574^\circ$ . The reaction activation energy and frequency factor are given in Table I.

**Table I:** Arrhenius Parameters for Acetate and Formate Decompositions

Rate equation	Frequency factor	Activation energy, kcal/mol
	KI Matrix	
$-\text{d}[\text{CH}_3\text{CO}_2^-]/\text{d}t = k_A[\text{CH}_3\text{CO}_2^-]$	$6.3 \times 10^8 \text{ sec}^{-1}$	$46.7 \pm 0.2$
$-\text{d}[\text{HCO}_2^-]/\text{d}t = k_F[\text{HCO}_2^-]^2$	$1.2 \times 10^9 M^{-1} \text{ sec}^{-1}$	$42 \pm 6$
	KBr Matrix	
$-\text{d}[\text{CH}_3\text{CO}_2^-]/\text{d}t = k_A[\text{CH}_3\text{CO}_2^-]$	$6.0 \times 10^2 \text{ sec}^{-1}$	$22.6 \pm 0.5$
$+\text{d}[\text{HCO}_2^-]/\text{d}t = k_A'[\text{CH}_3\text{CO}_2^-]$	$0.3 \times 10^2 \text{ sec}^{-1}$	$17.2 \pm 0.5$

At temperatures above about  $500^\circ$ , the decomposition of the formate ion itself in a KI matrix is appreciable.<sup>7</sup> Consequently, as the KI disk was heated, the optical density of a formate ir band first increased, then reached a maximum, and finally decayed. Throughout this process, the decay of the reactant acetate ion was still first order. When the maximum concentration of the formate was reached, there was usually about 10 to 20% of the original acetate still remaining, and the formate yield was about 75% of that expected on the basis of one-to-one stoichiometry between the acetate and the formate. Beyond the formate maximum both  $\text{HCO}_3^-$  and  $\text{CO}_3^{2-}$  ir bands increased with heating time, and the final yield of  $\text{CO}_3^{2-}$  was about 85% of the concentration expected from the second-order decomposition of the formate ion.<sup>7</sup> In fact, the second-order decomposition rate constant of the formate ion can be calculated from the experimental data at the formate maximum since at this reaction stage  $k_A[\text{CH}_3\text{CO}_2^-] =$

(3) I. C. Hisatsune, *Nippon Kagaku Zasshi*, **89**, 1143 (1968).

(4) K. O. Hartman and I. C. Hisatsune, *J. Phys. Chem.*, **71**, 392 (1967).

(5) I. C. Hisatsune, R. Passerini, R. Pichai, and V. Schettino, *ibid.*, **73**, 3690 (1969).

(6) I. C. Hisatsune and K. O. Hartman, *Science*, **145**, 1455 (1964).

(7) K. O. Hartman and I. C. Hisatsune, *J. Phys. Chem.*, **70**, 1281 (1966).

(8) I. C. Hisatsune, T. Adl, E. C. Beahm, and R. J. Kempf, *ibid.*, **74**, 3225 (1970).

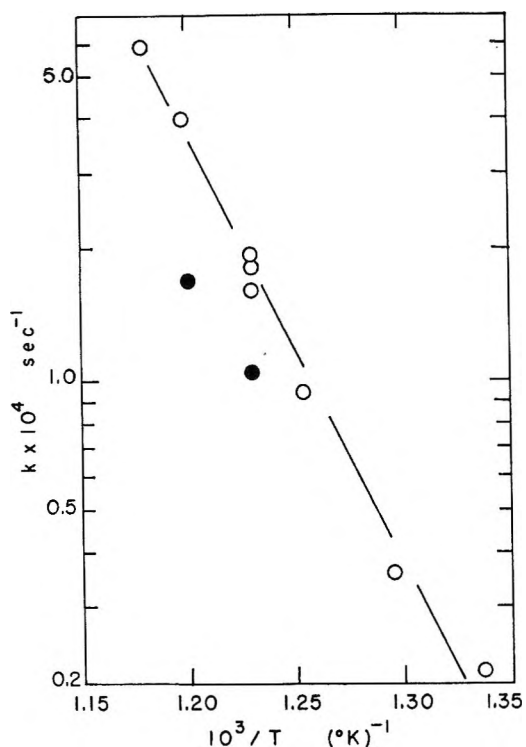


Figure 1. First-order decomposition rate constants for the acetate ion in a KI matrix:  $\circ$ ,  $CH_3CO_2^-$ ;  $\bullet$ ,  $CD_3CO_2^-$ .

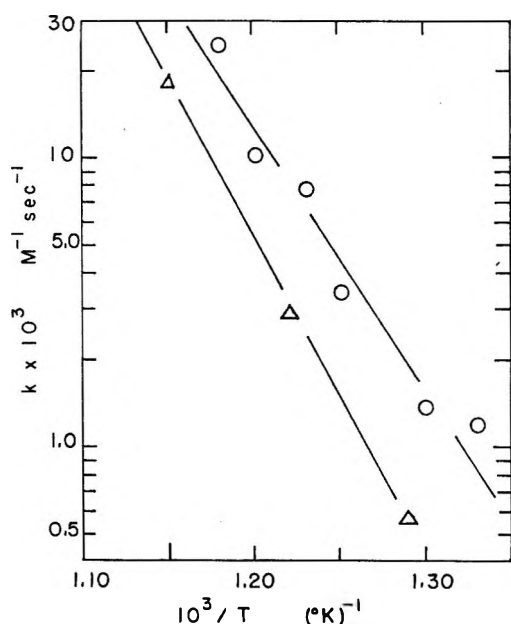


Figure 2. Second-order decomposition rate constants for the formate ion in a KI matrix:  $\circ$ , present work;  $\Delta$ , ref. 7.

$k_F[HCO_2^-]^2$ . The rate constants calculated from the maxima of the  $1615\text{-cm}^{-1}$  formate band optical densities are summarized in Figure 2 and in Table I. For comparison, the three experimental points obtained from the  $753\text{-cm}^{-1}$   $HCO_2^-$  band in an earlier study<sup>7</sup> are also displayed in Figure 2.

The first-order rate constant of  $CD_3CO_2^-$  decomposition in KI, which gave both  $HCO_2^-$  and  $DCO_2^-$ , was

obtained at two temperatures as illustrated in Figure 1. These constants are a factor of about 2 smaller than those of the normal isotopic molecule, but the temperature dependence appears to be the same within error limits in the two sets of data. Also, two samples of  $CH_3^{13}CO_2^-$  were decomposed at  $540^{\circ}$ , but the  $^{13}C$ -isotope effect was too small to measure. However, there appeared to be some isotopic dilution in these runs since in both samples the final  $^{13}C$  content of  $HCO_2^-$  was 29% while the initial isotopic content of the acetate was 34%. More extensive isotopic dilution was observed in the case of  $CH_3C^{18}O_2^-$  decomposition. We noted in an earlier study<sup>9</sup> that oxygen from air is often trapped in pressed disks during their fabrication, and in order to enhance the effects of this oxygen on our reaction, a KI disk containing 0.4 mg/g of  $^{18}O$ -isotopic sodium acetate and 0.4 mg/g of  $KClO_4$  was heated at  $390^{\circ}$ . After the first hour, there were no  $ClO_4^-$ , no  $HCO_2^-$ , a trace of  $IO_3^-$ , and small amounts of acetate,  $CO_3^{2-}$ ,  $HCO_3^-$ , and  $ClO_3^-$ . Further heating destroyed both the acetate and the chlorate, but no  $HCO_2^-$  nor additional  $IO_3^-$  was formed. The decomposition was completed in 2 hr at which time the only observable products were  $CO_3^{2-}$  and  $HCO_3^-$  with the latter ion displaying in the  $1680$  and  $1310\text{-cm}^{-1}$  regions four sets of sharp bands corresponding to  $HCO_3^-$  with different  $^{18}O$  content. When an excess of perchlorate was used, the final products contained more iodate ion.

It was very much more difficult to dissolve the acetate ion in a KBr matrix than in KI. Temperatures above  $500^{\circ}$  were required to produce the sharp acetate band at  $1611\text{-cm}^{-1}$ , and by the time the intensity of this band was sufficient for a kinetic run about 20 to 40% of the initial acetate had decomposed giving a dark disk with carbonate, bicarbonate, and formate ions. Nevertheless, the decay of the  $1611\text{-cm}^{-1}$  band followed a first-order dependence on the acetate concentration over 90% of the reaction, and  $0.77 \pm 0.06$  mol of formate was obtained from each mole of acetate. Since the formate decomposition in the KBr matrix is about one order of magnitude slower than in KI,<sup>7</sup> the rate of growth of the  $1633\text{-cm}^{-1}$  formate band could be followed throughout the reaction. However, rates from the formate band were generally larger than the rates from the acetate band even though both were still first-order rates. Thus, the rate constants from the formate band are displayed separately from those of the acetate in Figure 3 and in Table I. These rate constants were obtained from disks having initial solute concentrations of about 0.2 mg/g and with decomposition temperatures in the range  $399\text{--}640^{\circ}$ .

The high initial concentrations of carbonate generally present in the KBr disks precluded quantitative studies of isotope effects in the acetate decomposition. How-

(9) I. C. Hisatsune and N. Haddock-Suarez, *Inorg. Chem.*, **3**, 168 (1964).

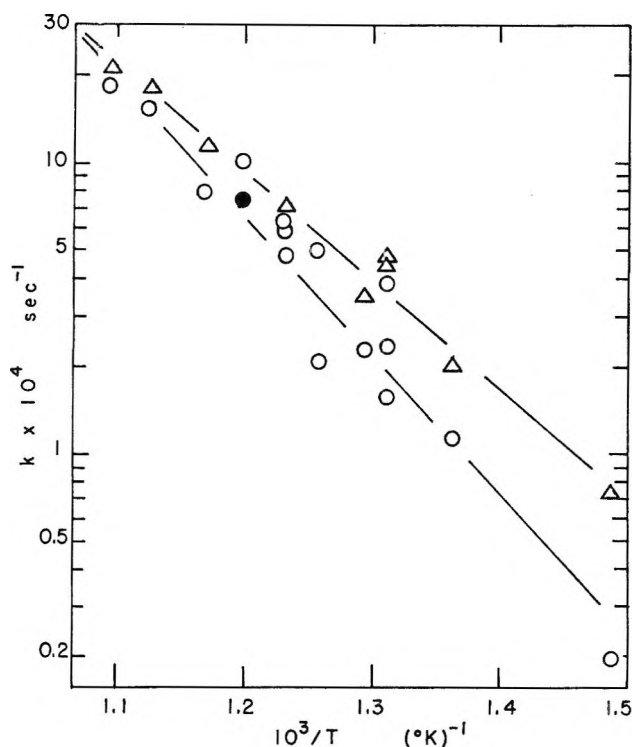


Figure 3. First-order decomposition rate constants for the acetate ion in a KBr matrix: O,  $\text{CH}_3\text{CO}_2^-$ ;  $\Delta$ ,  $\text{HCO}_2^-$ ;  $\bullet$ ,  $\text{CH}_3^{13}\text{CO}_2^-$ .

ever, two qualitative runs are included in Figure 3. Interestingly,  $\text{H}^{13}\text{CO}_3^-$  was produced by  $\text{CH}_3^{13}\text{CO}_2^-$  but not by  $^{13}\text{CH}_3\text{CO}_2^-$ . Also, the decomposition of  $\text{CD}_3\text{CO}_2^-$  again gave both  $\text{HCO}_2^-$  and  $\text{DCO}_2^-$ .

During the production of the formate ion, the acetate showed approximately a one-to-one mole ratio for the stoichiometry of the reactant and product. However, since there was much decomposition of the solute in the disk preparation, we examined the carbon balance in five disks after the absorption bands of the acetate ion had disappeared. The final infrared spectra of these disks showed only bands due to  $\text{HCO}_2^-$ ,  $\text{HCO}_3^-$ , and  $\text{CO}_3^{2-}$ . The concentrations of these ions were determined from appropriate calibration curves,<sup>8</sup> and the results are summarized in Table II. Here, the acetate concentrations are those calculated from the initial

Table II: Stoichiometry of Acetate Decomposition in a KBr Matrix at 520°

Initial mole, <sup>a</sup> $\text{CH}_3\text{CO}_2^-$	Final mole <sup>a</sup>			Carbon balance <sup>b</sup>
	$\text{HCO}_2^-$	$\text{CO}_3^{2-}$	$\text{HCO}_3^-$	
4.4	0.94	3.2	0.1	0.48
7.4	1.0	7.0	0.1	0.55
7.9	1.4	6.8	0.1	0.53
8.2	1.1	7.6	0.1	0.54
8.3	1.1	5.4	0.3	0.41

<sup>a</sup> Units in  $10^{-6}$  mol. <sup>b</sup> Mole ratio of  $(\text{HCO}_2^- + \text{CO}_3^{2-} + \text{HCO}_3^-)$  to  $(2\text{CH}_3\text{CO}_2^-)$ .

weights of the solute. Also, when these disks were heated further, both  $\text{HCO}_3^-$  and  $\text{HCO}_2^-$  decayed. However, the decay of  $\text{HCO}_2^-$  was closer to a first-order process with a low activation energy of about 17 kcal/mol than to a second-order process as observed previously.<sup>7</sup>

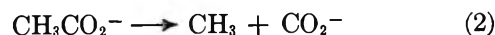
The decomposition kinetics of acetate in KCl matrix was not studied since the concentrations of the matrix isolated ion were too low as evidenced by the weakness of the  $1620\text{-cm}^{-1}$  ir band. The solute under this condition decomposed rapidly, but the reaction products still were  $\text{HCO}_2^-$ ,  $\text{HCO}_3^-$ , and  $\text{CO}_3^{2-}$ . A decomposition of  $8.4 \times 10^{-6}$  mol of acetate at  $516^\circ$  gave  $0.76 \times 10^{-6}$  mol of  $\text{HCO}_2^-$ ,  $0.43 \times 10^{-6}$  mol of  $\text{HCO}_3^-$ , and  $11.1 \times 10^{-6}$  mol of  $\text{CO}_3^{2-}$ . There is considerable uncertainty in the last value since the calibration curve does not follow Beer's law at high carbonate concentrations.

When a KBr disk containing the acetate ion was exposed to  $\gamma$  rays at room temperature, its esr spectrum showed only the formation of  $\text{CO}_2^-$  and  $\text{CO}_3^-$  free radicals which we had observed and characterized previously.<sup>3,8</sup> A hyperfine structure due to  $^{13}\text{CO}_2^-$  in natural abundance was barely detected, but no signals from the  $^{13}\text{CO}_3^-$  were seen. Irradiation of  $^{13}\text{CH}_3\text{CO}_2^-$  or  $\text{CD}_3\text{CO}_2^-$  in the KBr matrix gave identical results as before, but the irradiation of  $\text{CH}_3^{13}\text{CO}_2^-$  produced readily observable  $^{13}\text{C}$ -hyperfine signals from both  $\text{CO}_2^-$  and  $\text{CO}_3^-$  radicals. The esr pattern remained unchanged when the solute concentration was varied in the range 0.05–20 mg/g or when the irradiation time was changed from a few minutes to 4 days. However, longer irradiation eventually caused the esr signals from the two free radicals to decrease with the  $\text{CO}_2^-$  decaying faster.

In order to trace the fate of the hydrogen-containing fragment produced in the irradiation of the acetate ion, products trapped in 25 irradiated KBr disks were analyzed as follows. The disks, each of which originally contained 20 mg/g of acetate, were exposed together to a  $\gamma$ -ray dose of about  $10^7$  R in an evacuated tube. The tube was then opened, about 30 ml of water added, and the contents quickly frozen with liquid nitrogen. After the evacuation of the air from the tube, the sample was allowed to warm to room temperature and liquefy into a solution. A gas chromatographic analysis of the vapor showed the presence of both methane and ethane gases.

## Discussion

The pyrolysis reaction of the acetate ion in a KI matrix can be interpreted by a mechanism in which the elementary reaction



is the initial and the rate-determining step of the decomposition. Each  $\text{CO}_2^-$  then undergoes a rapid hydrogen abstraction reaction to generate the formate

ion. The principal hydrogen source for this reaction is water since we observed earlier<sup>8</sup> that water present in a pressed alkali halide disk is an effective scavenger for  $\text{CO}_2^-$  and since the decomposition of  $\text{CD}_3\text{CO}_2^-$  gave mostly  $\text{HCO}_2^-$  except when the disk was prepared by freeze-drying from  $\text{D}_2\text{O}$ . The latter  $\text{CD}_3\text{CO}_2^-$  reaction, however, indicates that some methyl radical and, to a lesser extent, acetate ion are also sources of hydrogen for the  $\text{CO}_2^-$  radical. We deduce that the acetate- $\text{CO}_2^-$  reaction must not be very extensive for otherwise we should have observed readily in our irradiation and esr studies the well known  $\text{CH}_2\text{CO}_2^-$  radical.

The irradiation work on the KBr disks suggests that the methyl radical produced in reaction 2 can dimerize to give ethane or abstract a hydrogen to give methane. The methyl radical, in addition, can be the source of the elemental carbon which gave the disks a dark color as the decomposition progressed, but the CO from the  $\text{HCO}_2^-$  decay is also known to give carbon by a disproportionation reaction.<sup>7</sup> The absence of  $\text{CO}_3^{2-}$  during the formation of  $\text{HCO}_2^-$  in the KI matrix, as well as the absence of  $\text{H}^{13}\text{CO}_3^-$  in the decomposition of  $^{13}\text{CH}_3\text{CO}_2^-$  in the KBr matrix, indicates that no oxidation of the methyl radical occurred.

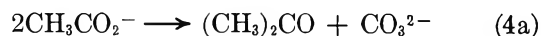
The second-order decay rate constants for  $\text{HCO}_2^-$  calculated from its maximum optical density during the acetate decomposition in the KI matrix are appreciably larger than those determined earlier<sup>7</sup> as shown in Figure 2. Both  $\text{HCO}_3^-$  and  $\text{CO}_3^{2-}$  ions were produced as the formate decayed whereas previously only the  $\text{CO}_3^{2-}$  was observed to increase with reaction time. Thus, we are observing a combination of  $\text{HCO}_2^-$  decay reactions, a slow bimolecular process studied before, and a faster process which gives essentially the same ionic products. The apparent first-order decay of  $\text{HCO}_2^-$  with an activation energy of about 17 kcal/mol that we observed after the acetate decomposition in the KBr matrix or the fast reaction of undiluted potassium formate<sup>10</sup> which gives formaldehyde and carbonate can be the additional  $\text{HCO}_2^-$  decomposition process taking place in our KI disks.

The low activation energy and the unusual frequency factor we obtained in KBr for the decomposition of the

acetate to the formate ion (Table I) are similar to the parameters in the rate constant  $7.2 \times 10^2 \exp(-14 \text{ kcal}/RT) \text{ sec}^{-1}$  determined for the dissociation of a cyclic bicarbonate dimer into two monomer ions in a KBr matrix.<sup>11</sup> The latter reaction was interpreted as a diffusion-controlled one, and we make a similar interpretation here. Since the stoichiometry  $\text{CH}_3\text{CO}_2^-/\text{HCO}_2^-$  is essentially one, this diffusion controlled disproportionation reaction can be



According to our experimental results, the carbonate-producing decomposition of the acetate ion in the KCl and KBr matrices is a separate process from reaction 3. We propose for this process the following sequence of reactions



Toyoda<sup>10</sup> observed reaction 4a with the potassium salt at about 390° and identified the product acetone as a hydrazone derivative. We also carried out the decomposition of undiluted potassium acetate in an evacuated infrared gas cell and observed directly the gas-phase infrared spectrum of acetone. Reaction 4b was attempted by fabricating a KBr disk containing acetone. Although only a small amount of acetone was trapped, it did decompose upon heating at 510° and gave the formate ion. Reaction 4a and 4b, which together is equivalent to reaction 1, and reaction 3 require that the observed ionic carbon products should account for one half of the initial gram-atoms of carbon and that the mole ratio  $\text{CO}_3^{2-}/\text{CH}_3\text{CO}_2^-$  should be close to 1 when the formate yield is low. Both of these expectations are essentially met by the data presented in Table II.

(10) R. Toyoda, *Bull. Inst. Chem. Res. Kyoto Univ.*, **20**, 11 (1950); **21**, 32 (1950).

(11) I. C. Hisatsune and T. Adl, *J. Phys. Chem.*, in press.

# Electrical Mobilities of Lithium-6, Calcium-45, and Nitrate Ions in Liquid Mixtures of Lithium Nitrate and Calcium Nitrate

by Jan C. T. Kwak,<sup>1</sup> J. A. A. Ketelaar, P. P. E. Maenaut, and A. J. H. Boerboom

Laboratory of Electrochemistry, University of Amsterdam, Amsterdam, The Netherlands, and F. O. M. Institute for Atomic and Molecular Physics, Amsterdam, The Netherlands (Received January 14, 1970)

The electrical mobility of  ${}^6\text{Li}$  and  ${}^{45}\text{Ca}$  ions is measured in liquid mixtures of  $\text{LiNO}_3$  and  $\text{Ca}(\text{NO}_3)_2$  in the temperature range 280–400° using a paper electrophoresis method. The mobility of the nitrate ion is calculated from the mobilities of the cations and the equivalent conductivity. The mobility of the Ca ions is found to be much lower than the mobility of the Li ions.

A paper electrophoresis method described earlier<sup>2</sup> has been used to measure the ionic mobilities of  ${}^6\text{Li}$  and  ${}^{45}\text{Ca}$  ions in the liquid mixtures  $\text{LiNO}_3$  (89 mol %)- $\text{Ca}(\text{NO}_3)_2$  (11 mol %) and  $\text{LiNO}_3$  (67 mol %)- $\text{Ca}(\text{NO}_3)_2$  (33 mol %). A quartz fiber "paper" strip (G. H. Dexter and Sons, Inc., Windsor Locks, Conn.) and an alumina support were used.  ${}^6\text{Li}$  as  $\text{LiNO}_3$  and  ${}^{45}\text{Ca}$  as  $\text{CaCl}_2$  were used as tracers. The displacement of the  ${}^{45}\text{Ca}$  ions is found by scanning the strip with a Geiger-Müller counter and determining the location of maximum activity. Less than 0.5 mg of  $\text{CaCl}_2$  containing  ${}^{45}\text{Ca}$  is used in an experiment. The strip is impregnated with about 30 mg of salt mixture/cm. This means that even during the first moments of an experiment the  $\text{CaCl}_2$  added to the strip constitutes only a small fraction of the total amount of salt present. As the experiment proceeds, the chloride ions migrate in a direction opposite to the Ca ions and the  ${}^{45}\text{Ca}$  ions may be considered to move solely in a nitrate environment.

$\text{LiNO}_3$  99.99% enriched in  ${}^7\text{Li}$  is used in the solvent mixtures in the experiments for measuring the mobility of  ${}^6\text{Li}$  ions.  $\text{LiNO}_3$  95% enriched in  ${}^6\text{Li}$  is used as the tracer salt, 2–4 mg in one experiment. When an experiment is finished small bands are cut from the strip and dissolved in concentrated HCl. After evaporation of water and nitric acid the  ${}^6\text{Li}/{}^7\text{Li}$  ratio of the remaining chloride mixture is determined using a mass spectrometer.<sup>3,4</sup> In most cases four or six sample analyses are enough to find the maximum of the  ${}^6\text{Li}$  distribution curve with an estimated accuracy of about 1 mm. A typical  ${}^6\text{Li}$  distribution curve is shown in Figure 1.

The  $\text{Ca}(\text{NO}_3)_2$  content of the salt mixtures on the strip is redetermined after each experiment by complexometric titration. No hydroxide could be detected with phenolphthalein when the cooled salt mixture was dissolved in water after an experiment.

## Results

The results of the measurements are presented in Tables I and II. One measurement of the ionic mo-

**Table I:** Ionic Mobilities  $u$  of  ${}^6\text{Li}$  and  ${}^{45}\text{Ca}$  (Measured) and of  $\text{NO}_3$  (Calculated) in the  $\text{LiNO}_3$  (89 mol %)- $\text{Ca}(\text{NO}_3)_2$  (11 mol %) Mixture

Temp. °C	$10^4 u({}^6\text{Li})$	$10^4 u({}^{45}\text{Ca})$	$10^4 \Lambda / F^a$	$10^4 [-u(\text{NO}_3)]$
282	$2.53 \pm 0.07$	$0.77 \pm 0.04$		
295	$2.92 \pm 0.08$	$0.92 \pm 0.04$	2.90 <sup>b</sup>	$0.38 \pm 0.09$
304	$3.16 \pm 0.10$	$1.08 \pm 0.05$	3.09	$0.35 \pm 0.12$
316	$3.23 \pm 0.13$	$1.09 \pm 0.04$	3.35	$0.56 \pm 0.14$
355	$3.78 \pm 0.12$	$1.24 \pm 0.05$	4.20	$1.03 \pm 0.15$
375	$4.06 \pm 0.12$	$1.27 \pm 0.05$	4.63	$1.13 \pm 0.15$
387	$4.47 \pm 0.14$	$1.32 \pm 0.05$	4.89	$1.05 \pm 0.16$

<sup>a</sup> Calculated from conductance (ref 6) and density (ref 7 and 8) data. <sup>b</sup> Extrapolated value.

**Table II:** Ionic Mobilities  $u$  of  ${}^6\text{Li}$  and  ${}^{45}\text{Ca}$  (Measured) and of  $\text{NO}_3$  (Calculated) in the  $\text{LiNO}_3$  (67 mol %)- $\text{Ca}(\text{NO}_3)_2$  (33 mol %) Mixture

Temp. °C	$10^4 u({}^6\text{Li})$	$10^4 u({}^{45}\text{Ca})$	$10^4 \Lambda / F^a$	$10^4 [-u(\text{NO}_3)]$
303	$1.96 \pm 0.06$	$0.59 \pm 0.03$	1.43 <sup>b</sup>	$0.16 \pm 0.06$
322	$2.21 \pm 0.12$	$0.64 \pm 0.07$	1.73	$0.30 \pm 0.11$
340	$2.56 \pm 0.06$	$0.70 \pm 0.08$	2.01	$0.38 \pm 0.09$
374	$2.86 \pm 0.07$	$0.97 \pm 0.06$	2.54	$0.63 \pm 0.09$
395	$3.09 \pm 0.09$	$0.87 \pm 0.05$	2.88	$0.91 \pm 0.09$

<sup>a</sup> Calculated from conductance (ref 6) and density (ref 7 and 8) data. <sup>b</sup> Extrapolated value.

bility of  ${}^6\text{Li}$  in pure  $\text{LiNO}_3$  was made for comparison with literature data. At 323° we found in pure  $\text{LiNO}_3$ :  $u({}^6\text{Li}) = (4.06 \pm 0.10) \times 10^{-4} \text{ cm}^2 \text{ V}^{-1} \text{ sec}^{-1}$ , to be compared with a value of  $(4.00 \pm 0.06) \times 10^{-4} \text{ cm}^2$

(1) Address inquires to the Department of Chemistry, Dalhousie University, Halifax, Nova Scotia, Canada.

(2) (a) E. P. Honig and J. A. A. Ketelaar, *Trans. Faraday Soc.*, **62**, 190 (1966); (b) J. A. A. Ketelaar and J. C. T. Kwak, *J. Phys. Chem.*, **71**, 1149 (1967).

(3) A. J. H. Boerboom, Thesis, University of Leiden, The Netherlands, 1957.

(4) A. J. H. Boerboom, A. de Jongh, and J. Kistemaker, *Rev. Sci. Instrum.*, **35**, 301 (1964).

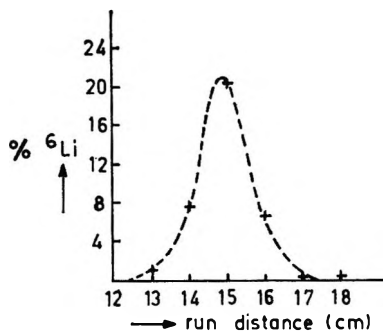


Figure 1. Distribution curve of  ${}^6\text{Li}$  after a migration experiment.

$V^{-1} \text{ sec}^{-1}$  calculated from the results of Lantelme.<sup>5</sup> The experimental errors in the data reported for the mobility of  ${}^{45}\text{Ca}$  are quite large due to the low migration velocity of this ion.

When the equivalent conductivities of these common anion binary mixtures are known, the mobility of the nitrate ion can be calculated from the equation

$$\Lambda/\mathcal{F} = x'(\text{Li})u(\text{Li}) + x'(\text{Ca})u(\text{Ca}) - u(\text{NO}_3^-)$$

where  $\Lambda$  is the equivalent conductivity,  $\mathcal{F}$  the Faraday, and  $x'$  the equivalent mole fraction. The specific conductances of these  $\text{LiNO}_3\text{-Ca}(\text{NO}_3)_2$  mixtures have recently been measured,<sup>6</sup> but no data on the densities have been reported. McAuley, Rhodes, and Ubbelohde<sup>7</sup> have measured the densities of  $\text{NaNO}_3\text{-Ca}(\text{NO}_3)_2$  and  $\text{KNO}_3\text{-Ca}(\text{NO}_3)_2$  mixtures. They found ideal behavior for the volume of mixing within measurement accuracy (0.1%), as well as a linear dependence of the equivalent volume on the temperature. When the equivalent volumes of these mixtures are extrapolated to  $x'(\text{Ca}(\text{NO}_3)_2) = 1$  identical values for the equivalent volume of  $\text{Ca}(\text{NO}_3)_2$  are found. This value may be used for estimating the equivalent volumes of  $\text{LiNO}_3\text{-Ca}(\text{NO}_3)_2$  mixtures, even though the melting point of  $\text{Ca}(\text{NO}_3)_2$  is much higher than the temperatures used in this investigation. Zero excess volume of mixing and linear dependence of the equivalent volume on temperature was assumed for the mixtures under investigation. For pure  $\text{LiNO}_3$  the density measurements of Jaeger and Kapma<sup>8</sup> were used. An error of 1% in  $\Lambda/\mathcal{F}$  was assumed in the calculation of the maximum error in the ionic mobility of the nitrate ion.

## Discussion

Figure 2 shows the electrical mobilities of  ${}^6\text{Li}$ ,  ${}^{45}\text{Ca}$ , and  $\text{NO}_3^-$  ions (as calculated from the equivalent conductivity) in the  $\text{LiNO}_3\text{-Ca}(\text{NO}_3)_2$  system at  $350^\circ$ . Lantelme's<sup>5</sup> measurements were used for the ionic mobility of  ${}^6\text{Li}$  in pure  $\text{LiNO}_3$ . The ionic mobility of  ${}^{45}\text{Ca}$  in pure  $\text{LiNO}_3$  could not be measured reliably due to difficulties with the absorption of the Ca ions, present in tracer quantities, by the quartz fibers and possibly by the alumina plate. In  $\text{LiNO}_3$  containing 2 mol %

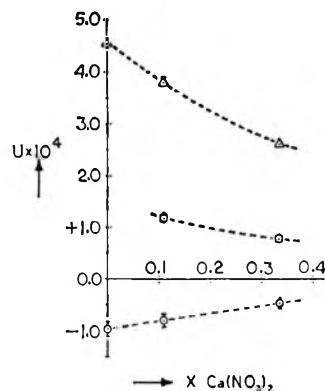


Figure 2. Ionic mobilities  $u$  of  ${}^6\text{Li}$  ( $\Delta$ ),  ${}^{45}\text{Ca}$  ( $\square$ ), and  $\text{NO}_3^-$  ( $\circ$ , negative) in the  $\text{LiNO}_3\text{-Ca}(\text{NO}_3)_2$  system at  $350^\circ$ .

$\text{Ca}(\text{NO}_3)_2$  less than 2% of the  ${}^{45}\text{Ca}$  was found in the quartz fibers and no  ${}^{45}\text{Ca}$  could be detected in the alumina support. In both mixtures used in the measurements reported here no  ${}^{45}\text{Ca}$  could be detected in the quartz fibers or in the support. The minimum detection level is about 1% of the total amount of  ${}^{45}\text{Ca}$  present. Thus it seems that if there is an influence of the support on the measured "external" mobilities, for instance because of bulk flow, the relative values of the ionic mobilities will not be changed and the conclusions drawn in this paper remain valid.

It is seen that the divalent  ${}^{45}\text{Ca}$  ion has a very low mobility compared with the  ${}^6\text{Li}$  ion. The same observation has been made in mixtures of  $\text{CdCl}_2$  with alkali chlorides.<sup>9</sup> The low mobility of the Cd ion in these mixtures and its low Nernst-Einstein parameter ( $RTu/\mathcal{F}D = 0.2$  in the equimolar  $\text{CdCl}_2\text{-KCl}$  mixture<sup>9</sup>) could be caused by the formation of cadmium chloride complex ions. But there is no reason at all to expect the existence of calcium nitrate complex ions in the conventional sense in  $\text{LiNO}_3\text{-Ca}(\text{NO}_3)_2$  mixtures. Indeed it seems that the strong Coulombic interaction of the divalent ions with the anions causes their low electrical mobility. This would be the case in  $\text{LiNO}_3\text{-Ca}(\text{NO}_3)_2$  mixtures as well as in  $\text{CdCl}_2\text{-alkali chloride}$  mixtures and there is no need for assuming the existence of specific complex ions in the latter systems. Apparently electromigration experiments do give information about the ionic interactions in molten salt mixtures but they cannot be used to distinguish between "complex formation" and the existence of strong Coulombic attractions causing drag effects on the ionic migration. Even the movement of some divalent cations in an  $\text{LiCl-KCl}$  solvent mixture towards the anode, as reported by

(5) F. Lantelme, Thesis, University of Paris, 1965.

(6) J. A. A. Ketelaar and P. P. E. Maenaut, to be published.

(7) W. J. McAuley, E. Rhodes, and A. R. Ubbelohde, *Proc. Roy. Soc., Ser. A*, **289**, 151 (1968).

(8) F. M. Jaeger and B. Kapma, *Z. Anorg. Chem.* **113**, 27 (1920).

(9) J. C. T. Kwak and J. A. A. Ketelaar, *Electrochim. Acta*, **14**, 955 (1969).

Alberti, Grassini, and Trucco,<sup>10</sup> is no definite proof for the existence of negatively charged complex ions. Only the relative movement of cation and anion is important and the migration of certain cations towards the anode only means there is a strong drag force exerted upon them by the anions, and not necessarily complex ion formation. Thus there is no special meaning attached to the fact that an ion may have zero electrical mobility. This just means that the drag force and the electric field are approximately counterbalanced. A diffusion experiment as proposed by Angell and Moynihan<sup>11</sup> would enable us to detect complex ions with lifetimes longer than the duration of the experiment. It is interesting to notice that when the temperature dependence of the ionic mobilities of  ${}^6\text{Li}$  and  ${}^{46}\text{Ca}$  is described with the Arrhenius equation, the Arrhenius coefficients  $\Delta H^*$  ("activation energy") for the two cations are equal within experimental error (Table III).<sup>12</sup> The large difference in ionic mobility at a certain temperature can be attributed completely to a

difference in preexponential constant  $u_\infty$ . The same observation has been made for the cations in alkali nitrates<sup>13</sup> and in  $\text{CdCl}_2$ -alkali chloride mixtures.<sup>9</sup> This is in agreement with some of the assumptions of the free volume theory for transport processes as applied to the electrical conductivity of molten salt mixtures.<sup>14</sup> However, the strong interaction between the  $\text{NO}_3^-$  and the  $\text{Ca}^{2+}$  ionic flows in the electrical transport process, as indicated by our results, seem to contradict the physical model on which this theory is based. On the other hand, other transport theories based on cooperative rearrangement models, like the theory proposed by Adam and Gibbs,<sup>15</sup> also predict equal "activation energies."

*Acknowledgments.* The present investigations have been carried out under the auspices of the Netherlands Foundation for Chemical Research (S. O. N.) and with financial aid from the Netherlands Organization for the Advancement of Pure Research (Z. W. O.).

**Table III:** Arrhenius Coefficients  $\Delta H^*$  (kcal/mol) and Preexponential Constants  $u_\infty$  ( $\text{cm}^2/\text{vol sec}$ ) of  ${}^6\text{Li}$  and  ${}^{46}\text{Ca}$  in  $\text{LiNO}_3$ - $\text{Ca}(\text{NO}_3)_2$  Mixtures

LiNO <sub>3</sub> (89 mol %)- Ca(NO <sub>3</sub> ) <sub>2</sub> (11 mol %) 282-387°		LiNO <sub>3</sub> (67 mol %)- Ca(NO <sub>3</sub> ) <sub>2</sub> (33 mol %) 303-395°			
${}^6\text{Li}$	$\Delta H^*$	$3.44 \pm 0.26$	${}^6\text{Li}$	$\Delta H^*$	$3.75 \pm 0.25$
	$10^3 \times u_\infty$	$6.0 \pm 1.4$		$10^3 \times u_\infty$	$5.3 \pm 1.0$
${}^{46}\text{Ca}$	$\Delta H^*$	$3.2 \pm 1.4$	${}^{46}\text{Ca}$	$\Delta H^*$	$4.0 \pm 1.5$
	$10^3 \times u_\infty$	$1.5 \pm 0.9$		$10^3 \times u_\infty$	$1.8 \pm 1.0$

(10) G. Alberti, G. Grassini, and R. Trucco, *J. Electroanal. Chem.*, **3**, 283 (1962).

(11) C. A. Angell and C. T. Moynihan in "Molten Salts, Characterization and Analysis," G. Mamantov, Ed., Marcel Dekker, New York, N. Y., 1969.

(12) The electrical mobility of the nitrate ion is obtained by subtracting two large numbers and thus has a high estimated error. This would result in a very high uncertainty in the value of  $\Delta H_u^*(\text{NO}_3)$ . For this reason no value for  $\Delta H_u^*(\text{NO}_3)$  is given in Table III.

(13) J. C. T. Kwak and J. A. A. Ketelaar, *J. Phys. Chem.*, **73**, 94 (1969).

(14) C. A. Angell, *ibid.*, **68**, 1917 (1964).

(15) G. Adam and J. H. Gibbs, *J. Chem. Phys.*, **43**, 139 (1965).

# Chemiluminescence from the Reaction of Oxygen Atoms

## with Dicyanoacetylene<sup>1</sup>

by J. A. Meyer and D. W. Setser<sup>2</sup>

Chemistry Department, Kansas State University, Manhattan, Kansas 66502 (Received April 30, 1970)

The reaction of oxygen atoms with dicyanoacetylene has been investigated in a discharge flow apparatus. The rate constant for removal of oxygen atoms at 300°K is  $2.2 \pm 0.4 \times 10^{10}$  cc mol<sup>-1</sup> sec<sup>-1</sup>. The reaction generates intense CN(A<sup>2</sup>Π-X<sup>2</sup>Σ<sup>+</sup> and B<sup>2</sup>Σ<sup>+</sup>-X<sup>2</sup>Σ<sup>+</sup>) chemiluminescence. These emissions were characterized and shown to be identical with CN chemiluminescence from the O + C<sub>2</sub>N<sub>2</sub> reaction. Kinetic analysis implies that the same excitation mechanism produces all of the observed vibrational levels,  $v' = 0-15$ , of the CN(B<sup>2</sup>Σ<sup>+</sup>) state; it is also likely that the CN(A) and (B) states are both excited by the same mechanism. The excitation mechanism for CN radical chemiluminescence in oxygen atom reaction systems is discussed; a firm conclusion could not be reached although the evidence favors collisional energy transfer as the excitation step. The reaction of oxygen atoms with C<sub>4</sub>N<sub>2</sub> and C<sub>2</sub>N<sub>2</sub> also gives strong CO(A<sup>1</sup>Π-X<sup>1</sup>Σ) emission in the vacuum ultraviolet. Addition of NO to the O + C<sub>4</sub>N<sub>2</sub> reaction system produces strong NO(A<sup>2</sup>Σ<sup>+</sup>-X<sup>2</sup>Π) emission and addition of mercury gives 2537-Å emission. Estimates of the  $\Delta H_f^\circ(\text{C}_2\text{O})$ ,  $\Delta H_f^\circ(\text{C}_3\text{N})$ , and  $\Delta H_f^\circ(\text{C}_2\text{H})$  are provided in an Appendix.

### Introduction

Chemiluminescence by CN radicals is of widespread occurrence in the reactions of active nitrogen with various organic compounds.<sup>3,4</sup> In contrast, only one example of CN chemiluminescence in an oxygen atom reaction system has been reported, namely, the reaction of oxygen atoms with cyanogen,<sup>5,6</sup> which is a relatively slow reaction with an activation energy of 11 kcal mol<sup>-1</sup>. We wish to report the rapid room temperature reaction of oxygen atoms with dicyanoacetylene (C<sub>4</sub>N<sub>2</sub>) as a second example of CN chemiluminescence, CN(B<sup>2</sup>Σ<sup>+</sup>-X<sup>2</sup>Σ<sup>+</sup>) and (A<sup>2</sup>Π-X<sup>2</sup>Σ<sup>+</sup>), in an oxygen atom reaction system. Cyanide radical chemiluminescence has been observed from the reacting mixtures of oxygen and nitrogen atoms with carbon suboxide<sup>7</sup> and various other molecules.<sup>8</sup> An enhancement in CN emission has been observed when oxygen atoms were added to the active nitrogen-cyanogen system.<sup>7,9</sup> The excitation mechanisms in these mixed nitrogen-oxygen atom reactions may be related to that in the oxygen atom plus C<sub>2</sub>N<sub>2</sub> or C<sub>4</sub>N<sub>2</sub> reactions.

The reaction of oxygen atoms with C<sub>4</sub>N<sub>2</sub> is of interest for several reasons. It is a convenient room temperature system for study of CN radical kinetics and for spectroscopic study of the emission spectra from high vibrational levels of CN(B<sup>2</sup>Σ<sup>+</sup>). Another reason is the close relationship to other current investigations of the reaction of oxygen atoms with acetylenic or related molecules. However, our main objective was to gain insight into the excitation mechanism of CN chemiluminescence in gas phase oxygen atom reaction systems. The mechanisms responsible for CN chemiluminescence in the oxygen atom-cyanogen reaction,<sup>5,6</sup> or for that matter in the more extensively studied active nitrogen

systems,<sup>3,4,10-12</sup> have not been fully explained. In fact, much controversy and very little agreement characterizes the literature concerned with CN radical excitation mechanism in active nitrogen. This paper will only make reference to CN chemiluminescence in active nitrogen if a point is thought to have a direct bearing upon the oxygen atom excitation mechanism.

The experiments were conducted in a discharge-flow reactor. The rate of removal of oxygen atoms was measured, emission intensity kinetics were established, and spectroscopic measurements were made from 10,000 to 1500 Å. Emission intensities gave relative CN vibrational level populations and, in some cases, estimates of relative rotational level populations. The quenching of CN and NO emissions with such added

(1) Abstracted from a thesis submitted by J. A. Meyer in partial fulfillment of the requirements for the Ph.D. degree, Kansas State University, 1969.

(2) Alfred P. Sloan Fellow; to whom correspondence should be addressed.

(3) A. N. Wright and C. A. Winkler, "Active Nitrogen," Academic Press, New York, N. Y., 1968.

(4) B. Brocklehurst and K. R. Jennings, *Progr. React. Kinet.*, **4**, 1 (1967).

(5) D. W. Setser and B. A. Thrush, *Proc. Roy. Soc., Ser. A*, **288**, 256, 275, (1965).

(6) J. C. Boden and B. A. Thrush, *ibid.*, **305**, 107 (1968).

(7) G. Liuti, C. Kunz, and S. Dondes, *J. Amer. Chem. Soc.*, **89**, 5542 (1967).

(8) (a) A. Fontijn and R. Ellison, *J. Phys. Chem.*, **72**, 3701 (1968); (b) A. Fontijn, *J. Chem. Phys.*, **43**, 1829 (1965).

(9) D. Safrany and W. Jaster, *J. Phys. Chem.*, **72**, 3305, 3318 (1968).

(10) J. C. Boden and B. A. Thrush, *Proc. Roy. Soc., A*, **305**, 93 (1968).

(11) (a) T. Iwai, D. W. Pratt, and H. P. Broida, *J. Chem. Phys.*, **49**, 919 (1968); (b) T. Iwai, M. I. Savadatti, and H. P. Broida, *ibid.*, **47**, 3861 (1967); (c) K. D. Bayes, *Can. J. Chem.*, **39**, 1074 (1961)

(12) C. A. Arrington, Jr., O. O. Bernardini, and G. B. Kistiakowsky, *Proc. Roy. Soc., Ser. A*, **310**, 161 (1969).

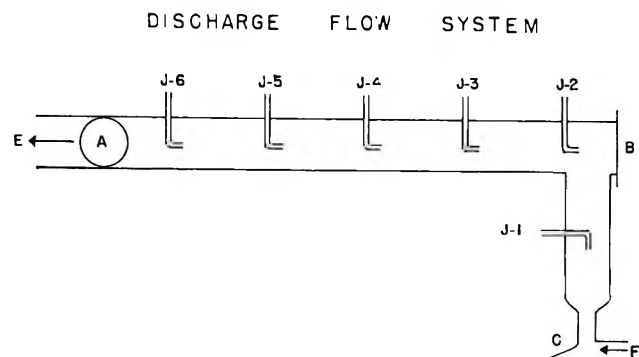


Figure 1. Discharge flow reaction vessel. The vessel was constructed from 30-mm o.d. Pyrex; the jets through which reagents are added have 1-mm orifices. Spectroscopic observations can be made at position A and B through quartz plates. Carrier gases enter at F and exit at E to a mechanical pump.

gases as  $\text{NH}_3$ ,  $\text{SO}_2$ ,  $\text{CO}_2$ , and  $\text{O}_2$  was measured. The CN excitation mechanisms in  $\text{O} + \text{C}_2\text{N}_2$  and  $\text{O} + \text{C}_4\text{N}_2$  reactions were shown to be the same. In spite of all these observations and others described in the text, an unequivocal identification of the excitation mechanism could not be made. However, useful information was collected; some questions are answered and others are raised.

### Experimental Section

The discharge-flow reactor used for the  $\text{O} + \text{C}_4\text{N}_2$  and the  $\text{O} + \text{C}_2\text{N}_2$  experiments is shown in Figure 1. The  $\text{O} + \text{C}_4\text{N}_2$  reaction was studied at room temperature; however, the  $\text{O} + \text{C}_2\text{N}_2$  reaction is very slow at room temperature, so the reaction tube was heated to approximately  $350^\circ$  for those experiments. Operating pressures ranged from 1 to 5 Torr and were measured with silicone oil manometers. Gas flows were regulated with needle valves and measured with calibrated capillary flow meters or with precalibrated floating-ball flow meters. Linear flow velocities ranged from 1 to 10 m/sec and were regulated with a large throttling stopcock in front of a 425 l./min mechanical pump. Concentrations and flow times were calculated in the usual way.<sup>5,6</sup> Intensity measurements were made at the quartz emission window, which was 10 cm downstream of jet 6. The emission intensities of CN, NO, and Hg were measured by selecting the wavelength of interest with a Jarrell-Ash 0.75-m monochromator using a grating blazed at  $3000 \text{ \AA}$  and fitted with a EMI 9558Q photomultiplier tube. The output was amplified by a PAR JB-5 phase lock amplifier. The  $\text{NO}_2$  air afterglow intensity was followed by placing a Baird Atomic interference filter ( $\lambda 5200 \text{ \AA}$  with  $100\text{-\AA}$  bandpass) over an RCA 1P28 photomultiplier tube. The emission in the vacuum ultraviolet and from 7000 to  $10,000 \text{ \AA}$  was studied by use of a McPherson 0.3-m monochromator. The vacuum ultraviolet measurements were done in a reaction vessel (different from that in Figure 1) fitted

with an LiF window, which was directly attached to the monochromator.

Oxygen atoms, free from molecular oxygen, were produced by passing molecular nitrogen through a microwave discharge and titrating the resulting nitrogen atoms with an equivalent amount of nitric oxide at jet 1.<sup>13</sup> For a few runs oxygen atoms were produced by discharging a flow of argon containing a few per cent  $\text{O}_2$ ; this technique introduced additional complexity into the kinetic interpretations due to the presence of  $\text{O}_2$ . The nitrogen carrier gas was purified by passage through a glass wool-packed trap cooled to  $195^\circ\text{K}$  and at reduced pressure through a second at  $78^\circ\text{K}$ . This purification procedure removed most of the water impurity. The trace of  $\text{O}_2$  in the tank nitrogen (which was probably dissociated) did not affect the reaction to a noticeable extent and, in fact, some impurity is necessary to promote dissociation of molecular nitrogen in the discharge.<sup>14</sup> The discharged nitrogen flowed through a Wood's horn light trap before entering the flow tube and, with external shielding, prevented light from the discharge reaching the observation region. A glass wool plug was placed beyond the discharge region; the plug reportedly quenches vibrationally excited ground-state nitrogen molecules or other excited species produced by the discharge.<sup>15</sup>

Dicyanoacetylene ( $\text{C}_4\text{N}_2$ ) was prepared by a standard method<sup>16,17</sup> using dimethylacetylenedicarboxylate as the starting material. The  $\text{C}_4\text{N}_2$  was collected in a Dry Ice trap and stored at  $195^\circ\text{K}$  under vacuum. The purity of  $\text{C}_4\text{N}_2$  was checked by comparison to the known infrared, ultraviolet, and electron impact spectra. The  $\text{C}_4\text{N}_2$  was expanded into a 12 l. Pyrex glass reservoir for an experiment; it seemed to react very slowly with the storage vessel as evidenced by the formation of some polymer and small amounts of noncondensable gas. Conditioning the storage vessel for a few days reduced the formation of the noncondensable component to a negligible amount. No attempt was made to condition the reaction tube since oxygen atoms probably would have affected the conditioning.

### Results

*General Kinetic Observations.* The addition of  $\text{C}_4\text{N}_2$  to a flow of oxygen atoms at room temperature gave a bright purple glow which filled the reaction flow tube, and the oxygen atoms were removed at a rate amenable

(13) (a) F. Kaufman and J. R. Kelso, *J. Chem. Phys.*, **27**, 1209 (1957); **28**, 992 (1958). (b) An up to date summary of this technique is given in ref 3 and 4.

(14) I. M. Campbell and B. A. Thrush, *Proc. Roy. Soc., Ser. A*, **296**, 201 (1967).

(15) (a) J. E. Morgan, L. F. Phillips, and H. I. Schiff, *Discuss. Faraday Soc.*, **33**, 118 (1962); (b) P. N. Clough and B. A. Thrush, *Proc. Roy. Soc., Ser. A*, **309**, 419 (1969).

(16) C. Moureu and J. C. Bongrand, *Justus Liebig's Ann. Chem.*, **14**, 5 (1920).

(17) J. A. Meyer, Ph.D. Thesis, Kansas State University, 1969. This reference contains more experimental details.

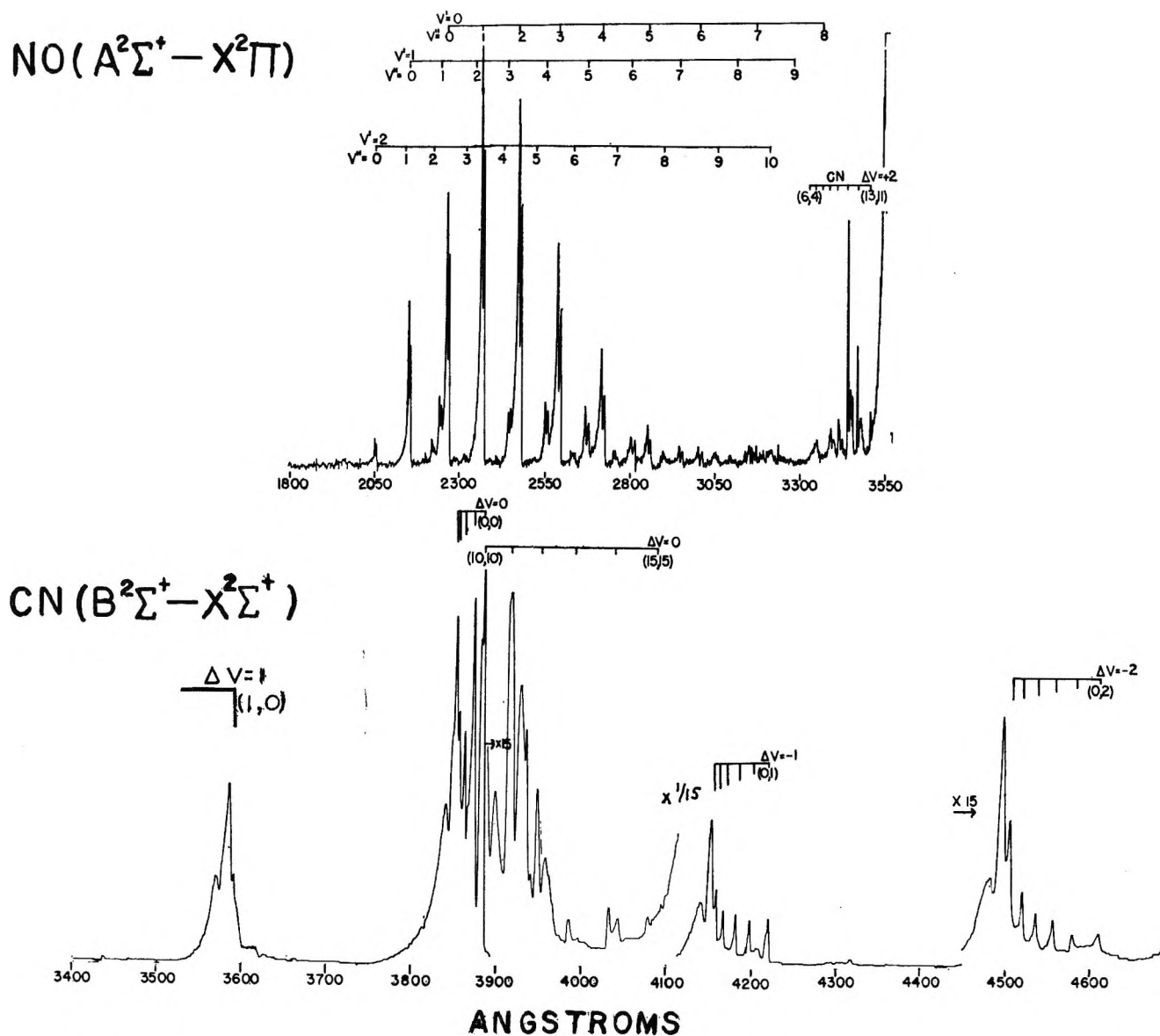


Figure 2. CN(B-X) and NO(A-X) emission spectra. Typical emission spectra from O + C<sub>4</sub>N<sub>2</sub> at 2.5 Torr. A small excess of NO was added to enhance the NO bands. The highest CN vibrational level observed was v' = 15. The structure between 3050 and 3300 Å corresponds to additional CN tail bands.

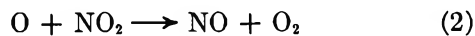
to study with a discharge flow apparatus. The heterogeneous component to the reaction was insignificant in contrast to the room temperature reaction of active nitrogen with C<sub>4</sub>N<sub>2</sub>, which also gave intense CN emission but left brown surface deposits around the mixing jet. The CN(A-X), CN(B-X), and NO(A-X) emission spectra are shown in Figures 2 and 3. Detailed considerations of the spectra and the kinetics of the emission intensities are presented in the next section.

The rate constant for the removal of oxygen atoms was measured by employing the NO<sub>2</sub> air afterglow as a method of following relative oxygen atom concentration.<sup>5</sup> The conditions were adjusted such that [C<sub>4</sub>N<sub>2</sub>] ≫ [O] in anticipation that the oxygen atom removal rate would be reduced to pseudo-first-order kinetics. The air afterglow<sup>18</sup> is due to the slow com-

bination of O and NO



The nitric oxide concentration remained approximately constant down the flow tube because of the very fast reaction



which immediately regenerates NO. There is, therefore, little net removal of oxygen atoms and no net removal of nitric oxide from reaction 1 under our conditions.

(18) (a) M. A. A. Clyne and B. A. Thrush, *Proc. Roy. Soc., Ser. A*, **269**, 404 (1962); (b) N. Jonathan and R. Petty, *Trans. Faraday Soc.*, **64**, 1240 (1968); (c) A more detailed formulation of reaction 1 may be made but is unnecessary for our purposes.

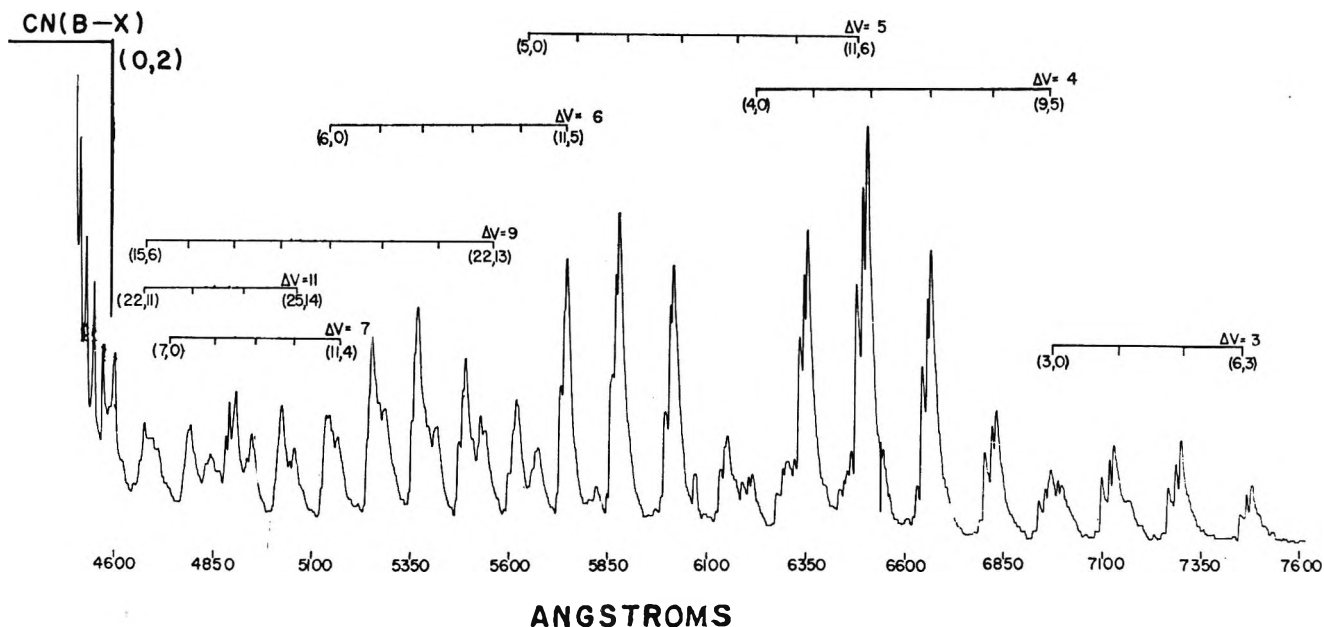


Figure 3. CN(A-X) emission spectra. Typical emission spectra from  $\text{O} + \text{C}_4\text{N}_2$  at 2.5 Torr. The (A-X) bands extend to the (B-X)  $\Delta v = 2$  sequence indicating the presence of populations in high vibrational levels of the A state. The sensitivity of the 9558 Q photomultiplier tube declines sharply beyond 5000 Å.

The air afterglow emission intensity is independent of pressure in the 1–10 Torr range and is given by<sup>18</sup>  $I_{\text{NO}_2} = I_{\text{NO}_2}^0 [\text{O}][\text{NO}]$ ;  $I_{\text{NO}_2}^0$  is a constant which depends upon the temperature, the third body, and the geometry.  $I_{\text{NO}_2}$  is directly proportional to  $[\text{O}]$  and if a small quantity of NO is added to a stream of oxygen atoms, the decrease in light intensity along the flow tube measures the decay of  $[\text{O}]$ ; i.e.,  $-dI_{\text{NO}_2}/dx = -d[\text{O}]/dx$ . In our experiments the nitrogen atoms were titrated with NO at jet 1 to obtain an absolute value of  $[\text{O}]$ , and a small excess of NO then was added at that jet. Additional quantities of nitric oxide were added at jet 6 and  $I_{\text{NO}_2}$  was measured at A. Plots of  $I_{\text{NO}_2}$  against  $[\text{NO}]$  yielded a straight line with slope equal to  $I_{\text{NO}_2}^0 [\text{O}]$ . The  $\text{C}_4\text{N}_2$  was added to the oxygen atom flow at jets 2–6. For each reaction time the relative concentration of oxygen atoms at the observation window was measured by adding NO at jet 6 and measuring  $I_{\text{NO}_2}$ . An example of such a plot is shown in Figure 4; the slopes of the lines decrease with increase in the reaction time or  $[\text{C}_4\text{N}_2]$ . The right side of the abscissa represents the NO added at jet 6, and the left side shows excess NO added at J-1 plus NO generated in the reaction. Nitric oxide is a product of the reaction since the intercept is larger with  $\text{C}_4\text{N}_2$  present. But the  $[\text{NO}]$  seemed to reach a steady state and did not increase with reaction time.

The data of Figure 4 were analyzed according to  $-d[\text{O}]/dt = k[\text{O}][\text{C}_4\text{N}_2]$ ; removal of oxygen atoms by  $\text{O} + \text{O} + \text{M}$  or  $\text{O} + \text{O}_2 + \text{M}$  is negligible. Since  $[\text{C}_4\text{N}_2] \gg [\text{O}]$ , integration gives  $\ln [\text{O}]/[\text{O}]_0 = -k[\text{C}_4\text{N}_2]t$

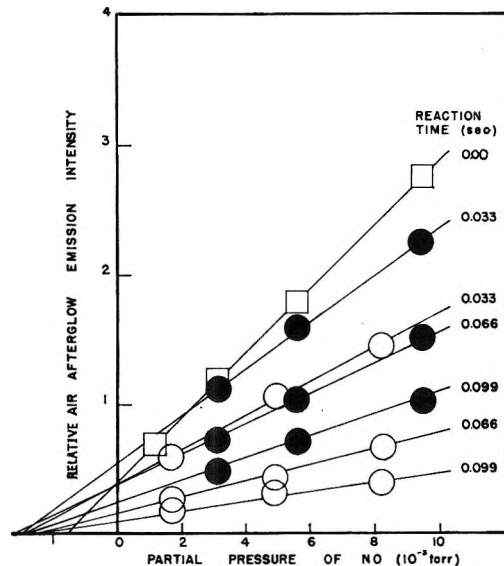


Figure 4. Measurement of  $[\text{O}]$  in the  $\text{O} + \text{C}_4\text{N}_2$  reaction. The air-afterglow intensity ( $\text{O} + \text{NO}$ ) was measured at window A vs. added  $[\text{NO}]$  through J-6. The reaction times are the flow times from jets 3, 4, 5, to the window. Total pressure = 2.4 Torr,  $[\text{O}] = 2.5 \times 10^{-3}$  Torr,  $[\text{C}_4\text{N}_2] = 7.0 \times 10^{-3}$  Torr, ●;  $[\text{C}_4\text{N}_2] = 1.6 \times 10^{-2}$  Torr, ○; No  $\text{C}_4\text{N}_2$  added, □.

$\text{N}_2]t$  and the appropriate plot, Figure 5, gave  $k = 2.2 \times 10^{10} \text{ cc mol}^{-1} \text{ sec}^{-1}$ . This procedure was repeated for various  $[\text{C}_4\text{N}_2]$ , but always under pseudo-first-order conditions, and the average value of  $k$  was  $2.2 \pm 0.4 \times 10^{10} \text{ cc mol}^{-1} \text{ sec}^{-1}$ .

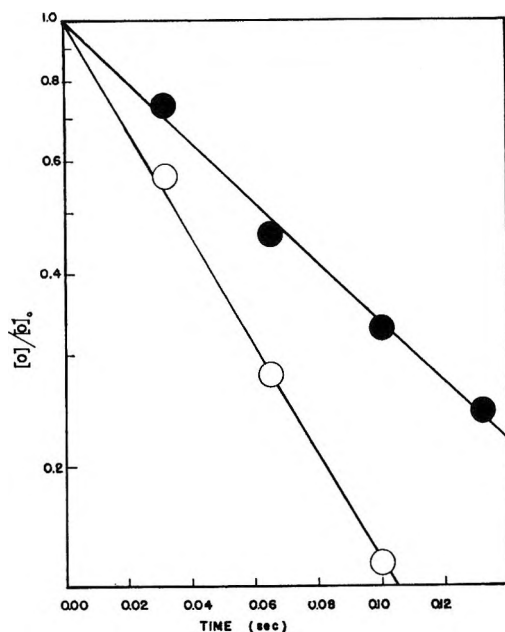


Figure 5. Oxygen atom removal by  $C_4N_2$ . Semilog plot of data in Figure 4;  $[C_4N_2] = 1.6 \times 10^{-2}$  Torr, O;  $[C_4N_2] = 7.0 \times 10^{-3}$  Torr, ●.

The overall  $O + C_4N_2$  reaction is, without doubt, quite complex and the measured rate constant is related to the slowest step in the oxygen atom removal sequence. The secondary reactions involve intermediate radicals, and their reactions with oxygen atoms and with  $C_4N_2$  probably are fast. Attempts were made to measure the stoichiometry for various  $[C_4N_2]/[O]$  ratios by using the CN emission intensity to measure  $[C_4N_2]$  (see later section) and  $I_{NO}$  to measure  $[N]$ . For  $[C_4N_2]/[O] < 0.2$ , 3–5 oxygen atoms were used for each  $C_4N_2$  molecule. As the ratio was increased the oxygen atom consumption diminished, and for  $[C_4N_2]/[O] = 10$  only 0.5 oxygen atom was consumed per molecule of  $C_4N_2$ . This implies that intermediate radicals react with  $C_4N_2$ , which is not surprising in view of the acetylenic bond in the molecule. The rate constant reported above was for  $[C_4N_2]/[O] = 3$ –6.

**Emission Spectra.** The  $CN(B^2\Sigma^+ - X^2\Sigma^+)$  emission is quite intense and extends up to  $v' = 15$ , which corresponds to an excitation energy of  $149 \text{ kcal mol}^{-1}$ . Approximate relative populations can be obtained by inspection of the  $\Delta v = 0$  sequence since the Franck-Condon factors are approximately constant.<sup>19</sup> The emissions from  $v' > 10$  are about a factor of 15 less intense than from the 0–5 levels. Figure 3 shows a low resolution spectrum from the Jarrell-Ash monochromator of the  $CN(A^2\Pi - X^2\Sigma)$  bands with transitions from  $v' = 3$ –11 definitely identified. Scans from 10,000 to 7000 Å with the McPherson monochromator show bands down to  $v' = 1$ ; the (0,0) band is above 10,000 Å. Transitions from levels with  $v' > 11$  could not be unambiguously identified, but bands originating from levels up to  $v' \approx 20$  may be present. A search

was made for the recently discovered  $CN(B^2\Sigma^+ - A^2\Pi)$  bands but a definite assignment could not be made. This is understandable since LeBlanc<sup>20</sup> found the  $CN(B, v' = 7 - X, v'' = 7)$  band to be about 50 times more intense than the  $CN(B, v' = 7 - A, v'' = 4)$  band.

The  $NO(A-X)$  emission resulted if  $NO$  was added to the reaction. If excess  $NO$  was not added in the titration of nitrogen atoms or downstream, the  $NO(A-X)$  emission was weak. The  $NO(A-X)$  emission was more than ten times as intense as the  $NO(B-X)$  emission.

Both the  $C_2N_2$  (at 300°K) and  $C_4N_2$  reactions showed<sup>21</sup> CO Fourth Positive  $CO(A^1\Pi - X^1\Sigma^+)$  emission in the vacuum ultraviolet (1500–1850 Å), and the emissions appeared to be identical. The appearance of the Fourth Positive emission spectrum was very similar to that from  $O + C_2H_2$ ,<sup>22</sup> which was obtained in our apparatus for the purpose of comparison. A search for the CO “triplet system” was unsuccessful, perhaps due to overlap from  $CN(A-X)$  bands.

The low resolution  $CN(B-A)$  and  $(A-X)$  spectra from the  $O + C_4N_2$  and  $O + C_2N_2$  reactions are very similar in appearance. Figure 6 compares the rotational structure of the  $CN(B^2\Sigma^+, v' = 0 - X^2\Sigma^+, v'' = 0)$  band at the same pressure from three reactions:  $O + C_2N_2$ ,  $O + C_4N_2$ , and “active nitrogen” +  $CH_2Cl_2$ . The rotational structure of the bands in Figure 6 from the two oxygen reactions is virtually identical. The “active nitrogen” plus  $CH_2Cl_2$  system has been thoroughly studied<sup>11,23</sup> and the enhancement of the  $K' = 4, 7, 11,$  and  $15$  rotational lines is caused by perturbations from the  $CN(A^2\Pi)$  rotational levels in  $v' = 10$ . In fact at lower pressure (0.045 Torr) emission from only the perturbed rotational levels is found in the  $CN(B, v' = 0 - X, v'' = 0)$  band from “active nitrogen” plus  $CH_2Cl_2$ ; at higher pressures rotational relaxation spreads the population to other rotational levels and additional rotational structure is observed. The most obvious differences between the spectra obtained from the “active  $N_2$ ” and oxygen atom reactions in Figure 6 are the presence of the  $v' = 1$  and 2 band heads, the lesser enhancement of the perturbed rotational lines, and a higher rotational temperature for the oxygen atom cases. Comparing the spectrum from “active nitrogen” +  $CH_2Cl_2$  in Figure 6 to lower pressure spectra<sup>23c</sup> indicates a considerable degree of rotational relaxation under our conditions. Therefore the original rotational populations of  $CN(B^2\Sigma^+)$  from  $O +$

(19) R. J. Spindler, *J. Quant. Spectrosc. Radiat. Transfer*, **5**, 165 (1965).

(20) F. J. LeBlanc, *J. Chem. Phys.*, **48**, 1841 (1968).

(21) W. C. Richardson, D. W. Setser, and J. A. Meyer, unpublished results.

(22) (a) K. H. Becker and K. D. Bayes, *J. Chem. Phys.*, **48**, 653 (1968); (b) K. D. Bayes, *ibid.*, **52**, 1093 (1970).

(23) (a) H. P. Broida and S. Golden, *Can. J. Chem.*, **38**, 1666 (1960); (b) H. E. Radford and H. P. Broida, *J. Chem. Phys.*, **38**, 644 (1963); (c) K. M. Evenson and H. P. Broida, *ibid.*, **44**, 1637 (1966).

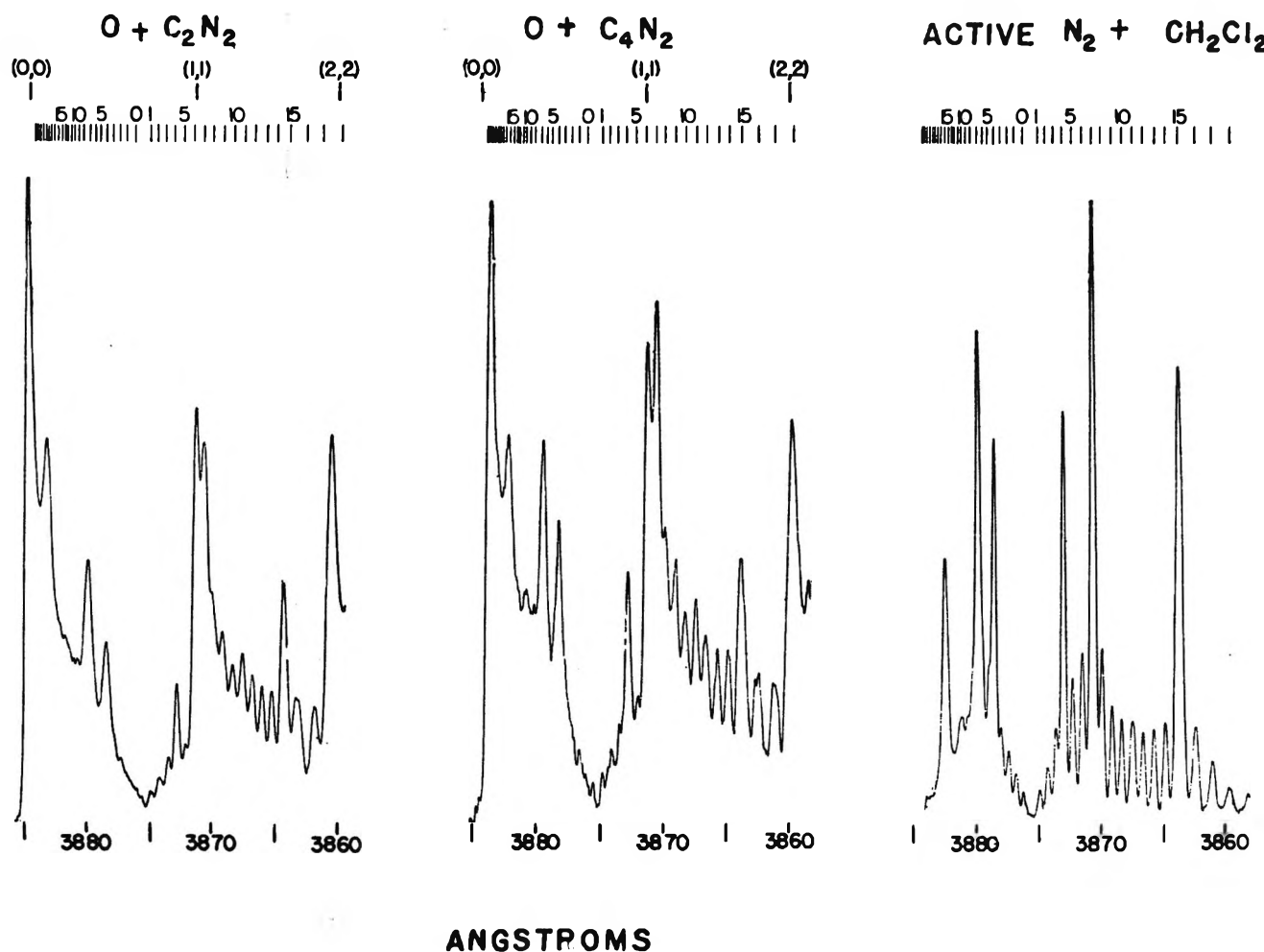


Figure 6. Rotation populations of  $\text{CN}(B^2\Sigma^+, v' = 0)$ . Higher resolution,  $30\text{-}\mu$  slit, spectra of the (0,0) band at 0.8 Torr for the three indicated reactions. The  $\text{N} + \text{CH}_2\text{Cl}_2$  shows the strongly enhanced populations of the perturbed levels  $K' = 4, 7, 11, 15$ . The lines are identified by the upper rotational level.

$\text{C}_4\text{N}_2$  must have extended to very high rotational levels indeed.

*Relative Vibrational Populations of  $\text{CN}(B^2\Sigma^+$  and  $A^2\Pi)$ .* The relative vibrational populations of the  $\text{CN}(A)$  and  $\text{CN}(B)$  states in the oxygen atom excitation systems were measured in order to more fully characterize the excitation mechanism. Relative populations were calculated from relative intensities (corrected for detector-monochromator sensitivity) using the expression

$$N_{v'} \propto I_{v'0''} / \bar{\nu}_{v'0''}^4 S_{v'0''}$$

$I_{v'0''}$  is the intensity of the band head,  $\bar{\nu}_{v'0''}$  is the frequency at the band head in  $\text{cm}^{-1}$ ,  $N_{v'}$  is the population of level  $v'$ , and  $S_{v'0''}$  is the band strength. The  $S_{v'0''}$  values were approximated by Franck-Condon factors and taken from Spindler.<sup>19</sup> For the B state the  $\Delta v = 0, 1, 2$  sequences were used to obtain the relative populations for  $v' = 0-5$ ; the  $v' = 10-15$  levels were obtained from the  $\Delta v = 0$  tail bands. The populations of levels 6-9 cannot be estimated due to severe overlapping of bands for all sequences. However, the gen-

eral appearance of the spectra suggest a smooth curve connecting the two groups of levels as implied in Figure 7. The  $\text{CN}(A^2\Pi)$  state relative vibrational populations were estimated from the A-X spectrum of Figure 3 and from scans of the 6000-10,000-Å region obtained with the McPherson monochromator fitted with a RCA 7102 photomultiplier tube. It should be noted that band head intensities were used to determine relative vibrational populations. This is actually quite unreliable if the rotational temperature varies from one vibrational level to another, as implied by Figure 6. Using band heads for the  $\text{CN}(B^2\Sigma^+ - X^2\Sigma^+)$  system introduces additional uncertainty because perturbations strongly affect the shapes of some vibrational bands.

Figure 7 shows the B state vibrational populations relative to  $v' = 0$  populations from  $\text{O} + \text{C}_4\text{N}_2$ , "active nitrogen" +  $\text{CNBr}$ , and  $\text{O} + \text{C}_2\text{N}_2(350^\circ)$  at 1.0 Torr pressure. Variation of the pressure ( $\text{N}_2$  carrier gas) from 1 to 5 Torr, did not change the  $\text{CN}(B)$  relative populations in  $v' = 0-5$ , but the relative populations for  $v' > 10$  were decreased by  $\sim 1.5$ . Since the  $\text{CN}(B^2\Sigma^+)$

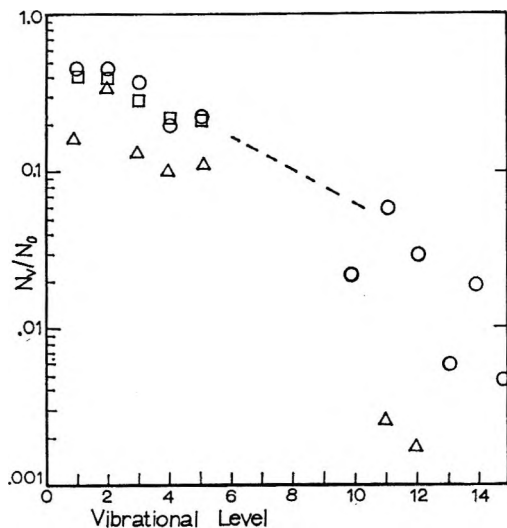


Figure 7. Relative vibrational populations of  $\text{CN}(\text{B}^2\Sigma^+)$ .  $\text{O} + \text{C}_4\text{N}_2$ ,  $\circ$ ;  $\text{O} + \text{C}_2\text{N}_2$ ,  $\square$ ; "active nitrogen" and  $\text{CNBr}$ ,  $\Delta$ .

radiative lifetime<sup>24</sup> is  $3 \times 10^{-8}$  sec, little vibrational relaxation occurs at pressures  $\leq 1$  Torr. The "normal active nitrogen" +  $\text{CNBr}$  emission was used as a check on our technique for obtaining relative populations; our values are in reasonably good agreement with relative populations quoted elsewhere.<sup>11b</sup> Figure 7 clearly shows that, within experimental error, the relative vibrational populations from  $\text{O} + \text{C}_4\text{N}_2$  and  $\text{O} + \text{C}_2\text{N}_2$  are identical.

The relative vibrational populations of  $\text{CN}(\text{A})$  from  $\text{O} + \text{C}_4\text{N}_2$  were estimated as  $\nu_1:\nu_2:\nu_3:\nu_4:\nu_5:\nu_6:\nu_7:\nu_8:\nu_9 = 1.0:0.6:0.5:0.5:0.3:0.2:0.1:0.05:0.03$ . These relative populations were not studied in detail but the trend of increasing occupation of lower vibrational levels should be correct. The vibrational distribution in the  $\text{CN}(\text{A})$  state is similar to that obtained from active nitrogen with compounds containing the  $\text{CN}$  group.<sup>11c</sup>

Another common type of  $\text{CN}(\text{B-X})$  emission in active nitrogen is the "blue flame,"<sup>10,11b</sup> which occurs at high pressure ( $\sim 5$  Torr) with trace amounts of fuel. The "blue flame" vibrational distribution<sup>11b,25</sup> is highest for  $\nu' = 0$ , declines strongly through  $\nu' = 1-4$ , then increases for  $\nu' = 5-11$  before declining again for higher  $\nu'$ . This distribution is much different than the relative populations from the oxygen atom or the "normal" active nitrogen +  $\text{CNBr}$  reactions shown in Figure 7. In fact, the general shape of the  $\text{CN}(\text{B})$  vibrational distribution in oxygen atom system resembles that from active nitrogen plus cyanogen,<sup>11b</sup> however, the levels from 6 to 15 are probably more highly populated in oxygen atom excitation reactions.

Since the  $\text{CN}(\text{B})$  vibrational populations were the same for  $\text{O} + \text{C}_4\text{N}_2$  and  $\text{O} + \text{C}_2\text{N}_2$  and since the (0,0) band had the same rotational structure in both systems, the excitation mechanisms must be the same in each case. The experiments described below also strongly suggest that all vibrational levels in the B state were

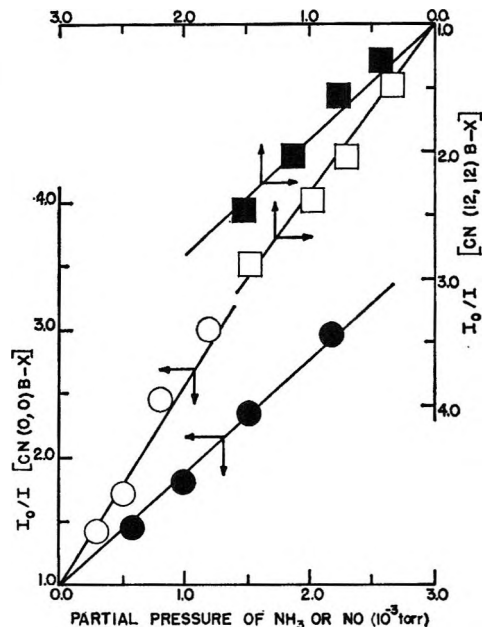


Figure 8. Quenching of the  $\text{CN}(\text{B-X})$ , (0,0), and (12,12) bands by  $\text{NH}_3$  or  $\text{NO}$ . The quenching gases  $\text{NH}_3$ ,  $\circ$ ,  $\square$  and  $\text{NO}$  ( $\bullet$ ,  $\blacksquare$ ) were added at jet 6. The  $\text{C}_4\text{N}_2$  was added at jet 5; the total pressure was 1.3 Torr.

produced by the same mechanism (and by implication a single mechanism). The quenching of  $\text{CN}$  emission by the addition of foreign gases to the  $\text{O} + \text{C}_2\text{N}_2$  reaction, which is described later, was similar to that for the  $\text{O} + \text{C}_2\text{N}_2$  reaction.<sup>5,6</sup> At this point we wish demonstrate that the  $\text{CN}(\text{B}) \nu' = 0$  and  $\nu' = 1$  levels are quenched in identical ways. This is shown in Figure 8 for  $\text{NO}$  and  $\text{NH}_3$  as added gases. In addition scans of the entire  $\Delta\nu = 0$  sequence were made and sufficient  $\text{NO}$  and  $\text{NH}_3$  added to give half-quenching the relative intensities of the vibrational bands were changed from scans without  $\text{NH}_3$  or  $\text{NO}$ . In similar quenching experiments,<sup>17</sup> the intensity ratio,  $I(\text{B-X})/I(\text{A-X}, \text{high } \nu' \text{ levels})$ , was found to be invariant with degree of quenching.

*Kinetics of CN, NO, and Hg Emission Intensities.* The kinetics of the emission intensities from  $\text{CN}(\text{B-X})$ ,  $\text{CN}(\text{A-X})$ , and  $\text{NO}(\text{A-X})$  were determined by following the emission from a specific band and varying the concentration of reactants. The results for the  $\text{CN}(\text{B}, \nu' = 0-X, \nu'' = 0)$  band are shown in Figure 9; the intensity was first order in  $[\text{O}]$  and  $[\text{C}_4\text{N}_2]$  except for high  $[\text{C}_4\text{N}_2]$ . If the  $[\text{C}_4\text{N}_2]/[\text{O}]$  ratio was increased sufficiently, the intensity became approximately second order in oxygen atom concentration. In the experi-

(24) (a) J. H. Moore, Jr., and D. Robinson, *J. Chem. Phys.*, **48**, 4870 (1968); (b) T. Wentink, *et al.*, *ibid.*, **41**, 278 (1964).

(25) (a) For the "blue flame" active nitrogen reaction conditions, Boden and Thrush<sup>10</sup> showed that three well defined groups ( $\nu' = 0-2$ ,  $5-12$ , and  $13-15$ ) of levels must be considered separately in explaining the collisional excitation of  $\text{CN}(\text{X-B})$ . (b) The high-resolution  $\text{CN}(\text{B-X})$  spectrum from the "blue flame" active nitrogen excitation has been discussed by R. L. Brown and H. P. Broida, *J. Chem. Phys.*, **41**, 2053 (1964).

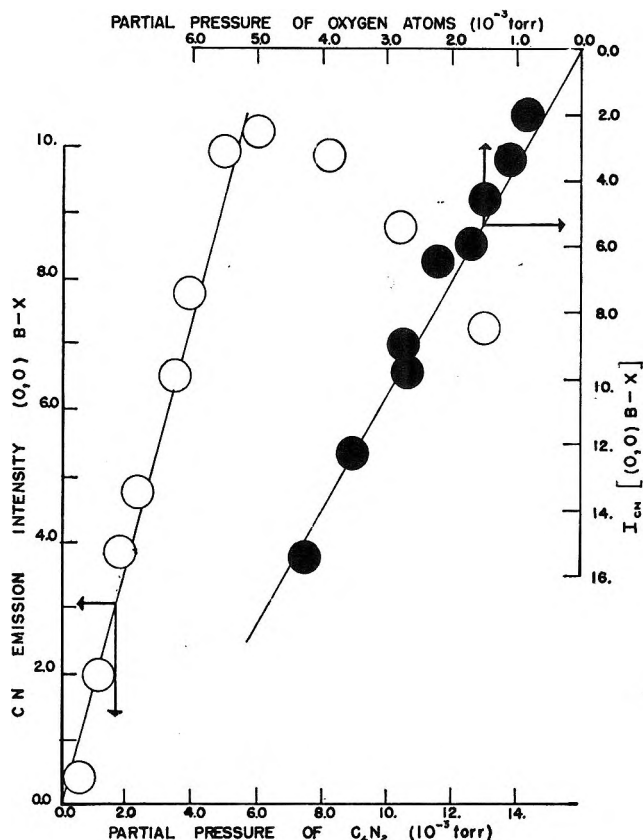


Figure 9. Dependence of CN(B-X) emission intensity upon [O] and  $[C_4N_2]$ . The experiments were done by adding  $C_4N_2$  at J-6; the NO titration was done at J-3. The total pressure was 1.5 Torr;  $\circ$ ,  $[O] = 3.2 \times 10^{-3}$  Torr and  $[C_4N_2]$  was varied;  $\bullet$ ,  $[C_4N_2] = 0.6 \times 10^{-3}$  Torr and [O] was varied.

ment of Figure 9, the second-order effect began at a ratio of 1. The intensity from the B-X (12,12) band and the CN(A,  $v' = 7-X$ ,  $v' = 2$ ) band showed the same dependence on reactant concentrations as displayed in Figure 9.

The dependence of NO(A-X) emission intensity upon  $[NO]$ ,  $[O]$ , and  $[C_4N_2]$  was investigated by following emission from the  $v' = 0$  and 1 bands. The results were identical and the intensity was first order in  $[O]$ ,  $[C_4N_2]$ , and  $[NO]$  at low concentrations, but deviations were observed at high concentrations<sup>17</sup> probably from interference of  $[NO]$  or  $[C_4N_2]$  with the "normal" sequence of radical reactions. The radiative NO(A-X) lifetime is sufficiently short ( $\tau = 2 \times 10^{-7}$  sec)<sup>26</sup> that the vibrational populations of NO(A) [0:1:2 = 100:40:10]<sup>27</sup> nearly reflect the distribution produced by the excitation mechanism.

The Hg emission (2537 Å) can be used to identify metastable  $N_2(A^3\Sigma_u^+)$  molecules,<sup>27,28</sup> although other metastables, such as  $CO(A^3\Pi)$ ,<sup>29</sup> also excite  $Hg(^3P_1)$ . Experiments were done in which mercury vapor was excluded from the gas flow, except at jet 6 where nitrogen saturated with mercury vapor was added to the  $O + C_4N_2$  reaction. The  $Hg(2537\text{-}\text{Å})$  emission was absent unless both mercury vapor and  $C_4N_2$  was added.

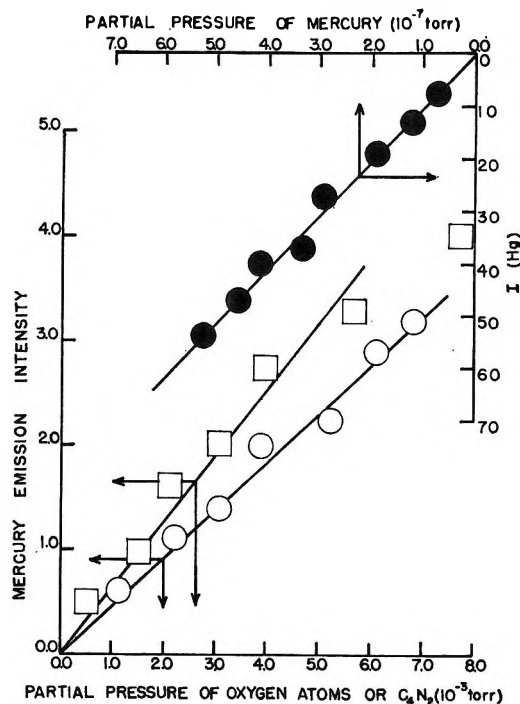


Figure 10. Dependence of  $Hg(^3P_1-^1S_0)$  emission intensity upon  $[O]$ ,  $[C_4N_2]$ , and  $[Hg]$ . Hg was added to J-6,  $C_4N_2$  was added at J-5 and  $[O]$  was varied by altering the discharge power and titrating the  $[N]$  with NO at J-3; the total pressure was 2 Torr:  $\bullet$ ,  $[O] = 4.6 \times 10^{-3}$  Torr,  $[C_4N_2] = 4.4 \times 10^{-3}$  Torr, variable  $[Hg]$ ;  $\circ$ ,  $[C_4N_2] = 5.3 \times 10^{-3}$  Torr, constant  $[Hg]$  and variable  $[O]$ ;  $\square$ ,  $[O] = 4.6 \times 10^{-3}$  Torr, constant  $[Hg]$  and variable  $[C_4N_2]$ .

Thereupon it was observed and the intensity, Figure 10, was first order in  $[Hg]$ ,  $[O]$ , and  $[C_4N_2]$ . Similar experiments were tried in the  $O + C_2N_2$  system. The 2537-Å intensity was too weak for accurate measurement; it was, however, definitely present.

*Effect of Quenching Gases on CN and NO Emission.* Information on the CN excitation mechanism and CN reactions can be obtained by studying CN emission in the presence of various added gases.<sup>5,6</sup> Such data are displayed, Figures 8 and 11, in Stern-Volmer fashion.  $I_0/I$  was plotted against concentration of added quenching gas;  $I_0$  and  $I$  are the emission intensities in the absence and presence of quenching gas, respectively. The CN(A-X) emission shows the same quenching kinetics. A full discussion of such quenching experiments may be found in references 5, 6, and 10. Here we merely note that the fast CN radiative lifetime precludes direct physical quenching of CN(A or

(26) M. Jeunehomme, *J. Chem. Phys.*, **45**, 4433 (1966).

(27) D. H. Stedman and D. W. Setser, *Chem. Phys. Lett.*, **2**, 542 (1968). The NO(A) vibrational distribution produced by collisions with  $N_2(A)$  is  $N_0:N_1:N_2 = 100:20:<2$ ; band strengths for converting intensities to relative populations were taken from D. C. Jains and R. C. Sahni, *Trans. Faraday Soc.*, **64**, 3169 (1968).

(28) D. H. Stedman, J. A. Meyer, and D. W. Setser, *J. Chem. Phys.*, **48**, 4320 (1968).

(29) (a) C. H. Dungan, *Can. J. Chem.*, **47**, 2314 (1969); (b) G. W. Taylor and D. W. Setser, unpublished results (1970).

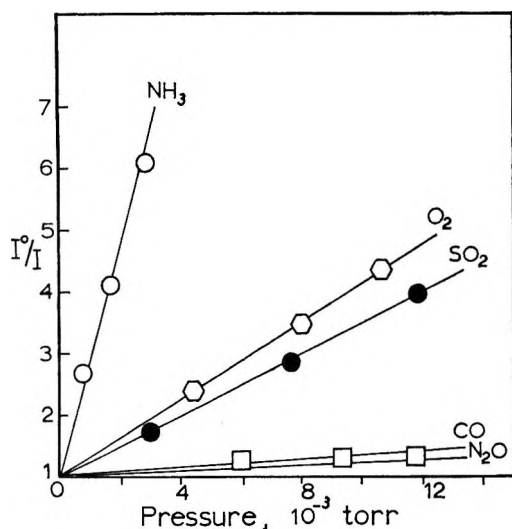


Figure 11. Stern-Volmer quenching plots for CN(B-X) emission. For all cases the pressure was 1 Torr, and  $[C_4N_2] = [O] = 2.9 \times 10^{-3}$  Torr. The emission intensity of the CN( $B^2\Sigma^+$ ,  $v' = 0$ - $X^2\Sigma^+$ ,  $v'' = 0$ ) band was observed at the quartz window, A, as quenching gas was added to J-6;  $C_2N_2$  was added at J-5.

B). The quenching arises from first-order chemical removal of CN radicals or from removal of the energy carrier which excites the CN radicals. The relative quenching efficiencies for CN were  $NH_3:NO:O_2:SO_2:CO:N_2O = 1.0:0.46:0.17:0.14:0.018$  and  $0.014$ . The  $NH_3$  quenching of the NO  $\gamma$ -band emission is presumably by removal of the energy carrier, and the relative efficiencies were  $NH_3:SO_2:O_2:CO:N_2O = 1.0:0.23:0.11:0.043:0.032$ . The  $NH_3$  half quenching pressures for quenching of CN and NO emission were  $0.5 \times 10^{-3}$  and  $1.3 \times 10^{-3}$  Torr, respectively. Since their relative quenching efficiencies for NO and CN were similar,  $SO_2$ , CO, and  $N_2O$  probably quench CN emission by removing an energy carrier. Boden and Thrush<sup>6</sup> showed that  $O_2$  chemically reacts with CN but that NO removed the energy carrier or the precursor of the energy carrier. Ammonia mainly quenches CN emission by chemical reaction, although our NO quenching data and Boden and Thrush's work show that  $NH_3$  also rapidly removes the energy carrier.

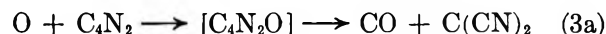
## Discussion

**General Reaction Scheme.** The following information is available for constructing a reaction scheme: CN, NO, and CO are reaction products, about four oxygen atoms are consumed per molecule of  $C_4N_2$  at high  $[O]/[C_4N_2]$ , oxygen atoms are removed by a reaction that is first order in  $[O]$  and  $[C_4N_2]$  with a rate constant of  $2.2 \times 10^{10}$  cc mol<sup>-1</sup> sec<sup>-1</sup> for  $[C_4N_2] \gg [O]$ , the CN emission is very similar and probably identical with that from oxygen atom plus cyanogen, and an energy carrier is produced by the reaction as evidenced by the excitation of Hg or NO upon addition of these gases to the

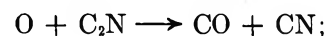
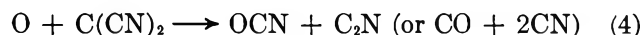
reaction. This information, however, is not sufficient to form a complete picture of the total, very complex reaction mechanism. We only can indicate a plausible set of reactions which may serve as a starting point for future studies.

Recent work<sup>30</sup> gives  $\Delta H_f^\circ(CN) \leq 103$  kcal mol<sup>-1</sup> rather than 111 kcal mol<sup>-1</sup> as recommended by the JANAF<sup>31</sup> tables. The  $\Delta H_f^\circ(C_2N)$  was estimated as 184 kcal mol<sup>-1</sup> by taking  $D(NCC\equiv N)$  equal to  $D(HC\equiv N)$ . The JANAF<sup>31</sup> values were used for the heats of formation of other species. We have included our estimate of the  $\Delta H_f^\circ(C_2O)$ ,  $\Delta H_f^\circ(C_2H)$ , and  $\Delta H_f^\circ(C_3N)$ , based upon metastable rare gas atom impact studies with  $C_2O_2$ ,  $C_4N_2$ , and  $HC_2CN$ , in the Appendix.

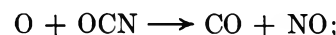
The room temperature rate constant for the  $O + C_4N_2$  reaction is comparable to that for  $O + C_2H_2$  reaction<sup>32</sup> ( $9.2 \times 10^{10}$  cc mol<sup>-1</sup> sec<sup>-1</sup> at 300°K). Since the  $O + C_2N_2$  reaction has a fairly large activation energy, it can be inferred that atomic oxygen initially attacks the triple bond of  $C_4N_2$ . One of the main initial steps<sup>32</sup> in the oxygen atom-acetylene reaction is thought to be formation of CO and  $CH_2$ , followed by  $O + CH_2 \rightarrow CO + 2H$ . Another reaction seems to give  $HC_2O + H$ ; the formation of  $C_2O + H_2$  is a minor, but important, process. By analogy the reactions below are proposed as initial steps for  $O + C_4N_2$ .



Dicyanocarbene,  $C(CN)_2$  is known,<sup>33</sup> although its  $\Delta H_f^\circ$  is not available. Reaction 32 could be written to give  $CO + CN + C_2N$  and would lead to approximately the same end result. Secondary reactions lead to CO, NO, and CN.



$$\Delta H^\circ = -166 \text{ kcal mol}^{-1} \quad (6)$$



$$\Delta H^\circ = -80 \text{ kcal mol}^{-1} \quad (7)$$

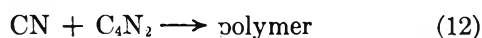
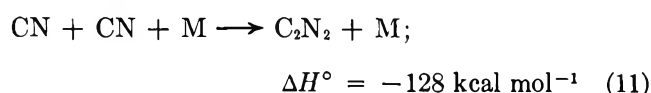
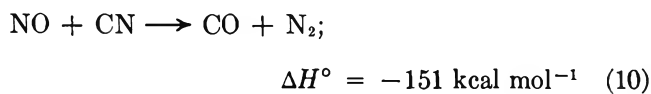
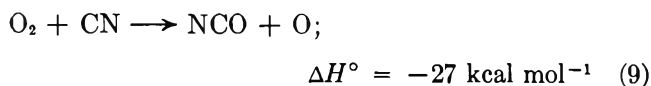
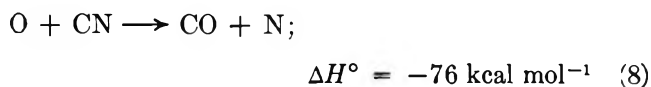
(30) (a) D. W. Setser and D. H. Stedman, *J. Chem. Phys.*, **49**, 467 (1968); (b) V. H. Dibeler and S. K. Liston, *ibid.*, **47**, 4548 (1967).

(31) "JANAF Thermochemical Tables," The Dow Chemical Co., Midland, Mich. Obtainable from the Clearinghouse for Federal Scientific and Technical Information, Springfield, Va.

(32) (a) A. A. Westenberg and N. deHaas, *J. Phys. Chem.*, **73**, 1181 (1969), and references quoted therein; (b) D. G. Williamson and K. D. Bayes, *ibid.*, **73**, 1232 (1969). (c) Controversy still exists about many of the secondary and minor reactions in the  $O + C_2H_2$  reaction.

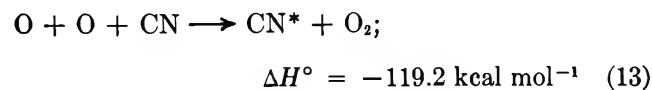
(33) W. H. Smith and G. E. Leroi, *J. Chem. Phys.*, **45**, 1784 (1966); *Spectrochim. Acta*, **25A**, 1917 (1969).

Reaction 7 is well known;<sup>34</sup> reaction 6 was written by analogy to the  $O + C_2O$  reaction, which has been suggested from studies<sup>7,22,35</sup> of  $O + C_3O_2$ . Reactions that remove CN are



Boden and Thrush have measured  $k_8$ ,  $k_9$ , and  $k_{10}$  at higher temperatures. Reaction 9 is fast ( $k_9 = 4 \times 10^{12} \text{ cc mol}^{-1} \text{ sec}^{-1}$  at  $687^\circ\text{K}$ ) with nearly zero activation energy; however, it will not be important unless  $[O_2]$  is large (oxygen atom sources having high  $[O_2]$  would be a discharged  $Ar + O_2$  flow or, perhaps, flash photolysis<sup>34</sup> of  $O_3$  and  $C_2N_2$  mixtures). The quenching of  $CN(B-X)$  by deliberate addition of  $O_2$  is from 9. Reaction 10 is relatively slow ( $k_{10} \sim 3 \times 10^{11} \text{ cc mol}^{-1} \text{ sec}^{-1}$  at  $687^\circ\text{K}$ ) and since  $[O]$  and  $[C_4N_2] > [NO]$  it should be relatively unimportant for our conditions except that it helps to maintain a steady state for  $[NO]$ . The main CN removal steps are probably (8), with an estimated rate constant of  $1 \times 10^{12} \text{ cc mol}^{-1} \text{ sec}^{-1}$  at  $300^\circ\text{K}$ , and reaction 12. Nitrogen atoms produced in reaction 8 will be removed by reaction with  $NO$  or with  $C_4N_2$ ; the absence of  $NO \beta$ -band emission from  $N + O + M$  shows that  $[N]$  was low. We favor reaction 6 or  $O + C_2O$  as the source of the CO Fourth Positive emission.

*Excitation Mechanism of CN.* The excitation mechanism for CN emission in oxygen atom systems is still open to conjecture. One<sup>5</sup> of the first suggestions was reaction 13



Boden and Thrush<sup>6</sup> subsequently showed this to be incorrect for the  $O + C_2N_2$  reaction. Also this reaction can only account for  $CN(B^2\Sigma^+)$  excitation up to  $v' = 8$ , whereas levels up to  $v' = 15$  ( $150 \text{ kcal mol}^{-1}$ ) are excited. An important conclusion of our work is that the CN excitation mechanism for  $O + C_2N_2$  and  $O + C_4N_2$  is the same. A second conclusion is that the high

vibrational levels of  $CN(B)$ , at least up to  $v' = 12$ , follow the same kinetics (dependence upon  $[O]$ ,  $[C_4N_2]$  and quenching gases) as the  $v' = 0$  level. In this sense the CN excitation mechanism in oxygen atom reaction systems appears to be more straightforward than in active nitrogen systems<sup>25</sup> where several excitation mechanisms<sup>10</sup> often operate concurrently.

Formation<sup>36</sup> of high vibrational levels of  $CN(B)$  by direct chemical reaction of  $N$  and  $O$  atoms with intermediate radicals such as  $C_2O$ ,  $NCN$ , and  $C_2N$  (reaction 6, for example) has been suggested,<sup>7,9</sup> and the possibility should be reexamined for oxygen atom excitation of  $CN$ . Without doubt an energy carrier exists in the  $O + C_4N_2$  system with concentration proportional to  $[O][C_4N_2]$  as demonstrated by the  $Hg$  and  $NO$  emission data; however, the question is whether or not this is the major source of the CN excitation. The work of Boden and Thrush<sup>6</sup> with  $O + C_2N_2$ , in which  $[CN]$  was directly measured by absorption spectroscopy, provides the best direct evidence. Oxygen and nitric oxide both quenched  $CN(B$  and  $A)$  emission but  $O_2$  mainly quenched by removing  $CN$  (reaction 9), whereas  $NO$  did not reduce  $[CN]$  to a significant extent, but removed an energy carrier or possibly the precursor to the carrier.<sup>35b</sup> Further support for excitation of  $CN(X)$  by collision is that the emission intensity<sup>6</sup> was directly proportional to  $[CN]$ . Of course some of the quenching gases can react with the precursor to  $CN$  (at least for the  $O + C_4N_2$  reaction). However, only if the intermediate radical (such as  $C_2N$ ) followed exactly the same kinetics as  $CN$  can these direct observations of Boden and Thrush be made to be consistent with a mechanism giving  $CN^*$  by some direct reaction. Our own quenching data from the  $O + C_4N_2$  reaction support Boden and Thrush's conclusion, but they are not as convincing since  $[CN]$  was not directly observed. A diagnostic experiment was attempted in order to identify the energy carrier. A source of  $N_2(A^3\Sigma_u^+)$  molecules has been developed in our laboratory<sup>17,27</sup> and a flow of  $N_2(A)$  was directly added to the  $O + C_4N_2$  reaction in front of the observation window. The  $NO(A-X)$  emission was greatly enhanced (a factor of 10), but the  $CN$  emission remained virtually unchanged. This experiment provides conclusive evidence that the  $CN$  emissions in the  $O + C_4N_2$  reaction was not pro-

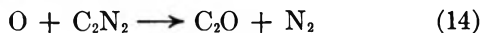
(34) (a) T. Morrow and W. D. McGrath, *Trans. Faraday Soc.*, **62**, 642 (1969); (b) N. Basco, *Proc. Roy. Soc., Ser. A*, **283**, 302 (1965); (c) C. W. Hand, *J. Amer. Chem. Soc.*, **92**, 1825 (1970).

(35) (a) K. H. Becker and K. D. Bayes, *J. Chem. Phys.*, **45**, 396 (1966); (b) D. G. Williamson and K. D. Bayes, *J. Amer. Chem. Soc.*, **89**, 3390 (1967); **90**, 1957 (1968). The authors show that  $C_2O$  reacts rapidly with  $O_2$  and  $NO$ .

(36) The direct production of  $CN(A, B)$  by chemical reactions of the type  $N + C-X \rightarrow CN(A, B) + X$  has been proposed [D. W. Setser and B. A. Thrush, *Nature*, **200**, 864 (1963)] as the excitation mechanism in active nitrogen systems giving the high population in the upper  $v$ , levels of the  $A$  state and high populations in the perturbed rotational levels of the  $v' = 0$  level of  $CN(B^2\Sigma^+)$ . The suggestion has gathered support<sup>11a,10</sup> but its acceptance is not universal.

duced by  $N_2(A^3\Sigma_u^+)$ .<sup>37a</sup> The NO(A) vibrational distribution from  $O + C_4N_2$  also is significantly different from that generated by the  $N_2(A) + NO$  reaction. Thus  $N_2(A)$  is not present in significant amounts in the  $O + C_4N_2$  reaction.

Another possible energy carrier is  $CO(a^3\Pi)$  or some other excited state of carbon monoxide.<sup>37b</sup> Formation of such states *via* reaction 6 or from  $O + C_2O$  is feasible and, with some assumptions, such a mechanism can be made to fit the emission kinetics. The presence of strong Fourth Positive emission provides support<sup>35,22</sup> for the presence of triplet CO states, since ( $d^3\Delta$ ), ( $e^3\Sigma^-$ ), ( $a^3\Pi$ ), ( $A^1\Pi$ ) states are often found together. Bayes also suggests that the  $CO(I^1\Sigma)$  and ( $a^3\Sigma^+$ ) states may be important. However, one must explain how  $C_2N$  or  $C_2O$  is produced in sufficient quantity, or find a similar radical so that reactions such as (6) can serve as the excitation source in the  $C_2N_2$  reaction. Safrany<sup>9</sup> has proposed carbon atoms as a chain carrier in the reaction of active nitrogen with  $C_2N_2$  ( $N + CN \rightarrow N_2 + C$ ,  $C + C_2N_2 \rightarrow C_2N + CN$ ,  $C_2N + N \rightarrow 2CN$ , etc.). The analogous reaction,  $O + CN \rightarrow NO + C$ , is endothermic and other channels, reaction 8, are favored. A possibility is reaction 14, which is analogous to reaction 3c and is  $\approx 70$  kcal exothermic.



This step could accompany the two other suggested reactions (formation of CN and OCN or NCN and CO). Also, the NCN radical could be the precursor to the energy carrier if reaction 15 was important.<sup>38</sup>



Further speculation is not warranted without additional information. Correlation of the CO Fourth Positive emission with the CN and NO emissions might be useful. However, the important information needed to understand these complex systems<sup>39</sup> is knowledge of the elementary reactions of the very reactive radical intermediates. Direct monitoring of reaction intermediates or study of the kinetics of intermediate radicals in clean reaction systems is highly desirable. In this connection the  $O + C_4N_2$  reaction can serve as a satisfactory low-temperature CN radical source for continuing the measurements of CN radical kinetics started by Boden and Thrush.<sup>10</sup>

## Conclusions

Oxygen atoms diluted in molecular nitrogen readily react with dicyanoacetylene at room temperature and the initial interaction is with the acetylenic bond. Subsequent oxygen atom reactions with intermediate radicals are highly exothermic and produce CO and CN chemiluminescence having up to 150 kcal mol<sup>-1</sup> of excitation energy. The addition of NO or Hg produces  $\gamma$ -band and 2537-Å emission which serves to identify the presence of an energy carrier. This energy carrier

is thought to excite the CN emission by collisional energy transfer to CN(X). The metastable states of carbon monoxide are suggested as possibly being the energy carrier(s).

*Acknowledgments.* This work was supported by the National Air Pollution Control Administration, Consumer Protection and Environmental Health Service, Public Health Service, Grant AP-00391.

We thank Dr. Donald Stedman for many stimulating discussions and suggestions during the course of the work. We also thank Mr. Michael Braeckel, a summer N. S. F. undergraduate research participant (Grant GY-2681), for preparing the monocyanoacetylene and Mr. Richard Suenraun for assistance with early experiments. We also wish to acknowledge discussions of CN radical excitation mechanisms with Professors B. A. Thrush (Cambridge University) and K. D. Bayes (University of California, Los Angeles).

## Appendix

The collisions of metastable rare gas atoms with substrate molecules can be used to estimate bond energies and heats of formation of radical fragments providing one of the fragments is produced in an electronically excited radiative state.<sup>40,30a</sup> We investigated the reactions of  $Ar(^3P_{0,2})$  with  $C_4N_2$  and  $HC\equiv CCN$  and  $Ar(^3P_{0,2})$ ,  $Kr(^3P_2)$ , and  $Xe(^3P_2)$  with  $C_3O_2$  in order to estimate  $\Delta H_f^\circ(C_3N)$ ,  $\Delta H_f^\circ(C_2H)$ , and  $\Delta H_f^\circ(C_2O)$ . These experiments are described and characterized elsewhere.<sup>40b</sup>

The  $C_4N_2$  was prepared as described in the text. Monocyanoacetylene was prepared by a standard method.<sup>41</sup> The purity was checked by mass spectroscopy and no other CN-containing compound was present. The reactions of interest are

(37) (a) We have attempted to obtain a spectrum from  $N_2(A^3\Sigma_u^+) + CN$ . So far the emission has been very weak and we have not obtained sufficient intensity to obtain relative vibrational populations; however the main excitation is to the  $v' = 0$  level of CN(B). The experiments suggest that the energy transfer reaction may be slow, relative to the  $N_2(A) + NO$  reaction. These experiments seriously question the assignment<sup>10,26</sup> of the CN "blue flame" to collisional excitation by  $N_2(A)$ . Boden and Thrush<sup>10</sup> grouped the CN levels into three classes. If any of the classes can be attributed to  $N_2(A) + CN$ , it must be the group they designate as (a) *i.e.*,  $v' = 0-2$ . Our experiments, of course, do not eliminate the possibility of other  $N_2$  excited states (for example  $^3\Delta$ ) being responsible for the CN excitation; (b) G. W. Taylor and D. W. Setser, unpublished results. The addition of NO to a flow of oxygen containing  $CO(a^3\Pi)$  molecules give both NO(A-X) and (B-X) emission. Since the NO emission is the  $O + C_4N_2$  reaction shows only very weak NO(B-X) bands, the energy carrier can not be just  $CO(a^3\Pi)$  molecules.

(38) W. Braun, A. N. Bass, D. D. Davis, and J. D. Simmons, *Proc. Roy. Soc., Ser. A*, **312**, 417 (1969). This paper which is concerned with the reactions of carbon atoms, shows that  $C(^3P)$  combines with  $N_2$  to give  $CN_2$ .

(39) K. H. Becker and K. D. Bayes, *J. Phys. Chem.*, **71**, 371 (1967). The NO  $\gamma$ -band chemiluminescence from the  $O + N_2H_4$  reaction has been attributed to the presence of  $N_2(A^3\Sigma_u^+)$ . The reactions which give  $N_2(A^3\Sigma_u^+)$  were not identified.

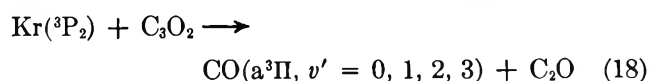
(40) (a) J. F. Prince, C. A. Collins, and W. W. Robertson, *J. Chem. Phys.*, **40**, 2619 (1964); (b) D. H. Stedman, *ibid.*, **52**, 3966 (1970).

(41) A. A. Westenber and E. B. Wilson, *J. Amer. Chem. Soc.*, **72**, 199 (1950).



The flow system mainly contains  $\text{Ar}(^3\text{P}_2)$  metastables, but the small concentration of the 270-kcal metastable,  $^3\text{P}_0$ , requires that this energy limit be used. The highest  $\text{CN}(\text{B}^2\Sigma^+)$  vibrational level found was  $v' = 14$  for reaction 16 and  $v' = 12$  for reaction 17. These observations provide upper limits to the bond energies ( $\text{kcal mol}^{-1}$ ) from the relationship  $\text{D.E.} < 270 - E_{\text{max}}(\text{CN})$ . If the rotational energy of CN is ignored,  $E_{\text{max}}(\text{CN})$  for  $v' = 14$  and 12 are 146 and 137 kcal.<sup>42</sup> Thus  $D(\text{NC}_3-\text{CN}) \leq 124$  kcal and  $D(\text{HC}_2-\text{CN}) \leq 133$  kcal. Using  $\Delta H_f^\circ(\text{C}_4\text{N}_2)^{31}$  and  $\Delta H_f^\circ(\text{CN})^{40b}$  values of 127 and 102 kcal give  $\Delta H_f^\circ(\text{C}_3\text{N}) < 99$  kcal  $\text{mol}^{-1}$ . The  $\Delta H_f^\circ(\text{HC}_2\text{CN})$  has not been reported, but bond additivity tables<sup>43</sup> give 91 kcal, which leads to  $\Delta H_f^\circ(\text{C}_2\text{H}) \leq 122$  kcal  $\text{mol}^{-1}$ . This upper limit to  $\Delta H_f^\circ(\text{C}_2\text{H})$  is virtually identical with that adopted by JANAF Tables. A mass spectrometric<sup>44</sup> study has yielded  $\Delta H_f^\circ(\text{C}_3\text{N}) = 131$  kcal; our value is a significant improvement. The value for  $\Delta H_f^\circ(\text{CCN})$  suggested by Dibeler, Reese, and Franklin<sup>44</sup> also is suspect.

Metastable argon impact with  $\text{CO}_2$  gives dissociation to  $\text{O} + \text{CO}(\text{a}^3\Pi)$ , as well as other reactions. The highest observed vibrational level from  $\text{CO}(\text{a}^3\Pi)$  gives an upper limit that is in good agreement<sup>30a</sup> with the known  $D(\text{O}-\text{CO})$  value. The  $\text{CO}(\text{a}^3\Pi-\text{X}^1\Sigma^+)$  emission is much less satisfactory for determining bond energies than the  $\text{CN}(\text{B}^2\Sigma^+-\text{X}^2\Sigma^+)$  emission because it is weak and because emission has never been observed for  $v' > 4$ . We used Ar, Kr, and Xe metastables to study the bond energy of carbon suboxide. The  $\text{Kr}^*$  reaction was the most useful and is shown below.



The flow conditions were adjusted so that only the lower krypton metastable ( $^3\text{P}_2$ ) was present. Carbon

suboxide was prepared by dehydration of malonic acid. Care was taken to remove all traces of  $\text{CO}_2$  from the  $\text{C}_3\text{O}_2$ . The bond energy relationship is  $\text{D.E.} \leq 229 - E_{\text{max}}(\text{CO})$ ;  $E_{\text{max}}(\text{CO})^{45}$  for  $v' = 3$  is 153 kcal  $\text{mol}^{-1}$  and  $D(\text{OC}_2-\text{CO}) \leq 76$  kcal  $\text{mol}^{-1}$ . Metastable argon impact gave Cameron bands up to  $v' = 4$  (the maximum observable in emission from  $\text{CO}(\text{a}^3\Pi)$ ) which leads to  $D(\text{O}_2\text{C}-\text{CO})$  of  $\leq 112$ . Metastable  $\text{Xe}(^3\text{P}_2)$  did not give CO emission. If it is assumed that the absence of emission was from lack of sufficient energy, a lower limit to  $D(\text{OC}_2-\text{CO})$  of  $> 54$  kcal  $\text{mol}^{-1}$  is obtained. Combining the upper limit obtained from  $\text{Kr}^*$  with  $\Delta H_f^\circ(\text{C}_3\text{O}_2)^{46} = -23.4$  and  $\Delta H_f^\circ(\text{CO})^{31} = -26.4$  gives  $\Delta H_f^\circ(\text{C}_2\text{O}) \leq 79$  kcal  $\text{mol}^{-1}$ . This is considerably lower than the  $\sim 92$  kcal  $\text{mol}^{-1}$  value often quoted in the literature.<sup>22,47</sup> Laufer<sup>48</sup> has suggested reaction 19 as a primary process in ketene photolysis for wavelengths up to 3130 Å.



This gives  $\Delta H_f^\circ(\text{C}_2\text{O}) \leq 77$  kcal which supports our measurements. Palmer and Cross<sup>49</sup> favor  $\Delta H_f^\circ(\text{C}_2\text{O}) = 57$  kcal which is only slightly above our tentative lower limit from the metastable xenon impact result.

(42) L. Wallace, *Astrophys. J. Suppl. Ser.*, **7**, 165 (1962).

(43)(a) S. W. Benson, F. R. Cruickshank, D. M. Golden, G. R. Haugen, H. E. O'Neal, A. S. Rodgers, R. Shaw, and R. Walsh, *Chem. Rev.*, **69**, 279 (1969); (b) R. Walsh, private communication. Assuming a zero heat of reaction for the disproportionation reaction between  $\text{C}_2\text{N}_2$  and  $\text{HC}\equiv\text{C}-\text{C}\equiv\text{CH}$  gives  $\Delta H_f^\circ(\text{HC}\equiv\text{CCN}) = 92.5 \pm 2$  kcal  $\text{mol}^{-1}$ .

(44) V. H. Dibeler, R. M. Reese, and J. L. Franklin, *J. Amer. Chem. Soc.*, **83**, 1813 (1961).

(45) P. H. Krupenie, "The Band Spectrum of Carbon Monoxide," NSRDS-NBS-5 (1966).

(46) B. D. Kybett, G. K. Johnson, C. K. Barker, and J. L. Margrave, *J. Phys. Chem.*, **69**, 3603 (1965).

(47) L. J. Stief and V. J. DeCarlo, *J. Amer. Chem. Soc.*, **91**, 839 (1969).

(48) A. H. Laufer, *J. Phys. Chem.*, **73**, 959 (1969).

(49) H. B. Palmer and W. D. Cross, *Carbon*, **3**, 475 (1966).

# The Reactions of Energetic Fluorine-18 Atoms with Tetrafluoroethylene<sup>1a</sup>

by Thomas Smail, George E. Miller, and F. S. Rowland<sup>1b</sup>

Department of Chemistry, University of California, Irvine, California 92664 (Received February 6, 1970)

Energetic <sup>18</sup>F atoms react with CF<sub>2</sub>=CF<sub>2</sub> to form CF<sub>2</sub>=CF<sup>18</sup>F and CF<sub>2</sub>CF<sub>2</sub><sup>18</sup>F\*. More than 89% of CF<sub>2</sub>=CF<sup>18</sup>F\* molecules are excited enough to decompose to CF<sub>2</sub> plus CF<sup>18</sup>F (>76 kcal/mol excitation energy) at several atmospheres pressure; CF<sup>18</sup>F is conveniently trapped by insertion in HI to form CHF<sup>18</sup>FI. The decomposition of excited CF<sub>2</sub>CF<sub>2</sub><sup>18</sup>F\* by C-C bond rupture is followed by measurement of CHF<sub>2</sub>CF<sub>2</sub><sup>18</sup>F and CHF<sub>2</sub><sup>18</sup>F yields in the presence of HI. The half-stabilization pressure for CF<sub>2</sub>CF<sub>2</sub><sup>18</sup>F radicals formed by thermal <sup>18</sup>F atom addition is 218 Torr of C<sub>2</sub>F<sub>4</sub>. The formation of <sup>18</sup>F in gas ampoules by the <sup>19</sup>F(n,2n)<sup>18</sup>F reaction was monitored with a system utilizing a Teflon sleeve around the standard glass ampoule. The average recoil range of <sup>18</sup>F from the (n,2n) reaction is about 0.1 cm in 760 Torr of C<sub>2</sub>F<sub>4</sub>.

## Introduction

Investigations of the reactions of thermal fluorine atoms with organic compounds have been mainly concerned with the abstraction of hydrogen atoms from hydrocarbons,<sup>2</sup> although some studies of the addition reaction have been made with olefins.<sup>3,4</sup> Usually, the thermal F atoms are generated by reaction between F<sub>2</sub> and the substrate,<sup>2,3</sup> although the photolysis of NOF has been the source in recent studies.<sup>4</sup> Additional reaction paths, especially the substitution of F for atoms or groups in the substrate molecule, can readily be observed with energetic <sup>18</sup>F atoms formed by the nuclear reactions <sup>16</sup>O(T,n)<sup>18</sup>F,<sup>5</sup> <sup>19</sup>F(γ,n)<sup>18</sup>F,<sup>6-10</sup> or <sup>19</sup>F(n,2n)-<sup>18</sup>F.<sup>10</sup>

The inclusion of increasing amounts of an inert moderator (*e.g.*, neon) in a system in which hot <sup>18</sup>F atoms are formed leads to a continual reduction in the average kinetic energy of the atoms at the time of reaction and permits the observation of the chemical reactions of F atoms with energies nearer and nearer to thermal energies. The nuclear methods of fluorine atom production have two strong advantages: (a) only tracer concentrations of fluorine atoms are involved; and (b) the fluorine atoms can be formed from stable, unreactive precursors such as CF<sub>4</sub>, SF<sub>6</sub>, etc. Consequently, the chemical difficulties of handling reactive precursors and macroscopic amounts of reactive products are avoided. Solids, liquids, and gases are all readily studied, and the reaction products can be identified and detected through radio gas chromatography.

The present experiments form part of a general investigation of <sup>18</sup>F atom reactions with olefinic compounds and have been carried out with the intention of discovering the general features of both hot and thermal fluorine atom reactions with these substrates.

## Experimental Section

**Chemicals.** Tetrafluoroethylene (Peninsular Chemical Co.) was distilled at -78° to free it from traces of

the polymerization inhibitor (bp 170°) present in the original tank; it was then degassed at -196° prior to use and stored in a -78° bath. Hydrogen iodide (Research Chemical Co.) was degassed and stored at -196°. Sulfur hexafluoride (Matheson Co.) was degassed at -196° and used without further purification; a trace of CF<sub>4</sub> (<<1%) was detected in it by gas chromatography.

**Sample Preparation.** The samples were sealed in Pyrex or quartz ampoules of 10-12 cm<sup>3</sup> volume. The volume of each ampoule was measured with calipers and checked in a few cases by weighing the water contained in them; the accuracy is estimated as ±0.1 cm<sup>3</sup>. The required amount of each component was measured as pressure-volume (PV) units and then condensed into an evacuated ampoule maintained at -196°. The ampoules were filled on a calibrated vacuum line, fitted with a mercury manometer, and final pressures were calculated from the known volume of the individual ampoule, assuming all gases as ideal. Hydrogen iodide was measured in a calibrated volume with a Kern glass spiral manometer isolated from any connection with the mercury manometer. Traces of I<sub>2</sub> in the HI were removed by allowing the HI storage bulb

(1) (a) This research was supported by AEC Contract No. AT-(11-1)-34, Agreement No. 126. Part of this work was presented at the 157th National Meeting of the American Chemical Society, Minneapolis, Minn., April 1969. (b) To whom correspondence should be addressed.

(2) G. C. Fettis and J. H. Knox, *Progr. React. Kinet.*, **2**, 2 (1964).

(3) A. S. Rodgers, *J. Phys. Chem.*, **72**, 3407 (1968).

(4) A. L. Flores and D. deB. Darwent, *ibid.*, **73**, 2203 (1969).

(5) M. Anbar and P. Neta, *J. Chem. Phys.*, **37**, 2757 (1962).

(6) J. F. J. Todd, N. Colebourne, and R. Wolfgang, *J. Phys. Chem.*, **71**, 2875 (1967).

(7) N. Colebourne, J. F. J. Todd, and R. Wolfgang, "Chemical Effects of Nuclear Transformations," International Atomic Energy Agency, Vienna, 1965, Vol. 1, p 149.

(8) L. Spicer, J. F. J. Todd, and R. Wolfgang, *J. Amer. Chem. Soc.*, **90**, 2425 (1968).

(9) Y.-N. Tang and F. S. Rowland, *J. Phys. Chem.*, **71**, 4576 (1967).

(10) Y.-N. Tang, T. Smail, and F. S. Rowland, *J. Amer. Chem. Soc.*, **91**, 2130 (1969).

to warm up slowly from  $-196^\circ$ , thereby distilling the HI away from the much less volatile  $\text{I}_2$ . No  $\text{I}_2$  was visible in any sample prior to irradiation. Samples were thoroughly degassed at  $-196^\circ$  after filling and before sealing, and were stored in the dark at  $-196^\circ$  until irradiation.

**Irradiation and Analysis.** Energetic  $^{18}\text{F}$  atoms were produced by the  $^{19}\text{F}(n,2n)^{18}\text{F}$  reaction with fast neutrons from a Kaman A-711 neutron generator. The average fast neutron flux in the irradiation position was crudely estimated by dosimetry with copper foils to be  $4\text{--}6 \times 10^8 \text{ n/cm}^2 \text{ sec}$ . Irradiation times ranged from 10 to 30 min; the sample temperature was maintained at about  $10^\circ$  by a cooling system incapable of precision temperature control. A pneumatic transfer system was used to place the samples in position for irradiation, with a neutron flux/beam current reproducibility of about  $\pm 20\%$  for successively positioned samples. The irradiation geometry placed the target ampoules—roughly cylindrical with length twice the diameter—crosswise to the neutron beam. The beam is well collimated initially but spreads rapidly, resulting in marked inhomogeneity in the irradiation of the ampoule; the intensity in the middle of cylinder was several times that at the ends, while the intensity at the nearer wall of the cylinder was several times that at the far wall.

The  $^{18}\text{F}$ -labeled reaction products were separated and analyzed by radio gas chromatography, using an "external" flow proportional counter for the assay of the radioactivity. The "external" counter, in which the helium-propane counting gas is separated by a thin Mylar window from the column effluent containing the  $^{18}\text{F}$  compounds in a helium stream, was used because many fluoro compounds (*e.g.*,  $\text{SF}_6$ ) severely quench by electron scavenging the multiplying action of a proportional counter. The products ( $\text{SF}_5^{18}\text{F} + \text{C}_2\text{F}_3^{18}\text{F}$ ),  $\text{CHF}_2^{18}\text{F}$ ,  $\text{C}_2\text{HF}_4^{18}\text{F}$ , and  $\text{CH}_2\text{F}^{18}\text{F}$  were separated with a 50-ft di-*n*-butyl phthalate (DBP) column (30% by weight, DBP on 30–60 mesh Chromosorb P) operated at  $0^\circ$ . In most experiments, this column was preceded by a 25-ft silicone oil column (30% by weight Dow-Corning 705 silicone oil on 40–60 mesh Chromosorb P) operated at  $68^\circ$ . In operation, the silicone oil column was isolated after the passage of  $\text{C}_2\text{F}_3^{18}\text{F}$  and  $\text{C}_2\text{HF}_4^{18}\text{F}$  from it into the DBP column. After elution of these compounds from the DBP column, the silicone oil column was reinserted into the flow stream and  $\text{CHF}^{18}\text{FI}$  was eluted, as shown in Figure 1. Macroscopic quantities of  $\text{CHF}_2\text{I}$  have not been available for column calibration, so its retention times on various column combinations were measured through observations on tracer-level  $\text{CHF}^{18}\text{FI}$ .<sup>11</sup>

The number of radioactive decays observed in each product was corrected for decay of  $^{18}\text{F}$  and for any variations in the mass flow rate (accompanying the emergence of large macroscopic peaks) through the radioactivity detector.

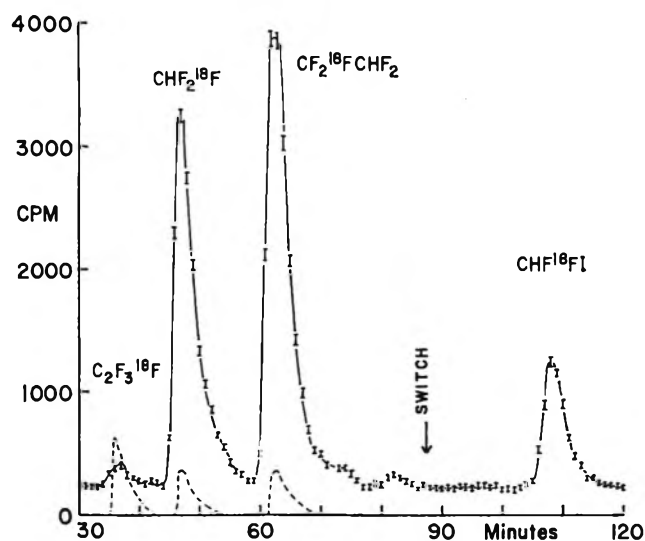


Figure 1. Gas chromatographic traces of products from  $^{18}\text{F}$  reaction with HI-scavenged  $\text{C}_2\text{F}_4$ . Solid line:  $^{18}\text{F}$  radioactivity. Dotted line: macroscopic peaks of parent  $\text{C}_2\text{F}_4$  plus carrier  $\text{CHF}_3$  and  $\text{C}_2\text{HF}_6$  (added after irradiation and prior to chromatographic separation). "Switch" indicates the resinertion of the silicone oil column into the gas stream (see text).

**Absolute Yield Measurements.** The relative yields of various  $^{18}\text{F}$ -labeled compounds can be readily measured in a single radio gas chromatographic run. However, the absolute yields—the fraction found as a given product of the total  $^{18}\text{F}$  formed—are likewise important in the interpretation of  $^{18}\text{F}$  experiments. Absolute yields for hot  $^{18}\text{F}$  reactions have been reported earlier for fluorine atoms created in the  $^{19}\text{F}(\gamma,n)^{18}\text{F}$  reaction, but not for the  $^{19}\text{F}(n,2n)^{18}\text{F}$  reaction. Barring very unusual and unexpected complications in the nuclear processes, the absolute yields for particular chemical reactions under otherwise identical conditions should be the same for both nuclear reaction sources, and absolute measurements for both furnish a useful check upon the general reliability of such determinations.

We have developed an absolute yield monitoring technique for the  $^{18}\text{F}$  atoms formed in our fast neutron generator and have here applied it to the determination of absolute yields for reactions with  $\text{C}_2\text{F}_4$ . A thin Teflon cylindrical sleeve, slightly larger in diameter than the standard ampoule for gas samples, was placed around each sample during irradiation and acted as monitor for the formation of  $^{18}\text{F}$  by fast neutron reaction. The use of Teflon permits monitoring with the same isotope used in the reactions being studied. The Teflon-sleeve monitor had essentially the same cross-sectional geometry as the ampoule, and effectively integrates the fast neutron flux incident on the sample, while the inhomogeneity of the fast neutron flux was determined by counting small sections of such a monitor.

(11)  $\text{CHF}^{18}\text{FI}$  is formed by the insertion reaction of  $\text{CF}^{18}\text{F}$  with HI. See T. Smail and F. S. Rowland, *J. Phys. Chem.*, **74**, 1866 (1970).

The  $^{18}\text{F}$  activity was measured with a 2-in. diameter sodium iodide well counter and a single-channel analyzer with a window set on the annihilation radiation peak (approximately 0.4 to 0.8 meV range). Counter reproducibility was checked frequently using a standard  $^{22}\text{Na}$  source. Measurements of  $^{18}\text{F}$  activity with the scintillation counter were always delayed for at least 2 hr after the end of the irradiation to avoid counting interference by shorter-lived isotopes. A few samples were counted to follow the  $^{18}\text{F}$  decay; no long-lived contaminants were found in the energy region examined. Routine sample measurements involved comparison of the radioactivity observed in the flow proportional counter for particular labeled compounds to that found for the Teflon-sleeve monitor in the scintillation counter. The conversion of these into absolute percentage yields was accomplished by calibration of the Teflon-sleeve monitor as described below.

*Calibration of Teflon-Sleeve Monitors.* Quartz ampoules were used during the calibration experiments because irradiation of an empty quartz bulb with no Teflon sleeve produced a negligible quantity of  $^{18}\text{F}$  (or other radioactivity after 2 hr) with the usual  $^{18}\text{F}$  window setting of the analyzer. (Pyrex bulbs are used in most regular experiments. The amount of radioactivity produced in the gases contained in quartz and Pyrex bulbs is essentially the same, but some radioactivity is induced in the Pyrex itself. This is inconvenient in calibration experiments, but presents no difficulty in experiments measuring the relative radioactivities of a Teflon-sleeve monitor and of the volatile products in the radio gas chromatograph.) When an empty quartz bulb is irradiated with a Teflon-sleeve monitor around it, a small amount of  $^{18}\text{F}$  (0.2% of the total  $^{18}\text{F}$  formed in the Teflon) recoils into the quartz surface. Measurements of the total  $^{18}\text{F}$  contained in a quartz ampoule containing a fluorinated gas have always been corrected for this recoil contamination of the quartz bulb. This correction factor depends upon the pressure of fluorocarbon in the bulb and upon the number of fluorine atoms in the molecule, but was always less than 5% of the  $^{18}\text{F}$  activity assigned to the contents of the bulb in these calibration experiments.

In the actual calibrations, a quartz bulb containing a particular fluorocarbon was irradiated while sheathed with a Teflon-sleeve monitor. The monitor and the quartz bulb were then separately counted in the well scintillation counter, and a ratio was obtained for the counts per second of  $^{18}\text{F}$  per gram  $^{19}\text{F}$  in the gas (after correction for the recoil contamination) to the counts per second of  $^{18}\text{F}$  in the Teflon sleeve per gram  $^{19}\text{F}$  in this monitor: the mean of six separate experiments gave a value of 0.87 for this calibration factor.<sup>12</sup> The original irradiated ampoule was then broken open on the vacuum line in the presence of several carrier molecules, the "Volatile" contents frozen into a second ampoule of the same geometry as the original, and the  $^{18}\text{F}$  activity

was redetermined. The ratio of the "Volatile" activity to that of the original irradiated bulb is shown in Table I for several fluorocarbon systems. The section of

**Table I:** Absolute Yield Measurements for  $^{19}\text{F}(n,2n)^{18}\text{F}$  Reactions with Various Substrates as Monitored by the Teflon-Sleeve Method

System composition, mol %	Per cent $^{18}\text{F}^a$	
	Volatile	Identified volatile
$\text{CF}_4$ , 96.0; $\text{C}_2\text{H}_4$ , 3.5; HI, 0.5	73 <sup>b</sup>	62
$\text{CF}_4$ , 95.2; $\text{C}_2\text{H}_4$ , 4.0; $\text{H}_2\text{S}$ , 0.8	11	8 <sup>c</sup>
$\text{CF}_4$ , 64.0; $\text{C}_2\text{H}_6$ , 31.5; $\text{C}_2\text{H}_4$ , 4.0; HI, 0.5	42	9 <sup>c</sup>
$\text{C}_2\text{F}_4$ , 92.0; HI, 8.0	...	59 <sup>d</sup>

<sup>a</sup> Normalized to total  $^{18}\text{F}$  activity in irradiated, but unopened and untreated ampoule. <sup>b</sup> In this sample, 13% of the  $^{18}\text{F}$  activity remained in the original ampoule as nonvolatile activity. <sup>c</sup> Sum of ( $\text{C}_2\text{H}_5^{18}\text{F}$  +  $\text{C}_2\text{H}_3^{18}\text{F}$  +  $\text{CF}_3^{18}\text{F}$ ). <sup>d</sup> Sum of ( $\text{C}_2\text{HF}_4^{18}\text{F}$  +  $\text{CHF}_2^{18}\text{F}$  +  $\text{C}_2\text{F}_3^{18}\text{F}$ ). The yield of  $\text{CHF}^{18}\text{F}$  was not included in this measurement. See Table III.

vacuum line used in this transfer contained, in addition to fresh glass surfaces, the brass of the ampoule breaker and the Viton A diaphragms of the greaseless stopcocks. Related experiments have shown that some  $^{18}\text{F}$  radioactivity is able to transfer from the original ampoule onto fresh glass surfaces and there reacts in such a way as to be nonvolatile in subsequent treatment. Consequently, the "Volatile"  $^{18}\text{F}$  recovered in Table I is only a lower limit on the amount of actual volatile material originally formed—some  $^{18}\text{F}$  activity, perhaps in the form  $\text{H}^{18}\text{F}$ , may volatilize from the original bulb and then react in the vacuum transfer system, and not be recovered as "Volatile" in these tests. In addition, some originally volatile  $^{18}\text{F}$  compounds may have reacted with the glass surface of the original ampoule, and been converted at that stage into nonvolatile forms. While macroscopic HF reacts with glass walls to form  $\text{SiF}_4$ , the species formed in our tracer level experiments is undetermined. Since the total  $^{18}\text{F}$  formed in an ampoule is only about  $10^7$  atoms, the successive reaction of two or more  $^{18}\text{F}$  containing molecules with each other is negligibly important, and the ultimate fate of the reactive species formed by the initial reaction of carrier-free  $\text{H}^{18}\text{F}$  with silicate is simply not known.

A second form of loss—recoil of  $^{18}\text{F}$  atoms created in the gas phase onto the inner walls of the ampoule—must also be considered for the energetic  $^{18}\text{F}$  atoms formed by nuclear reactions. These  $^{18}\text{F}$  atoms,

(12) The variation from unity in cps of  $^{18}\text{F}$  from  $^{19}\text{F}$  in the gas and in Teflon arises both from the extreme inhomogeneity of the fast neutron flux, and from the different geometries of the two objects in the well counter. Both of these geometrical factors are essentially constant in the routine use of the Teflon-sleeve monitor

imbedded in the surface layers of silicate, are also non-volatile during the opening of an irradiated ampoule. This recoil loss from the gas phase becomes appreciable only at pressures of <200 Torr (see below), but will always leave a minor fraction of nonvolatile  $^{18}\text{F}$  contamination in the irradiated bulb. Measurements of the irradiated bulbs after evacuation consistently showed small amounts of nonvolatile  $^{18}\text{F}$  activity from gas recoil loss and from surface reactions of reactive compounds formed in the original primary reactions of the  $^{18}\text{F}$  atoms.

The subsequent handling of the ampoules containing the separated "Volatile" activity has varied. In some instances, these bulbs were opened, and the contents passed through a radio gas chromatograph, and then trapped again in the third ampoule of the same geometry.<sup>13</sup> In this third ampoule only  $^{18}\text{F}$  atoms bonded in known compounds (as identified by peaks on the radio gas chromatograph) were present. The  $^{18}\text{F}$  activity of this third ampoule was then redetermined in the well scintillation counter, with the results shown in Table I as "Identified Volatile." The  $^{18}\text{F}$  compounds included in the "Volatile" category but missing from "Identified Volatile" represent either known molecules with retention times longer than the operating time of the trapping procedure, unknown compounds of only moderate volatility and long chromatographic retention times, or nonvolatile  $^{18}\text{F}$ -products formed by reaction in the "Volatile" ampoule of a reactive volatile species. As indicated in Table I,  $\text{CHF}^{18}\text{FI}$  has been identified as an important product in  $\text{CF}_4$ -HI and  $\text{C}_2\text{F}_4$ -HI systems, but was still on the chromatographic column when trapping was discontinued in the experiments listed there. The glass surfaces of the "Volatile" ampoules showed varying amounts of nonvolatile  $^{18}\text{F}$  reactivity, reflecting chiefly changes in the chemical composition of the irradiated mixtures and of the  $^{18}\text{F}$  product spectra.

Calibration factors for conversion of counts observed in the radio gas chromatograph to absolute yields were obtained by comparison of the proportional counter observations during the passage of various  $^{18}\text{F}$  peaks with the fractional yield found in the "Identified Volatile" ampoule filled with the  $^{18}\text{F}$  compounds trapped from the chromatographic stream after passage through the proportional counter. The agreement among the various systems indicated in Table I, as well as other similar ones, was excellent, and leads us to estimate that the overall Teflon-sleeve monitoring system permits the measurement of  $^{18}\text{F}$  production in a given ampoule (and therefore of absolute yields) to  $\pm 10\%$ .

The data of Table I show substantial variations both in the fraction of "Volatile"  $^{18}\text{F}$  and in the ratio of "Identified Volatile" to "Volatile" for different target molecules. The introduction of  $\text{C}_2\text{H}_6$  into a mixture of  $\text{CF}_4$ - $\text{C}_2\text{H}_4$ -HI causes an abrupt drop in the yield of  $\text{C}_2\text{H}_5^{18}\text{F}$ , the product obtained by the addition of a thermal or low-energy  $^{18}\text{F}$  atom to  $\text{C}_2\text{H}_4$  when followed

by scavenging of the  $\text{C}_2\text{H}_4^{18}\text{F}$  radical with HI. Since the abstraction of hydrogen atoms from alkanes is postulated to occur in almost every collision of thermal fluorine atoms,<sup>2</sup> the decrease in "Volatile" activity can be readily assigned to the greatly increased probability that  $^{18}\text{F}$  will react by formation of  $\text{H}^{18}\text{F}$  in abstraction from  $\text{C}_2\text{H}_6$  rather than by addition to  $\text{C}_2\text{H}_4$ . Similarly, the decrease by more than a factor of 4 in  $^{18}\text{F}$  activity from "Volatile" to "Identified Volatile" for the  $\text{C}_2\text{H}_6$ -containing sample probably means that substantial quantities of this  $\text{H}^{18}\text{F}$  (or some reactive species formed by its attack on silicate walls) have been transferred from the irradiated bulb to the "Volatile" bulb and have there reacted on the surface to become nonvolatile. Comparison of  $\text{C}_2\text{H}_4$ -HI and  $\text{C}_2\text{H}_4$ - $\text{H}_2\text{S}$  indicates that the former system is much more efficient in converting  $^{18}\text{F}$  atoms and radicals into organic species readily identified with the radio gas chromatograph.

The values of the absolute yields for  $^{18}\text{F}$  products formed by hot reactions with some fluoromethanes are given in Table II, together with previously reported

**Table II:** Measured Absolute Yields for  $^{18}\text{F}$  Products from Energetic  $^{18}\text{F}$  Reactions with Various Substrates

Substrate molecule	Product	—Absolute yield (% $^{18}\text{F}$ )—	
		This work <sup>a</sup>	Ref 7 <sup>b</sup>
$\text{CF}_4$	$\text{CF}_3^{18}\text{F}$	2.0	2.8
	$\text{CF}_2^{18}\text{F}$	1.2	2.5
$\text{CHF}_3$	$\text{CHF}_2^{18}\text{F}$	1.0	1.4
	$\text{CF}_2^{18}\text{F}$	0.9	1.3
$\text{CH}_2\text{F}_2$	$\text{CH}_2\text{F}^{18}\text{F}$	1.5	2.6
	$\text{CHF}_2^{18}\text{F}$	0.8	0.9

<sup>a</sup> Total pressure and scavengers present:  $\text{CF}_4$ , 3 atm,  $\text{C}_2\text{H}_4$ -HI;  $\text{CHF}_3$ , 4 atm,  $\text{C}_2\text{H}_4$ -HI;  $\text{CH}_2\text{F}_2$ , 6 atm, HI- $\text{O}_2$ . <sup>b</sup> Total pressure: 1 atm, scavenger:  $\text{C}_2\text{H}_4$ - $\text{I}_2$ .

values obtained in experiments with  $^{19}\text{F}(\gamma, n)^{18}\text{F}$ . The present numbers are all lower by as much as a factor of 2, and are somewhat outside the combined limits of error indicated for the two monitor calculations. There does not seem to be a systematic constant discrepancy in the calibration for the two methods, although the relatively large limits of error (*e.g.*,  $\text{CF}_3^{18}\text{F}$ :  $2.0 \pm 0.3$  and  $2.8 \pm 0.4$ ) do not completely preclude a constant calibration error together with a random scatter of individual assays. While the pressures are not

(13) As a check on the possibility that the trap might in some way interfere with the operation of the proportional flow counter, an alternate procedure was adopted in two experiments. The irradiated ampoule was counted after the 2-hr delay, and then injected directly into the radio gas chromatograph after the addition of carriers. The eluted compounds were trapped as before, transferred to another ampoule, counted in the scintillation counter, and then rechromatographed without a trap. Calibration factors could then be obtained between the radioactivity found in the radio gas chromatograph and the "Identified Volatile" measured before radio gas chromatography; both sets of calibration factors were in good agreement with each other.

**Table III:** Yields of  $^{18}\text{F}$ -Labeled Products from Reactions of Energetic  $^{18}\text{F}$  Atoms with HI-Scavenged  $\text{C}_2\text{F}_4$  as a Function of  $\text{C}_2\text{F}_4/\text{HI}$  Ratio

Mole ratio $\text{C}_2\text{F}_4/\text{HI}$	Absolute yields, % <sup>a</sup>			
	Observed Product			
	$\text{CHF}_2\text{CF}_2^{13}\text{F}$	$\text{CHF}_2^{18}\text{F}$	$\text{CHF}^{18}\text{FI}$	$\text{CF}_2=\text{CF}^{18}\text{F}$
	Radical Precursor			
	$\text{CF}_2\text{CF}_2^{18}\text{F}$	$\text{CF}_2^{18}\text{F}$	$\text{CF}^{18}\text{F}$	...
2.92	22.4 ± 0.5	20.4 ± 0.4	12.0 ± 0.3	1.0 ± 0.2
10.6	38.5 ± 0.4	26.6 ± 0.3	13.2 ± 0.3	1.6 ± 0.1
20.4	34.0 ± 0.3	24.1 ± 0.3	12.7 ± 0.3	1.5 ± 0.1
210	15.5 ± 0.2	12.6 ± 0.2	12.7 ± 0.3	1.5 ± 0.1

<sup>a</sup> Total Pressure 1060 ± 60 Torr. The listed errors represent the statistical counting error alone. The actual errors in absolute yield for all data must be at least ±10% of the listed yields because of the ±10% uncertainty in the monitoring system for absolute measurements.

identical in the two sets of measurements, the quantitative effects of such differences should be relatively small—in any event, the yield of all of these  $^{18}\text{F}$  products, except  $\text{CF}_2^{18}\text{F}$  from  $\text{CF}_4$ , should increase with increasing pressure, which is not the direction of the discrepancy in Table II. One earlier monitor method relied upon injection of an aliquot of the sample directly into a proportional counter for determination of the total gaseous  $^{18}\text{F}$  activity.<sup>7</sup> In our experimental apparatus, such a procedure would almost invariably lead to a substantial underestimate (although not by a constant ratio) of the total gaseous  $^{18}\text{F}$  through loss in transit of  $\text{H}^{18}\text{F}$ , reactive intermediates formed by  $\text{H}^{18}\text{F}$  reaction with silicates, etc. Errors of the requisite magnitude seem to us to be unlikely in our own experiments, since we have recovered as much as 80% of the total  $^{18}\text{F}$  activity in the form of organic products (see Table III).

At this stage of experimentation, the question of the precise values of absolute yields is essentially just a technical one, for none of the qualitative or quantitative explanations used below are sensitive to the discrepancies shown in Table II.

*Charge and Excitation of Reacting  $^{18}\text{F}$  Species.* All of the interpretations given below assume that the reacting  $^{18}\text{F}$  species is in the neutral, ground electronic state, designated as "hot" if it possesses excess kinetic energy and "thermal" if it does not. The possibility that the resulting species is either charged or electronically excited cannot be rigorously excluded. However, the general pattern of reaction of  $^{18}\text{F}$  from nuclear recoil—especially the yield behavior in the presence of inert moderators of varying ionization potential—has not yet shown any evidence inconsistent with the neutral, ground state hypothesis.<sup>4-10</sup> The very high energies (*vs.* the ground state of F) for the first excited electronic state (12.7 eV) and the ionization limit (17.4 eV) make appreciable fractions of these species very unlikely at energies comparable to chemical bond energies.

## Results and Discussion

*Reaction Products.* The three general classes of primary reactions usually observed for the reactions of  $^{18}\text{F}$  atoms with olefinic molecules are indicated for  $\text{C}_2\text{F}_4$ .

### (a) Substitution of $^{18}\text{F}$ -for-F



### (b) Addition to the $\pi$ -bond

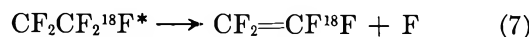
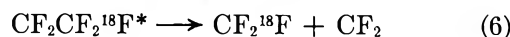
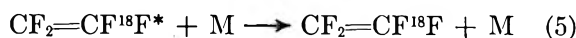


### (c) Abstraction



With hydrogen-containing molecules, the abstraction of H to form  $\text{H}^{18}\text{F}$  must also be considered and is actually an important reaction in most systems. No attempt has been made in our experiments to investigate the possible abstraction of F atoms as in (3), and we have neither positive nor negative evidence regarding the existence of this reaction. However, the weakness of the product  $\text{F}-^{18}\text{F}$  bond makes this reaction much less favorable energetically than the other  $^{18}\text{F}$  reactions considered here.

When the products of reactions 1 and 2 are sufficiently vibrationally excited, the secondary decomposition reactions, (4), (6), and probably (7) occur in competition with the collisional stabilization reactions 5 and 8.

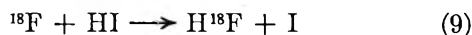


Labeled  $\text{CF}_2=\text{CF}^{18}\text{F}$  can be formed by direct substitution, as in (1), or by addition-plus-atom elimination, as in (2) + (7). Monoradicals, *e.g.*,  $\text{CF}_2^{18}\text{F}$ ,  $\text{CF}_2\text{CF}_2^{18}\text{F}$ , etc., react with HI scavenger by hydrogen atom ab-

straction to give stable saturated products. Diradicals such as  $\text{CF}^{18}\text{F}$  react with HI by insertion to form  $\text{CHF}^{18}\text{FI}$ .<sup>11</sup>

Four major products have been identified from the reaction of  $^{18}\text{F}$  with  $\text{C}_2\text{F}_4$ —the substituted parent,  $\text{CF}_2=\text{CF}^{18}\text{F}$ ; two monoradicals (observed after H abstraction from HI),  $\text{CF}_2^{18}\text{F}$  and  $\text{CF}_2\text{CF}_2^{18}\text{F}$ ; and one di-radical,  $\text{CF}^{18}\text{F}$ , found as  $\text{CHF}^{18}\text{FI}$ . Iodine atom abstraction, *i.e.*, formation of  $\text{CF}_2^{18}\text{FI}$  or  $\text{CF}_2^{18}\text{FCF}_2\text{I}$ , was not found with HI.<sup>14</sup>

*Competition between  $\text{C}_2\text{F}_4$  and HI for  $^{18}\text{F}$  Atoms.* The reaction of fluorine atoms with HI, as in (9), is expected to have little or no activation energy<sup>15</sup> and should compete effectively with reaction 2 for lower energy  $^{18}\text{F}$  atoms. Reaction 9 (and perhaps the abstraction of I to form  $\text{I}^{18}\text{F}$ ) is presumably not limited to low energy  $^{18}\text{F}$  atoms, but the removal of  $^{18}\text{F}$  by direct, hot reaction should be relatively unimportant, especially for  $\text{C}_2\text{F}_4/\text{HI} > 10$ . The effect on absolute product yields of var-



iations in the  $\text{C}_2\text{F}_4/\text{HI}$  ratio at constant total pressure is shown in Table III. The maximum in absolute yields in this table identifies two separate mechanistic influences. At the lowest  $\text{C}_2\text{F}_4/\text{HI}$  ratios, direct reaction of  $^{18}\text{F}$  with HI is lowering the overall yields of all products which have precursors which originate at least partially from low-energy or thermal  $^{18}\text{F}$  atoms. The formation of  $\text{CF}^{18}\text{F}$  *via* decomposition of an excited  $\text{CF}_2=\text{CF}^{18}\text{F}^*$  molecule has the greatest energy requirement of any of the observed reactions, and presumably is initiated by the highest energy  $^{18}\text{F}$  atoms on the average. As expected for the hottest process, the yield of  $\text{CF}^{18}\text{F}$  as  $\text{CHF}^{18}\text{FI}$  is least affected by a decrease in  $\text{C}_2\text{F}_4/\text{HI}$  ratio and is essentially constant throughout Table III. The other products show decreases in absolute yield as the relative concentration of HI increases. At the lowest HI concentration,  $\text{C}_2\text{F}_4$  begins to compete effectively with HI as a monoradical scavenger and the yields of  $\text{CHF}_2^{18}\text{F}$  and  $\text{CHF}_2\text{CF}_2^{18}\text{F}$  are markedly reduced. The yield of  $\text{CHF}^{18}\text{FI}$  is not affected by this ratio change, consistent with the unreactivity of  $\text{C}_2\text{F}_4$  toward  $\text{CF}^{18}\text{F}$ .<sup>16</sup> A ratio of  $\text{C}_2\text{F}_4/\text{HI}$  of 10 has been chosen for subsequent experiments in order to maximize low-energy  $^{18}\text{F}$  reaction with  $\text{C}_2\text{F}_4$  rather than HI, while still preserving the role of HI as efficient scavenger of monoradicals.

*Hot vs. Thermal Reactions.* One distinguishing test for hot and thermal reactions in a particular system involves the measurement of the effect of an inert moderator. A completely inert moderator, such as neon, will remove the kinetic energy of  $^{18}\text{F}$  atoms and reduce the probability that the  $^{18}\text{F}$  atom will possess high kinetic energy at the time of its reaction with  $\text{C}_2\text{F}_4$  or other reactive substance in the system. In the present case, completely inert moderators are ruled out by the necessity that substantial quantities of  $^{18}\text{F}$  atoms are needed

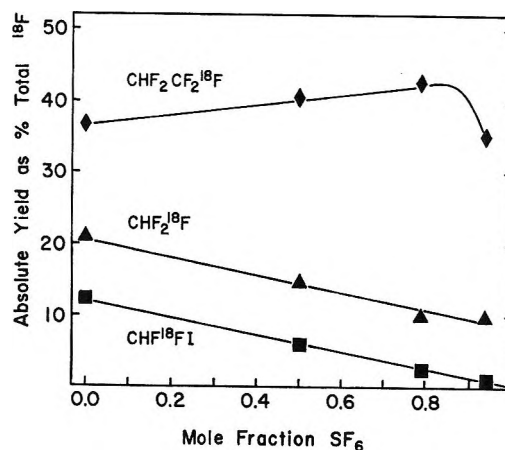


Figure 2. Absolute yields of products from  $^{18}\text{F}$  plus  $\text{C}_2\text{F}_4$  vs. mole fraction of  $\text{C}_2\text{F}_4\text{-SF}_6$ :  $\blacklozenge$ ,  $\text{CHF}_2\text{CF}_2^{18}\text{F}$ ;  $\blacktriangle$ ,  $\text{CHF}_2^{18}\text{F}$ ;  $\blacksquare$ ,  $\text{CHF}^{18}\text{FI}$ .

in the system as targets for the nuclear reaction forming  $^{18}\text{F}$ . Wolfgang, *et al.*, have previously shown that  $\text{CF}_4$  and neon are about equally efficient as moderators for F atoms.<sup>6</sup> However, since  $\text{CF}_4$  can also be a reactive source of  $\text{CF}^{18}\text{F}$  and  $\text{CF}_2^{18}\text{F}$ , we have substituted  $\text{SF}_6$  as a moderator in this work. To a first approximation,  $\text{SF}_6$  is inert toward reaction with  $^{18}\text{F}$ —the absolute yield of  $\text{SF}_6^{18}\text{F}$  is only 1.3% and no other volatile products are readily observed. The absolute yields obtained from a series of experiments with varying  $\text{C}_2\text{F}_4/\text{SF}_6$  ratios are summarized in Figure 2.

The three products in this data set are obviously ordered by their slope/intercept behavior in Figure 2 into decreasing order of the average energy of the primary  $^{18}\text{F}$  reaction involved:  $\text{CF}^{18}\text{F} > \text{CF}_2^{18}\text{F} > \text{CF}_2\text{CF}_2^{18}\text{F}$ . The yield of  $\text{CF}^{18}\text{F}$  extrapolates to zero for pure  $\text{SF}_6$  (complete moderation of kinetic energy of  $^{18}\text{F}$ ) and is thereby identified as entirely of "hot" origin. The steady decrease in  $\text{CHF}_2^{18}\text{F}$  yield to a nonzero intercept indicates both some loss of kinetic energy used in this reaction, as well as underlying yield of thermal  $^{18}\text{F}$  origin. The  $^{18}\text{F}$  content as  $\text{SF}_6^{18}\text{F}$  and  $\text{CF}_2=\text{CF}^{18}\text{F}$  was not resolved into its components in the ratio gas chromatograms, but the combined yields do not increase as would be required if the decrease in yield of  $\text{CHF}^{18}\text{FI}$  with increasing  $\text{SF}_6$  concentration were matched by an increase in the yield of  $\text{CF}_2=\text{CF}^{18}\text{F}$ . The reaction forming  $\text{CF}^{18}\text{F}$  is clearly identified as initiated by energetic  $^{18}\text{F}$  atoms, consistent with the minimum endothermicity of 76 kcal/mol for the dissociation of  $\text{C}_2\text{F}_4$  into  $2\text{CF}_2$ .<sup>17</sup>

(14) See D. M. Golden and S. W. Benson, *Chem. Rev.*, **69**, 125 (1969).

(15) H. S. Johnston and C. Parr, *J. Amer. Chem. Soc.*, **85**, 2544 (1963).

(16) W. J. Tyerman, *Trans. Faraday Soc.*, 1188 (1969), and references therein.

(17) H. F. Zmbov, O. M. Uy, and J. L. Margrave, *J. Amer. Chem. Soc.*, **90**, 5090 (1968).

The rate of formation of  $\text{CF}_2^{18}\text{F}$  by the decomposition of  $\text{CF}_2\text{CF}_2^{18}\text{F}$  radicals, as in reaction 6, certainly will decrease as the average energy of  $^{18}\text{F}$  decreases, but the nonzero moderated yield implies that the rate of decomposition at these pressures is not negligibly small for thermal  $^{18}\text{F}$  addition to  $\text{C}_2\text{F}_4$ —both hot and thermal  $^{18}\text{F}$  atoms are involved in the formation of  $\text{CF}_2^{18}\text{F}$  in this system. This finding is consistent with the pressure studies described below.

If a smaller fraction of  $\text{CF}_2\text{CF}_2^{18}\text{F}$  radicals fails to decompose to  $\text{CF}_2^{18}\text{F}$ , and if lower energy  $^{18}\text{F}$  atoms are still scavenged by  $\text{C}_2\text{F}_4$ , then the yield of  $\text{CHF}_2\text{CF}_2^{18}\text{F}$  should show a complementary increase in yield with increasing mole fraction of  $\text{SF}_6$ . Although the yield of  $\text{CHF}_2\text{CF}_2^{18}\text{F}$  does increase with increasing  $\text{SF}_6$ , the increase is not complementary to the other decreases. Finally, at the highest  $\text{SF}_6$  concentration, the  $\text{CHF}_2\text{CF}_2^{18}\text{F}$  yield decreases again, indicating that some other reaction is removing some  $^{18}\text{F}$  when  $\text{SF}_6$  is in almost 20-fold excess *vs.* the 10:1 mixture of  $\text{C}_2\text{F}_4$ -HI. This other reaction path has not been identified, but could involve rather low energy processes in which the reaction of  $^{18}\text{F}$  with HI is favored in competition with  $\text{C}_2\text{F}_4$ .

**Addition of  $^{18}\text{F}$  to  $\text{CF}_2=\text{CF}_2$ .** The addition of thermal  $^{18}\text{F}$  to  $\text{CF}_2=\text{CF}_2$  creates an excited  $\text{CF}_2\text{CF}_2^{18}\text{F}^*$  radical with 70–75 kcal/mol excitation energy, while the initiation by a hot  $^{18}\text{F}$  atom will provide still more excitation energy as well as a broad spectrum of excitation energies for the excited pentafluoroethyl- $^{18}\text{F}$  radicals. Pentafluoroethyl radicals from the pyrolysis of  $\text{C}_2\text{F}_5\text{N}=\text{NC}_2\text{F}_5$  have been observed by Lossing, *et al.*, to decompose into  $\text{CF}_3 + \text{CF}_2$  above  $950^\circ$ ; <sup>18</sup> this observation was rationalized by the fact that the C–C split of reaction 6 is about 17 kcal/mol more exothermic than the loss of F as in reaction 7. The pathways for decomposition of excited radicals formed in this  $^{18}\text{F}$  system can also be determined by study of the effects of pressure upon the absolute and relative product yields. The data from such a study of  $\text{C}_2\text{F}_4$ -HI over the range from 110–4500 Torr is shown in Figure 3. The scatter in the magnitude of the yields is within the 10% accuracy attributed to the Teflon-sleeve monitor technique, and most of the scatter seems to arise in a systematic shift of all absolute yields from a particular sample and not in the relative ratio of product yields within a given sample.

The steady decrease in the yields of all products below about 650 Torr is attributed to recoil loss of  $^{18}\text{F}$  at low pressures. By assuming that HI is a completely efficient scavenger for  $\text{CF}^{18}\text{F}$  and noting that most of the excited  $\text{CF}_2=\text{CF}^{18}\text{F}$  molecules have decomposed to  $\text{CF}^{18}\text{F}$  at all pressures, the yield of  $\text{CHF}^{18}\text{FI}$  can be assumed to be essentially independent of pressure and used as the standard for a recoil loss correction. The open triangles in Figure 3 indicate the expected yield of  $\text{CHF}_2^{18}\text{F}$  after such a correction has been applied. Similar corrections could also be made for the other two products, but would not alter the qualitative conclusion

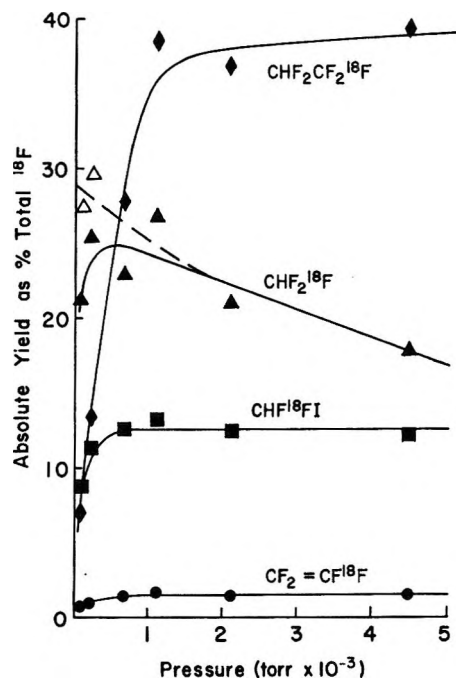


Figure 3. Pressure dependence of product yields from  $^{18}\text{F}$  plus  $\text{C}_2\text{F}_4$ :  $\blacklozenge$ ,  $\text{CHF}_2\text{CF}_2^{18}\text{F}$ ;  $\blacktriangle$ ,  $\text{CHF}_2^{18}\text{F}$ ;  $\blacksquare$ ,  $\text{CHF}^{18}\text{FI}$ ;  $\bullet$ ,  $\text{CF}_2=\text{CF}^{18}\text{F}$ ;  $\triangle$ ,  $\text{CHF}_2^{18}\text{F}$  corrected for recoil loss using  $\text{CHF}^{18}\text{FI}$  data.

that  $\text{CF}_2\text{CF}_2^{18}\text{F}$  yields decrease at low pressure; the yields of  $\text{CF}_2=\text{CF}^{18}\text{F}$  are discussed below. The decomposition/stabilization ( $D/S$ ) ratio for  $\text{C}_2\text{F}_4^{18}\text{F}$  radicals is plotted in Figure 4.

The behavior of the graphs of Figure 4 suggests that there are two populations of  $\text{CF}_2\text{CF}_2^{18}\text{F}^*$  radicals—a roughly monoenergetic group formed by the exothermic addition of thermal  $^{18}\text{F}$  to  $\text{C}_2\text{F}_4$ , and a more energetic group formed by the addition of hot  $^{18}\text{F}$  atoms with a spread of kinetic energies. Assuming that those radicals which decompose at the highest pressures are chiefly the result of the addition of hot  $^{18}\text{F}$  atoms (and that this 30/70 ratio of hot/thermal  $^{18}\text{F}$  atom addition is independent of pressure), the observed  $D/S$  ratios can be corrected for the hot contribution, and a set of  $D/S$  values obtained which correspond to the behavior of the radicals formed by the addition of thermal  $^{18}\text{F}$  atoms. These “corrected” values are also plotted in Figure 4, and give a straight line passing through the origin of the reciprocal pressure plot, as required for a monoenergetic group of radicals. The half-stabilization pressure for these pentafluoroethyl radicals formed by thermal addition of  $^{18}\text{F}$  is 218 Torr, which corresponds to an average decomposition rate of  $\sim 2 \times 10^9 \text{ sec}^{-1}$  assuming a strong-collision deexcitation mechanism.

**Recoil Losses for Energetic  $^{18}\text{F}$  Atoms Formed in the  $^{19}\text{F}(n,2n)^{18}\text{F}$  Reaction.** The loss of energetic tritium atoms to the walls of the vessel has been the source of a

(18) I. P. Fisher, J. B. Homer, and F. P. Lossing, *J. Amer. Chem. Soc.*, **87**, 957 (1965).

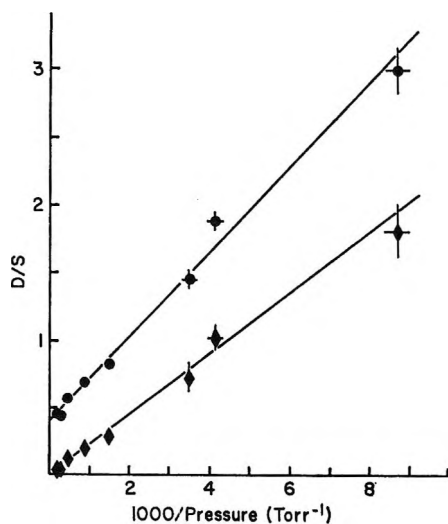


Figure 4. Decomposition (stabilization ( $D/S$ ) ratios for  $\text{CF}_2^{18}\text{FCF}_2$  from  $^{18}\text{F} + \text{C}_2\text{F}_4$ : ●, ( $D/S$ ) all data— $\text{CHF}_2^{18}\text{F}/\text{CHF}_2\text{CF}_2^{18}\text{F}$ ; ◆, ( $D/S$ ) after subtraction of "high energy"  $\text{CF}_2\text{CF}_2^{18}\text{F}$  radicals.

routine correction for many years<sup>19,20</sup> in the studies of the hot atom chemistry of tritium. Several of the simplifications available in recoil tritium systems are absent in the study of  $^{18}\text{F}$  recoils: the  $^{18}\text{F}$  atoms are not monoenergetic, are not isotropically emitted, and are not produced homogeneously throughout the reaction vessel because of the severe inhomogeneity of the fast neutron flux. Consequently, only a very approximate estimate can be simply made of the recoil losses in  $^{18}\text{F}$  systems. By making the unjustified but crudely applicable assumption that the fractional recoil losses of  $^{18}\text{F}$  can be converted into an average recoil range with the diagrams constructed for isotropic, monoenergetic homogeneously produced atoms,<sup>20</sup> the average range of  $^{18}\text{F}$  is calculated to be about 0.1 cm in 760 Torr of  $\text{C}_2\text{F}_4$ .

*Formation of Vibrationally Excited  $\text{CF}_2=\text{CF}^{18}\text{F}$ .* The molecules of  $\text{CF}_2=\text{CF}^{18}\text{F}$  found in these experiments can conceivably be formed by either of two mechanisms: by the direct substitution of  $^{18}\text{F}$  for F in  $\text{C}_2\text{F}_4$ , in analogy with similar replacements for  $\text{CF}_4$  and other saturated molecules, and by the decomposition of excited  $\text{CF}_2\text{CF}_2^{18}\text{F}^*$  radicals formed by addition of hot  $^{18}\text{F}$  atoms to  $\text{C}_2\text{F}_4$ . From a pragmatic experimental point of view, these two mechanisms are essentially in-

distinguishable, differing only in the time delay between the arrival of  $^{18}\text{F}$  and the departure of the displaced F atom. Since the lower energy decomposition path of an excited pentafluoroethyl radical is through the C-C split discussed earlier, the loss of an F atom from pentafluoroethyl can only occur if the total excitation energy is very high. Experimentally, such higher energy paths are very difficult to stabilize at any gas pressure, so that the reaction (if it occurs) will proceed to completion without any distinguishable trace, nor will it be readily disclosed by a study of the pressure dependence of product yields even over a very wide range of pressures. We can certainly conclude that most  $\text{CF}_2\text{CF}_2^{18}\text{F}$  radicals formed by hot or thermal  $^{18}\text{F}$  atom addition decompose to  $\text{CF}_2^{18}\text{F}$  and not by F loss; however, we are unable to estimate the contribution of F atom loss to the small yield of  $\text{CF}_2=\text{CF}^{18}\text{F}$  formed in this system.

The yield of  $\text{CHF}^{18}\text{FI}$  greatly exceeds that of  $\text{CF}_2=\text{CF}^{18}\text{F}$  at all pressures (Figure 3), with average yields for six determinations of 12.6% and 1.5%, respectively, corresponding to >89% decomposition of  $\text{CF}_2=\text{CF}^{18}\text{F}$ . Hence, we can conclude that the hot replacement of F in  $\text{C}_2\text{F}_4$  results in the deposition of >>76 kcal/mol of excitation energy in >89% of the cases. This conclusion is quite consistent with the very large energy depositions found for  $^{18}\text{F}$ -for-F in  $\text{CF}_4$ <sup>21</sup> and  $\text{CH}_3\text{CF}_3$ .<sup>22</sup>

The data of Figure 3 show little if any dependence of  $\text{CF}_2=\text{CF}^{18}\text{F}$  yield with pressure—the apparent decrease at low pressure is chiefly attributable to the recoil loss of  $^{18}\text{F}$ . If a recoil loss correction is made, the yield of  $\text{CF}_2=\text{CF}^{18}\text{F}$  is constant over this 110–4500 Torr pressure range within the not very stringent accuracy limits of this series of measurements. The ratios of  $\text{CHF}^{18}\text{FI}/\text{CF}_2=\text{CF}^{18}\text{F}$ , in which all monitor fluctuations are canceled, also indicate no change in the fraction decomposition of  $\text{CF}_2=\text{CF}^{18}\text{F}$  over this pressure range.

(19) P. Estrup and R. Wolfgang, *J. Amer. Chem. Soc.*, **82**, 2665 (1960).

(20) J. W. Root and F. S. Rowland, *Radiochim. Acta*, **10**, 104 (1968).

(21) Y.-N. Tang, T. Smail, and F. S. Rowland, *J. Amer. Chem. Soc.*, **91**, 2130 (1969).

(22) C. McKnight, N. J. Parks, and J. W. Root, *J. Phys. Chem.*, **74**, 217 (1970).

# Optical Filter Effect in the Photolysis of Solid Potassium

## Trisoxalatocobaltate(III) Trihydrate

by H. E. Spencer\* and M. W. Schmidt

Research Laboratories, Eastman Kodak Company, Rochester, New York 14650 (Received May 12, 1970)

A two-parameter equation is derived to describe the optical filter effect of the surface-formed photoproduct generated during photolysis of solids. One parameter is the quantum yield for production of photoproduct; the other is an attenuation factor characteristic of the solid photoproducts. Values of quantum yields are obtained conveniently by fitting the equation to photolysis data. This is illustrated by analysis of Co(II) yields in the photolysis of  $K_3[Co(C_2O_4)_3] \cdot 3H_2O$ .

### Introduction

Radiation absorbed by photoproducts, an important consideration in photochemistry, can do two things: it can diminish the apparent quantum yield, and it can cause the absorbing photoproduct itself to undergo photolysis, either producing different photoproducts or reproducing the starting material.

There have been several discussions of the inner filter effect, the case in which the apparent quantum yield is diminished, in photolysis of solutions of inorganic materials.<sup>1-3</sup> The most comprehensive is by Schlafer, *et al.*,<sup>2</sup> who analyze mathematically the case of one reactant producing one product in a homogeneous solution.

The case in which reactant and photoproduct are not homogeneously mixed, namely, photolysis of a solid in which the photoproduct forms on the surface of the reactant and attenuates part or all of the incident radiation, has received less attention. For this case we present here a relatively simple model involving only two parameters, quantum yield and an attenuation factor characteristic of one or more photoproducts.

After completion of most of this work, another analysis by Purnell, *et al.*,<sup>4</sup> was published. Their analysis, although more general, requires three parameters: quantum yield, absorption coefficient of reactant, and absorption coefficient of product.

Our general purpose is to find an accurate method of extracting a value of quantum efficiency from the raw data. We illustrate here the use of our two-parameter equation. Of course, it is advantageous to have two rather than three adjustable parameters, and we believe that our equation is preferable to a three-parameter one except for situations where the optical properties of the materials are known.

Although only two materials are used to illustrate this solid-state filter effect, the phenomenon should be commonly encountered. For instance, Purnell, *et al.*,<sup>4</sup> discussed the photolysis of solid hydrogen iodide. Absorption by photolytic silver in silver halides has long

been a concern in photographic systems.<sup>5</sup> Simmons and Wendlandt,<sup>6</sup> in studying potassium trisoxalato-manganate(III) trihydrate, found that the rate of photolysis decreased with radiation time. We believe that the explanation is the optical filter effect of surface photoproducts and will discuss this more fully in a later section.

Recently, it was observed<sup>7</sup> that the quantum yields for production of Co(II) and Fe(II) from solid  $K_3[Co(C_2O_4)_3] \cdot 3H_2O$  and  $K_3[Fe(C_2O_4)_3] \cdot 3H_2O$ , respectively, decreased appreciably with increasing time of exposure, and the explanation given was that the photoproduct absorbed some of the radiation. Some sort of extrapolation of quantum yield values to zero time of exposure was necessary to correct for this absorption. One specific purpose of this paper is to present a mathematical model to describe the phenomenon. New, more extensive data for various wavelengths and times of exposure are given. Also our reflectivity measurements are compared briefly with those of Wendlandt and Simmons.<sup>6</sup>

Most of the experiments reported here were made with  $K_3[Co(C_2O_4)_3] \cdot 3H_2O$ . With this compound both amount of photoproduct and reflectivity could be measured quantitatively. The intensity dependence of the Fe(II) quantum yield<sup>7</sup> in  $K_3[Fe(C_2O_4)_3] \cdot 3H_2O$  discouraged us initially from studying this compound, but we have found that irradiation under vacuum eliminates

\* To whom correspondence should be addressed.

(1) J. Jortner and G. Stein, *J. Phys. Chem.*, **66**, 1258 (1962).

(2) O. Kling, E. Nikolaiski, and H. L. Schlafer, *Ber. Bunsenges. Physik. Chem.*, **67**, 883 (1963).

(3) A. W. Adamson, W. L. Waltz, E. Zinato, D. M. Watts, P. D. Fleischauer, and R. D. Lindholm, *Chem. Rev.*, **68**, 541 (1968).

(4) P. G. Barker, M. P. Halstead, and J. H. Purnell, *Trans. Faraday Soc.*, **65**, 2404 (1969).

(5) C. E. K. Mees and T. H. James, "The Theory of the Photographic Process," 3rd ed, Macmillan, New York, N. Y., 1966, Chapters 5 and 12; T. R. Sliker, *J. Opt. Soc. Amer.*, **53**, 454 (1963).

(6) E. L. Simmons and W. W. Wendlandt, *J. Inorg. Nucl. Chem.*, **27**, 2325 (1965).

(7) H. E. Spencer, *J. Phys. Chem.*, **73**, 2316 (1969).

this intensity dependence. However, the changes in reflectivity upon irradiation of the iron compound are slight and few spectra were obtained. At present there is no good analytical technique for measuring solid or gaseous photoproducts of  $K_3[Mn(C_2O_4)_3] \cdot 3H_2O$  because of the appreciable thermal decomposition at room temperature.

### Experimental Section

Techniques for purification and coating on glass slides have been given previously.<sup>7,8</sup> A somewhat modified scheme for Co(II) analysis was used. The coatings were washed into a weighed beaker with a jet of oxalate buffer made up of 0.05 mol of  $K_2C_2O_4 \cdot H_2O$  and 5 ml of 1.0 *N*  $H_2SO_4$ , diluted to 1 l. The oxalate buffer was used to maintain all of the Co(II) in solution,<sup>9</sup> enough buffer being added to make 10 g of solution. The concentration of  $Co(C_2O_4)_3^{3-}$  was monitored by measuring the optical density at 600 nm.<sup>7</sup> A 2- or 4-ml aliquot of the solution was pipetted into a 25-ml volumetric flask; 5 ml of 0.006 *M*  $Fe(C_2O_4)_3^{3-}$  in 0.1 *M*  $H_2SO_4$ , 5 ml of an acetate buffer solution (0.6 mol of sodium acetate and 360 ml of 1 *N*  $H_2SO_4$  diluted to 1 l.), and 10 ml of 0.005 *M* 1,10-phenanthroline solutions were added. Because the Co(II) concentration increases slightly with time, the optical density at 510 nm, which is proportional to the Co(II) concentration, was measured successively at several times after mixing. Since the optical density varied linearly with time, at least during the first 30 min, the values were extrapolated back to time zero with a least-squares procedure. After correction for the amount of Co(II) impurity in the coating,<sup>7</sup> the Co(II) produced photochemically was calculated from the extrapolated value.

The procedure for analysis of Fe(II) in solid  $K_3[Fe(C_2O_4)_3] \cdot 3H_2O$  was described previously.<sup>7</sup>

An acidic solution of  $K_3[Fe(C_2O_4)_3] \cdot 3H_2O$  was used as an actinometer according to the procedure of Hatchard and Parker.<sup>10</sup> The radiation source used previously,<sup>11</sup> a 200-W high-pressure mercury arc focused upon a grating monochromator, produced radiation of somewhat nonuniform intensity across the illuminated area. To obtain a more uniform intensity, it was necessary to magnify the emerging beam to a large area with a quartz lens. A blackened metal plate with a small opening (either 0.7 or 1.0 cm<sup>2</sup> in area) was used to pick out an area of the beam. The uniformity of the intensity in the selected area was judged visually both by observing the luminescence or reflectance from a piece of white cardboard held in front of the opening and by examination of the pink photoproduct produced by exposure of a  $K_3[Co(C_2O_4)_3] \cdot 3H_2O$  coating taped across the opening. To achieve uniformity of intensity, which was important to this study, the wavelength dial on the monochromator was adjusted slightly around each wavelength. Measurements at 546 and 578 nm with a

0.1-cm<sup>2</sup> area photocell indicated maximum intensity variations of about  $\pm 15\%$ .

Reflection and transmission measurements were made using either a Beckman DK 2A or a General Electric recording spectrophotometer. Corrections for reflection losses in  $K_3[Co(C_2O_4)_3] \cdot 3H_2O$  of 4.3, 13.4, and 1.4% at 332, 363, and 405 nm, respectively, were made in the number of incident photons.

*Model.* The basis for the proposed model is the observation that photoproduct forms on the surface of the coating. In the case of  $K_3[Co(C_2O_4)_3] \cdot 3H_2O$ , Wendlandt and Simmons<sup>12</sup> identified the solid photoproduct as 2 parts of  $K_2Co(C_2O_4)_2$ , 1 part of  $KHC_2O_4$ , and 1 part of  $KHCO_3$ . Initially the surface facing the radiation source turns from green to pink, and at this stage the pink photoproduct may be scraped off the unreacted green material underneath. Only after considerably more exposure does the pink photoproduct finally become visible on the backside of the coating.

We assume a skin of Co(II) photoproduct  $x$  cm thick which increases as irradiation proceeds. It can only be an approximation that the skin is pure Co(II) photoproduct covering a pure Co(III) substrate because there certainly must be an intermediate region containing both Co(II) and Co(III). Thus  $x$  may represent some average thickness such that if all the Co(II) were concentrated in the skin, its thickness would be  $x$ .

Another assumption is that the intensity  $I$  transmitted through the skin of photoproduct is an exponential function of the thickness

$$I = I_0 e^{-\kappa x} \quad (1)$$

where  $I_0$  is the incident intensity and  $\kappa$  is a constant, which we will call an attenuation constant. If the photoproduct is not a scattering medium,  $\kappa$  is the absorption coefficient. However, if scattering is important, as it is for the microcrystalline system discussed here,  $\kappa$  must represent a constant made up of absorption and scattering factors. Kubelka showed that an equation identical in form with eq 1 is obeyed for a scattering medium in which the reflectivity is low.<sup>13</sup> This condition is certainly met at the four shortest wavelengths in this study. At the two longer wavelengths, eq 1 is probably only an approximation.

Let  $\varphi$  = quantum efficiency,  $[Co(II)]$  = number of Co(II) ions/cm<sup>2</sup>, and  $\rho$  = density of Co(II) in the

(8) H. E. Spencer, *Photogr. Sci. Eng.*, **13**, 147 (1969).

(9) J. E. Barney, W. J. Argersinger, and C. A. Reynolds, *J. Amer. Chem. Soc.*, **73**, 3785 (1951).

(10) (a) C. G. Hatchard and C. A. Parker, *Proc. Roy. Soc. (London)*, **A235**, 518 (1956); (b) J. G. Calvert and J. N. Pitts, Jr., "Photochemistry," John Wiley and Sons, Inc., New York, N. Y., 1966, pp 783-786.

(11) H. E. Spencer and J. O. Darlak, *J. Phys. Chem.*, **72**, 2384 (1968).

(12) W. W. Wendlandt and E. L. Simmons, *J. Inorg. Nucl. Chem.*, **28**, 2420 (1966).

(13) P. Kubelka, *J. Opt. Soc. Amer.*, **38**, 448 (1948).

photoproduct (ions/cm<sup>3</sup>). Then the rate of change of surface concentration of Co(II) is

$$\frac{d[\text{Co(II)}]}{dt} = \frac{\rho dx}{dt} = \varphi I = \varphi I_0 e^{-\kappa x}$$

assuming no transmission through the entire coating, a realistic situation for these experiments. Another assumption is that  $\varphi$  does not vary with  $x$ .

Integration and rearrangement gives

$$x = \frac{1}{\kappa} \ln \left( 1 + \frac{\kappa \varphi}{\rho} I_0 t \right)$$

If a normalized attenuation constant  $\kappa'$  is defined as  $\kappa' = \kappa/\rho$ , and  $x$  is converted to [Co(II)], we have a two-parameter equation

$$[\text{Co(II)}] = \frac{1}{\kappa'} \ln (1 + \kappa' \varphi I_0 t) \quad (2)$$

relating the number of incident photons/cm<sup>2</sup>,  $I_0 t$ , to the number of Co(II) ions/cm<sup>2</sup>, [Co(II)].

For the case of low absorption by the photoproducts (low values of either  $\kappa'$  or  $I_0 t$ ), eq 2 reduces to [Co(II)] =  $\varphi I_0 t$ . Thus eq 2 properly describes the fact that  $\varphi$  is the initial slope of the [Co(II)]- $I_0 t$  curve.

At each wavelength, eq 2 was fitted to the data by computer using a nonlinear regression program. From this fitting, a value of  $\varphi$  and a value of  $\kappa'$  were obtained.

## Results and Discussion

Figure 1 shows data for three wavelengths; the curves are those calculated by computer. Table I contains all the values of the normalized attenuation constant,  $\kappa'$ , and the quantum efficiency,  $\varphi$ . The listed uncertainties are standard deviations as calculated by computer. The examples chosen for Figure 1 represent extremes in values of  $\kappa'$  and  $\varphi$ . For instance, the curves for 296 and 313 nm begin steeply, which indicates high values of  $\varphi$ , but bend over as exposure is increased, which indicates intensity losses due to the photoproduct. The fact that the curve for 296 nm bends over more rapidly than the one for 313 nm indicates higher losses at 296 nm, and Table I lists  $\kappa'_{296} > \kappa'_{313}$ . In contrast, the curve for 405 nm has a lower initial slope and a lower value of  $\varphi$ , but eventually crosses the other two because the loss due to the photoproduct is less.

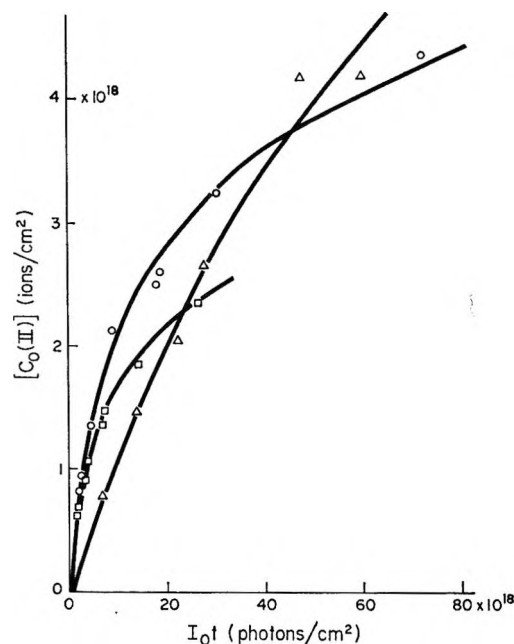


Figure 1. Amount of Co(II) vs. exposure:  $\square$ , 296 nm;  $\circ$ , 313 nm;  $\triangle$ , 405 nm.

Although the values of  $\varphi$  in Table I are known with more accuracy than those reported in ref 7, the values are not greatly different; their significance was discussed in ref 7 and will not be reconsidered here.

We have confirmed for the cobalt compound an assumption made by Simmons and Wendlandt<sup>6</sup> in analyzing the photolysis of  $\text{K}_3[\text{Mn}(\text{C}_2\text{O}_4)_3] \cdot 3\text{H}_2\text{O}$  that the quantity  $R - R_0$ , where  $R_0$  and  $R$  are the reflectivities at a particular wavelength before and after irradiation, is proportional to the amount of photoproduct produced. Although such a linear relationship between reflectivity and amount of material is empirical, it has been found for other systems as well.<sup>14</sup> Yet we find that plots of  $(R - R_0)^2$  vs.  $I_0 t$  are not linear for irradiation of either  $\text{K}_3[\text{Co}(\text{C}_2\text{O}_4)_3] \cdot 3\text{H}_2\text{O}$  or  $\text{K}_3[\text{Mn}(\text{C}_2\text{O}_4)_3] \cdot 3\text{H}_2\text{O}$ . This is contrary to the findings of Simmons and Wendlandt; possibly the important difference is that they used unfiltered radiation from a mercury arc, whereas we used monochromatic radiation.

In Figure 2 are plotted all the data collected at the six wavelengths. The abscissa represents the values of [Co(II)] calculated according to eq 2 after values of  $\kappa'$  and  $\varphi$  were determined by the computer, whereas the ordinate represents the experimental values.

It is clear that the model describes the data well. Unfortunately, this does not prove its uniqueness. In fact, the same type of final equation can be derived if, instead of the assumption that  $\varphi$  is constant throughout photolysis, it is assumed that  $\varphi$  is an exponential function of  $x$ ,  $\varphi = \varphi_0 e^{\alpha x}$ , where  $\alpha$  and  $\varphi_0$  are constants. This assumption leads to eq 3.

Table I: Values of  $\kappa'$  and  $\varphi$  Obtained from Computer Analysis

Wavelength, nm	$\kappa'$ , cm <sup>2</sup> /ion $\times 10^{18}$	$\varphi$ , ions/photon
274	0.40 $\pm$ 0.02	0.31 $\pm$ 0.01
296	1.30 $\pm$ 0.05	0.59 $\pm$ 0.03
313	0.82 $\pm$ 0.05	0.55 $\pm$ 0.06
332	0.41 $\pm$ 0.05	0.41 $\pm$ 0.04
363	0.22 $\pm$ 0.03	0.23 $\pm$ 0.02
405	0.24 $\pm$ 0.07	0.13 $\pm$ 0.02

(14) W. W. Wendlandt and H. G. Hecht, "Reflectance Spectroscopy," Interscience, New York, N. Y., 1966, Chapter V.

$$[\text{Co(II)}] = \frac{\rho}{\kappa - \alpha} \ln \left( 1 + \frac{\kappa - \alpha}{\rho} \varphi_0 I_0 t \right) \quad (3)$$

If  $\kappa' = (\kappa - \alpha)/\rho$ , eq 2 is obtained.

Presumably the constant  $\alpha$  would have the same value for all six wavelengths. Thus, the variation in  $\kappa'$ , almost a factor of 6, must be due to variation in values of  $\kappa$ . With the exception of the low values of  $\kappa'_{274}$ , the values of  $\kappa'$  approximately follow the trend of absorption of the photoproduct as determined by transmission and reflection measurements on coatings fully

and use eq 2 to obtain a value of  $\varphi$ . Although the use of a computer simplifies curve fitting of eq 2 to photolysis data, it can be accomplished readily by use of log tables and a hand calculator.

An equation identical in form with eq 2 also fits photolysis data for both microcrystals and single crystals of  $\text{K}_3[\text{Fe}(\text{C}_2\text{O}_4)_3] \cdot 3\text{H}_2\text{O}$ , provided the samples are evacuated.

Experimentally, small variations in intensity across the irradiated area seem to lead to negligible changes in values of  $\varphi$ . Analysis by computer simulation of the effects of major variations in intensity indicates minor influence on values of  $\varphi$  but major influence on values of  $\kappa'$ . Thus, the parameter of most interest,  $\varphi$ , is the parameter determined with the most accuracy.

Finally, some discussion of the generality of eq 2 is required. Except for photolysis caused by weakly absorbed radiation, surface accumulation of solid photoproducts probably is the rule rather than the exception for photosensitive solids. Certainly this is one bothersome feature that has contributed to the paucity of quantitative solid-state photochemical studies. The use of eq 2 overcomes the problem in large measure, but more applications of it to other materials will be required to prove its generality. In particular, it will be necessary to assess both the approximation that there is a sharp line of demarcation between photoproduct skin and reactant substrate and the approximation that transmission through the skin decreases exponentially with skin thickness. In order to correct for the unwanted attenuation by photoproducts, whatever the outcome of these assessments, eq 2 or some modified form of it will be required for accurate extrapolation of amounts of photoproducts to zero time of exposure.

However, we do not agree with Barker, Halstead, and Purnell<sup>4</sup> that self-filtering by products cannot be important unless absorption per unit thickness of products is greater than or equal to that of reactants. We believe *any* absorption by photoproducts is important in determining  $\varphi$ .

Yet the analysis of Barker, Halstead, and Purnell<sup>4</sup> should be particularly useful in obtaining quantum efficiencies for cases in which absorption coefficients of both products and reactants are known. On the other hand, eq 2, because it contains only two parameters, should be more useful where the optical properties are not known.

*Acknowledgment.* We appreciate the many reflection measurements made by R. M. Peden, the computer program made available by Leonard Tiefel, and helpful discussions with J. F. Hamilton and J. Yudelso.

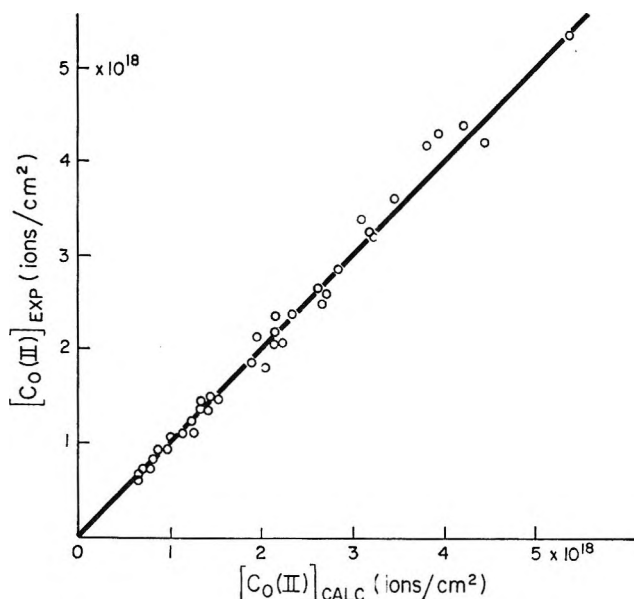


Figure 2. Calculated *vs.* experimental amount of Co(II).

converted to photoproduct.<sup>7</sup> Thus, it seems improbable that  $\alpha$  could be large enough to be important. Furthermore, since the coatings are made up of an arrangement of microcrystals something like a brushpile, it seems unlikely that the value of  $\varphi$  would vary systematically from crystal to crystal, although it is easy to conceive the photolysis of the surface would differ from photolysis of the volume of an individual microcrystal.

Values of  $\kappa'$  should be compared with optical constants of the solid photoproducts, but unfortunately they are not known. Thus, it is impossible at present to understand the low value of  $\kappa'_{274}$ .

Because eq 2 described the data accurately, the use of it provides a convenient way of obtaining values of  $\varphi$ . The initial slope of the  $[\text{Co(II)}]-I_0 t$  curve is simply the value of  $\varphi$  also, but experimental errors can be large in that region of small amounts of Co(II). It is much more convenient and accurate to produce more Co(II)

# The Radiation Chemistry of Tetramethylsilane. I. Vapor Phase<sup>1</sup>

by Gilbert J. Mains<sup>2</sup> and Jonas Dedinas

Department of Chemistry, Carnegie-Mellon University, Pittsburgh, Pennsylvania (Received March 20, 1970)

The radiolysis of tetramethylsilane (TMS) induced by 50-pkeV X-rays has been investigated in the dose range  $9.53 \times 10^{15}$  to  $4.20 \times 10^{17}$  eV/ml and at pressures of 60 to 300 Torr. Reaction mechanisms were deduced from studies using 1:1 TMS-TMS-*d*<sub>12</sub> mixtures and from experiments in which O<sub>2</sub> and NO were added as free radical scavengers. H<sub>2</sub> and CH<sub>4</sub> are produced by atomic reactions, molecular elimination reactions, and, to a lesser extent, by "hot" intermediates. C<sub>2</sub>H<sub>6</sub> is formed almost exclusively *via* methyl radical combination. Internal free radical scavengers, C<sub>2</sub>H<sub>2</sub>, C<sub>2</sub>H<sub>4</sub>, and C<sub>3</sub>H<sub>6</sub>, are radiolysis products and observed in appreciable *G* yields at low conversions or in the presence of O<sub>2</sub> or NO. The principal carbosilane products are (C<sub>2</sub>H<sub>5</sub>)Si(CH<sub>3</sub>)<sub>3</sub>, (CH<sub>3</sub>)<sub>3</sub>-SiSi(CH<sub>3</sub>)<sub>3</sub>, (CH<sub>3</sub>)<sub>3</sub>SiCH<sub>2</sub>Si(CH<sub>3</sub>)<sub>3</sub>, and (CH<sub>3</sub>)<sub>3</sub>SiCH<sub>2</sub>CH<sub>2</sub>Si(CH<sub>3</sub>)<sub>3</sub>, all of which appear to arise from the intercombination of CH<sub>3</sub>·, (CH<sub>3</sub>)<sub>3</sub>Si·, and (CH<sub>3</sub>)<sub>3</sub>SiCH<sub>2</sub>· radicals. A diradical intermediate, (CH<sub>3</sub>)<sub>3</sub>SiCH<sub>2</sub>· is also postulated to account for radiolysis products obtained in small yields.

## Introduction

Although the photochemistry of monosilane<sup>3,4</sup> and its methyl-substituted derivatives<sup>5,6</sup> have been reported, analogous radiolysis studies are less complete. The radiolysis of monosilane has been reported by this laboratory<sup>7</sup> and, more recently, by Schmidt and Lampe.<sup>8</sup> The *G* yields of monosilane decomposition are rather high, suggesting a chain mechanism for the decomposition. An ionic chain has been proposed,<sup>8</sup> but in view of the observed high quantum yields for the photolysis, a concurrent radical chain is also possible. An ionic chain mechanism has also been suggested for the radiation-induced addition of methylsilane and dimethylsilane to ethylene,<sup>9</sup> although the low *G* yield of methylsilane dimer in the absence of ethylene does not require a chain mechanism explanation. Except for a study of the chemical ramifications of neutron capture<sup>10</sup> and an epr study of the free radicals produced by the  $\gamma$  radiolysis<sup>11</sup> at 77°K, the effects of ionizing radiation on tetramethylsilane have not been investigated.

The present study, a logical extension of our earlier monosilane research,<sup>7</sup> was undertaken to extend knowledge of the nature of the radiolysis of silane systems.

## Experimental Section

The radiation source was a Machlett OEG-50 X-ray tube operated at 50 pkeV and 40 mA anode current. The dose rate was  $1.06 \times 10^{13}$  eV/(ml sec) measured by the N<sub>2</sub> yield from N<sub>2</sub>O radiolysis at 25° and 565 Torr assuming *G*(N<sub>2</sub>) to be 9.7 from Harteck and Dondes study,<sup>12</sup> a value in excellent agreement with more recent ionization chamber measurements.<sup>13</sup> The reaction vessel was a Pyrex cylinder 45 mm in diameter, 70 mm long, and 75 ml in volume. The end of the reactor facing the X-ray tube had a thin in-blown window; the other end was attached by means of a transfer line to a mercury float valve. Except for the absence of stop-

cock grease throughout the vacuum system, standard high-vacuum techniques were employed.

**Reagents.** Tetramethylsilane (TMS) was obtained from Peninsular ChemResearch Inc. and was 99.5% pure as received. The purity was improved to 99.7% by means of vacuum distillation. This TMS was used to study the effects of impurities. Pure TMS was prepared by bromination of the distilled TMS, initially at 0° and then slowly allowing the temperature to rise to 25°. The brominated material was passed through a packed column at 0°. The column contained basic alumina, coconut charcoal, and silica gel in equal amounts. The eluted and degassed TMS was stored over Na and KOH pellets for 12 hr to remove CO<sub>2</sub> and water. Further degassing was performed by slow distillation through a trap held at -130°. Analysis of the pure TMS by gas chromatography employing flame ionization and thermal conductivity detectors revealed no impurities.

Perdeuteriotetramethylsilane (TMS-*d*<sub>12</sub>) obtained from Merck Sharp and Dohme of Canada, Ltd., was

- (1) Supported by U. S. AEC Contract No. AT(30-1)2007.
- (2) To whom correspondence should be addressed at Department of Chemistry, University of Detroit, Detroit, Mich. 48221.
- (3) H. Niki and G. J. Mains, *J. Phys. Chem.*, **68**, 304 (1964).
- (4) M. Ring, G. Beverly, F. Koester, and R. Hollandsworth, *Inorg. Chem.*, **8**, 2033 (1969).
- (5) M. Nay, G. Woodall, O. Strausz, and H. Gunning, *J. Amer. Chem. Soc.*, **87**, 179 (1965).
- (6) K. Obi, A. Clement, H. Gunning, and O. Strausz, *ibid.*, **91**, 1622 (1969).
- (7) G. J. Mains and T. Tiernan, U. S. Atomic Energy Commission Report NYO-2007-8.
- (8) J. Schmidt and F. Lampe, *J. Phys. Chem.*, **73**, 2706 (1969).
- (9) J. Snyderman, W. Johnston, and F. Lampe, *ibid.*, **70**, 3934 (1966).
- (10) D. K. Snediker, Ph.D. Thesis, Pennsylvania State University, University Park, Pa. 16802.
- (11) J. Roncin, *Mol. Cryst.*, **3**, 117 (1967).
- (12) P. Harteck and S. Dondes, *Nucleonics*, **14**, 66 (1956).
- (13) F. Jones and T. Sworski, *J. Phys. Chem.*, **70**, 1546 (1966).

similarly purified. The isotopic purity was found to be 90.8 mol % after purification; the only isotopic impurity detected was TMS- $d_{11}$ .

$N_2O$ , NO, and  $O_2$  were 98, 99, and 99.6% pure as received from Matheson and were used without further purification.

**Product Analysis.** The irradiated samples were degassed at  $-196$  and at  $-140^\circ$ . The gas fractions so obtained were analyzed using a Consolidated Electro-dynamics Co., Type 21-103C mass spectrometer. Mass spectrometer standards were determined daily.  $O_2$ ,  $N_2$ ,  $CO_2$ ,  $H_2$ , and  $C_1$ ,  $C_2$ , and  $C_3$  hydrocarbon standards were at least 99% pure (CP grade). HD,  $D_2$ , and deuteriohydrocarbons,  $C_1$ ,  $C_2$ , and  $C_3$  (Merck), contained at least 98 atom % deuterium. The degassed sample was transferred to a Pyrex ampoule and sealed off for subsequent analysis by gas chromatography. To minimize the loss of volatile liquids both the ampoule and the injection syringe were precooled to  $-10^\circ$ . A Perkin-Elmer Model 800 gas chromatograph equipped with dual 12-ft,  $1/4$ -in. diameter, Apiezon L columns operated at  $100^\circ$  and an He carrier gas flow rate of 50 ml/min was used for all liquid product analysis. Radiolysis products were identified by retention time and mass spectral analysis of the effluent from the gas chromatograph. Authentic samples were also prepared for direct comparison. Trimethylsilane was obtained from Peninsular ChemResearch.  $C_2H_5Si(CH_3)_3$ ,  $n-C_3H_7Si(CH_3)_3$ , and  $(CH_3)_3SiCH_2Si(CH_3)_3$  were synthesized from  $(CH_3)_3SiCl$  and the appropriate Grignard reagents and purified by fractional distillation.  $(CH_3)_3SiSi(CH_3)_3$  was prepared from  $(CH_3)_3SiCl$  using Na-K alloy and similarly purified.  $(CH_3)_3SiCH_2CH_2Si(CH_3)_3$  was prepared by ( $^{63}P_1$ ) Hg-sensitized decomposition to pure TMS in the gas phase.<sup>5</sup> The mass spectrum of a collected gas chromatograph fraction was in agreement with literature data.<sup>14</sup> Ethylpentamethylsilane was not prepared but identified from the mass spectra of undeuterated and perdeuterated fractions. Similarly, the oxygenated silicon compounds from the radiolysis of TMS in the presence of  $O_2$  were identified by mass spectrometry.<sup>15</sup> Dimethylsilane was identified tentatively by gas chromatography retention time. The identification of radiolysis products was confirmed by infrared analysis whenever possible.<sup>16</sup>

## Results and Discussion

**Products and Radiation Yields.** The radiolysis of tetramethylsilane (TMS) induced by 50-pkeV X-rays was studied over a dose range from  $9.53 \times 10^{15}$  to  $4.20 \times 10^{17}$  eV/ml and over a pressure range from 60 to 300 Torr. Also, the effects of thermal free radical scavengers and of low level impurities were investigated. The products and their  $G$  yields, molecules/100 eV absorbed energy, are summarized in Table I. Hydrogen, hydrocarbon gases, and methyl-substituted silanes and disilanes were found as radiolysis products. The

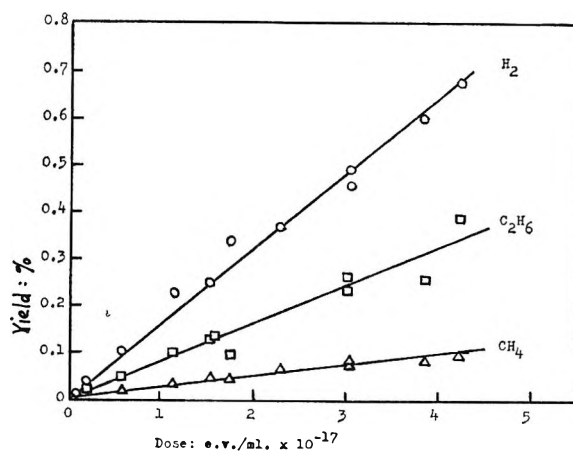


Figure 1. Effect of dose on yields of principal gases in the radiolysis of pure tetramethylsilane at 150 Torr and  $25^\circ$ .

effect of dose was studied at a pressure of 150 Torr and is depicted in Figure 1. The linearity of the yields *vs.* dose indicate that the  $G$  yields reported in Table I are dose independent in the dose range investigated. The reduction of product  $G$  yields in the presence of small amounts of oxygen and nitric oxide suggests that thermal free radicals are important intermediates. Taking average  $G$  yields for the scavenger experiments reported in Table I, it may be seen that 81% of the  $H_2$ , 35% of the  $CH_4$ , 96% of the  $C_2H_6$ , and 94% of the  $C_3H_8$  is suppressed by free radical scavengers.

The unsaturated hydrocarbons,  $C_2H_4$ ,  $C_2H_2$ , and  $C_3H_6$ , are obtained at constant concentration in the irradiated samples regardless of dose, the average yields being  $3.1 \times 10^{-3}\%$ ,  $7.8 \times 10^{-4}\%$ , and  $4.7 \times 10^{-4}\%$ , respectively. Thus, as shown in Figure 2, the  $G$  yields of these products decrease rapidly with dose. Because the *initial*  $G$  yields of these unsaturated products are essentially the same as the  $G$  yields obtained in the presence of scavengers, they probably represent the primary radiolysis yields. The subsequent decrease in  $G$  yield with dose indicates that the unsaturated hydrocarbons undergo rapid subsequent reactions in the radiolysis of pure TMS. These reactions do not occur in the presence of oxygen or nitric oxide and suggest that free radical addition reactions are responsible for olefin removal. Since the steady-state concentrations of these olefins are relatively low, it is seen that  $C_2H_4$ ,  $C_2H_2$ , and  $C_3H_6$  are effective internal free radical scavengers in the TMS system. It should be noted that the steady-state concentrations of the olefins were found to be approximately the same throughout the pressure range of this study.

(14) G. Fritz, *et al.*, *Z. Anorg. Allgem. Chem.*, **312**, 202 (1961).

(15) A. G. Sharkey, R. A. Friedel, and H. Langer, *Anal. Chem.*, **29**, 770 (1957).

(16) D. G. White and E. G. Rochow, *J. Amer. Chem. Soc.*, **76**, 3897 (1954).

Table I: Effect of Pressure and Scavenger on Radiation Yields

	Pressure, Torr								
	60	105	150	150 <sup>a</sup>	300	300	150	150	150
	Scavenger (%) and dose, eV/ml								
	1.16 × 10 <sup>17</sup>	1.16 × 10 <sup>17</sup>	1.53 × 10 <sup>17</sup>	0.0953-4.20 × 10 <sup>17</sup>	1.16 × 10 <sup>17</sup>	2.32 × 10 <sup>-17</sup>	O <sub>2</sub> (4.5%) 1.53 × 10 <sup>17</sup>	O <sub>2</sub> (2.0%) × 10 <sup>16</sup>	NO (6.0%) × 10 <sup>16</sup>
	G yields:								
H <sub>2</sub>	8.63	10.8	7.60	8.56	8.68	9.18	1.58	1.90	1.72
CH <sub>4</sub>	1.53	1.78		1.28	1.30	1.43	0.78	0.96	
C <sub>2</sub> H <sub>6</sub>	6.19	6.99	4.34	4.23	5.35	5.16	0.13	0.23	0.13
C <sub>2</sub> H <sub>4</sub>	~0.0	~0.0	0.12	1.54 <sup>b</sup> -0.039	0.036	0.056	1.20	1.12	1.16
C <sub>2</sub> H <sub>2</sub>	0.024	~0.0	0.022	0.52 <sup>b</sup>	0.025	0.20	0.65	0.42	0.58
C <sub>3</sub> H <sub>8</sub>	0.32	0.20	0.12	0.17	0.096	0.078	0.016	0.0	0.0
C <sub>3</sub> H <sub>6</sub>	0.21	0.016	0.12	0.043 <sup>c</sup> -0.0049	0.23	0.025	0.11	0.014	0.043
(CH <sub>3</sub> ) <sub>2</sub> SiH <sub>2</sub>				0.02	0.06				
(CH <sub>3</sub> ) <sub>3</sub> SiH			0.10	0.18					
(CH <sub>3</sub> ) <sub>3</sub> SiC <sub>2</sub> H <sub>5</sub>	5.66	4.76	4.39	4.52	5.50	4.79	0.0		
(CH <sub>3</sub> ) <sub>3</sub> SiC <sub>3</sub> H <sub>7</sub>	0.31	0.31	0.17	0.20	0.32	0.25	0.0		
(CH <sub>3</sub> ) <sub>3</sub> SiSi(CH <sub>3</sub> ) <sub>3</sub>	1.92	1.77	1.47	1.40	1.69	1.67	0.0		
(CH <sub>3</sub> ) <sub>3</sub> SiCH <sub>2</sub> Si(CH <sub>3</sub> ) <sub>3</sub>	0.99	1.32	1.19	1.22	1.30	1.63	0.0		
(CH <sub>3</sub> ) <sub>3</sub> SiSi(CH <sub>3</sub> ) <sub>2</sub> C <sub>2</sub> H <sub>5</sub>	0.24	0.26	0.069	0.17	0.21	0.14	0.0		
(CH <sub>3</sub> ) <sub>3</sub> SiCH <sub>2</sub> CH <sub>2</sub> Si(CH <sub>3</sub> ) <sub>3</sub>	0.33	0.46	0.44	0.47	0.68	0.60	0.0		
(CH <sub>3</sub> ) <sub>3</sub> SiOSi(CH <sub>3</sub> ) <sub>3</sub>							~5.3		
CH <sub>3</sub> OSi(CH <sub>3</sub> ) <sub>3</sub>							~5.7		

<sup>a</sup> Average values. <sup>b</sup> Dose = 9.53 × 10<sup>15</sup> eV/ml. <sup>c</sup> Dose = 5.72 × 10<sup>16</sup> eV/ml.

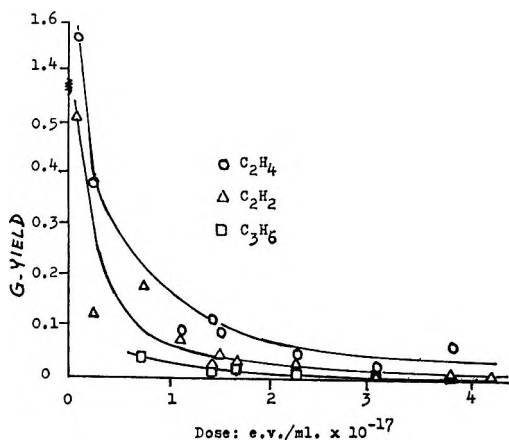


Figure 2. Effect of dose on the *G* yields of unsaturated hydrocarbons in the radiolysis of pure tetramethylsilane at 150 Torr and 25°.

The silicon-containing products vary over a molecular weight range from 60 to 174. Only two silicon-containing gases were found, (CH<sub>3</sub>)<sub>2</sub>SiH<sub>2</sub> and (CH<sub>3</sub>)<sub>3</sub>SiH, with *G* yields of approximately 0.1 and 0.2, respectively. These gases were retained in the liquid fraction from the degassing at -140°. It should be noted that SiH<sub>4</sub> and CH<sub>3</sub>SiH<sub>3</sub> have vapor pressures higher than propane and, had they been formed, would have been recovered in the gas fractions. There was no indication of SiH<sub>4</sub> or CH<sub>3</sub>SiH<sub>3</sub> among the radiolysis products. The *G* yields of the principal carbosilanes, (CH<sub>3</sub>)<sub>3</sub>SiC<sub>2</sub>H<sub>5</sub>, (CH<sub>3</sub>)<sub>3</sub>SiSi(CH<sub>3</sub>)<sub>3</sub>, (CH<sub>3</sub>)<sub>3</sub>SiCH<sub>2</sub>Si(CH<sub>3</sub>)<sub>3</sub>, and (CH<sub>3</sub>)<sub>3</sub>SiCH<sub>2</sub>CH<sub>2</sub>Si(CH<sub>3</sub>)<sub>3</sub>, are reported in Table I and, from

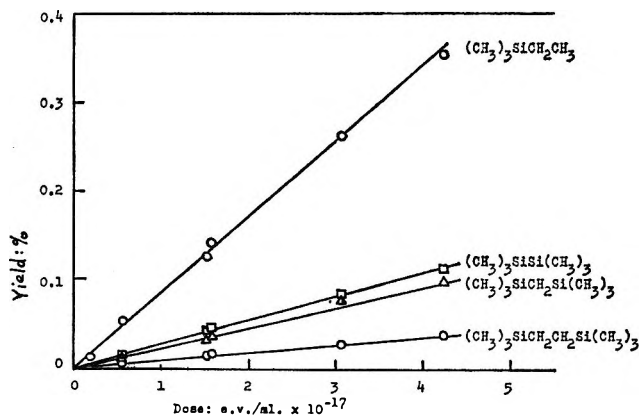


Figure 3. Effect of dose on the yields of principal carbosilanes in the radiolysis of pure tetramethylsilane at 150 Torr and 25°.

Figure 3, may be seen to be dose independent. Inasmuch as these products are completely removed by the addition of free radical scavengers, they are probably formed from CH<sub>3</sub>·, (CH<sub>3</sub>)<sub>3</sub>Si·, and (CH<sub>3</sub>)<sub>3</sub>SiCH<sub>2</sub>· precursors *via* combination reactions. The remaining carbosilanes, (CH<sub>3</sub>)<sub>3</sub>SiC<sub>3</sub>H<sub>7</sub> and (CH<sub>3</sub>)<sub>3</sub>SiSi(CH<sub>3</sub>)<sub>2</sub>C<sub>2</sub>H<sub>5</sub>, are obtained in small yields and could arise from secondary reactions involving the principal carbosilanes. It should be noted that these product yields are only slightly affected by pressure.

In the presence of oxygen, the main silicon-containing compounds are hexamethyldisiloxane and methoxytrimethylsilane, suggesting that CH<sub>3</sub>· and (CH<sub>3</sub>)<sub>3</sub>Si· are the predominant free radical precursors in this system. Small yields of hexamethyldisiloxane were obtained

**Table II:** Radiolysis of TMS-*d*<sub>12</sub> and 1:1 TMS:TMS-*d*<sub>12</sub> Mixture.  
(Relative Yields with Respect to TMS Radiolysis.<sup>a</sup> Dose:  $2.32 \times 10^{17}$  eV/ml; Pressure: 300 Torr)

Reactant	TMS- <i>d</i> <sub>12</sub>	1:1 TMS and TMS- <i>d</i> <sub>12</sub>	Scavenger	
			TMS- <i>d</i> <sub>12</sub> O <sub>2</sub> (6.3%)	1:1 TMS and TMS- <i>d</i> <sub>12</sub> O <sub>2</sub> (5.9%)
Hydrogen	0.556	0.867	0.548	0.773
Methane	1.05	1.00	0.609	0.732
Ethane	1.12	1.04	0.54	...
Ethyltrimethylsilane	0.539	0.878		
Propyltrimethylsilane	0.638	0.785		
Hexamethyldisilane	0.978	0.956		
2,2,4,4-Tetramethyl- 2,4-disilapentane	0.503	0.669		
Ethylpentamethyldisilane	1.10	1.10		
2,2,5,5-Tetramethyl- 2,5-disilahexane	0.244	0.475		
Methoxytrimethylsilane			...	0.74
Hexamethyldisiloxane			1.12	0.84

<sup>a</sup> All yields have been normalized by dividing by the appropriate yield from Table I (column 6).

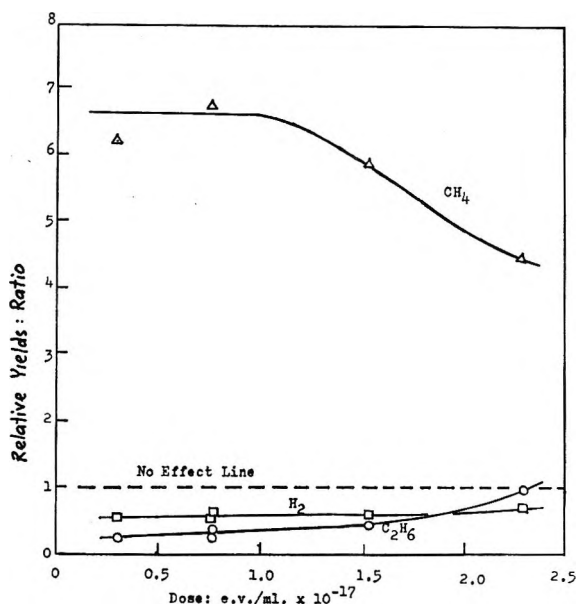


Figure 4. Relative yields in the radiolysis of tetramethylsilane containing 0.3% impurities with respect to pure tetramethylsilane.

even after extensive degassing of the TMS and prolonged evacuation (12 hr) of the reactor. It would appear that reactive oxygen was available in small amounts from the walls of the vessel.

The original impurities present in TMS at a concentration of 0.3% have a pronounced effect on the product distribution obtained from radiolysis. On the basis of mass spectral identification the impurities were trimethylsilane, vinyltrimethylsilane, ethyldimethylsilane, and cyclotetramethylenesilane. The yields of the major product gases, H<sub>2</sub>, CH<sub>4</sub>, and C<sub>2</sub>H<sub>6</sub>, increase nonlinearly with time (dose) in the presence of these impurities. Comparisons, presented in Figure 4, show the yields of hydrogen and ethane to be lower and methane to be 6.5 times higher than in the radiolysis of

pure TMS. The higher methane yield may be attributed to a rapid hydrogen abstraction reaction between methyl radicals and the reactive impurities containing secondary and tertiary hydrogens. The decreased ethane yield is consistent with a lower methyl radical concentration. The reduced hydrogen yield increases after the removal of vinyltrimethylsilane is complete.

*Radiolysis of TMS-*d*<sub>12</sub> and 1:1 TMS and TMS-*d*<sub>12</sub>.* The radiolysis of TMS-*d*<sub>12</sub> and the 1:1 mixture of TMS and TMS-*d*<sub>12</sub> was studied in the absence and presence of free radical scavengers. The yields of methane, ethane, and hexamethyldisilane are reported in Table II and may be seen to be unaffected by isotopic substitution when compared with the data in Table I. Hydrogen and products that require a single trimethylsilylmethyl radical precursor are lower from TMS-*d*<sub>12</sub> than from TMS by slightly more than 50%. Furthermore, the dimer formed by combination of two trimethylsilylmethyl radicals is reduced to 25% of the TMS yield by isotopic substitution, consistent with a 50% reduction of the trimethylsilylmethyl radical concentration in the TMS-*d*<sub>12</sub> system. The total yields from the radiolysis of the 1:1 mixture of TMS and TMS-*d*<sub>12</sub> are approximately equal to the average yields calculated from TMS and TMS-*d*<sub>12</sub> alone.

The isotopic distribution of several fractions from the radiolysis of 1:1 TMS and TMS-*d*<sub>12</sub> was determined mass spectrometrically and is reported in Table III. The high yields of H<sub>2</sub> and HD are consistent with a predominantly thermal H and D atom abstraction mechanism, *i.e.*

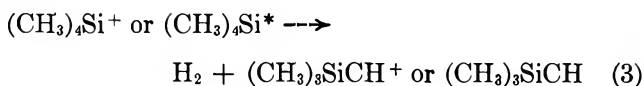


with a normal isotope effect, H favored over D, in both reactions 1 and 2. In the presence of oxygen, reaction

**Table III:** Isotopic Distribution of Major Gases in the Radiolysis of TMS- $d_{12}$  and 1:1 TMS- $d_{12}$ -TMS Mixture. (Dose:  $2.32 \times 10^{17}$  eV/ml; Pressure: 300 Torr)

	Reactant			
	TMS- $d_{12}$	1:1 TMS:TMS- $d_{12}$		1:1 TMS:TMS- $d_{12}$
		Scavenger		
	Hydrogen, %			
	Methane, %			
	Ethane, %			
H <sub>2</sub>		49.4	2.4	48.6
HD	13.7	42.7	2.7	17.7
D <sub>2</sub>	86.3	7.9	94.9	33.7
CH <sub>4</sub>		34.9		39.8
CH <sub>3</sub> D		3.8		6.8
C <sub>2</sub> H <sub>2</sub> D <sub>2</sub>		≤13.4		≤9.0
CHD <sub>3</sub>	10.5	23.3	0.0	8.1
CD <sub>4</sub>	89.5	24.6	100.0	36.3
C <sub>2</sub> H <sub>6</sub>		18.6		
C <sub>2</sub> H <sub>5</sub> D		0.0		
C <sub>2</sub> H <sub>4</sub> D <sub>2</sub>		≤4.8		
C <sub>2</sub> H <sub>3</sub> D <sub>3</sub>		46.3		
C <sub>2</sub> H <sub>2</sub> D <sub>4</sub>		≤2.6		
C <sub>2</sub> HD <sub>3</sub>	2.2	1.3		
C <sub>2</sub> D <sub>6</sub>	97.8	26.4		

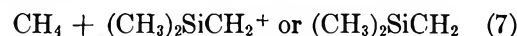
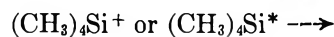
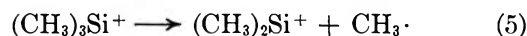
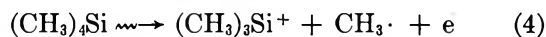
2 would be totally suppressed for both H and D atoms. Any resultant hydrogen formed under these conditions must arise from rapid, unscavengable reactions involving ions, excited molecules and/or "hot" intermediates. Because H<sub>2</sub> and D<sub>2</sub> predominate among the hydrogens formed in the presence of oxygen, molecular elimination reactions must occur in the system. However, these experiments are insufficient to identify the precursor as ionic or neutral and, therefore, the reaction is written ambiguously as



where the asterisk denotes electronic excitation of the neutral molecule. Although it is necessary to postulate reaction 3 to account for the high yields of H<sub>2</sub> and D<sub>2</sub> in the presence of oxygen, molecular elimination reactions cannot account for the totality of unscavengable hydrogen. The yield of HD under these conditions (17.7%) is much too large to be attributed to TMS- $d_{11}$  impurity and requires a rapid, intermolecular reaction for explanation. While these experiments cannot uniquely identify this reaction, one possibility is that reactions analogous to (1) and (2) involving translationally "hot" hydrogen atoms, *i.e.*, H·\*, are the most probable explanation. On this basis the authors estimate 81% of the hydrogen arises from thermal atoms, 7% from "hot" H atoms, and 12% by molecular elimination. Another possibility, suggested by a

referee, is that oxygen participates in a chain reaction with silyl-type radicals to produce HD (and, of course, H<sub>2</sub> and D<sub>2</sub>) in a manner analogous to the mechanism proposed by Nay, Woodall, Strausz, and Gunning<sup>5</sup> for NO inhibition. While this sequence cannot be ruled out as contributing to the hydrogen production in the presence of O<sub>2</sub>, the contribution cannot be a major one. The *G* yields of siloxanes, Table I, are too small to support a free radical chain mechanism and, contrary to the observations using NO scavenger (Table II, ref 6), hydrogen is suppressed by the addition of O<sub>2</sub>.

The distribution of the methane fraction from the radiolysis of 1:1 TMS-TMS- $d_{12}$  in the presence of oxygen suggests that a large fraction of the methane (73% in the mixture) is formed by unscavengable reactions and, further, that these are largely molecular elimination reactions. The remaining 27% of the methane probably arises from thermal methyl radicals undergoing hydrogen abstraction reactions. The reactions which may be postulated are



In addition, the yields of CH<sub>3</sub>D and CD<sub>3</sub>H in the presence of oxygen suggest an intermolecular reaction which is not scavenged, probably the "hot" methyl analog of reaction 6. These data suggest that 40% of the methane arises from molecular elimination, reaction 7, 25% from "hot" methyl radical abstraction reactions, and the remainder from thermal methyl radical reactions, such as reaction 6, in the radiolysis of pure TMS.

Because reaction 6 is known<sup>17</sup> to have an appreciable activation energy, 10.3 kcal/mol, other reactions might be expected to compete in the removal of methyl radicals from the system. Thus, ethane formation could arise from methyl radical combination reactions, *i.e.*



Because the ethane is almost completely scavenged in the presence of oxygen (Table I) and the isotopic ethanes are statistically distributed among the  $d_6$ ,  $d_3$ , and  $d_0$  compounds, reaction 8 is postulated as the source of ethane. Since the yields of ethane- $d_6$  and ethane- $d_0$  are essentially equal, the stationary-state concentrations of CH<sub>3</sub>· and CD<sub>3</sub>· must be nearly equal, implying the absence of a significant isotope effect for reactions 4 and 5 and their neutral analogs.

Ethylene, acetylene, propane, and propylene were obtained in such low yields that analysis for isotopic

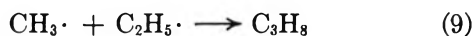
(17) E. R. Morris and J. C. J. Thynne, *J. Phys. Chem.*, **73**, 3294 (1969).

**Table IV:** Isotopic Distribution of Principal Carbosilanes in Radiolysis of 1:1 TMS:TMS- $d_{12}$  Mixture. (Dose:  $2.32 \times 10^{17}$  eV/ml; Pressure: 300 Torr)

Ethyltrimethylsilane	$-d_0$	$-d_1$	$-d_2$	$-d_3$	$-d_{11}$	$-d_{13}$	$-d_{14}$
%	38.3	4.7	9.3	37.4	4.7	0.93	4.7
Hexamethyldisilane	$-d_0$	$-d_3$	$-d_6$	$-d_9$	$-d_{12}$	$-d_{15}$	$-d_{18}$
%	17.2	4.8	4.8	39.4	5.4	5.2	23.2
2,2,4,4-Tetramethyl- 2,4-disilapentane <sup>a</sup>	$-d_0$	$-d_3$	$-d_{11}$	$-d_{20}$			
%	39.4	43.0	9.7	7.9			
2,2,5,5-Tetramethyl- 2,5-disilahexane	$-d_0$	$-d_3$	$-d_{11}$	$-d_{22}$			
%	65.4	11.5	23.1	Nd			

<sup>a</sup> Distribution relative to four compounds indicated.

distribution was not feasible. Although little can be said about the origins of most of these minor products, the fact that 90% of the propane is scavenged by oxygen suggests a free radical formation reaction such as



with the ethyl radical arising from the internal scavenging of H atoms by ethylene, *viz.*

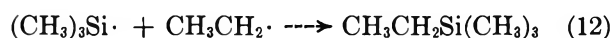
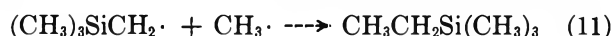


Because the unsaturated hydrocarbons are formed in the presence of oxygen with a yield approximately equivalent to the *initial G* yield in the absence of oxygen, the authors believe these products to arise from the primary radiolysis act and/or from rapid ion neutralization processes.

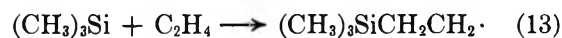
The isotopic distribution of the major silicon-containing compounds from the radiolysis of the equimolar TMS and TMS- $d_{12}$  mixture was determined by comparison of the mass spectra of the product gc peaks from the radiolysis of pure TMS, TMS- $d_{12}$ , and the equimolar mixture. Since the mass spectral patterns of these compounds indicated the loss of an alkyl group as the principal mode of parent ion fragmentation, it appeared justifiable to use this observation to estimate the distribution of the isotopic molecules. These estimates, assuming no isotope effect for alkyl fragmentation, are reported in Table IV. These estimates are probably too high for the perdeuterio and partially deuterated compounds because it is known<sup>18,19</sup> that perdeuterio methyl groups are eliminated 1.1 to 1.3 times more preferentially from TMS and hydrocarbons. In spite of the uncertainty of the analyses it is nonetheless instructive to consider the qualitative implications of the observations.

Of the carbosilanes, ethyltrimethylsilane is obtained in largest yield. The approximate equality of the  $d_0$  and  $d_3$  compounds, and the  $d_{11}$  and  $d_{14}$  compounds, reflects the equal  $\text{CH}_3\cdot$  and  $\text{CD}_3\cdot$  concentrations cited earlier and the pronounced isotope effect on the formation of trimethylsilylmethyl radical from the TMS- $d_{12}$

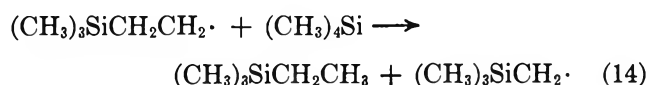
as compared to TMS. Thus, the low  $d_{11}$  and  $d_{14}$  are compatible with the low HD and D<sub>2</sub> yields from the 1:1 TMS-TMS- $d_{12}$  mixture. The significant yields of the  $d_1$ ,  $d_2$ , and  $d_{13}$  are indicative of at least one additional path for the formation of ethyltrimethylsilane. The following reactions are congruous with the observations.



The ethyl radical, formed by hydrogen scavenging, can introduce amounts of deuterium in the ethyltrimethylsilane which differ from the  $d_3$  introduced or lost *via* the methyl radical. However, the addition of trimethylsilyl radicals to ethylene, *viz.*



as suggested by Thynne<sup>20</sup> and followed by a hydrogen abstraction reaction, such as



can also account for the unexpected deuterioethyltrimethylsilanes. No decision can be reached regarding the various possible alternatives without additional experimental studies.

The carbosilane observed in second highest yield, hexamethyldisilane, appears to be formed almost exclusively by combination of trimethylsilyl radicals, *i.e.*



since there is a preponderance of the  $d_0$ ,  $d_9$ , and  $d_{18}$  compounds in almost exactly statistical distribution. However, the yields of the  $d_3$ ,  $d_6$ ,  $d_{12}$ , and  $d_{15}$  compounds, although small, are indicative of either methyl exchange or other modes of product formation. Since the hexamethyldisilane is totally scavenged by oxygen,

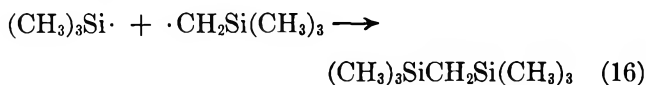
(18) F. E. Condon, *J. Amer. Chem. Soc.*, **73**, 4675 (1951).

(19) W. H. McFadden and A. Wahrhaftig, *ibid.*, **78**, 1572 (1956).

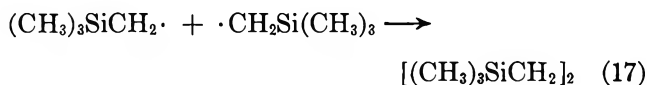
(20) J. C. J. Thynne, *J. Organometal. Chem.*, **17**, 155 (1969).

reactions which involve methylene or silene intermediates can probably be ruled out as the sole precursors to the  $d_3$ ,  $d_6$ ,  $d_{12}$ , and  $d_{15}$  compounds. Further speculation seems unwarranted at this time.

The isotopic distributions calculated for the remaining major carbosilane products,  $(\text{CH}_3)_3\text{SiCH}_2\text{Si}(\text{CH}_3)_3$  and  $[(\text{CH}_3)_3\text{SiCH}_2]_2$ , are in accord with simple free radical paths of formation, *viz.*

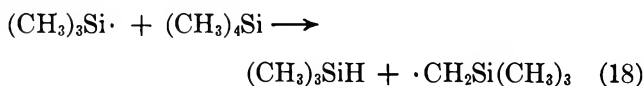


and

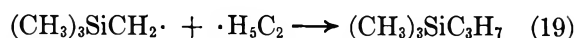


when it is borne in mind that  $(\text{CD}_3)_3\text{Si}\cdot$  and  $(\text{CH}_3)_3\text{Si}\cdot$  are in essentially equal concentrations whereas the concentration of  $(\text{CD}_3)_3\text{SiCD}_2\cdot$  is at least 50% lower than the concentration of  $(\text{CH}_3)_3\text{SiCH}_2\cdot$ . Thus, the failure to detect  $[(\text{CD}_3)_3\text{SiCD}_2]_2$  among the radiolysis products does not negate reaction 17 but, instead, reflects the low probability of two  $(\text{CD}_3)_3\text{SiCD}_2\cdot$  radicals combining under the conditions of the experiment.

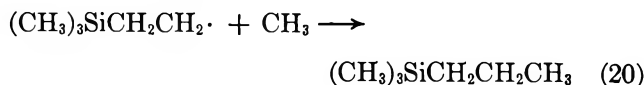
Although isotopic distributions could not be determined for the remaining carbosilanes, the following reactions do not seem unreasonable in light of the foregoing discussion. For the formation of trimethylsilane, the hydrogen abstraction by trimethylsilyl radicals



is probably responsible. Reaction 18 may be expected to have a rather large activation energy<sup>17</sup> in accord with the very low yields of trimethylsilane observed here. Propyltrimethylsilane can be attributed to the reaction of ethyl radicals with trimethylsilylmethyl radicals

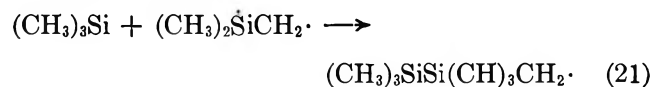


by analogy from reaction 12 or to the addition of a methyl radical to the trimethylsilylethyl radical formed from reaction 13, *viz.*



Similarly, ethylpentamethyldisilane could arise from secondary reactions of the hexamethyldisilane product or, alternately, from the addition of trimethylsilyl

radical to the diradical postulated as a product in reaction 7, *i.e.*



which reacts with methyl radicals to produce ethylpentamethyldisilane. It is interesting to note that the diradical postulated in reactions 7 and 21 has been suggested as the precursor of cyclic carbosilanes in the pyrolysis of TMS.<sup>21</sup> However, in the absence of dose dependency data or isotopic distributions of products from the 1:1 TMS-TMS- $d_{12}$  radiolysis no decision can be reached regarding reactions 19, 20, and 21 and their alternatives.

Finally, it should be mentioned that a careful study of the effect of pressure on the mass spectrum of TMS accompanied this research, the details of which are reported elsewhere.<sup>22</sup> It is sufficient here to simply point out that no evidence for ion-molecule reactions could be found. Except for a diminution of the parent peak attributed to a collision-induced fragmentation into  $(\text{CH}_3)_3\text{Si}^+$ , pressure effects were negligible up to over 1000  $\mu$  inlet pressure. The corresponding source pressure, estimated at 0.1  $\mu$ , should have permitted the detection of ion-molecule reactions with cross sections of the order of 1.0  $\text{\AA}^2$  without any difficulty. Although it is always dangerous to extrapolate from the low pressures in a mass spectrometer ion source to the higher pressures of the radiolysis experiments of Table I, the present measurements rule out the occurrence of rapid ion-molecule reactions in the tetramethylsilane system. The possible importance of ion-molecule reactions at high pressures, while deemed unlikely, cannot be ruled out. In the absence of high-pressure mass spectrometric studies of tetramethylsilane it seems reasonable to assume that the ions formed in the radiolysis of tetramethylsilane act primarily as the precursors for the radicals and atoms postulated to account for the radiolysis products.

*Acknowledgment.* The authors gratefully acknowledge the financial support provided by the U. S. Atomic Energy Commission. Mr. S. Wrbican is to be thanked for careful determination of product mass spectra. Also, Professor Yves Rousseau (University of Montreal), Professor C. H. Van Dyke, and Dr. David Lewis (Notre Dame) have participated in stimulating discussions which are gratefully acknowledged here.

(21) G. Fritz, J. Grobe, and D. Kummer, *Advan. Inorg. Radiochem.*, **7**, 364 (1965).

(22) J. Dedinas, "Radiation Chemistry of Tetramethylsilane," Ph.D. Thesis, Carnegie Institute of Technology, 1965.

## The Radiation Chemistry of Tetramethylsilane. II. Liquid Phase<sup>1</sup>

by Gilbert J. Mains<sup>2</sup> and Jonas Dedinas

Department of Chemistry, Carnegie-Mellon University, Pittsburgh, Pennsylvania (Received March 20, 1970)

The radiolysis of tetramethylsilane (TMS) liquid induced by 50-pkeV X-rays has been investigated at 25° in the dose range  $0.713 \times 10^{20}$  to  $3.56 \times 10^{20}$  eV/ml and compared with the previously reported vapor phase radiolysis study. The condensed phase was found to enhance the hydrogen abstraction reaction of methyl radicals resulting in an increased yield of methane,  $G(\text{CH}_4) = 4.8$ , and  $(\text{CH}_3)_2\text{SiCH}_2\text{CH}_2\text{Si}(\text{CH}_3)_3$  and  $(\text{CH}_3)_3\text{SiCH}_2\text{Si}(\text{CH}_3)_3$  products. Correspondingly, the yields of ethane and ethyltrimethylsilane are reduced in the liquid phase. The yields of internal scavengers,  $\text{C}_2\text{H}_4$ ,  $\text{C}_2\text{H}_2$ , and  $\text{C}_3\text{H}_6$ , are 50–100 times lower in the liquid phase, suggesting an electronically excited precursor. Nonhomogeneous radical distribution is suggested to account for product formation in the presence of scavengers.

### Introduction

Although the radiolysis of tetramethylsilane vapor has been reported in some detail by this laboratory,<sup>3</sup> corresponding studies of the liquid phase radiolysis have been restricted to the chemical effects of neutron capture<sup>4</sup> and an epr study of the radicals produced by the  $\gamma$  radiolysis<sup>5</sup> of solid TMS at 77°K. The latter study is especially interesting because of the detection of a weak signal attributed to  $(\text{CH}_3)_3\text{Si}\cdot$  in the intense  $(\text{CH}_3)_3\text{SiCH}_2\cdot$  signal. However, in order to obtain comparable data for product yields in the liquid phase, the investigation reported herein was undertaken.

It was deemed of special interest to compare the yields of unsaturated hydrocarbon radiolysis products,  $\text{C}_2\text{H}_4$ ,  $\text{C}_2\text{H}_2$ , and  $\text{C}_3\text{H}_6$ , with the corresponding yields in the vapor phase study. These internal free radical scavengers, found to achieve a steady-state concentration at very low conversion in the vapor phase radiolysis, were attributed to unspecified primary processes. Whether or not these primary processes, as well as those resulting in H atoms,  $\text{CH}_3\cdot$ ,  $(\text{CH}_3)_3\text{Si}\cdot$ , and  $(\text{CH}_3)_3\text{SiCH}_2\cdot$  radicals, were phase dependent could only be ascertained by a comparison study.

### Experimental Section

The radiation source has been described previously.<sup>3</sup> A constant dose rate,  $9.9 \times 10^{15}$  eV/(ml sec) as determined using the Fricke dosimeter,<sup>6,7</sup> was employed for all irradiations. The reaction vessel was a Pyrex cylinder, 12 mm in diameter, 2.8 cm in length, 0.1 to 0.2 mm wall thickness, and was equipped with a 5-mm transfer line at the top. This reactor, 2.35 ml in volume, was reproducibly positioned below the X-ray tube such that the beam was perpendicular to the cylinder axis. This design facilitated rapid evolution of gas from the zone of intense radiation.

The tetramethylsilane used for these studies was 99.9% pure as obtained from Peninsular ChemResearch Inc. The sole impurity detected by gc analysis was found to be inert on the basis of a negative bromination test. Degassed TMS was stored over Na and KOH

for 12 hr to remove  $\text{CO}_2$  and  $\text{H}_2\text{O}$ . Prior to distillation into the reaction vessel the TMS was degassed again by slow distillation at  $-130^\circ$ . Completion of degassing was checked using a Toepler pump. Free radical scavenger studies were made using either DPPH<sup>8</sup> (diphenylpicrylhydrazyl) or oxygen. The runs with  $\text{O}_2$  were carried out intermittently. Every 15 min the power supply to the X-ray tube was shut off and the reactor contents mixed to resaturate the liquid TMS with oxygen. The partial pressure of  $\text{O}_2$  was from 18 to 20 cm. Standard vacuum techniques were employed except for the absence of stopcock grease throughout the system. The irradiated samples were degassed at  $-196$  and  $-140^\circ$ . The gases and liquids were analyzed as previously described.<sup>3</sup>

One experiment was performed using a 1:1 mixture of TMS and TMS- $d_{12}$  in the presence of  $\text{O}_2$ . TMS- $d_{12}$  was purified as described earlier.<sup>3</sup> In this experiment three gas fractions were separated at  $-196$ ,  $-160$ , and  $-140^\circ$ , respectively. The first fraction was analyzed for  $\text{H}_2$ , HD,  $\text{D}_2$ ,  $\text{CH}_4$ ,  $\text{CD}_3\text{H}$ , and  $\text{CD}_4$ . Because of background water, no attempt was made to determine  $\text{CH}_3\text{D}$  and  $\text{CH}_2\text{D}_2$ . The second fraction contained only isotopically substituted  $\text{C}_2$  compounds and was successfully analyzed for the isotopic distributions of ethane and ethylene.

### Results and Discussion

*Effect of Dose.* The observed radiolysis products and their  $G$  yields (molecules/100 eV of absorbed energy)

- (1) Supported by U. S. AEC Contract No. AT(30-1)2007.
- (2) To whom correspondence should be addressed at Department of Chemistry, University of Detroit, Detroit, Mich. 48221.
- (3) G. J. Mains and J. Dedinas, *J. Phys. Chem.*, **74**, 3476 (1970).
- (4) D. K. Snediker, Ph.D. Thesis, Pennsylvania State University, University Park, Pa. 16802.
- (5) J. Roncin, *Mol. Cryst.*, **3**, 117 (1967).
- (6) J. W. T. Spinks and R. J. Woods, "An Introduction to Radiation Chemistry," John Wiley and Sons, New York, N. Y., 1964, p 111.
- (7) M. H. Back and N. Miller, *Nature*, **179**, 321 (1957).
- (8) A. Chapiro, *et al.*, *J. Chem. Phys.*, **50**, 468 (1958).

**Table I:** *G* Values of Products Obtained in Radiolysis of Liquid Tetramethylsilane by 50-pkeV X-Rays. Effect of Thermal Free Radical Scavengers

Reactants	Dose, eV ml <sup>-1</sup>		
	TMS 0.713-3.56 × 10 <sup>20</sup>	TMS and DPPH (sat.) 0.713 × 10 <sup>20</sup>	TMS and O <sub>2</sub> (20 cm) 0.713 × 10 <sup>20</sup>
Methane	4.8	2.8	1.1
Hydrogen	2.9	1.7	1.4
Ethane	0.71	0.53	0.49
Ethylene	0.026	0.035	0.12
Acetylene	0.0058	0.029	0.029
Propane	0.017	~0.0	0.015
Propylene	0.0065	0.0061	0.34
(CH <sub>3</sub> ) <sub>3</sub> SiCH <sub>2</sub> Si(CH <sub>3</sub> ) <sub>3</sub>	1.2	0.40	0.39
(CH <sub>3</sub> ) <sub>3</sub> SiCH <sub>2</sub> CH <sub>2</sub> (CH <sub>3</sub> ) <sub>3</sub>	1.2	<0.13	0.0
CH <sub>3</sub> CH <sub>2</sub> Si(CH <sub>3</sub> ) <sub>3</sub>	0.60	0.35	0.32
(CH <sub>3</sub> ) <sub>3</sub> SiSi(CH <sub>3</sub> ) <sub>3</sub>	0.26	0.15	0.20
C <sub>3</sub> H <sub>7</sub> Si(CH <sub>3</sub> ) <sub>3</sub>	0.068	...	...
CH <sub>3</sub> CH <sub>2</sub> Si(CH <sub>2</sub> ) <sub>2</sub> Si(CH <sub>3</sub> ) <sub>3</sub>	0.086	...	...
(CH <sub>3</sub> ) <sub>3</sub> SiH	0.083	...	...

are listed in Table I. The radiation yields are independent of dose over the range investigated, 0.713 × 10<sup>20</sup> to 3.56 × 10<sup>20</sup> eV/ml, and were calculated from the slopes of the lines in Figures 1 to 3, inclusive. The product distribution is significantly different from that obtained from gas-phase radiolysis.<sup>3</sup> Except for methane, all the gases were obtained in lower yields. This decrease is not unexpected in view of the increased quenching of excited species and the enhancement of geminate recombination in the liquid phase. The decrease in the hydrogen *G* yield from 8.6 to 2.9 suggests that a large fraction of the hydrogen arises from excited molecule precursors since cage effects are minimal for this substance. The high yield of methane, *G*<sub>CH<sub>4</sub></sub> = 4.8 as compared with 1.3 in the gas phase,

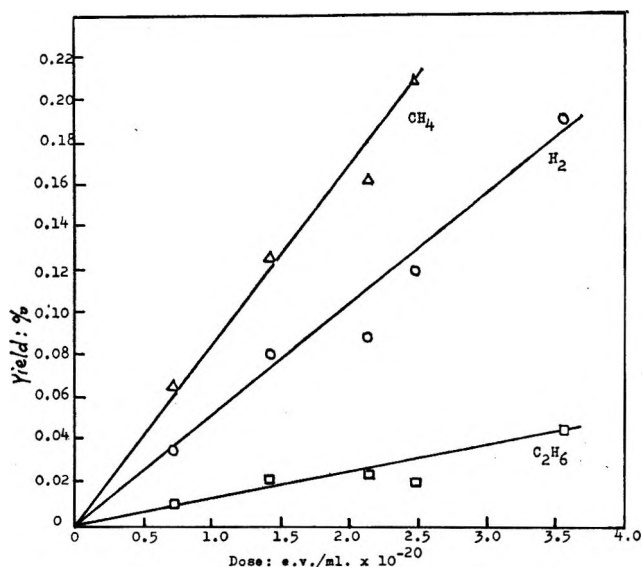


Figure 1. Effect of dose on the yields of principal gases.

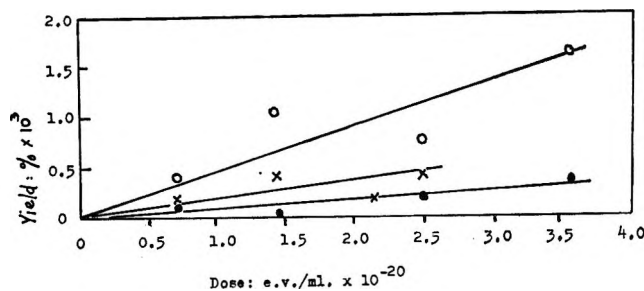
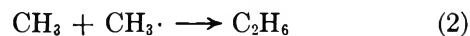


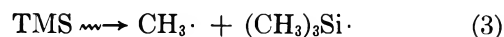
Figure 2. Effect of dose on the yields of unsaturated hydrocarbons: O, C<sub>2</sub>H<sub>4</sub>; X, C<sub>3</sub>H<sub>6</sub>; ●, C<sub>2</sub>H<sub>2</sub>.

reflects the competition between hydrogen abstraction and radical combination reactions such as (1) and (2).



Because of the higher concentration of TMS in the liquid phase, reaction 1 predominates over reaction 2 in spite of the lower activation energy of the latter. The relative importance of reaction 1 in the liquid phase is also suggested by the higher yield of dimer, (CH<sub>2</sub>)<sub>3</sub>-SiCH<sub>2</sub>CH<sub>2</sub>Si(CH<sub>3</sub>)<sub>3</sub>, *G* = 1.2 vs. 0.5-0.6, in the liquid phase. Correspondingly, the yield of ethane is significantly lower in the liquid phase.

Another important observation is the low yield of hexamethyldisilane in the liquid phase (*G* = 0.26). A much lower yield of (CH<sub>3</sub>)<sub>3</sub>Si· radicals is suggested in the liquid phase. Based upon the relative yields of hexamethyldisilane and dimer, the ratio of (CH<sub>3</sub>)<sub>3</sub>-Si·/(CH<sub>3</sub>)<sub>3</sub>SiCH<sub>2</sub>· is 1.7 in the gas phase and 0.46 in the liquid phase, values which are consistent with the ratio 0.02 estimated by Roncin<sup>5</sup> for solid TMS at 77°K. Assuming reaction 3 for the formation of trimethylsilyl radicals, *viz.*



reaction 4, geminate recombination, must be postulated to account for the reduced yield of trimethylsilyl radicals in the liquid. Both reactions 1 and 4 occur primarily within the solvent cage in which the radicals are formed and both processes might be expected to become important in the liquid phase. Thus, methyl radicals are consumed near their site of generation. This argument is consistent with the low yields of ethane and ethyltrimethylsilane in the liquid phase relative to the gas phase.

The *G* yields of unsaturated hydrocarbons are very low: *G*(C<sub>2</sub>H<sub>4</sub>) = 0.026, *G*(C<sub>2</sub>H<sub>2</sub>) = 0.0058, and *G*(C<sub>3</sub>-H<sub>6</sub>) = 0.0065. These yields are 50 to 100 times lower than the corresponding gas-phase yields, and a factor of 10 or more greater reduction than is observed for any of the other radiolysis products. On this basis, it appears that these hydrocarbon unsaturates arise

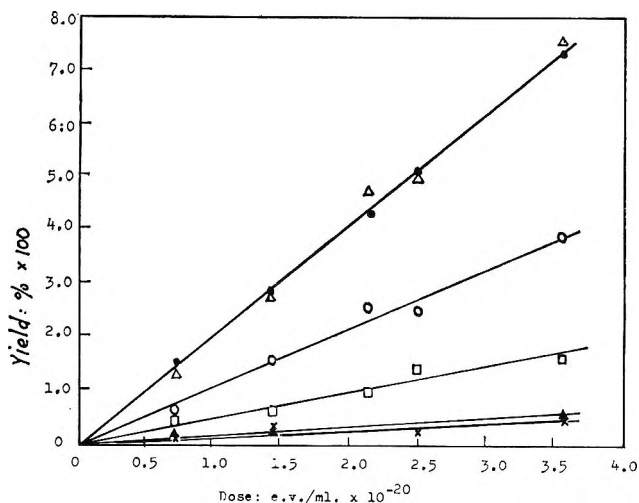


Figure 3. Effect of dose on the yields of carbosilanes:  $\Delta$ ,  $(\text{CH}_3)_3\text{SiCH}_2\text{Si}(\text{CH}_3)_3$ ;  $\bullet$ ,  $(\text{CH}_3)_3\text{SiCH}_2\text{CH}_2(\text{CH}_3)_3$ ;  $\circ$ ,  $\text{C}_2\text{H}_5\text{Si}(\text{CH}_3)_3$ ;  $\square$ ,  $(\text{CH}_3)_3\text{SiSi}(\text{CH}_3)_3$ ;  $\blacktriangle$ ,  $\text{C}_2\text{H}_5(\text{CH}_3)_2\text{SiSi}(\text{CH}_3)_3$ ; and  $\times$ ,  $\text{C}_3\text{H}_7\text{Si}(\text{CH}_3)_3$ .

primarily from electronically excited precursors which are quenched in the liquid phase.

**Effect of Scavengers.** Although it was realized that the concentration of scavengers in the liquid phase may be too low to remove all of the thermal free radicals efficiently, the study was carried out in the hope that qualitative information might be forthcoming which would provide insight into the reaction mechanism. DPPH has low solubility in TMS and, therefore, proved to be less effective as a scavenger than  $\text{O}_2$ . The  $G$  yields presented in Table I show that both  $\text{O}_2$  and DPPH reduce the yields of the major products.  $G$ - $(\text{CH}_4)$ , for example, is reduced from 4.8 to 2.8 by DPPH and to 1.1 by  $\text{O}_2$ . The unsaturated hydrocarbons,  $\text{C}_2\text{H}_4$  and  $\text{C}_2\text{H}_2$ , are obtained in higher yield in the presence of scavenger as was observed in the gas phase; however, the extent is much lower.

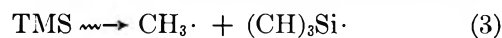
It is interesting to note that the yields of carbosilane products are about the same in the presence of either scavenger. The greatest effect is seen in the dimer yield which is essentially zero in the presence of scavenger. This suggests that one of the main high molecular weight products is produced by an entirely free radical mechanism. The other products,  $(\text{CH}_3)_3\text{SiCH}_2\text{Si}(\text{CH}_3)_3$ ,  $(\text{CH}_3)_3\text{SiSi}(\text{CH}_3)_3$ , and  $\text{C}_2\text{H}_5\text{Si}(\text{CH}_3)_3$ , are reduced to 32%, 58%, and 53% of the unscavenged yields by  $\text{O}_2$ . While these data may suggest nonradical mechanisms, especially since the same yields were obtained with both scavengers, there is the distinct possibility that the scavengers are not equally accessible to all the free radicals in the system because of track and cage effects.

**Radiolysis of 1:1 TMS-TMS- $d_{12}$  Mixture With  $\text{O}_2$ .** Only the gas fractions were analyzed in this experiment. The product distributions, presented in Table II, further substantiate the importance of free radical

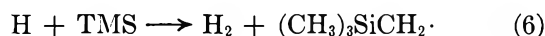
reactions in the radiolysis of TMS. The hydrogen fraction reveals a significant isotope effect,  $\text{D}_2$  being low and  $\text{H}_2$  being high. Furthermore, the HD yield is lower than expected from a random combination of H and D atoms suggesting the formation of molecular hydrogen and unscavengable H and D atom products. However, because it is not possible to assume complete scavenging of thermal H and D atoms in this system, no estimates can be made regarding the extent of molecular elimination and "hot" atom reactions.

The isotopic distribution of methanes also suggests the presence of radical reactions and an isotope effect for H atom abstraction. Again, because of the possibility of incomplete scavenging, no definite conclusions can be reached about the extent of the thermal radical, "hot" radical, and molecular elimination mechanisms of methane formation. The isotopic ethane yield, on the other hand, is consistent with a random combination of  $\text{CH}_3\cdot$  and  $\text{CD}_3\cdot$  radicals and supports incomplete scavenging in this system. The ethylenes were predominately  $\text{C}_2\text{H}_4$  and  $\text{C}_2\text{D}_4$ , suggesting a molecular elimination mechanism for formation, consistent with the postulated excited electronic precursor.

**Distribution of Free Radicals.** The observation in Table I that oxygen completely eliminated the formation of dimer but only partially reduced the yields of  $(\text{CH}_3)_3\text{SiCH}_2\text{Si}(\text{CH}_3)_3$ ,  $\text{CH}_3\text{CH}_2\text{Si}(\text{CH}_3)_3$ , and  $[(\text{CH}_3)_3\text{Si}]_2$  suggests that the radical precursors are not homogeneously distributed throughout the solution and, hence, not equally accessible to  $\text{O}_2$ . The primary radiolysis process along the secondary electron tracks is



with reaction 5 predominating by a factor of 2 in the liquid phase. Because of their size, the H atoms mainly escape the solvent cage and react in the bulk liquid to abstract hydrogen *via* reaction 6.



Since reaction 6 occurs after the escape from the solvent cage, the distribution of  $(\text{CH}_3)_3\text{SiCH}_2\cdot$  radicals is essentially random. On the other hand, the methyl radicals which produced reaction 3 are too bulky to escape the cage readily and reactions 1 and 4 are likely within or very near the solvent cage of formation. Thus, there is a rather high probability that a  $(\text{CH}_3)_3\text{Si}\cdot$  will find a  $(\text{CH}_3)_3\text{SiCH}_2\cdot$  in its immediate environment as a result of reaction 1. On this basis it is easy to understand why  $[(\text{CH}_3)_3\text{SiCH}_2]_2$  is completely suppressed by small amounts of  $\text{O}_2$  whereas  $(\text{CH}_3)_3\text{SiCH}_2\text{Si}(\text{CH}_3)_3$  is not.

While the cage effect can adequately explain the effect of  $\text{O}_2$  on the dimer and  $(\text{CH}_3)_3\text{SiCH}_2\text{Si}(\text{CH}_3)_3$  formation, it cannot readily explain the formation of  $(\text{CH}_3)_3\text{SiSi}(\text{CH}_3)_3$  and ethyltrimethylsilane in the pres-

**Table II:** Product Distribution in Radiolysis of 1:1 TMS and TMS- $d_{12}$  in the Presence of Oxygen (18 cm)  
(Dose,  $0.713 \times 10^{20}$  eV ml $^{-1}$ )

Hydrogen %	H <sub>2</sub> 56.9	HD 32.2	D <sub>2</sub> 10.9				
Methane	CH <sub>4</sub> :CD <sub>3</sub> H:CD <sub>4</sub> = 2.30:1.00:0.684						
Ethane %	C <sub>2</sub> H <sub>6</sub> 39.5	C <sub>2</sub> DH <sub>5</sub> 0.0	C <sub>2</sub> D <sub>2</sub> H <sub>4</sub> 0.0	CD <sub>3</sub> H <sub>3</sub> 44.6	CD <sub>4</sub> H <sub>2</sub> 0.0	C <sub>2</sub> D <sub>5</sub> H 0.3	C <sub>2</sub> D <sub>6</sub> 15.6
Ethylene %	C <sub>2</sub> H <sub>4</sub> 55.5	C <sub>2</sub> DH <sub>3</sub> 0.0	C <sub>2</sub> D <sub>2</sub> H <sub>2</sub> 10.5	C <sub>2</sub> D <sub>3</sub> H 0.0	C <sub>2</sub> D <sub>4</sub> 34.0		

ence of O<sub>2</sub>. Ethyltrimethylsilane can be attributed to incomplete quenching of reaction 7



by O<sub>2</sub> in the radiation track. A similar explanation can be offered to explain [(CH<sub>3</sub>)<sub>3</sub>Si]<sub>2</sub> formation along the radiation track. It should be noted that unscavengable insertion reactions of CH<sub>2</sub> and (CH<sub>3</sub>)<sub>2</sub>Si might be invoked to explain the observations. However, the recent observation of Bowrey and Purnell<sup>9</sup> that SiH<sub>2</sub> does not insert into TMS would appear to rule out this

mechanism for the formation of (CH<sub>3</sub>)<sub>3</sub>SiSi(CH<sub>3</sub>)<sub>3</sub>. Under the circumstances it seems advisable to await additional studies rather than speculate further.

*Acknowledgment.* This research was performed under the auspices of the U. S. Atomic Energy Commission and grateful acknowledgement is made thereto. Mr. S. Wrbican is thanked for careful determinations of the mass spectra used in this research.

(9) M. Bowrey and J. H. Purnell, *J. Amer. Chem. Soc.*, **92**, 2594 (1970).

## The Yield of Thermal Hydrogen Atoms from the

### $\gamma$ Radiolysis of Liquid 2,2,4-Trimethylpentane<sup>1</sup>

by Krishan M. Bansal and Stefan J. Rzad

Radiation Research Laboratories, Mellon Institute, Carnegie-Mellon University, Pittsburgh, Pennsylvania 15213  
(Received April 20, 1970)

In the  $\gamma$  radiolysis of 2,2,4-trimethylpentane, the decrease in the hydrogen yield observed upon the addition of ethylene is equal to the yield of ethyl radicals. This result is interpreted in terms of simple scavenging of thermal hydrogen atoms by ethylene since complications arising from the positive ion reactions of the latter do not appear to occur. The lack of ionic complications in this system is also supported by the absence of positive ion reactions with cyclopropane. A treatment of the data accordingly gives a yield of thermal hydrogen atoms ( $G(\text{H})_0$ ) of 1.0 and a ratio of rate constants for the abstraction of hydrogen atom from the solvent to the addition to ethylene of 0.0043.

#### Introduction

In several studies, ethylene has been used as a thermal hydrogen atom scavenger and the ethyl radicals thus produced have been measured with the <sup>14</sup>C-methyl radical sampling technique<sup>2</sup> or by titration with iodine.<sup>3,4</sup> The yields of thermal hydrogen atoms determined in cyclohexane radiolysis by these two methods are 1.80<sup>2</sup> and 1.46.<sup>4</sup> The latter measurement seems more accurate since the absolute yield of the ethyl radicals is measured directly. In such studies the inter-

pretation of the data is difficult because complications arising from the participation of ethylene in ionic reactions are known to occur, at least in the case of cyclohexane.<sup>4</sup> Preliminary experiments have shown that cyclopropane does not undergo positive ion reactions in

(1) Supported in part by the U. S. Atomic Energy Commission.

(2) R. A. Holroyd, *J. Phys. Chem.*, **70**, 1341 (1966).

(3) J. L. McCrumb and R. H. Schuler, *ibid.*, **71**, 1953 (1967).

(4) K.-D. Asmus, J. M. Warman, and R. H. Schuler, *ibid.*, **74**, 246 (1970).

2,2,4-trimethylpentane. This observation is further substantiated by the absence of an effect of cyclopropane on the hydrogen yield. Since the positive ion reactions of cyclopropane and ethylene are analogous, one can expect the absence of such reactions in 2,2,4-trimethylpentane. This simplifies greatly the interpretation of the mode of ethyl radical formation, and as a result the kinetic parameters derived from the treatment of the experimental data are expected to be more reliable. These observations prompted us to determine the thermal hydrogen atom yield and the ratio of rate constants for the abstraction of hydrogen atom from the solvent to the addition to ethylene in the radiolysis of 2,2,4-trimethylpentane using the iodine titration method.

### Experimental Section

Phillips Research grade 2,2,4-trimethylpentane was purified to remove the olefinic impurities by passage through an activated silica gel column. Ethylene, sulfur hexafluoride, nitrous oxide, and cyclopropane were outgassed and distilled at  $-80^\circ$  and stored. Radioiodine ( $^{131}\text{I}_2$ ) was prepared in a manner described elsewhere.<sup>5</sup>

A known amount of 2,2,4-trimethylpentane (5 cm<sup>3</sup>) containing radioiodine ( $\sim 5 \times 10^{-4}$  M) of known specific activity was outgassed by three freeze-pump-thaw cycles. To this a known amount of the solute, determined by a pressure-volume measurement, was added. The sample was sealed off the vacuum line in such a way that the vapor volume was  $\sim 0.5$  cm<sup>3</sup>. The concentration of the solute in 2,2,4-trimethylpentane was calculated on the assumption of complete solubility. The samples were irradiated in a tubular  $^{60}\text{Co}$   $\gamma$ -ray source. The dose rate, determined by the Fricke dosimeter and corrected for electron density differences, was  $6 \times 10^{16}$  eV cm<sup>-3</sup> min<sup>-1</sup> in 2,2,4-trimethylpentane. The dose received by the sample was usually  $3 \times 10^{17}$  eV cm<sup>-3</sup>. After irradiation, 0.5 cm<sup>3</sup> of the sample was chromatographed, the ethyl iodide fraction was collected, and the total activity in this fraction was determined by a method similar to that reported in studies of scavenging of methyl radicals.<sup>5</sup>

For experiments in which the gases noncondensable at liquid nitrogen temperature were measured, 5 cm<sup>3</sup> of the purified and outgassed 2,2,4-trimethylpentane containing a known amount of the scavenger was irradiated to a total dose of  $3 \times 10^{18}$  eV cm<sup>-3</sup> at a dose rate of  $3 \times 10^{17}$  eV cm<sup>-3</sup> min<sup>-1</sup> in the 2,2,4-trimethylpentane. After irradiation, the gases noncondensable at liquid nitrogen temperature were collected in a Toepler-McLeod apparatus and subsequently analyzed by mass spectrometry. In certain experiments, 2,2,4-trimethylpentane was dried over sodium mirror and the dissolved CO<sub>2</sub> was removed by pumping at room temperature.

<sup>14</sup>C-Cyclopropane, of known specific activity, was purified by gas chromatography.<sup>6</sup> Then, 1 cm<sup>3</sup> of

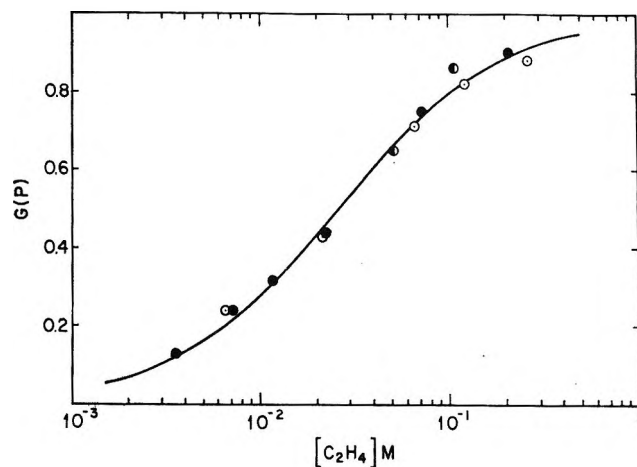


Figure 1. Yield of products as a function of ethylene concentration in the  $\gamma$  radiolysis of 2,2,4-trimethylpentane-ethylene solutions:  $\circ$ ,  $\Delta G(\text{H}_2)$ ;  $\bullet$ ,  $G(\text{C}_2\text{H}_5\text{I})$ ;  $\ominus$ ,  $G(\text{C}_2\text{H}_5\text{I})$  in the presence of 0.31 M cyclopropane. The solid line is calculated using eq I as described in the text.

2,2,4-trimethylpentane, dried over sodium, degassed, and stored on the vacuum line, was transferred into the irradiation cell. To this a known amount of <sup>14</sup>C-cyclopropane, determined by a pressure-volume measurement, was added. After sealing of the vacuum line the vapor volume was  $\sim 0.2$  cm<sup>3</sup>. The samples were irradiated in a tubular  $^{60}\text{Co}$   $\gamma$ -ray source to a total dose of  $3.2 \times 10^{18}$  eV. The dose rate was  $3.2 \times 10^{17}$  eV cm<sup>-3</sup> min<sup>-1</sup> in 2,2,4-trimethylpentane. The radiochromatographic analysis of the <sup>14</sup>C-containing products has been previously described.<sup>6,7</sup>

### Results

The hydrogen yield from the  $\gamma$  radiolysis of pure 2,2,4-trimethylpentane, carefully degassed to remove any dissolved CO<sub>2</sub> by pumping at room temperature, was found to be 2.44 and independent of the dose over the range  $1.5 \times 10^{18}$  to  $6 \times 10^{18}$  eV cm<sup>-3</sup>. This is slightly higher than the values of 2.34<sup>5</sup> and 2.20<sup>8,9</sup> reported in the literature. An identical hydrogen yield (2.44) was obtained from samples dried over sodium.

The addition of ethylene results in a decrease of the hydrogen yield. The ethylene concentration dependence of this decrease ( $\Delta G(\text{H}_2)$ ) is shown in Figure 1. Cyclopropane had virtually no effect on the yield of hydrogen. Two experiments at 0.13 and 0.35 M cyclopropane both gave a yield of hydrogen of 2.40 which should be compared with the value of 2.44 obtained in the pure solvent.

Ethyl radicals produced upon irradiation of 2,2,4-trimethylpentane-ethylene solutions were measured as

- (5) R. H. Schuler and R. R. Kuntz, *J. Phys. Chem.*, **67**, 1004 (1963).
- (6) S. J. RZad and R. H. Schuler, *ibid.*, **72**, 228 (1968).
- (7) J. M. Warman and S. J. RZad, *J. Chem. Phys.*, **52**, 485 (1970).
- (8) J. A. Knight, R. L. McDaniel, and F. Sicilio, *J. Phys. Chem.*, **67**, 2273 (1963).
- (9) T. Kudo, *ibid.*, **71**, 3681 (1967).

ethyl iodide and the variation of the yield of the latter as a function of ethylene concentration is shown in Figure 1. The presence of 0.31 *M* of cyclopropane did not affect the yield of ethyl iodide as illustrated in Figure 1.

The irradiation of 2,2,4-trimethylpentane-<sup>14</sup>C-cyclopropane solutions resulted in the formation of only a small yield of radioactive propane. No high boiling radioactive products (*e.g.*, propyloctanes) were observed as had been found in the radiolysis of cyclohexane-<sup>14</sup>C-cyclopropane mixtures.<sup>6</sup> This <sup>14</sup>C-propane yield is given in Table I for different concentrations of cyclopropane in the presence and absence of electron scavengers.

**Table I:** Yields of <sup>14</sup>C Products in the Radiolysis of Solutions of <sup>14</sup>C-Cyclopropane in 2,2,4-Trimethylpentane and Cyclohexane

Solute	[S], mM	[Δ], mM	<i>G</i> ( <sup>14</sup> C <sub>3</sub> H <sub>8</sub> )	<i>G</i> ( <sup>14</sup> C products) <sup>b</sup>
		1.2	0.039 <sup>a</sup>	0.18
		10	0.039	0.33
		11	0.026	0.34
		56	0.058	0.59
		113	0.071	0.77
CH <sub>3</sub> Br	100	1.3	0.023	0.42
CCl <sub>4</sub>	208	1.2	0.044	0.41
	208	1.2	0.017	0.41

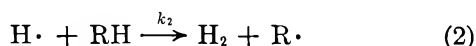
<sup>a</sup> This yield corresponds to 4459 counts with an accuracy of  $\pm 50$  counts. No high boiling <sup>14</sup>C-containing compounds were found in the 2,2,4-trimethylpentane solutions. <sup>b</sup> Yield of <sup>14</sup>C products (C<sub>3</sub>H<sub>8</sub> + C<sub>3</sub>H<sub>7</sub>C<sub>4</sub>H<sub>11</sub>) in cyclohexane.<sup>14</sup>

## Discussion

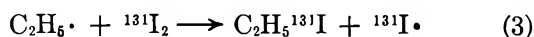
The thermal hydrogen atoms produced in the  $\gamma$  radiolysis of 2,2,4-trimethylpentane-ethylene solutions can either add to ethylene (reaction 1) to produce ethyl



radicals or abstract a hydrogen atom from the solvent (reaction 2). The ethyl radicals produced in reaction 1



can then be scavenged by radioiodine



which has been shown to be a very efficient radical scavenger.<sup>5</sup> Therefore, the quantitative measurements of the ethyl iodide yield will, in turn, give the yield of thermal hydrogen atoms provided there are no other sources of ethyl radicals and that ethylene does not react with the precursors of the hydrogen atoms. However, it has been shown that in hydrocarbons<sup>10-12</sup> ethylene also participates in positive ion reactions which not only affect the hydrogen yield formation by interfering with the neutralization processes but also contribute to the production of ethyl radicals.<sup>4</sup> Fortu-

nately, these complications do not seem to occur in 2,2,4-trimethylpentane since it has been shown that in this case the reactions of primary positive ions with ethylene, such as occur in cyclohexane,<sup>4,12</sup> do not take place.<sup>13</sup>

Bearing in mind the similarity between the ionic reactions of ethylene and cyclopropane<sup>4,10-12</sup> the above-mentioned conclusion is further substantiated by the results presented in Table I. The yield of radioactive propane ( $\sim 0.05$ ), obtained over a cyclopropane concentration range between  $1.2 \times 10^{-3}$  and 0.1 *M*, is much smaller than the yield given in the last column of Table I. This latter yield is the yield of positive ion reaction in cyclohexane at the given concentration of cyclopropane.<sup>14</sup> Moreover, it has been shown that the presence of scavenger increases the yield of the positive ion reaction by increasing the ion-pair lifetimes. This results from the conversion of more rapidly diffusing electrons to more slowly diffusing negative ions.<sup>10,14</sup> Data in Table I show, however, that the yield of radioactive propane is essentially unaffected by the presence of efficient scavengers such as CH<sub>3</sub>Br and CCl<sub>4</sub>.<sup>4,7</sup> This absence of positive ion reaction in 2,2,4-trimethylpentane-cyclopropane solutions is also reflected by the lack of an effect of cyclopropane on the hydrogen yield, which is known to arise at least partly from ionic processes,<sup>4</sup> and by the unchanged yield of ethyl iodide upon addition of cyclopropane to 2,2,4-trimethylpentane-ethylene solutions. The fact that cyclopropane or ethylene do not react with positive ions in 2,2,4-trimethylpentane can be understood if one considers the type of reactions both solutes undergo in cyclohexane. It has been shown that the reactions occurring between the positive ion of the latter and cyclopropane or ethylene consist of an H<sub>2</sub> transfer to give propane<sup>6,11</sup> or ethane,<sup>11,13</sup> of an H transfer to give propyl<sup>6,11</sup> or ethyl<sup>4,11,13</sup> radicals and of a "condensation reaction" giving rise to propylcyclohexane<sup>6</sup> or ethylcyclohexane.<sup>13,15</sup> No contribution from charge transfer

(10) A. A. Scala, S. G. Lias, and P. Ausloos, *J. Amer. Chem. Soc.*, **88**, 5701 (1966).

(11) P. Ausloos, A. A. Scala, and S. G. Lias, *ibid.*, **89**, 3677 (1967).

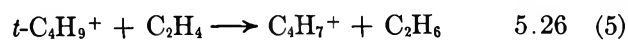
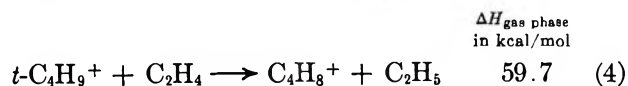
(12) S. J. Rzad, Abstracts, 158th National Meeting of the American Chemical Society, New York, N. Y., Sept 1969, p 239.

(13) G. Klein, private communication. Radioactive ethane with a yield less than 0.04 and no ethylisooctane were observed from a 0.05 *M* <sup>14</sup>C<sub>2</sub>H<sub>4</sub> solution in 2,2,4-trimethylpentane containing  $\sim 1.5 \times 10^{-3}$  *M* I<sub>2</sub>. A *G*(<sup>14</sup>C<sub>2</sub>H<sub>6</sub>I)  $\sim 0.50$  similar to that in this work was, however, obtained. For comparison, significant yields of radioactive ethane (*G* = 0.2) and ethyl cyclohexane (*G* = 0.2) were observed from a 0.04 *M* <sup>14</sup>C<sub>2</sub>H<sub>4</sub> solution in cyclohexane containing  $\sim 10^{-3}$  I<sub>2</sub>. In this experiment the yield of <sup>14</sup>C<sub>2</sub>H<sub>6</sub>I was  $\sim 0.6$ .

(14) S. J. Rzad, R. H. Schuler, and A. Hummel, *J. Chem. Phys.*, **51**, 1369 (1969). In the absence of electron scavengers this yield is calculated by eq 1 given in this reference. In the presence of electron scavenger this yield is determined from  $G(\text{P}) = G_{\text{fi}} + G_{\text{gi}}F(c_n, c_p)$  with  $F(c_n, c_p)$  given by eq 14. The parameters used in these equations are  $G_{\text{fi}} = 0.1$ ,  $G_{\text{gi}} = 3.8$ ,  $\tau_D = 17$ ,  $\alpha_{\Delta} = 0.4 \text{ M}^{-1}$  and  $\alpha_{\text{CH}_3\text{Br}} = \alpha_{\text{CCl}_4} = 16 \text{ M}^{-1}$ . These calculated values are those one would interpolate from the experimental data given in Figures 3 and 4 of the above reference.

(15) W. A. Cramer and G. J. Piet, *Trans. Faraday Soc.*, **63**, 1402 (1967).

should occur since the ionization potentials of cyclopropane (10.06 eV)<sup>16</sup> and ethylene (10.52 eV)<sup>16</sup> are higher than the ionization potential of cyclohexane (9.88 eV).<sup>16</sup> The ionization potential of 2,2,4-trimethylpentane being 9.86 eV,<sup>16</sup> charge transfer can also be ruled out in this case and the simplest explanation for the lack of reaction with the two solutes under consideration would be the nonoccurrence of H<sub>2</sub> and H transfers and of the "condensation reaction." However, there is no reason why these reactions should not occur in 2,2,4-trimethylpentane more so than they were found to occur in *n*-hexane,<sup>6</sup> cyclopentane,<sup>11</sup> and in 2-methylbutane and 3-methylpentane at 195°K.<sup>10</sup> On the other hand, Williams carried out thermochemical calculations which showed that C–C scission is energetically preferred for branched alkane ions whereas the corresponding dissociation of linear hydrocarbon ions is less favored.<sup>17</sup> More recently, the radiolysis of mixtures of methylamine in neopentane and 2,2,4-trimethylpentane has been interpreted in terms of a proton transfer from the *t*-C<sub>4</sub>H<sub>9</sub><sup>+</sup> fragment ion to the solute.<sup>18</sup> The present results are consistent with such a fragmentation of the 2,2,4-trimethylpentane primary ion to give the *t*-C<sub>4</sub>H<sub>9</sub><sup>+</sup> ion. If one considers, for example, the energetics<sup>19</sup> of the hydrogen transfer reactions to ethylene, one readily sees that while exothermic in cyclohexane they are not energetically favored in 2,2,4-trimethylpentane. Similar calculations can be performed in the cyclopropane case and the conclusion reached concerning the energetics of the reactions are identical (reaction 4, 54.2 kcal/mol; reaction 5, 0.44 kcal/mol; reaction 6, –35.56 kcal/mol).



From the results and arguments presented above one can conclude that since no ionic complications occur in the radiolysis of 2,2,4-trimethylpentane–ethylene solutions, the only source of ethyl radicals is the thermal hydrogen atoms addition to ethylene and therefore the problem is one of simple competition between reactions 1 and 2. The yield of ethyl radicals, measured as ethyl iodide, will then be given at any ethylene concentration by

$$G(\text{C}_2\text{H}_5\text{I}) = G(\text{H})_0 \left[ \frac{1}{1 + \frac{k_2[\text{RH}]}{k_1[\text{C}_2\text{H}_4]}} \right] \quad (I)$$

where  $G(\text{H})_0$  represents the yield of thermal hydrogen atoms in the pure solvent.  $[\text{RH}]$ , the solvent concentration, has a value of 6.06 *M* in the case of 2,2,4-trimethylpentane. According to eq I,  $1/G(\text{C}_2\text{H}_5\text{I})$  should be linearly dependent on  $1/[\text{C}_2\text{H}_4]$  and indeed such a

dependence is observed. From a best fit of eq I to the experimental data (solid line in Figure 1), the following parameters are obtained:  $G(\text{H})_0 = 1.00$  and  $k_2/k_1 = 0.0043$ . Holroyd<sup>2</sup> reported values of  $G(\text{H})_0 = 1.63$  and  $k_2/k_1 = 0.0063$ , which are much higher than the values found in the present study. The reason for such high values lies most probably in the indirect method used for their determinations. The rate constants ratio  $k_2/k_1 = 0.0043$  is very similar to that of 0.0048 reported for cyclohexane–ethylene solutions<sup>4</sup> and implies that the rate constant for hydrogen atom abstraction from both solvents is almost identical (provided of course that the rate constant for hydrogen atom scavenging by ethylene does not change with change in solvent). The relative probabilities of rupture of the primary, secondary, and tertiary C–H bonds reported to be 0.33:1.00:3.00, in hydrocarbons<sup>20</sup> (*e.g.*, isopentane) are in agreement with the observed similarity in hydrogen atom abstraction rate constants in cyclohexane and in 2,2,4-trimethylpentane provided that the probabilities of C–H bond rupture and hydrogen abstraction are proportional. Indeed the total probability  $P(\text{H})$  (proportional to  $k_2$ ) of hydrogen abstraction from a given molecule is equal to  $\sum p_i n_i$  where  $p_i$  is the probability of abstraction of a hydrogen of type *i* (primary, secondary, tertiary) and  $n_i$  is the number of such hydrogens in the molecule. Assuming similar probability for abstraction of secondary hydrogen atoms in both solvents the ratio  $k_2/k_1$  in cyclohexane can be obtained by multiplying  $k_2/k_1 = 0.0043$  obtained in 2,2,4-trimethylpentane by the ratio of the total probabilities of abstraction from cyclohexane and 2,2,4-trimethylpentane normalized to the secondary hydrogen atom abstraction. Using relative efficiencies of C–H bond rupture of 0.33:1.00:3.00, these total probabilities are  $(12 \times 1.00) = 12$  and  $(15 \times 0.33) + (2 \times 1.00) + (1 \times 3.00) = 9.95$  for cyclohexane and 2,2,4-trimethylpentane, respectively. From these values one obtains a ratio  $k_2/k_1 = 0.0052$  in cyclohexane. It should be pointed out, however, that the rupture of the secondary C–H bond in 2,2,4-trimethylpentane has been shown to be 2.67 times more efficient than in the less branched hydrocarbons.<sup>21</sup> Therefore, using the following rela-

(16) K. Watanabe, T. Nakayama, and J. Mottl, *J. Quant. Spectrosc. Radiat. Transfer*, **2**, 369 (1962).

(17) T. F. Williams, *Trans. Faraday Soc.*, **57**, 755 (1961).

(18) K. Tanno, T. Miyazaki, K. Shinsaka, and S. Shida, *J. Phys. Chem.*, **71**, 4290 (1967).

(19) The heat of formation of different hydrocarbon ions can be obtained from the Appendix of "Electron Impact Phenomena and the Properties of Gaseous Ions," F. H. Field and J. L. Franklin, Academic Press, Inc., New York, N. Y., 1957. The heat of formation of free radicals and stable products can be obtained from the Appendix of "Photochemistry," J. G. Calvert and J. N. Pitts, Jr., Wiley, New York, N. Y., 1967.

(20) R. A. Holroyd and G. W. Klein, *J. Amer. Chem. Soc.*, **87**, 4983 (1965).

(21) R. H. Schuler and R. W. Fessenden, "Radiation Research," G. Silini, Ed., Interscience, New York, N. Y., 1967, p 99.

tive ratios of C-H bond rupture, 0.33:2.67:3.00, one calculates the total probability of abstraction from 2,2,4-trimethylpentane normalized to secondary hydrogen atom abstraction in cyclohexane:  $(15 \times 0.33) + (2 \times 2.67) + (1 \times 3.00) = 13.29$ . A value of  $k_2/k_1 = 0.0043 \times (12/13.29) = 0.0039$  is then obtained in cyclohexane. The calculations given above indicate that the  $k_2/k_1$  ratio in cyclohexane should be somewhere be-

tween 0.0039 and 0.0052. The reported value is 0.0048.<sup>4</sup> In view of the assumption involved in the calculations of these ratios the agreement is rather satisfactory.

*Acknowledgments.* The authors wish to thank Dr. R. H. Schuler for his helpful comments and Mr. R. Parenti for carrying out the <sup>14</sup>C-cyclopropane experiments.

## Further Observations on Products Formed in the Radiolysis of

### Alkali Metal Halates and Perhalates by Cobalt-60 $\gamma$ Rays<sup>1</sup>

by G. E. Boyd and L. C. Brown

Oak Ridge National Laboratory, Oak Ridge, Tennessee 37830 (Received April 1, 1970)

Spectroscopic and chemical techniques were employed to identify and measure the concentrations of the stable radiolytic products formed at room temperature in crystalline KClO<sub>3</sub>, CsBrO<sub>3</sub>, CsIO<sub>3</sub>, KClO<sub>4</sub>, KBrO<sub>4</sub>, and KIO<sub>4</sub> by <sup>60</sup>Co  $\gamma$  rays. The ultraviolet absorptions of KClO<sub>3</sub> and CsBrO<sub>3</sub> measured with diffuse reflectance techniques indicated the presence of ClO<sup>-</sup>, ClO<sub>2</sub><sup>-</sup>, O<sub>3</sub><sup>-</sup>, and BrO<sup>-</sup> and O<sub>3</sub><sup>-</sup> ions, respectively, in these solids. The spectrum of heavily irradiated CsIO<sub>3</sub>, however, showed no new features except for a broad band at 460 nm attributable to I<sub>2</sub> in the crystal. The infrared absorptions of KClO<sub>4</sub>, KBrO<sub>4</sub>, and KIO<sub>4</sub> showed that ClO<sub>3</sub><sup>-</sup>, ClO<sub>2</sub><sup>-</sup>, BrO<sub>3</sub><sup>-</sup>, IO<sub>3</sub><sup>-</sup> ions, respectively, were formed by radiolysis. Chemical determinations of the amounts of BrO<sup>-</sup>, BrO<sub>2</sub><sup>-</sup>, and BrO<sub>4</sub><sup>-</sup> ions produced in CsBrO<sub>3</sub> by increasing  $\gamma$ -ray exposure revealed that constant concentrations were approached for large doses, suggesting that decomposition reactions of a thermal and/or radiolytic nature must occur. The rate of increase in the BrO<sup>-</sup> ion concentration at very low dose suggested that this species is not a primary radiolysis product. The excess oxidizing power of CsBrO<sub>3</sub> above that from hypobromite and bromite ions was attributed to O<sub>3</sub><sup>-</sup> ion rather than to BrO<sub>2</sub> as assumed earlier. A synopsis of the current state of knowledge about the radiolysis of halate ions in crystals is given.

A diversity of products stable at room temperatures and above are formed when the crystalline alkali metal and alkaline earth halates and perhalates are decomposed by energetic ionizing radiations. Previous investigations<sup>2a,b</sup> on the bromates, for example, have shown that Br<sup>-</sup>, BrO<sup>-</sup>, and BrO<sub>2</sub><sup>-</sup> ions and oxygen gas are produced by irradiation with <sup>60</sup>Co  $\gamma$  rays. In addition, the creation of BrO<sub>2</sub> was assumed tentatively to account for the excess oxidizing power of the crystals over that attributable to BrO<sup>-</sup> + BrO<sub>2</sub><sup>-</sup>. The generation of still other products such as (BrO-BrO<sub>3</sub>)<sup>-</sup>, O<sub>2</sub><sup>-</sup>, (Br-BrO<sub>3</sub>)<sup>-</sup>, O<sub>3</sub><sup>-</sup>, and BrO<sub>3</sub><sup>2-</sup> has been inferred<sup>3</sup> from chemical, ultraviolet spectroscopic, and thermoluminescence measurements on KBrO<sub>3</sub> irradiated at 25° with  $\gamma$  rays or 10-MeV electrons. Electron spin resonance measurements<sup>4,5</sup> at 77°K on NaBrO<sub>3</sub> have confirmed the presence of O<sub>3</sub><sup>-</sup>, and, quite recently, the production of perbromate ion, BrO<sub>4</sub><sup>-</sup>, in CsBrO<sub>3</sub> has been established<sup>6</sup> by infrared spectroscopy and by

chemical analysis of aqueous solutions of the irradiated solid.

Much of the information available on the identities and concentrations of radiolytic species produced in halate and perhalate crystals is based on chemical analyses in which the irradiated solid is dissolved in aqueous solutions. There has been uncertainty, therefore, as to whether the chemical forms observed in solution were

(1) Research sponsored by the U. S. Atomic Energy Commission under contract with the Union Carbide Corporation.

(2) (a) For a review see J. W. Chase and G. E. Boyd, "The Radiolytic Decomposition of Crystalline Alkaline Earth Bromates," ASTM Special Publication No. 400, 1966, p 17 ff; (b) J. W. Chase and G. E. Boyd, *J. Phys. Chem.*, **70**, 1031 (1966).

(3) T. Andersen, H. E. Lundager-Madsen, and K. Olesen, *Trans. Faraday Soc.*, **62**, 2049 (1966).

(4) F. T. Gamble, *J. Chem. Phys.*, **47**, 1193 (1967).

(5) T. Andersen, J. R. Byberg, and K. J. Olsen, *J. Phys. Chem.*, **71**, 4129 (1967).

(6) L. C. Brown, G. M. Begun, and G. E. Boyd, *J. Amer. Chem. Soc.*, **91**, 2250 (1969).

the same as those trapped in the crystal lattice, or if the stable species found in solution were derived from unstable precursors in the solid. Spectroscopic methods (uv and ir absorption, Raman scattering, esr, etc.) can be applied for the direct identification of radiolytic fragments in solids, and these techniques have been employed in addition to chemical analysis in this research. A number of examples can now be cited where the same species occurs in the irradiated crystal and in its aqueous solution; moreover, the concentration of the species has been demonstrated to be the same in the two phases as determined by independent methods. Chemical analysis of aqueous solutions of radiolyzed halates and perhalates, therefore, appears to be generally reliable. However, exceptions are known and one of these is mentioned below.

### Experimental Section

**Irradiations.** Irradiations at *ca.* 35° with <sup>60</sup>Co  $\gamma$  rays were conducted at constant geometry with sources of 3 and 11.5-kCi strength, respectively. The dose rate in the 3-kCi source measured with a Fricke dosimeter was  $9.1 \times 10^{17}$  eV/g of H<sub>2</sub>O min; the rate in the 11.5-kCi source was  $3.8 \times 10^{18}$  eV/g of H<sub>2</sub>O min. The doses absorbed by the crystalline halates and perhalates were estimated by multiplying the dose in water by the ratio of the number of electrons per gram in the respective solids to that in water. The crystals were stored in CO<sub>2</sub> ice after irradiation until the time of the measurements which were at room temperature.

**Spectral Measurements.** A Cary Model 14 PM recording spectrophotometer equipped with a Model 1411 ring collector reflectance attachment was employed to determine the ultraviolet absorbance of finely divided polycrystalline KClO<sub>3</sub>, CsBrO<sub>3</sub>, and CsIO<sub>3</sub>. Measurements were conducted relative to the unirradiated salts; MgCO<sub>3</sub> served to standardize the optical measurements following accepted procedures.<sup>7</sup> Infrared absorption measurements on the finely divided crystalline solids were performed with KBr pressed pellet (0.20 wt % in 400 mg of KBr) or Nujol mull sampling techniques. Dry Nujol mulls were examined to establish that absorption bands from water were absent in the salts. A Beckman IR-12 grating infrared spectrophotometer operated in the double-beam mode with dry air in the reference beam was employed. Frequency calibration was done with polystyrene film.

**Chemical Analysis.** When radiolyzed chlorates and bromates are dissolved in slightly alkaline aqueous solutions at room temperature oxygen trapped in the crystal is released, and its volume may be estimated by gas chromatography.<sup>8</sup> The degassed solutions show oxidizing properties and the ultraviolet absorption spectrum of the bromate solution possesses bands characteristic of BrO<sup>-</sup> (330 nm) and BrO<sub>2</sub><sup>-</sup> (285 nm) ions.<sup>9</sup> The procedure for the analysis for oxidizing fragments produced in the crystalline bromates was as follows.

The total oxidizing power of the solution (*i.e.*, oxidizing capacity with respect to arsenite ion) was determined by dissolving the irradiated solid in 0.1 *N* NaOH solution containing a known excess of arsenite and back-titrating at pH 9.0–9.5 with standard iodine solution.<sup>10</sup> Hypobromite and bromite were determined on radiolyzed bromate dissolved in 0.3 *M* NaHCO<sub>3</sub> solution by micropotentiometric titration with standard NaAsO<sub>2</sub> to determine BrO<sup>-</sup>, which is reduced rapidly and quantitatively, followed by adjustment of the pH to 9.7–9.9, addition of OsO<sub>4</sub> catalyst, and titration of BrO<sub>2</sub><sup>-</sup> with AsO<sub>2</sub><sup>-</sup>. Perbromate ion was determined with a newly developed microanalytical solvent extraction-spectrophotometric method based on the use of crystal violet.<sup>11</sup>

Ozonide ion, O<sub>3</sub><sup>-</sup>, trapped in the crystal would be expected to react instantaneously with arsenite upon dissolution according to



and thus may contribute to the total oxidizing power. An attempt was made to devise a procedure for the analysis of ozonide ion in radiolyzed KClO<sub>3</sub> by preparing polycrystalline mixtures of KO<sub>3</sub> + KClO<sub>3</sub> and measuring their uv absorptions with reflectance techniques. Solid KO<sub>3</sub> was synthesized by the reaction of dry KOH with ozone gas,<sup>12</sup> followed by extraction of KO<sub>3</sub> with liquid ammonia.<sup>13</sup> This purified KO<sub>3</sub> was mixed in a drybox in varying proportions with finely divided KClO<sub>3</sub>. To exclude water during the optical measurements, the mixtures were placed in a black metal dish equipped with an "O"-ring over which a planar quartz window could be tightly bolted. The assembly was scanned at room temperature between 300 and 650 nm (Figure 1). The band at 450 nm showed a vibrational fine structure identical with that reported<sup>14</sup> for O<sub>3</sub><sup>-</sup> ion dissolved in liquid ammonia or dimethylformamide. The absorption at 360 nm is attributed to nitrite ion impurity introduced by slight oxidation of the liquid ammonia into which the KO<sub>3</sub> was extracted. Similar observations on the incidence NO<sub>2</sub><sup>-</sup> in KO<sub>2</sub> prepared in nitrogen-containing solvents have been reported.<sup>15</sup> The attempt to develop standards for the assay of O<sub>3</sub><sup>-</sup> ion in irradiated KClO<sub>3</sub> was

(7) G. Kortüm, "Reflectance Spectroscopy," translated by J. E. Lohr, Springer-Verlag, Inc., New York, N. Y., 1969.

(8) G. E. Boyd, E. W. Graham, and Q. V. Larson, *J. Phys. Chem.*, **66**, 300 (1962).

(9) G. E. Boyd and Q. V. Larson, *ibid.*, **69**, 1413 (1965).

(10) Bromate and perbromate ions are not reduced by AsO<sub>2</sub><sup>-</sup> in alkaline solutions.

(11) L. C. Brown and G. E. Boyd, *Anal. Chem.*, **42**, 291 (1970).

(12) A. W. Petrocelli, A. Capotosto, and R. Uno, *ibid.*, **36**, 2509 (1964).

(13) T. P. Whaley and J. Kleinberg, *J. Amer. Chem. Soc.*, **73**, 79 (1951).

(14) I. J. Solomon and A. J. Kacmerek, *J. Phys. Chem.*, **64**, 168 (1960).

(15) G. Czapski and B. Halperin, *Israel J. Chem.*, **5**, 185 (1967).

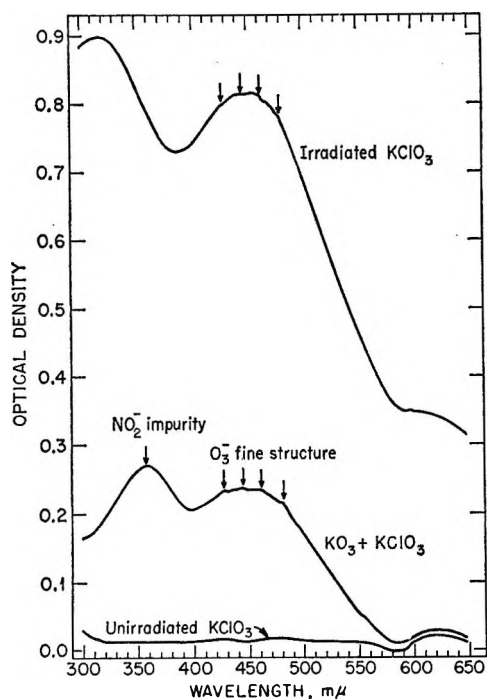


Figure 1. Diffuse reflectance spectrum of  $\text{KO}_3 + \text{KClO}_3$  (dose to irradiated  $\text{KClO}_3$ : ca.  $4 \times 10^{23}$  eV/mol).

abandoned when it was observed that the absorbancies of the synthetic  $\text{KO}_3 + \text{KClO}_3$  mixtures decreased with time, presumably because of decomposition according to



## Results

**Ultraviolet Absorption Measurements.** The diffuse reflectance spectrum of  $^{60}\text{Co}$   $\gamma$ -irradiated  $\text{KClO}_3$  (Figure 2) possessed three absorption bands. These may be assigned to  $\text{ClO}_2^-$  (265 nm),  $\text{ClO}^-$  (305 nm), and  $\text{O}_3^-$  (452 nm) ions, respectively. The uv cutoff of  $\text{ClO}_2^-$  ion at 225 nm can be observed in the spectrum taken with unirradiated  $\text{KClO}_3$ . The absorptions by hypochlorite and chlorite ions in radiolyzed  $\text{KClO}_3$  have been reported by Heal<sup>16</sup> in transmission measurements on the crystal and on aqueous solutions of the solid. A band at 450 nm was observed in the crystal, but not in aqueous solution, and was assigned provisionally by him to dichlorine hexoxide,  $\text{Cl}_2\text{O}_6$ . This species was assumed to explain the fact that perchlorate ion was found in aqueous solutions of irradiated  $\text{KClO}_3$  presumably as a hydrolysis product of  $\text{Cl}_2\text{O}_6$ . Infrared absorption investigations,<sup>17</sup> however, have demonstrated that  $\text{ClO}_4^-$  ion occurs in the solid in concentrations sufficient to account for all the perchlorate observed in solution. Furthermore, measurements<sup>18</sup> of the ultraviolet spectrum of  $\text{Cl}_2\text{O}_6$  dissolved in carbon tetrachloride have shown that this compound absorbs at 305 and 340 nm, respectively, rather than at 450 nm. The assignment of the absorption at 452 nm to  $\text{O}_3^-$  ion is supported by our investigations with solid  $\text{KO}_3$  noted

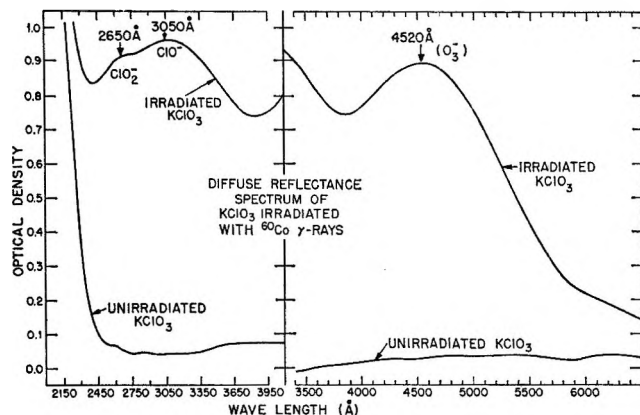


Figure 2. Diffuse reflectance spectrum of crystalline  $\text{KClO}_3$  irradiated at  $35^\circ$  with  $^{60}\text{Co}$   $\gamma$  rays (absorbed dose =  $4.1 \times 10^{23}$  eV/mol; vibrational structure in 450-nm band not observed because of high scan rate employed).

earlier. The absorption of  $\text{ClO}_2$  (360 nm) was not observed in the diffuse reflectance measurements (Figure 2) because of the overlap between the stronger absorption bands of  $\text{ClO}^-$  (305 nm) and  $\text{O}_3^-$  (452 nm) ions.

The ultraviolet absorption spectrum (Figure 3) of radiolyzed solid  $\text{CsBrO}_3$  clearly indicated the presence of hypobromite ion (330 nm). The evidence for ozonide, however, was less definite although the inflection at ca. 450 nm occurs close to the maximum of the absorption band for  $\text{O}_3^-$  ion. The spectrum of  $\text{BrO}_2^-$  (285 nm) was not seen probably because of overlap with the intense uv cutoff of bromate ion at 270 nm. The stabilization of the thermally unstable bromine dioxide,  $\text{BrO}_2$ , in radiolyzed solid bromates may occur. This species is reported<sup>19,20</sup> to absorb at 460 to 475 nm and thus would be eclipsed by the strong absorption of  $\text{O}_3^-$  ion at the same wavelengths. Bromine dioxide would not be observed readily in aqueous solutions of irradiated solid bromates. Recent studies<sup>21</sup> on the flash photolysis of aqueous halate ion solutions have indicated that the half-life of  $\text{BrO}_2$  in neutral  $10^{-3}$  M  $\text{NaBrO}_3$  at room temperatures is about 400  $\mu\text{sec}$ .

The reflectance spectrum measured with highly irradiated ( $3.6 \times 10^{24}$  eV/mol) crystalline  $\text{CsIO}_3$  showed but few features compared with the spectra for  $\text{CsBrO}_3$  and  $\text{KClO}_3$ . A broad band at 460 nm attributable to  $\text{I}_2$  could be seen, however, when the absorption by non-irradiated  $\text{CsIO}_3$  was subtracted from that for the irradiated salt. The spectrum of a solution of radio-

(16) H. G. Heal, *Can. J. Chem.*, **37**, 979 (1959).

(17) L. C. Brown and G. E. Boyd, *J. Phys. Chem.*, **73**, 396 (1969).

(18) Z. Spurný, *Talanta*, **9**, 885 (1962).

(19) G. V. Buxton and F. S. Dainton, *Proc. Roy. Soc. Ser. A*, **304**, 427 (1968).

(20) (a) O. Amichai, G. Czapski, and A. Treinin, *Israel J. Chem.*, **7**, 351 (1969); (b) O. Amichai and A. Treinin, *J. Phys. Chem.*, **74**, 830 (1970).

(21) F. Barat, L. Gilles, B. Hickel, and J. Sutton, *Chem. Commun.*, 1969, 1485.

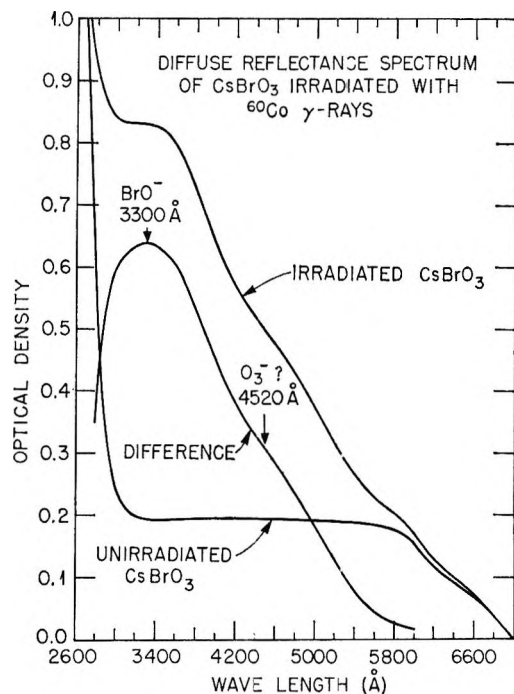


Figure 3. Diffuse reflectance spectrum of crystalline  $\text{CsBrO}_3$  irradiated at ca.  $35^\circ$  with  $^{60}\text{Co}$   $\gamma$  rays (absorbed dose =  $2.2 \times 10^{24}$  eV/mol).

lyzed solid in pure water showed bands which could be assigned to  $\text{I}_2$  (461 nm) and  $\text{I}_3^-$  (350 nm), respectively. Neither  $\text{IO}^-$  nor  $\text{IO}_2^-$  ions will be observed in aqueous solutions because of their great instability.<sup>22</sup> A 100 eV radiolytic yield for iodine,  $G(\text{I}_2) \geq 0.0034$ , was estimated from the optical density of the 461-nm band using the molar absorptivity value,  $\epsilon_{\text{I}_2(\text{aq})} = 740$ . This "yield" is a lower limit, as there was evidence for the loss of molecular iodine from the irradiated solid. The magnitude of  $G(\text{I}_2)$  is consistent, however, with values of  $G(-\text{IO}_3^-)$  of 0.003 and 0.012 determined with  $\text{KIO}_3$ <sup>23</sup> and with  $\text{CsIO}_3$  previously in this laboratory, respectively.

**Infrared Absorption.** The spectra of radiolyzed  $\text{KClO}_3$ <sup>17</sup> and  $\text{CsBrO}_3$ <sup>6</sup> have been reported and several species have been identified in these compounds. Bands were observed with  $\text{KClO}_3$  ( $4.2 \times 10^{23}$  eV/mol) at 806 and 844 and at  $1108 \text{ cm}^{-1}$ , which could be assigned to  $\text{ClO}_2^-$  and  $\text{ClO}_4^-$  ions, respectively. However, no band for  $\text{ClO}^-$  ion (ca.  $713 \text{ cm}^{-1}$ ) was detected probably because of its lower concentration:  $G(\text{ClO}^-) \approx (1/7)G(\text{ClO}_2^-)$ , and  $G(\text{ClO}^-) \approx (1/3)G(\text{ClO}_4^-)$ . Radiolyzed  $\text{CsBrO}_3$  ( $2.9 \times 10^{24}$  eV/mol) showed absorptions at 688 and 698 and at  $883 \text{ cm}^{-1}$  which were assigned to  $\text{BrO}_2^-$  and  $\text{BrO}_4^-$  ions, respectively. A very weak band at  $616 \text{ cm}^{-1}$  was also present which could be assigned to  $\text{BrO}^-$  ( $620 \text{ cm}^{-1}$ ). All of the absorption bands disappeared when the  $\text{CsBrO}_3$  was heated for one hour at  $250^\circ$  in air. No bands at frequencies other than at those attributable to  $\text{IO}_3^-$  ion were seen in the spectrum measured with  $\text{CsIO}_3$  ( $3.6 \times 10^{24}$  eV/mol).

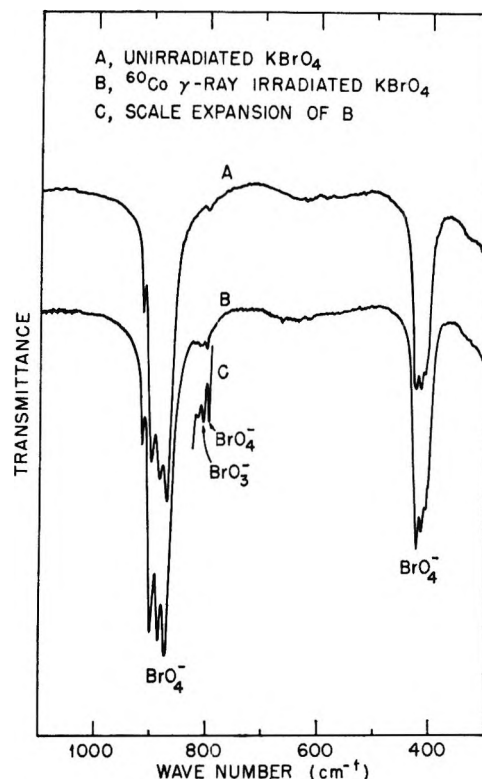


Figure 4. Infrared spectrum of crystalline  $\text{KBrO}_4$  irradiated at ca.  $35^\circ$  with  $^{60}\text{Co}$   $\gamma$  rays (absorbed dose =  $1.5 \times 10^{23}$  eV/mol; KBr pellet technique 0.2 wt %  $\text{KBrO}_4$  in KBr).

The irradiated crystalline perchalates gave ir spectra which suggested that halate ions were the dominant stable radiolytic species in the solids. Absorption bands characteristic of  $\text{ClO}_3^-$  ( $490$ ,  $940$ , and  $980 \text{ cm}^{-1}$ ) and one weak band at ca.  $845 \text{ cm}^{-1}$ , which may be assigned to chlorite ion, were observed in the spectrum of  $\text{KClO}_4$  ( $1.7 \times 10^{24}$  eV/mol), confirming and extending earlier observations.<sup>24</sup> The spectra (Figures 4 and 5) of  $\text{KBrO}_4$  ( $1.5 \times 10^{23}$  eV/mol) and  $\text{KIO}_4$  ( $1.9 \times 10^{24}$  eV/mol) showed absorption bands only for  $\text{BrO}_3^-$  ( $806$  and  $848 \text{ cm}^{-1}$ ) and  $\text{IO}_2^-$  ( $758 \text{ cm}^{-1}$ ) ions, respectively. No bands assignable to  $\text{BrO}_2^-$  were seen, possibly because of the relatively small dose absorbed in the  $\text{KBrO}_4$ . Infrared bands for  $\text{IO}^-$  and/or  $\text{IO}_2^-$  were not observed even in heavily irradiated  $\text{KIO}_4$ .

**Chemical Measurements.** The increase in the concentrations of  $\text{BrO}^-$ ,  $\text{BrO}_2^-$ , and  $\text{BrO}_4^-$  ions formed in crystalline  $\text{CsBrO}_3$  by  $^{60}\text{Co}$   $\gamma$  rays with dose is shown in Figure 6. Analyses of aqueous solutions of the irradiated solid were performed to determine these species. All species appeared to approach steady-state concentrations at large doses, suggesting that back-reactions were occurring or that their thermal

(22) C. H. Li and C. F. White, *J. Amer. Chem. Soc.*, **65**, 335 (1943).

(23) U. Bertocci, R. B. Jacobi, and G. N. Walton, Symposium on Chemical Effects of Nuclear Transformations, Vol. II, IAEA, 1961, p 337.

(24) L. A. Prince and E. R. Johnson, *J. Phys. Chem.*, **69**, 359 (1965).

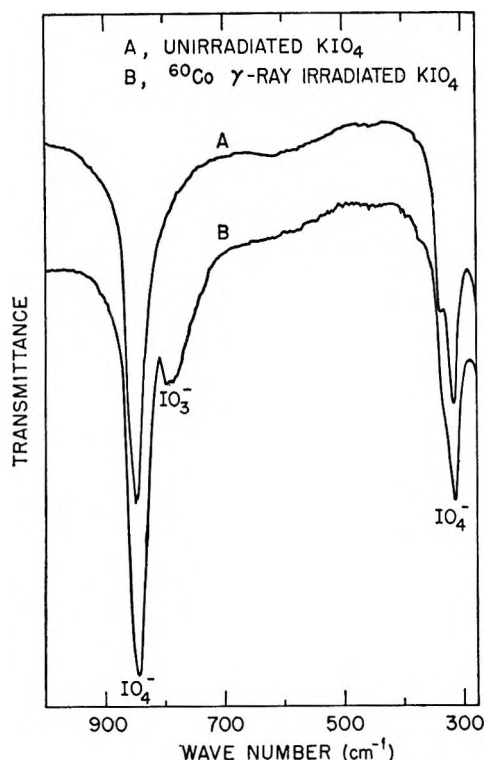


Figure 5. Infrared spectrum of crystalline  $\text{KIO}_4$  irradiated at ca.  $35^\circ$  with  $^{60}\text{Co}$   $\gamma$  rays (absorbed dose =  $1.9 \times 10^{24}$  eV/mol  $\text{KIO}_4$ ; KBr pellet technique).

and/or radiolytic decomposition was taking place. The initial 100-eV yields for the production of bromite and perbromate ions were  $G_0(\text{BrO}_2^-) = 3.7$  and  $G_0(\text{BrO}_4^-) \approx 0.7$ , respectively. A point of inflection was present at a dose of ca.  $5 \times 10^{23}$  eV/mol in the curve for the production of  $\text{BrO}^-$  ion (Figure 6). At vanishingly small doses, the value of  $G(\text{BrO}^-)$  appeared to approach zero, suggesting that hypobromite ion was not a primary product in the radiolysis.

The difference between the total oxidizing power of the solution of radiolyzed  $\text{CsBrO}_3$  and the oxidizing power of  $\text{BrO}^- + \text{BrO}_2^-$  was attributed to ozonide ion in the crystal. The  $\text{O}_3^-$  concentrations thus derived showed appreciable scatter because they were derived as differences between two relatively large quantities. The curve (not shown in Figure 6) for the dose dependence of ozonide ion concentration was qualitatively similar to those for  $\text{BrO}^-$ ,  $\text{BrO}_2^-$ , and  $\text{BrO}_4^-$  ions. At small doses (*i.e.*,  $< 2 \times 10^{23}$  eV/mol),  $G(\text{O}_3^-) \approx 0.7$ . This value is perceptibly larger than  $G(\text{O}_3^-) = 0.2$  for  $\text{KClO}_3$  exposed to an X-ray dose of  $1.3 \times 10^{23}$  eV/mol, which can be derived from the spectrum reported by H. G. Heal<sup>16</sup> for a crystal 0.12 mm thick, assuming that the molar absorbance index for ozonide ion in the solid is the same as that measured in aqueous solution at 430 nm<sup>25</sup> ( $\epsilon_{\text{O}_3^-} = 1900$ ).

The oxidizing power and the coloration of irradiated  $\text{CsBrO}_3$  may be removed completely by heating the crystals at  $300^\circ$  for 1 hr. Further experimental re-

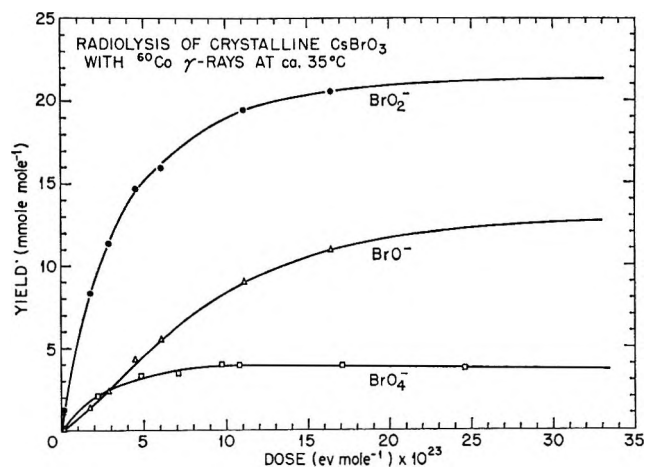


Figure 6. Dose dependence of the concentrations of radiolytic products formed at ca.  $35^\circ$  in crystalline  $\text{CsBrO}_3$  by  $^{60}\text{Co}$   $\gamma$  rays (concentration values based on chemical analyses of aqueous solutions of irradiated salt).

sults on the thermal annealing of irradiated  $\text{CsBrO}_3$  are summarized in Table I where it may be seen that heating also reduced the  $\text{BrO}_4^-$  ion concentration. Studies<sup>6,26</sup> with pure  $\text{KBrO}_4$  have shown that perbromate ion decomposes quantitatively to  $\text{KBrO}_3$  and  $\text{O}_2(\text{g})$  at  $275\text{--}280^\circ$ .

Table I: Changes of Perbromate Ion Concentration<sup>a</sup> in Radiolyzed  $\text{CsBrO}_3$  Caused by Thermal Annealing

Dose absorbed, eV/mol	Thermal treatment	$\text{BrO}_4^-$ concentration, mmoles $\text{BrO}_4^-/\text{mol BrO}_3^-$
$9.7 \times 10^{23}$	None	3.91
$9.7 \times 10^{23}$	None	3.98
$9.7 \times 10^{23}$	60 min @ $130^\circ$	2.99
$9.7 \times 10^{23}$	60 min @ $200^\circ$	0.98

<sup>a</sup> Determined by crystal violet solvent extraction-spectrophotometric method, ref 11.

## Discussion

A recapitulation of the information available at this time about the radiolysis of the alkali metal halates, including that given in this paper and recent results obtained by others, will be presented. Our discussion will not attempt to be exhaustive, as two comprehensive and thoughtful reviews<sup>27,28</sup> of papers published prior to 1968 have appeared. Several new interpretations of radiolysis mechanisms will be suggested.

(25) W. D. Felix, B. L. Gall, and L. M. Dorfman, *J. Phys. Chem.*, **71**, 384 (1967).

(26) E. H. Appelman, *Inorg. Chem.*, **8**, 223 (1969).

(27) Yu. A. Zaharov and V. A. Nevostruev, *Russ. Chem. Rev.*, **37** [1], 61 (1968).

(28) J. Cunningham, "Fragments in Irradiated Ionic Solids," "Radical Ions," E. T. Kaiser and L. Kevan, Ed., Interscience, New York, N. Y., 1968, Chapter 11.

*Radiation Chemistry of the Crystalline Alkali Metal Halates.* The major products formed in the crystalline alkali metal halates at room temperatures by small doses of  $\gamma$  radiation have been shown to be  $XO_2^-$ ,  $O_2$ , and  $X^-$ , where X denotes either chlorine or bromine. The ions  $XO^-$ ,  $XO_4^-$ , and  $O_3^-$  also are produced in smaller concentrations, and paramagnetic centers stable at 25° and above, such as  $XO_2$ ,  $O_3^-$ , and  $(X^-XO_2)$ , have been identified in chlorates,<sup>29</sup> but not in bromates except for  $O_3^-$ .

At low temperatures there is good evidence<sup>30</sup> for the creation of other paramagnetic species such as  $XO_3$  and  $XO_3^{2-}$  in chlorates. In addition, very small quantities of hydrogen gas are evolved and slight changes in alkalinity are observed when the radiolyzed halates are dissolved in water, suggesting that trapped electrons (F-centers) are present. Other products such as paramagnetic  $O_2^-$  and  $BrO_2$  have been reported, but the evidence for them has not been confirmed independently.

Many of the radiolysis products observed in the irradiated chlorates and bromates also have been found in aqueous solutions of the compounds, although ozonide ion,  $O_3^-$ , is an exception. The production of this ion<sup>30-32</sup> and of perchlorate<sup>6</sup> and perbromate<sup>17</sup> ions in alkali metal halate crystals has been established during the past 2 years.

Recognition of the large difference in the radiation stability of the chlorates and bromates on one hand and the iodates on the other has come about only recently. Iodate ion in  $KIO_3$ , for example, has been found to be approximately two orders of magnitude more stable toward radiation decomposition than the chlorates and bromates:  $G(-IO_3^-) = 0.01 G(-ClO_3^-) \approx 0.01 G(-BrO_3^-)$ . The radiolytic modes for the chlorates and bromates are quite similar in that the relative yields of many products are nearly the same and the concentrations of the ions  $XO^-$ ,  $XO_2^-$ , and  $XO_4^-$  produced in  $KClO_3$  and  $KBrO_3$ , respectively, all tend to saturation when large amounts of radiation are absorbed.

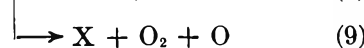
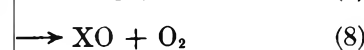
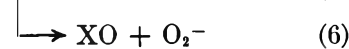
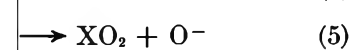
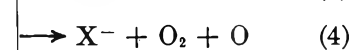
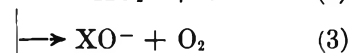
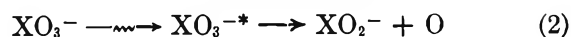
Current knowledge about the identity of the ions and free radicals produced by  $\gamma$  rays in crystalline  $KClO_3$ ,  $KBrO_3$ , and  $KIO_3$  is based on a range of physical and chemical evidence. Chemical analyses of  $KClO_3$  have been employed to determine the concentrations of chlorine dioxide,  $Cl^-$ ,  $ClO^-$ ,  $ClO_2^-$ , and  $ClO_4^-$  ions and the production of oxygen gas. Ultraviolet absorption measurements on aqueous solutions of the solid have revealed bands attributable to  $ClO^-$ ,  $ClO_2^-$ , and  $ClO_2$ , while reflectance and transmission spectra for irradiated  $KClO_3$  show bands characteristic of  $ClO^-$ ,  $ClO_2^-$ , and  $O_3^-$  ions. Infrared spectra measured at room temperature have demonstrated that  $ClO_4^-$  as well as  $ClO_2^-$  and  $ClO^-$  ions are produced in the solid, and, interestingly, polarized infrared radiation has been employed recently<sup>33</sup> to show that the chlorite ions occur in two groups, one family which conserves  $C_s$  symmetry, and the other which may occupy either of two orienta-

tions relative to the plane of symmetry of the lattice of  $KClO_3$  and retain  $C_{2v}$  symmetry approximately. Altogether, five paramagnetic species have been identified in radiolyzed  $KClO_3$ .<sup>30</sup> Three of these,  $ClO_2$ ,  $O_3^-$ , and  $(Cl-ClO_2)^-$ , are stable at room temperatures and above, while  $ClO_3$  and  $ClO_3^{2-}$  exist only at and below 77°K.

Many congeners of the  $KClO_3$  radiolysis products are found in radiolyzed  $KBrO_3$ . The concentrations of  $Br^-$ ,  $BrO^-$ ,  $BrO_2^-$ , and  $BrO_4^-$  ions and oxygen gas have been determined in this solid by chemical methods. Reflectance spectra measured on polycrystalline  $KBrO_3$  powders have exhibited bands attributable to  $BrO^-$  and possibly to  $O_3^-$  ion, while infrared absorption measurements have served to identify  $BrO^-$ ,  $BrO_2^-$ , and  $BrO_4^-$  ions in the solid. The only paramagnetic species identified by esr techniques thus far is  $O_3^-$  ion.<sup>31,34</sup> No bromine-containing free radical stable at room temperatures has been observed in  $NaBrO_3$ .<sup>34</sup>

Only two radiolysis products have been detected in  $\gamma$ -irradiated  $KIO_3$  and these,  $I^-$  and  $I_2$ , are formed in extremely small concentrations. The concentrations of  $I^-$  and  $I_2$  have been determined by chemical methods on aqueous solutions of the salt. Ultraviolet absorption spectra measured with these solutions also show bands characteristic of these species. No radiolytic fragment has yet been identified in the crystalline solid. Electron spin resonance measurements have failed to reveal any paramagnetic species.<sup>35</sup>

*Possible Radiolysis Mechanisms.* The primary steps in the radiolytic process are assumed to be the ionization (1) and excitation (2) of the halate anion,  $XO_3^-$ . The primary consequence of radiolysis is the breaking of halogen-oxygen bonds.



(29) R. S. Eachus, P. R. Edwards, S. Subramanian, and M. C. R. Symons, *J. Chem. Soc., A*, 1704 (1968).

(30) R. S. Eachus and M. C. R. Symons, *ibid.*, 2433 (1968).

(31) F. T. Gamble, *J. Chem. Phys.*, **47**, 1193 (1967).

(32) S. Schlick, *Chem. Phys. Lett.*, **4** [7], 421 (1969).

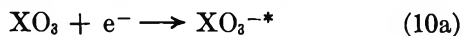
(33) D. Jumeau and J.-C. Fayet, *C. R. Acad. Sci. B*, **266**, 1614 (1968).

(34) M. M. Cosgrove and M. A. Collins, *J. Chem. Phys.*, **52**, 989 (1970).

(35) L. V. Serikov, Yu. A. Zakharov, and A. A. Vorob'ev, *High Energy Chem.*, **1**, 431 (1967).

Some of the foregoing reactions probably do not occur, and several products are highly unstable and will not exist in the halate crystal lattice at room temperatures. For example, experimental determinations of the yields of  $\text{ClO}^-$  and  $\text{BrO}^-$  at small doses in the radiolysis of alkali metal chlorates and bromates indicate that reaction 3 is absent. Further, the electron affinities of the species  $\text{XO}_2$  (2.8 eV) and  $\text{XO}$  (2.6–2.9 eV) are substantially larger than the affinities for  $\text{O}$  (1.5 eV) and  $\text{O}_2$  (0.9 eV), respectively, so that reactions 5 and 6 should not be favored. On the other hand, recent investigations<sup>20a,b</sup> on the photolysis of  $\text{BrO}_3^-$  and  $\text{IO}_3^-$  ions in aqueous solutions have been interpreted on the basis that the generation of  $\text{O}^-$  ions is a major decomposition route for excited oxyhalogen ions (e.g., eq 5). However, the identification of  $\text{O}^-$  ions in crystalline chlorates and bromates has not been reported. Regarding eq 6, the species  $\text{O}_2^-$  is paramagnetic and may be detected by esr techniques when present in ppm concentrations;<sup>36</sup> yet it has not been observed in radiolyzed halates. The free radicals produced in reactions 1, 7, and 8, with the exception of  $\text{ClO}_2$ , are quite unstable and appear to exist only at low temperatures in halate crystals. At 90°K, for example, half of the species  $\text{ClO}_3$  produced in  $\text{KClO}_3$  disappears within five minutes after irradiation,<sup>37</sup> and the recently reported<sup>38</sup>  $\text{BrO}_3$  radical formed in  $\text{KBrO}_3$  disappears above ca. 130°K. There is, however, good evidence for the production of  $\text{BrO}$  and  $\text{BrO}_2$  in the steady-state radiolysis of bromate ion in aqueous solutions.<sup>19</sup> The foregoing bromine radicals and the species  $\text{IO}_2$  and  $\text{IO}_3$  also are reported<sup>20a,b,21</sup> to be formed in the photolysis of  $\text{BrO}_3^-$  and  $\text{IO}_3^-$  ions in solution, respectively.

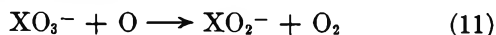
The trapping of electrons produced by ionization in solids also must be considered. Thus, electron capture by free radicals may lead to highly excited ions



which decompose because the electron affinities substantially exceed the bond strengths. In addition, electron trapping at anion vacancies in the lattice and by halate ions can be expected.



Recoil oxygen atoms produced in reactions 2, 4, 7, and 9 will react in the crystal lattice. The energetically favored abstraction reaction



will give oxygen gas and halite ions identical with those formed by reaction 2. Perhalate ions may be formed by addition



or by oxygen-atom transfer reactions



while correlated recombination reactions where the secondary electron does not escape the parent ion

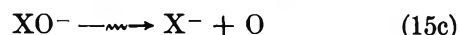
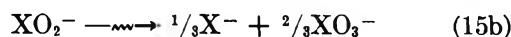
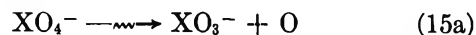


can reform the parent ion. Finally, direct combination of oxygen atoms



must occur to some extent and will be important in radiolysis with high LET radiations.

Thermal and/or radiolytic decomposition of the products of radiolysis also occurs in the chlorates and bromates. The distribution of the products formed in the alkali metal bromates, for example, are strongly dependent on the temperature at which the irradiation is conducted. At temperatures approaching the melting points of the crystals, only halide plus oxygen gas is produced.<sup>39</sup> Perhalate, formed by reaction 12, is radiolyzed as are halite<sup>40</sup> and hypohalite.



The mechanism for the formation of ozonide ion,  $\text{O}_3^-$ , is of special interest. Cosgrove and Collins<sup>34</sup> have suggested the process.



However, the electron affinities would favor the formation of  $\text{X}^- + \text{O}_3$  rather than  $\text{X} + \text{O}_3^-$ . Additionally, the optical studies of Heal<sup>16</sup> suggest that  $\text{O}_3^-$  is not a primary radiolysis product at low temperatures, but that it is created on warming  $\text{KClO}_3$  crystals to room temperature or is produced directly by irradiation at room temperature. The recent detailed esr studies of Eachus and Symons<sup>30</sup> have done much to clarify the observations of Heal. Three paramagnetic species,  $\text{ClO}_3$ ,  $\text{ClO}_2$ , and  $\text{ClO}_3^{2-}$ , were shown to be formed on irradiation of  $\text{KClO}_3$  at 77°K. On warming the crystal to room temperature, the  $\text{ClO}_3$  and  $\text{ClO}_3^{2-}$  disappeared and two new paramagnetic entities,  $\text{O}_3^-$  and  $(\text{Cl}^- \text{ClO}_2)$ , appeared. To explain the origin of these new species, Eachus and Symons postulate that at 77°K radiation induces an electron transfer according to



The resultant free radicals may occupy adjacent anion sites, or next nearest neighbor sites or distant sites,

(36) W. Holzer, W. F. Murphy, H. J. Bernstein, and J. Rolfe, *J. Mol. Spectrosc.*, **26**, 543 (1968).

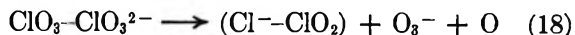
(37) J.-C. Fayet, C. Pariset, and B. Thiéblemont, *C. R. Acad. Sci. B*, **268**, 78 (1969).

(38) A. Begum, S. Subramanian, and M. C. R. Symons, *J. Chem. Soc.*, 1970, 918.

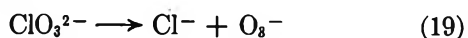
(39) G. E. Boyd and Q. V. Larson, *J. Phys. Chem.*, **69**, 1413 (1965).

(40) G. E. Boyd and L. C. Brown, *ibid.*, **92**, 1691 (1970).

depending on where the secondary electron is trapped. The pair,  $\text{ClO}_3\text{-ClO}_3^{2-}$ , on adjacent lattice sites decomposes on warming



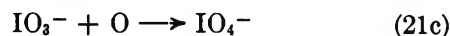
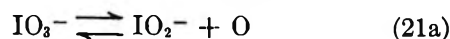
whereas  $\text{ClO}_3^{2-}$  and  $\text{ClO}_3$  on more distant sites decompose according to



At room temperature, dissociative electron capture can occur:  $\text{ClO}_3^- + e^- \longrightarrow \text{ClO}_3^{2-} \longrightarrow \text{Cl}^- + \text{O}_3^-$ . The  $V_k$  type center,  $(\text{Cl-ClO}_2)$ , which is favored by electron affinity over  $(\text{Cl-ClO}_2^-)$ , also is formed directly on room temperature irradiation presumably *via* a transient  $\text{ClO}_3$  radical.

The unusual stability of iodate ion has been remarked upon. No stable species such as  $\text{IO}^-$ ,  $\text{IO}_2^-$ , or  $\text{IO}_4^-$  have been observed in crystalline  $\text{KIO}_3$  exposed to heavy  $\gamma$ -ray doses. The radiolysis of iodate ion, how-

ever, shows a large LET effect: with  $^{60}\text{Co}$   $\gamma$  rays  $G(-\text{IO}_3^-) \leq 0.001$ , whereas with  $^6\text{Li}$  fission particles<sup>41</sup>  $G(-\text{IO}_3^-) = 2.85$ . An explanation of this behavior in terms of competitive reactions can be offered.



For low LET, the back-reaction 21a predominates, while with high LET radiations, oxygen-atom recombination (21b) becomes important and (21c) may take place. When the radiolyzed iodate is dissolved in aqueous solutions for analysis, the radiolytic iodite,  $\text{IO}_2^-$ , rapidly disproportionates to yield  $\text{I}^-$  and  $\text{IO}_3^-$  ions. Also, small quantities of  $\text{I}^-$  produced in the crystal are oxidized to give molecular iodine. The possible occurrence of (21c) remains to be checked experimentally.

(41) K. Hasegawa, *Nippon Kagaku Zasshi*, **90**, 135 (1969).

## The Crystal and Molecular Structure of

### Bisbipyridyl- $\mu$ -dihydroxo-dicopper(II) Nitrate

by Richard J. Majeste and Edward A. Meyers\*

Department of Chemistry, Texas A&M University, College Station, Texas 77843 (Received September 16, 1969)

The crystal and molecular structure of bisbipyridyl- $\mu$ -dihydroxo-dicopper(II) nitrate,  $[\text{Cu}(\text{C}_{10}\text{H}_8\text{N}_2)(\text{OH})(\text{NO}_3)]_2$ , has been determined by means of single crystal, X-ray diffraction techniques. The compound crystallizes in the triclinic space group  $\bar{1}$  with cell dimensions  $a = 7.637$ ,  $b = 16.989$ ,  $c = 8.504$  Å, and  $\alpha = 91.58^\circ$ ,  $\beta = 97.49^\circ$ ,  $\gamma = 90.36^\circ$ . Each half of the dimer, consisting of a copper atom and its bipyridyl ligand, is essentially planar. These two parallel planes are bridged across a center of symmetry by the two hydroxyl groups. The average Cu to OH bond distance is 1.92 Å, and the closest Cu to Cu distance is 2.85 Å. The hydrogen positions have been found and there is a close contact distance of 2.06 Å between a hydrogen of the OH group and an oxygen of the  $\text{NO}_3$  group. The final refinement gave a value of  $R = 0.035$  for 2844 independent reflections.

#### Introduction

Previous studies of thermodynamic equilibrium for copper bipyridyl systems<sup>1-3</sup> have neglected the possibility of dimerization. Recently, Rajan and Martell<sup>4a</sup> recalculated the equilibrium constants for similar systems and included a dimer as one of the species present. Measurements of spectral and magnetic properties also support the existence of a dimeric species<sup>4b</sup> in this system. This X-ray study was undertaken to substantiate the presence of the dimer in the crystalline state

and to elucidate its structure. Of particular interest in this compound is the effect of hydroxyl bridges on the copper-copper separation.

\* To whom correspondence should be addressed.

(1) G. Anderegg, *Helv. Chim. Acta*, **46**, 2397 (1963).

(2) G. Anderegg, *ibid.*, **46**, 2813 (1963).

(3) R. L. Davis and K. W. Dunning, *J. Chem. Soc.*, 4168 (1965).

(4) (a) K. S. Rajan and A. E. Martell, *J. Inorg. Nucl. Chem.*, **29**, 463 (1967); (b) private communication, F. J. Smentowski, D. W. Kingston, and A. E. Martell.

## Experimental Section

Crystals of the dimer suitable for X-ray studies were supplied to us by Drs. Kingston and Martell. The crystals are hard, and so dark blue as to appear black. One such crystal, with dimensions of approximately  $0.40 \times 0.48 \times 0.57$  mm, was mounted on a computer-controlled Syntex Autodiffractometer equipped with a full-circle E&A goniometer. Monochromatic Mo K $\alpha$  radiation was obtained from the (0,0,2) reflection of an oriented graphite crystal ( $2\theta$  mn =  $12^\circ 15'$ ).

The cell parameters were refined by least-squares to obtain optimum agreement between observed and calculated  $2\theta$  angles for 42 strong reflections. For the triclinic space group  $\bar{1}\bar{1}$ , these dimensions are  $a = 7.637 \pm 0.002$ ,  $b = 16.989 \pm 0.005$ ,  $c = 8.504 \pm 0.002$  Å,  $\alpha = 91.58 \pm 0.03^\circ$ ,  $\beta = 97.49 \pm 0.02^\circ$ ,  $\gamma = 90.36 \pm 0.02^\circ$  at  $t = 22^\circ$ . This led to a calculated density of  $1.81_4$  g/cc for two molecular dimers per unit cell, compared to a density of  $1.80_8$  g/cc measured by flotation techniques.

The data were collected by scanning in  $2\theta$  (scan range =  $2.6^\circ$ , scan rate =  $2^\circ/\text{min}$ ,  $2\theta_{\text{max}} = 65^\circ$ ) to obtain integrated intensities. A total of 3924 independent reflections were recorded. A check on the linearity of the counter and its circuitry showed that very high intensity ( $>10,000$  cps) data required correction. For this reason, the 11 most intense reflections were omitted from the data list, since it was felt that corrections for nonlinearity were too large to apply to them. Of the remaining reflections, the intensity of 1069 was less than  $3\sigma$ , and these were discarded. The 2844 reflections which remained were corrected for Lorentz and polarization effects. The polarization factor was taken as the average of the expressions<sup>5</sup>

$$P = \frac{\cos^2 2\theta + \cos^2 2\theta \text{ mn}}{1 + \cos^2 2\theta \text{ mn}}$$

$$P = \frac{\cos^2 2\theta + |\cos 2\theta \text{ mn}|}{1 + |\cos 2\theta \text{ mn}|}$$

the maximum difference being 0.8% for this structure.

**Structure Determination.** A three-dimensional Patterson function calculated with the 730 most intense reflections led directly to trial coordinates for the Cu atom. Least-squares refinement of these coordinates with the same limited data set gave  $R = \Sigma|F_o - F_c|/\Sigma|F_o| = 0.29_2$ . A three-dimensional difference Fourier map was then calculated, and from this map the coordinates were obtained for all atoms except hydrogen. Several cycles of least-squares refinement gave  $R = 0.06_0$ . This trial structure was then used to calculate a three-dimensional difference Fourier map which clearly showed the positions of the nine unique hydrogens. When the hydrogens were added to the trial structure as isotropic atoms, and all other temperature factors were converted to anisotropic,  $R$  became  $0.02_6$ .

The structure was then refined with all 2844 reflections. The scattering factors for H, C, N, and O were taken from the International Tables. The scattering factors for Cu were taken from an article by Cromer and Waber<sup>6</sup> (1965) with anomalous dispersion corrections calculated by Cromer<sup>7</sup> (1965). The hydrogen atom temperature factors were isotropic, while all other atom temperature factors were anisotropic. The weighting scheme was based on counting statistics, the function minimized was  $\Sigma\omega(F_o - F_c)^2$ ,  $R_2 = [\Sigma\omega(F_o - F_c)^2/\Sigma\omega F_o^2]^{1/2} = 0.031$ ,  $R = 0.035$ , and the standard deviation for an observation of unit weight was 1.90.

Both empirical ( $\phi$  scan) and spherical absorption ( $\mu R = 0.50$ ) corrections were applied to the data but they increased the final values of  $R$  and  $R_2$  to 0.036 and 0.032 and did not significantly alter the coordinates of the atoms. Since the crystal was rather irregular in shape the absorption corrections were of doubtful value, but fortunately small, and the final parameters given in Table I are based upon the refinements without absorption corrections included.

## Discussion

The dimer consists of two essentially planar sections composed of a bipyridyl ligand bonded to a copper atom. These sections are linked together by two hydroxyl bridges across a center of symmetry. The coordinates and anisotropic temperature factors for one such asymmetric unit of the dimer are given in Table I. Each copper atom has a slightly distorted [4 + 1] tetragonal pyramidal coordination. The copper rises from the base plane in the direction of its fifth bond to the nitrate group with a Cu-O distance of 2.379 Å. The other four bonds to copper occur in two sets: the copper to hydroxyl bridge oxygen, which average 1.92 Å, and the copper to bipyridyl nitrogen, which average 2.00 Å.

Chain or layer structures<sup>8-11</sup> which have copper bridged to copper by hydroxyl groups have a range of Cu-Cu separation from 2.88 to 3.21 Å, with an average separation of 3.07 Å. The binuclear copper complexes<sup>12-14</sup> have copper atom separations ranging from 2.63 to 2.65 Å, with an average separation of 2.64 Å. The Cu-Cu separation across the hydroxyl bridges in

(5) U. W. Arndt and B. T. M. Willis, "Single Crystal Diffractometry," Cambridge University Press, Cambridge, England, 1966.

(6) D. T. Cromer and J. T. Waber, *Acta Cryst.*, **18**, 104 (1965).

(7) D. T. Cromer, *ibid.*, **18**, 17 (1965).

(8) F. Aebi, *Helv. Chim. Acta*, **31**, 369 (1948).

(9) W. Nowacki and R. Scheidegger, *ibid.*, **35**, 375 (1952).

(10) A. F. Wells, *Acta Cryst.*, **4**, 200 (1951).

(11) G. Gattow and J. Zemmann, *ibid.*, **11**, 866 (1958).

(12) J. N. Niekerk and F. R. L. Schoening, *ibid.*, **6**, 227 (1953).

(13) F. Hanic, D. Stempelova, and K. Hanicova, *ibid.*, **17**, 633 (1964).

(14) G. A. Barclay and C. H. L. Kennard, *J. Chem. Soc.*, 5244 (1961).

**Table I:** Coordinates and Temperature Factors

Atom	X	Y	Z	$\beta_{11}^a$	$\beta_{22}$	$\beta_{33}$	$\beta_{12}$	$\beta_{13}$	$\beta_{23}$
Cu	0.5352	0.4295	0.4158	0.0102	0.0013	0.0073	0.0000	0.0022	-0.0007
O <sub>1</sub> (OH)	0.4259	0.4592	0.5992	0.0099	0.0015	0.0094	-0.0003	0.0038	-0.0006
O <sub>2</sub> (NO <sub>3</sub> )	0.9262	0.4956	0.6695	0.0363	0.0025	0.0179	-0.0033	0.0101	-0.0036
O <sub>3</sub> (NO <sub>3</sub> )	0.0872	0.3926	0.6379	0.0112	0.0042	0.0202	-0.0006	-0.0012	0.0031
O <sub>4</sub> (NO <sub>3</sub> )	0.8119	0.3904	0.5514	0.0103	0.0023	0.0189	-0.0003	-0.0015	-0.0010
N <sub>1</sub>	0.4705	0.3152	0.4083	0.0088	0.0015	0.0070	0.0000	0.0010	-0.0004
N <sub>2</sub>	0.6025	0.3993	0.2029	0.0110	0.0015	0.0073	0.0003	0.0017	-0.0005
N <sub>3</sub> (NO <sub>3</sub> )	0.9421	0.4275	0.6202	0.0132	0.0023	0.0074	-0.0014	0.0029	0.0001
C <sub>1</sub>	0.4093	0.2762	0.5259	0.0108	0.0019	0.0073	-0.0002	0.0010	0.0000
C <sub>2</sub>	0.3770	0.1956	0.5154	0.0124	0.0020	0.0100	-0.0004	0.0011	0.0007
C <sub>3</sub>	0.4084	0.1550	0.3800	0.0128	0.0015	0.0133	-0.0005	0.0009	-0.0003
C <sub>4</sub>	0.4703	0.1947	0.2573	0.0115	0.0016	0.0093	-0.0003	0.0007	-0.0009
C <sub>5</sub>	0.5010	0.2747	0.2763	0.0077	0.0015	0.0070	0.0002	0.0004	-0.0005
C <sub>6</sub>	0.5706	0.3238	0.1562	0.0082	0.0015	0.0063	0.0003	0.0003	-0.0003
C <sub>7</sub>	0.6001	0.2952	0.0074	0.0120	0.0022	0.0075	0.0002	0.0018	-0.0011
C <sub>8</sub>	0.6643	0.3474	0.9057	0.0138	0.0032	0.0068	0.0006	0.0024	-0.0006
C <sub>9</sub>	0.6979	0.4243	0.9534	0.0152	0.0028	0.0084	0.0003	0.0038	0.0007
C <sub>10</sub>	0.6669	0.4488	0.1033	0.0149	0.0019	0.0094	0.0000	0.0044	0.0003
H <sub>1</sub>	0.3881	0.3092	0.6231	0.0034	(0.0007)	(0.0038)	(0.0000)	(0.0004)	(0.0000)
H <sub>2</sub>	0.3333	0.1675	0.6084	0.0116	(0.0023)	(0.0094)	(0.0000)	(0.0014)	(0.0001)
H <sub>3</sub>	0.3827	0.0997	0.3762	0.0098	(0.0019)	(0.0079)	(0.0000)	(0.0012)	(0.0001)
H <sub>4</sub>	0.4913	0.1678	0.1583	0.0049	(0.0010)	(0.0040)	(0.0000)	(0.0006)	(0.0000)
H <sub>5</sub>	0.5790	0.2408	0.9717	0.0044	(0.0009)	(0.0035)	(0.0000)	(0.0005)	(0.0000)
H <sub>6</sub>	0.6892	0.3256	0.8050	0.0025	(0.0005)	(0.0020)	(0.0000)	(0.0003)	(0.0000)
H <sub>7</sub>	0.7366	0.4640	0.8806	0.0171	(0.0035)	(0.0138)	(0.0000)	(0.0021)	(0.0001)
H <sub>8</sub>	0.6901	0.5044	0.1398	0.0061	(0.0012)	(0.0049)	(0.0000)	(0.0007)	(0.0001)
H <sub>9</sub> (OH)	0.3163	0.4461	0.5903	0.0056	(0.0011)	(0.0045)	(0.0000)	(0.0007)	(0.0000)

<sup>a</sup> The temperature factors are given in the form:  $T = \exp[-(\beta_{11}h^2 + \beta_{22}k^2 + \beta_{33}l^2 + \beta_{12}hk + \beta_{13}hl + \beta_{23}kl)]$ . The temperature factors for the hydrogen atoms are isotropic and were obtained by refinement on  $\beta_{11}$  only.

this compound of 2.847 Å is intermediate but outside of both ranges. It agrees well with the separation of 2.78 Å found for coppers joined by hydroxyl bridges in the dimeric compound di- $\mu$ -hydroxobis(dimethylamine-copper(II)) sulfate monohydrate.<sup>15</sup>

The chain and layer structures have a range of copper to hydroxyl bridge distances from 1.92 to 2.08 Å, with an average of 2.00 Å, and a range of hydroxyl oxygen to hydroxyl oxygen separations from 2.67 to 3.03 Å, with an average separation of 2.85 Å as compared to Pauling's crystal diameter of 2.80 Å for oxygen. This compound has an average Cu-OH distance of 1.92 Å and a separation of 2.581 Å between the two hydroxyl oxy-

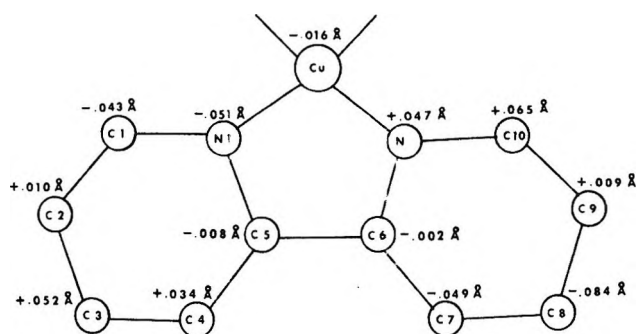


Figure 1. Deviations from the least-squares plane  $6.826X - 3.713Y + 2.388Z = -0.047$ .

**Table II:** Comparison of Average Distances (Å) and Angles (degrees) for Bipyridyl Systems

Compound	C-N	C-C	bipy-bipy	CNC	NCC	CCC
This study	1.346	1.382	1.485	119.1°	122.0°	119.0°
Bisbipyridyl copper <sup>16</sup>	1.36	1.40	1.52	118°	122°	119°
Bipyridine <sup>17</sup>	1.36	1.39	1.50	117°	123°	119°

gens. Both of these distances are somewhat shorter than the corresponding distances in the chain and layer structures but agree somewhat better with the average Cu-OH distance of 1.96 Å and the OH-OH separation of 2.497 Å found in the other copper dimer.

Each of the six-membered rings of the bipyridyl groups is planar with no atom being more than 0.006 Å from a least-squares plane. The deviations of the copper-bipyridyl system from a calculated plane are shown in Figure 1 and the bond distances and angles are given in Figure 2. A comparison of these distances and angles with those of iodobis(2,2'-bipyridyl)copper(II) iodide<sup>16</sup> and 2,2'-bipyridine<sup>17</sup> itself, in Table II,

(15) Y. Iitaka, K. Shimizu, and T. Kwan, *Acta Cryst.*, **20**, 803 (1966).

(16) G. A. Barclay, B. F. Hoskins, and C. H. L. Kennard, *J. Chem. Soc.*, 5691 (1963).

(17) L. Merritt and E. Schroeder, *Acta Cryst.*, **9**, 801 (1956).

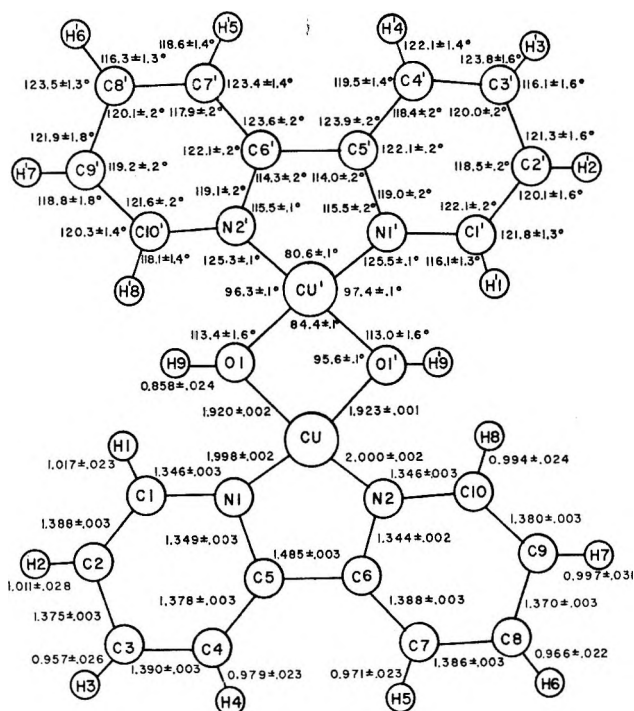


Figure 2. Bond distances and angles.

shows that there are no significant differences in the structures, when the standard deviations are considered. The bipyridyl nitrogen-copper-bipyridyl nitrogen angle of  $80.6^\circ$  is significantly less than  $90^\circ$  and may be due to the steric requirements of the bipyridyl ring system. This value is in good agreement with the value of  $82^\circ$  found for the same angle in the structure of bisbipyridyl copper.

The nitrate group has one oxygen bonded to a copper atom and another hydrogen bridged to the hydroxyl oxygen as shown in Figure 3. This bonding and bridging may be responsible for the evident distortion of the nitrate group. The geometry of this nitrate group is compared in Table III to that of other nitrate groups<sup>18,19</sup> which also show distortion. It is interesting to note

Table III: Comparison of Irregular Nitrate Groups

Compound	a, Å <sup>a</sup>	b, Å	c, Å	ab, deg	ac, deg	bc, deg
This study	1.232	1.244	1.254	120.4	122.2	117.4
Thorium nitrate pentahydrate <sup>18</sup>						
NO <sub>3</sub> (1)	1.202	1.250	1.270	123.2	121.7	115.2
NO <sub>3</sub> (2)	1.206	1.264	1.275	123.0	122.5	114.5
Cerium magnesium nitrate hydrate						
NO <sub>3</sub> (1)	1.220	1.259	1.268	122.8	121.2	116.1
NO <sub>3</sub> (2)	1.225	1.262	1.256	120.8	121.8	117.4

<sup>a</sup> The distance for the oxygen not involved in bonding to anything but the nitrate's nitrogen.

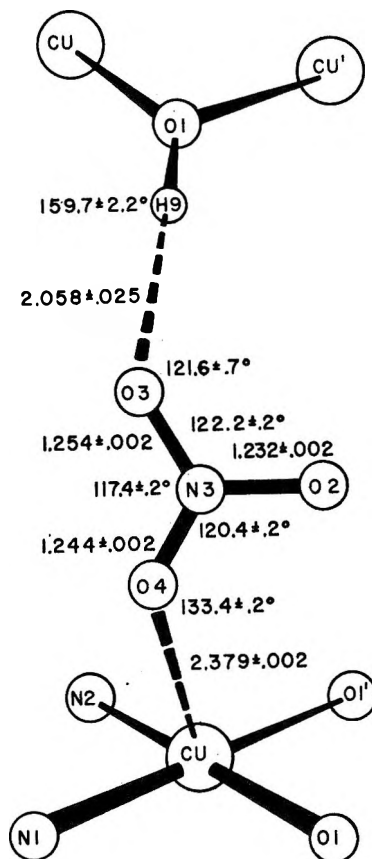


Figure 3. The nitrate group and its environment.

that these distortions in the bonds and angles do not alter the planarity of the species in this structure. The nitrogen is less than two standard deviations from the plane of the oxygens, despite O-N-O angles of  $117.4^\circ$  and  $122.2^\circ$ .

The two oxygens involved in the hydrogen bridging are separated by a distance of  $2.877 \text{ \AA}$ . The oxygen-hydrogen distance of  $0.858 \text{ \AA}$  is shorter than the average carbon-hydrogen distance of  $0.986 \text{ \AA}$ . All of these distances are shorter than the distances found in neutron diffraction work, but are in good agreement with X-ray results.<sup>20</sup> The bridging distance of  $2.058 \text{ \AA}$  is probably a slight overestimate of the separation between the hydroxyl hydrogen and the bridged nitrate oxygen.

*Acknowledgments.* We wish to thank the Robert A. Welch Foundation for its support of this work, and the National Science Foundation for a Departmental Equipment Grant, GP-8344, used for the purchase of the automated diffractometer.

(18) J. C. Taylor, M. H. Mueller, and R. L. Hitterman, *Acta Cryst.*, **20**, 842 (1966).

(19) A. Zalkin, J. D. Forrester, and D. H. Templeton, *J. Chem. Phys.*, **39**, 2881 (1963).

(20) W. C. Hamilton and J. A. Ibers, "Hydrogen Bonding in Solids," W. A. Benjamin, Inc., New York, N. Y., 1968.

# A Statistical-Thermodynamic Model of Aqueous Solutions of Alcohols

by Nora Laiken and George Némethy\*

*The Rockefeller University, New York, New York 10021 (Received December 5, 1969)*

A statistical-thermodynamic model for dilute aqueous solutions of the normal alcohols is presented. The model is a simple extension of the theoretical model for water structure proposed by Némethy and Scheraga, and retains all essential features and assumptions of the latter. Thus, the models are self-consistent in spite of the approximations inherent in them. The main assumption of the model presented here is the closely similar behavior between the OH group and a water molecule in aqueous environment. The partition function for the alcohol in water is based on a distribution of molecules over four energy levels, corresponding to zero, one, two, or three hydrogen bonds formed by the OH group. Due to a lack of spectroscopic data for alcohols in aqueous solution, the statistical weighting factors in the partition function had to be approximated and were selected in a manner consistent with the model for water. The results are insensitive to the exact assignment of these factors. In spite of the limitations and the simplicity of the model, it is able to predict thermodynamic parameters for the transfer of alcohols from dilute hydrocarbon solution to dilute aqueous solution which are in fairly close agreement with those observed experimentally. For the first four *n*-alkanols at 25°, the theoretical and experimental  $\Delta G^\circ$  values differ by less than 0.2 kcal/mol, while those for  $\Delta H^\circ$  differ by a maximum of 0.4 kcal/mol. The degree of hydrogen bonding of the OH group is found to be greater than either bulk water or water in contact with hydrocarbons.

## I. Introduction

Structural models for aqueous solutions are essential for a theoretical analysis of their behavior. The thermodynamic properties of aqueous solutions of hydrocarbons,<sup>1</sup> as well as those of hydrophobic interactions in proteins,<sup>2</sup> were explained several years ago by the extension of a statistical-thermodynamic model for liquid water.<sup>3</sup> In this paper, an application of this model<sup>1,3</sup> to the thermodynamic behavior of dilute solutions of *n*-alkanols in water is presented. The purpose of this investigation is to see whether a model for the latter can be constructed on the basis of the model for water<sup>3</sup> and consistent with its main features.

The model for liquid water was an approximate theory, containing many assumptions and simplifications, most of which were discussed in the original publication.<sup>3</sup> Recently, criticisms have been raised with respect to certain assumptions of the model, such as the assignments of some statistical weights and, more importantly, the approximations used in evaluating the combinatorial factor in the partition function.<sup>4,5</sup> A refinement of the model (while retaining some of its characteristic features) is expected to yield an improved theory,<sup>5</sup> although many uncertainties, due to shortcomings in the theories of liquids, cannot be eliminated at present. An exact model for alcohol-water solutions is even more difficult to construct, because of the uncertainty regarding many of the parameters required (such as reliable data on the strength of alcohol-water hydrogen bonds and on the modes of motion of the molecules in these mixtures).

However, it still appears of interest to see whether some of the basic concepts of the Némethy-Scheraga theory for water<sup>3</sup> (the presence of hydrogen-bonded water clusters, the description of the system in terms of

degree of hydrogen bonding, etc.) can be applied to the more complex alcohol-water solutions. The use of the simple model<sup>3</sup> has the advantage that the number of arbitrary new assumptions can be held to a minimum, even though the approximations inherent in the model for water<sup>3</sup> will render the results obtained here uncertain to some extent. In spite of the many approximations, the model presented here is able to predict successfully many thermodynamic properties of dilute aqueous solutions of *n*-alkanols. Thus, the insights gained in this study can be helpful in the construction of more refined models for such solutions, when the basis for such refinements has been given through improvements in the theories for water. In addition, the model can be used as a source of thermodynamic parameters for buried polar groups in a hydrophobic region of a protein, small molecule-protein interactions involving OH and CH<sub>2</sub> groups, the alcohol-induced denaturation of proteins, and similar phenomena.

## II. Description of the Model

The model is applicable to very dilute solutions in which interactions between alcohol molecules can be neglected. All thermodynamic parameters calculated refer to the transfer of one mole of alcohol from a state

\* To whom correspondence should be addressed.

(1) G. Némethy and H. A. Scheraga, *J. Chem. Phys.*, **36**, 3401 (1962).

(2) G. Némethy and H. A. Scheraga, *J. Phys. Chem.*, **66**, 1773 (1962).

(3) G. Némethy and H. A. Scheraga, *J. Chem. Phys.*, **36**, 3382 (1962).

(4) S. Levine and J. W. Perram in "Hydrogen-Bonded Solvent Systems," A. K. Covington and P. Jones, Ed., Taylor and Francis, Ltd., London, 1968, p 115.

(5) A. T. Hagler, G. Némethy, and H. A. Scheraga, work in progress.

of infinite dilution in a hydrocarbon solvent to a similar state in water.<sup>6</sup>

In keeping with the approach used earlier,<sup>1,3</sup> the changes in the thermodynamic parameters accompanying the transfer process are analyzed in terms of (a) interactions of an OH group attached to an alkyl chain and interacting with the solvent environment, (b) changes in water structure around the solute, and (c) the changing interaction energy of the alkyl group with the solvent environment. In the following expressions, these contributions are referred to by the subscripts OH, W, and R, respectively. Thus, the Gibbs free energy of transfer is expressed as

$$\Delta G^\circ = \Delta G_{\text{OH}} + \Delta G_{\text{W}} + \Delta G_{\text{R}} \quad (1)$$

and the other thermodynamic parameters are obtained using the standard relationships

$$\Delta H^\circ = -R \frac{\partial(\Delta G^\circ/T)}{\partial(1/T)} \quad (2)$$

$$\Delta S^\circ = \frac{\Delta H^\circ - \Delta G^\circ}{T} \quad (3)$$

The expression for  $\Delta G^\circ$  indicated in eq 1 is an approximation made for the sake of clarity in the description following. It does not imply that the free energy consists of additive contributions which can be ascribed individually to the hydroxyl group and the alkyl chain, respectively. For example,  $\Delta G_{\text{OH}}$  depends on the size of the alkyl chain, due to its effect on the vibrational contributions of the alcohol (see below) and it also includes a contribution from the interactions of the OH group with neighboring water molecules.

*A. Change of State of the Hydroxyl Group.* The three terms occurring in eq 1 now will be discussed separately. Using the superscripts aq and hc to represent aqueous and hydrocarbon solutions of the alcohol, respectively, the term  $\Delta G_{\text{OH}}$  may be written

$$\Delta G_{\text{OH}} = G_{\text{OH}}^{\text{aq}} - G_{\text{OH}}^{\text{hc}} \quad (4)$$

The terms on the right side of eq 4 are obtained from partition functions for the alcohol molecule in each state.

The partition function of the alcohol in aqueous solution is quite similar to that of liquid water.<sup>3</sup> Thus, alcohol molecules in aqueous solution may be divided into classes of varying energy and internal freedom depending upon the number of hydrogen bonds between the OH group and its neighboring water molecules. In the model for liquid water,<sup>3</sup> the difference in energy between classes,  $E_{\text{H}}$ , is composed of two contributions

$$1/2 n_{\text{H}} E_{\text{H}} = 1/2 n_{\text{H}} \epsilon_{\text{H}} - 1/2 (z_{\text{u}} - n_{\text{H}}) E_{\text{w}} \quad (5)$$

where  $n_{\text{H}}$  is the maximum number of hydrogen bonds possible per water molecule,  $z_{\text{u}}$  is the number of nearest neighbors of the nonhydrogen-bonded molecule,  $\epsilon_{\text{H}}$  is the intrinsic strength of the hydrogen bond, and  $E_{\text{w}}$

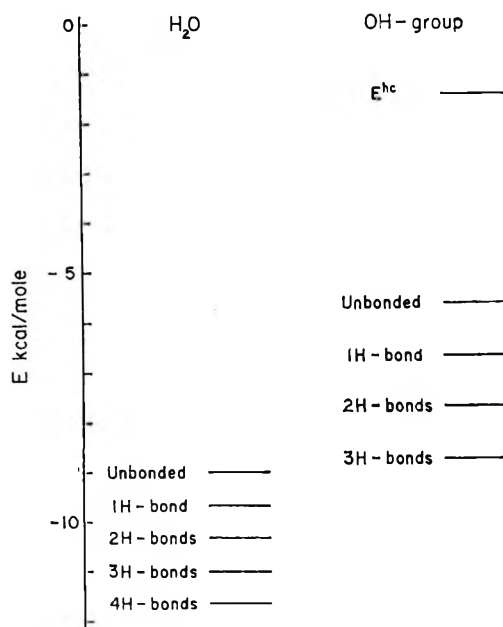


Figure 1. Energy levels for the species of  $\text{H}_2\text{O}$  molecules and OH groups in liquid water. Also included is  $E^{\text{hc}}$ , the energy of the OH group in hydrocarbon solution. The zero of the energy scale refers to an infinite separation between molecules.

represents the average van der Waals interaction energy between two water molecules not linked by a hydrogen bond. For liquid water,<sup>3</sup> assuming the values  $n_{\text{H}} = 4$  and  $z_{\text{u}} = 8$ , these parameters were found to be  $\epsilon_{\text{H}} = 3.57$  kcal/mol and  $E_{\text{H}} = 2.25$  kcal/mol, based on the parameter  $E_{\text{H}} = 1.32$  kcal/mol. If the OH group is assumed to be similar to a water molecule, the strength of the  $\text{OH} \cdots \text{H}_2\text{O}$  hydrogen bond and the  $\text{OH} \cdots \text{H}_2\text{O}$  van der Waals interaction energy can be assigned the above values of  $\epsilon_{\text{H}}$  and  $E_{\text{w}}$ , respectively. However, the energy level separation for the OH group given by eq 5 will differ from that for water since  $n_{\text{H}} = 3$  and  $z_{\text{u}} = 5$ . The latter was assigned with the aid of molecular models and is consistent with the value chosen for  $z_{\text{u}}$  in the water theory.<sup>3</sup> Thus,  $E_{\text{H}} = 2.07$  kcal/mol for the OH group. The energy levels of the various OH species are indicated in Figure 1, which also includes those of liquid water for purposes of comparison.<sup>7-10</sup>

(6) The hydrocarbon solvent, rather than the pure liquid alcohol, was chosen as the initial state in keeping with the use of the hydrocarbon theory as a parent model. If the pure alcohol were the initial state, it would be necessary to postulate a model for the liquid alcohols as well as their aqueous solutions.

(7) Some recent considerations on the nature of the hydrogen bond suggest that the energy of hydrogen bond in water depends on what other hydrogen bonds the water molecule makes,<sup>8,9</sup> an idea that is implicit in the Frank-Wen theory of flickering clusters<sup>10</sup> on which the model used here was based.<sup>3</sup> However, as an approximation, and in order to maintain consistency with the theory of water,<sup>3</sup> the approach used in the latter was retained here.

(8) J. Del Bene and J. A. Pople, *Chem. Phys. Lett.*, **4**, 426 (1969).

(9) D. Hankins, J. W. Moskowitz, and F. H. Stillinger, *ibid.*, **4**, 527 (1970).

(10) H. S. Frank and W.-Y. Wen, *Discuss. Faraday Soc.*, **24**, 133 (1957).

The mole fractions of the four species of OH groups are denoted by  $x_i^{\text{OH}}$  ( $i = 3, 2, 1, u$ ;  $u$  referring to the unbonded OH group), only three of which are independent due to the constraint

$$\sum_{i=u}^3 x_i^{\text{OH}} = 1 \quad (6)$$

In analogy to the model of liquid water,<sup>3</sup> the partition function for a mole of OH groups in dilute aqueous solution is given by

$$Z_{\text{OH}^{\text{aq}}} = \sum_{\{x_i^{\text{OH}}\}} g \prod_{i=u}^3 [f_i^{\text{aq}} \exp(-E_i^{\text{aq}}/RT)]^{N_0 x_i^{\text{OH}}} \quad (7)$$

where  $g$  is a combinatorial factor

$$\frac{N_0!}{\prod_{i=u}^3 (N_0 x_i^{\text{OH}})!} \quad (8)$$

$N_0$  is Avogadro's number,  $E_i^{\text{aq}}$  are the energy levels, and  $f_i^{\text{aq}}$  are the statistical weighting factors which allow for differences in vibrational, rotational, and translational freedom among the species (to be discussed below). The partition function is evaluated by the maximum term method, so that  $Z$  is equated with the maximum term in the summation of eq 7. The values of  $x_u^{\text{OH}}$ ,  $x_2^{\text{OH}}$ , and  $x_3^{\text{OH}}$  corresponding to the maximum term are found by setting  $W = \ln Z$ , using Stirling's approximation, and solving the three simultaneous equations

$$\partial W / \partial x_u^{\text{OH}} = 0 \quad (9)$$

$$\partial W / \partial x_2^{\text{OH}} = 0 \quad (10)$$

$$\partial W / \partial x_3^{\text{OH}} = 0 \quad (11)$$

These equations are linear in the unknowns and can be solved easily with Kramer's rule. Thus<sup>11</sup>

$$G_{\text{OH}^{\text{aq}}} = -RT \ln Z_{\text{OH}^{\text{aq}}} \quad (12)$$

It is important to note that this term does not contain contributions from the dispersion interaction between the alkyl chain and solvent molecules, nor the free energy of structural change of the water, since these are included in the terms  $\Delta G_R$  and  $\Delta G_w$  in eq 1, respectively.

The expression for the combinatorial factor,  $g$ , in eq 8 was chosen to maintain internal consistency with the model for water,<sup>3</sup> even though more recent studies have indicated that such a form results in an overcounting of configurations.<sup>4,5</sup>

In the infinitely dilute hydrocarbon solution, the alcohol is unable to form hydrogen bonds. Therefore, all OH groups have the same energy,  $E^{\text{hc}}$ , which is given by the nonbonded interaction energy per  $\text{CH}_2 \cdots \text{OH}$  contact,  $E_{\text{OH} \cdots \text{R}}$ , multiplied by the number of such contacts per OH group.

$E_{\text{OH} \cdots \text{R}}$  is found by evaluating the Slater-Kirkwood formula<sup>12,13</sup>

$$E_{\text{OH} \cdots \text{R}} = \frac{d}{r^{12}} - \frac{e}{r^6} - \frac{b}{r^6} \quad (13)$$

at  $r = r_{\text{OH} \cdots \text{R}}$ , where  $r$  is the distance between the  $\text{CH}_2$  and OH groups,  $r_{\text{OH} \cdots \text{R}}$  is the van der Waals contact distance, and  $d$ ,  $e$ , and  $b$  are the coefficients for repulsion, dispersion interactions, and the induction effect, respectively. The values of the coefficients were calculated from the parameters given by Gibson and Scheraga,<sup>14</sup> following the methods outlined by them. With the aid of molecular models, it is found that an average of seven such contacts are allowed per OH group, giving  $E^{\text{hc}} = -1.43$  kcal/mol (Figure 1).

The partition function for the OH group in hydrocarbon solution is

$$Z_{\text{OH}^{\text{hc}}} = f^{\text{hc}} \exp(-E^{\text{hc}}/RT) \quad (14)$$

where  $f^{\text{hc}}$  is the statistical weight assigned to the molecules.<sup>15</sup> As in eq 7 and 12, the dispersion interaction between the alkyl chain and the solvent is omitted from eq 14 and included in the term  $\Delta G_R$  of eq 1.

There is considerable uncertainty in the assignment of the frequencies entering the statistical weighting factors, due to a lack of experimental data and the approximate nature of the model. However, the results are not very sensitive to the exact values of these parameters, as discussed below. Thus, the values used were chosen to maintain internal consistency with the model for water<sup>3</sup> on which the present treatment is based.

In order to assign statistical weights  $f_i$  to the various alcohol species, it is only necessary to consider those intramolecular bond stretching and bending modes that are affected by hydrogen bonding and the external degrees of freedom, the translations and rotations, which are converted into new vibrational modes upon hydrogen bond formation. The intramolecular modes and the effect of hydrogen bonding upon them have been studied quite thoroughly.<sup>16,17</sup> Of the modes affected by hydrogen bonding, only the so-called C-O wagging or out-of-plane deformation contributes significantly to the partition function at ordinary temperatures. From

(11) Rigorously, the partition function gives the Helmholtz free energy and the internal energy rather than the Gibbs free energy and the enthalpy, as required for comparison with experimental data. However, the thermodynamic parameters are used in expressions such as eq 4 in which  $p\Delta V$  can be neglected. Therefore, the Helmholtz free energy and the internal energy are replaced by the Gibbs free energy and enthalpy, respectively, throughout this paper.

(12) K. S. Pitzer, *Advan. Chem. Phys.*, **2**, 59 (1959).

(13) R. A. Scott and H. A. Scheraga, *J. Chem. Phys.*, **42**, 2209 (1965).

(14) K. D. Gibson and H. A. Scheraga, *Proc. Nat. Acad. Sci.*, **58**, 420 (1967).

(15) Only those degrees of freedom need be included in  $f^{\text{hc}}$  which are affected by hydrogen bonding and therefore appear in the  $f_i^{\text{aq}}$  as well.

(16) A. V. Stuart and G. B. B. M. Sutherland, *J. Chem. Phys.*, **24**, 559 (1956).

(17) M. Falk and E. Whalley, *ibid.*, **34**, 1554 (1961).

infrared studies of pure liquid alcohols, a band centered at  $670\text{ cm}^{-1}$  has been assigned to this mode.<sup>18</sup> This vibration also can be regarded as a hindered rotation of the OH group about the C–O axis. Such frequencies are related to the barrier to rotation about the bond in question by<sup>19,20</sup>

$$\nu = n \sqrt{\frac{VA_1A_2}{A}} \quad (15)$$

where  $V$  is the barrier to rotation,  $n$  is the number of minima in a  $360^\circ$  rotation about the bond,  $A_1$  and  $A_2$  are the rotational constants corresponding to the moments of inertia  $I_1$  and  $I_2$  of the two parts of the molecule that rotate with respect to each other, and  $A$  is the rotational constant corresponding to  $I = I_1 + I_2$ . The rotational constants are of the form

$$A = \frac{h}{8\pi cI} \quad (16)$$

Three factors contribute to  $V^{\text{alc}}$ , the barrier to rotation about the C–O bond of an alcohol molecule in pure alcohol solution. First of all, there is a contribution  $V_0$  due to the intrinsic barrier to rotation. Secondly, intermolecular dipole–dipole interactions increase the barrier by the amount  $V_d^{\text{alc}}$ . Third, for each hydrogen bond formed a factor  $V_H$  must be added to the barrier. Equation 15 gives  $V^{\text{alc}} = 5.91\text{ kcal/mol}$  for the  $670\text{ cm}^{-1}$  vibration. In terms of the above contributions

$$V^{\text{alc}} = V_0 + V_d^{\text{alc}} + 2V_H \quad (17)$$

The multiplier two is used for  $V_H$  since di-bonded OH groups predominate in pure liquid alcohols.<sup>21</sup>

$V_0$  and  $V_H$  are assumed to be independent of the solution in which the alcohol molecule is situated. Thus, frequencies for the C–O wagging mode in the current model can be calculated from eq 15 with

$$V_i^{\text{aq}} = V_0 + V_d^{\text{aq}} + iV_H \quad (i = 1, 2, 3) \quad (18)$$

$$V_d^{\text{aq}} = V_0 + V_d^{\text{alc}} \quad (19)$$

$$V^{\text{hc}} = V_0 \quad (20)$$

The intrinsic barrier  $V_0$  has been assigned a value of approximately 1 kcal/mol on theoretical as well as experimental grounds.<sup>22–24</sup>  $V_H$  can be determined from eq 17 once  $V_d^{\text{alc}}$  is known. Values of  $V_d^{\text{alc}}$  and  $V_d^{\text{aq}}$  are derived from the dipole contribution for pure liquid water,  $V_d^{\text{w}}$ , as follows. The potential of a molecule with dipole moment  $\mu$  in a medium producing an effective field  $\mathbf{F}$  is given by<sup>25</sup>

$$V = -\mu \cdot \mathbf{F} \quad (21)$$

with

$$\mathbf{F} = \mu \frac{(\epsilon - 1)(\epsilon + 2)}{9\epsilon a^3} \quad (22)$$

where  $\epsilon$  is the dielectric constant of the medium and

$a$  is the molecular radius, calculated from molar volume data. Therefore

$$V_d^{\text{aq}} = V_d^{\text{w}} \left( \frac{\mu_{\text{ROH}}}{\mu_{\text{w}}} \right)^2 \left( 1 - \cos \frac{1}{2}\theta \right) \quad (23)$$

$$V_d^{\text{alc}} = V_d^{\text{w}} \left( \frac{\mu_{\text{ROH}}}{\mu_{\text{w}}} \right)^2 \left( 1 - \cos \frac{1}{2}\theta \right) \times \frac{(\epsilon_{\text{ROH}} - 1)(\epsilon_{\text{ROH}} + 2)a_{\text{w}}^3\epsilon_{\text{w}}}{(\epsilon_{\text{w}} - 1)(\epsilon_{\text{w}} + 2)a_{\text{ROH}}\epsilon_{\text{ROH}}} \quad (24)$$

where  $\theta$  is the angle through which the ROH dipole is rotated during a  $180^\circ$  rotation about the C–O bond. The ROH dipole makes an angle of  $62^\circ$  with the C–O bond,<sup>26</sup> so that  $\theta = 124^\circ$ . The factor

$$(1 - \cos 1/2\theta) \quad (25)$$

is necessary since  $V_d^{\text{w}}$  refers to a  $180^\circ$  rotation of the water dipole. Following Cartwright,<sup>27</sup>  $V_d^{\text{w}}$  was assigned the value  $5RT$ . The resulting dipole contributions are  $V_d^{\text{aq}} = 1.34\text{ kcal/mol}$  and  $V_d^{\text{alc}} = 0.25\text{ kcal/mol}$ .<sup>28</sup> From the latter, a value of  $V_H = 2.33\text{ kcal/mol}$  is obtained. Thus, the frequencies in the first row of Table I can be assigned to the C–O wagging mode.

The contributions of the external degrees of freedom to the statistical weights must be estimated due to the lack of spectral data in the low-frequency range where the excitation of these modes of motion occurs. The approximations made were those most consistent with the model for liquid water.<sup>3</sup> For alcohol molecules with OH groups involved in hydrogen bonding, the three translational degrees of freedom are converted into translational vibrations. Estimates of their frequencies were obtained from those for liquid water multiplied by a mass correction factor.<sup>29</sup>

(18) A. V. Stuart and G. B. B. M. Sutherland, *J. Chem. Phys.*, **20**, 1977 (1952).

(19) G. Herzberg, "Infrared and Raman Spectra," D. Van Nostrand Company, Inc., Princeton, N. J., 1945, p 225 ff.

(20) Equation 15 is strictly valid only for molecules with  $n$  identical potential minima such as methanol. Therefore, the constants used in eq 15–24 are those for methanol, and in the absence of additional information the frequencies for this mode are assumed to be independent of chain length.

(21) F. Franks and D. J. G. Ives, *Quart. Rev. (London)*, **20**, 1 (1966).

(22) D. G. Burkhard and D. M. Dennison, *Phys. Rev.*, **84**, 408 (1951).

(23) R. E. Hughes, W. E. Good, and D. K. Coles, *ibid.*, **84**, 418 (1951).

(24) E. V. Ivash and D. M. Dennison, *J. Chem. Phys.*, **21**, 1804 (1953).

(25) H. Fröhlich, "Theory of Dielectrics," Oxford University Press, London, 1958, Chapter II.

(26) C. P. Smyth, "Dielectric Behavior and Structure," McGraw-Hill, New York, N. Y., 1955, p 301.

(27) C. H. Cartwright, *Nature*, **135**, 872 (1935); *Phys. Rev.*, **49**, 470 (1936).

(28)  $V_d^{\text{w}}$ ,  $\epsilon$ , and  $a$  are temperature dependent. The calculations here are performed for  $t = 25^\circ$  since the variations of the frequencies with temperature would be small in the temperature range studied.

(29) The frequencies for an OH group with  $i$  hydrogen bonds were derived from those for a water molecule with  $i$  hydrogen bonds.

$$\sqrt{\frac{m_w}{m_{ROH}}} \quad (26)$$

where  $m_w$  and  $m_{ROH}$  are the masses of the water and alcohol molecules, respectively. The unbonded alcohol molecules in aqueous solution and the alcohol molecules in hydrocarbon solution have translational freedom within a cage, or "free volume," defined by their nearest neighbors, just as unbonded water molecules.<sup>3</sup>

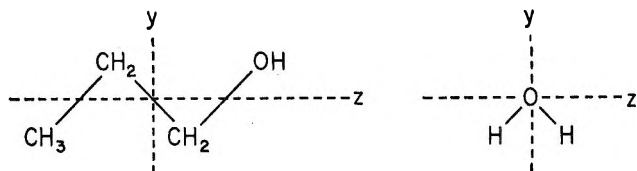


Figure 2. Coordinate axes for alcohol and water molecules. The  $x$  axis is perpendicular to the plane of the page.

In aqueous solution, the rotational degrees of freedom are converted to rotational vibrations, or librations, as a result of restrictions imposed on molecular motion by dipole-dipole interactions, hydrogen bonding (when it exists) and steric effects when rotation is about the  $x$  or  $y$  axis (see Figure 2). For alcohols in hydrocarbon solution, only steric restrictions are present. Therefore, while the  $x$  and  $y$  rotations become librations, rotation about the  $z$  axis is assumed to be free. The contributions of each restriction can be obtained in the form of a frequency, as described below. It is assumed that the force constants for each restriction contribute additively to the librational frequencies.

In aqueous solution, the restrictions on rotation due to dipole-dipole interactions result from the effect of the local potential field, due to neighboring dipoles, on the dipole moment of the alcohol molecule (eq 21). This potential for water is  $V_d^w = 5RT$ , as indicated above. In alcohols, the value of  $V_d$  for rotation about each axis depends on the corresponding component of the dipole moment. For most modes of motion, dipole-dipole interactions represent a small contribution to the frequency, because of the additional restrictions on rotation due to hydrogen bonding and steric effects. In water, the latter two effects are absent for the unbonded molecule rotating about the  $z$  axis, so that the use of the above  $V_d^w$  resulted in an assignment of 175  $\text{cm}^{-1}$  to this mode of motion.<sup>3</sup> Actually, this frequency has been shown more recently to correspond to a translational rather than a rotational vibration.<sup>30</sup> The value of  $V_d^w = 5RT$  for the assignment of dipole restrictions in the present model was retained for the sake of internal consistency with the model for water.<sup>3</sup> However, the dipole contribution represents only part of the total restriction to rotation (see above), and changes in its magnitude of as much as 20% would affect the  $f_i^{\text{aq}}$  values (eq 7) by an insignificant amount.

In water, the  $y$  axis coincides with the dipole axis, so that the 60, 450, and 650- $\text{cm}^{-1}$  librational frequencies about this axis<sup>3</sup> may be attributed solely to the restrictions imposed on rotation by one, two, and three hydrogen bonds, respectively. These frequencies were multiplied by the following correction factor to give contributions due to hydrogen bonding for unbonded, di-bonded and tri-bonded OH groups, respectively<sup>29</sup>

$$\sqrt{\frac{I_{w,v}}{I_{ROH}}} \quad (27)$$

Steric contributions were estimated by replacing the alcohol with a rigid, cylindrical rod<sup>31</sup> (of the appropriate length and cross-sectional area) surrounded by an empty shell whose width is determined by the "free volume" available to the center of mass of the molecule. In such a shell, rotation of the alcohol about the  $x$  and  $y$  axes is restricted to an angle  $\beta$  whose magnitude can be calculated from the dimensions of the rod and the width of the shell. Then, following Eyring,<sup>32</sup> the steric contribution can be determined from

$$f_{v, \text{steric}} = \frac{\beta}{360^\circ} f_r \quad (28)$$

where  $f_{v, \text{steric}}$  is the vibrational partition function corresponding to the steric frequency contribution and  $f_r$  is the partition function for free rotation about the axis under consideration (eq 35).

The frequencies calculated by the methods described above are listed in Table I. Although the methods by which they were calculated are quite approximate, random perturbations of their values by as much as 20% altered the final results by only 0.3 kcal/mol for  $\Delta G^\circ$  and 0.1 kcal/mol for  $\Delta H^\circ$ . These frequencies can be used to calculate statistical weighting factors as follows

$$f_i^{\text{aq}} = f_v^{\text{aq}} \quad (i = 1, 2, 3) \quad (29)$$

$$f_u^{\text{aq}} = f_v f_v^{\text{aq}} \quad (30)$$

$$f^{\text{hc}} = f_v f_r f_v^{\text{hc}} \quad (31)$$

with<sup>33</sup>

$$f_v^{\text{aq}} = \prod_{j=1}^s [1 - \exp(-h\nu_j/kT)]^{-1} \quad (32)$$

where  $s = 7$  for  $i = 1, 2, 3$ , and  $s = 4$  for  $i = u$

$$f_v^{\text{hc}} = \prod_{j=1}^3 \exp(-h\nu_j/2kT) [1 - \exp(h\nu_j/kT)]^{-1} \quad (33)$$

(30) G. E. Walrafen, *J. Chem. Phys.*, **40**, 3249 (1964).

(31) The use of a cylindrical rod model limits the application of this theory to those alcohols whose hydrocarbon chains retain extended conformations in aqueous solution, *i.e.*, methanol to butanol.<sup>1</sup>

(32) J. F. Kincaid and H. Eyring, *J. Chem. Phys.*, **6**, 620 (1938).

(33) The zero point contribution to the vibrational partition function is omitted for aqueous solutions of the alcohols since the energies (Figure 1) are measured from the vibrational ground state rather than from the bottom of the potential curve.

$$f_t = \left( \frac{2\pi m_{\text{ROH}} kT}{h^2} \right)^{1/2} V_t \quad (34)$$

where  $V_t$  is the "free volume"<sup>3</sup>

$$f_r = 2\pi \left( \frac{2\pi I kT}{h^2} \right)^{1/2} \quad (35)$$

The subscripts v, t, and r refer to vibration, translation, and rotation, respectively. The value of  $V_t$  has been taken directly from the model for liquid water<sup>3</sup> since it represents the volume available to the center of mass of a molecule in a given environment and therefore should not depend on the size of the molecule.<sup>34</sup> Thus,  $V_t = 4.4 \times 10^{-25} \text{ cm}^3$ .

**Table I:** Vibrational Frequency Assignments for Calculation of Weighting Factors  $f^{\text{hc}}$  and  $f^{\text{aq}}$

Mode of motion	OH group in hc	Frequency, $\text{cm}^{-1}$			
		OH group in aq			
		$i = u$	$i = 1$	$i = 2$	$i = 3$
C-O wagging	275	420	595	730	840
Rotational vibrations					
<i>x</i> axis:					
Methanol	125	125	130	160	195
Ethanol	90	95	95	110	125
Propanol	75	75	75	85	95
Butanol	65	65	65	70	80
<i>y</i> axis:					
Methanol	140	140	145	180	215
Ethanol	100	100	100	120	140
Propanol	80	80	80	90	100
Butanol	65	65	65	75	80
<i>z</i> axis:					
Methanol		45	55	245	350
Ethanol		35	40	145	205
Propanol		30	35	125	175
Butanol		25	30	105	155
Translational vibrations					
<i>x</i> , <i>y</i> , and <i>z</i> axes:					
Methanol		120	120	160	
Ethanol		100	100	130	
Propanol		90	90	115	
Butanol		80	80	105	

<sup>a</sup> Because of the approximations used in their calculation, the frequencies have been rounded to the nearest  $5 \text{ cm}^{-1}$ .

**B. Change of State of the Water.** When an alcohol molecule is transferred to an aqueous solution, the thermodynamic properties of the water molecules adjacent to its hydrocarbon chain are altered.<sup>1</sup> Parameters for these molecules are specified by superscript c while those for bulk water are indicated by o. Hence, it is possible to write

$$\Delta G_w = y(G_w^c - G_w^o) \quad (36)$$

in a manner analogous to that used for hydrocarbon solutions,<sup>1</sup> where  $y$  is the number of water molecules involved. Equation 36 assumes that water molecules in contact with the OH group but not the alkyl chain are equivalent to bulk water. This is consistent with the use of the parameters  $\mathcal{E}_H$  and  $E_w$  to describe  $\text{OH} \cdots \text{H}_2\text{O}$  as well as  $\text{H}_2\text{O} \cdots \text{H}_2\text{O}$  hydrogen bonds.

The values of the thermodynamic parameters in eq 36 are obtained from the models for water<sup>3</sup> and the aqueous solutions of the hydrocarbons.<sup>1</sup> The parameter  $y$  is composed of two parts

$$y = y_R + y_{\text{ROH}} \quad (37)$$

where  $y_R$  represents the number of water molecules touching only the hydrocarbon chain and  $y_{\text{ROH}}$  represents those in contact with both the hydrocarbon chain and the OH group. The  $y_R$  values, listed in Table II, were determined from molecular models and are consistent with the analogous parameters in the hydrocarbon theory.<sup>1</sup> Those for  $y_{\text{ROH}}$  were set equal to a fixed fraction of the total number of water neighbors of the OH group. From molecular models, the best value for this fraction was found to be 60%. Therefore

$$y_{\text{ROH}} = 0.6 \sum_{i=u}^3 x_i^{\text{OH}} z_i \quad (38)$$

where  $z_i$  is the number of water neighbors of an OH group with  $i$  hydrogen bonds. The parameter  $z_i$  is assumed to vary linearly between  $z_u = 5$  and  $z_3 = 3$ . Values for  $y_{\text{ROH}}$  at  $25^\circ$  are listed in Table II.

**Table II:** Nearest Neighbor Parameters for Hydrocarbon Chain

Alcohol	$y_R$	$y_{\text{ROH}}$ ( $25^\circ$ )	$c_R$
Methanol	7	2.26	8
Ethanol	10	2.27	13
Propanol	12	2.28	18
Butanol	14	2.29	23

**C. Change of State of the Hydrocarbon Chain.** Because the alcohol molecules were treated as cylindrical rods when calculating the weights, only alcohols retaining a fully extended conformation in aqueous solution are considered.<sup>31</sup> Therefore,  $\Delta S_R = 0^1$  and

$$\Delta G_R = \Delta H_R = y\Delta E_1 - c_R E_R \quad (39)$$

where  $y\Delta E_1$  is the energy gain upon establishment of  $y$  hydrocarbon-water contacts,  $E_R$  is the energy of a single methyl-methyl pairwise interaction, and  $c_R$  is the number of such contacts. The values of  $\Delta E_1$  and  $E_R$  were taken from the model of aqueous solutions of the hydrocarbons,<sup>1</sup> in which they are assigned values of  $-0.031$  and  $-0.15$  kcal/mol, respectively. The  $c_R$  values were determined from molecular models to conform approximately with hexagonal packing. They are listed in Table II.

### III. Results and Discussion

Using the model described in the previous section, thermodynamic parameters for the transfer of one mole

(34) In the absence of other information it is assumed that  $V_t$  will not be greatly different in the hydrocarbon environment.

**Table III:** Observed Thermodynamic Parameters for the Transfer of One Mole of Alcohol from Hydrocarbon to Aqueous Solution at 25°

Alcohol	Process	$\Delta G^\circ$ , kcal/mol	Ref	Process	$\Delta G^\circ$ , kcal/mol	Ref
Methanol	<i>n</i> -Hexane $\rightarrow$ methanol	$-2.66 \pm 1\%$	36	Methanol $\rightarrow$ water	$0.25 \pm 1.8\%$	36
	<i>n</i> -Heptane $\rightarrow$ methanol	$-2.65 \pm 1\%$	36			
Ethanol	<i>n</i> -Hexane $\rightarrow$ ethanol	$-2.34 \pm 1\%$	36	Ethanol $\rightarrow$ water	$0.72 \pm 1.8\%$	36
	<i>n</i> -Heptane $\rightarrow$ ethanol	$-2.33 \pm 1\%$	36			
	<i>n</i> -Heptane $\rightarrow$ ethanol	$-2.37 \pm 1\%$	37			
1-Propanol	<i>n</i> -Hexane $\rightarrow$ propanol	$-2.24 \pm 1\%$	36	Propanol $\rightarrow$ water	$1.44 \pm 1.8\%$	36
	<i>n</i> -Heptane $\rightarrow$ propanol	$-2.23 \pm 1\%$	36			
	<i>n</i> -Heptane $\rightarrow$ propanol	$-2.30 \pm 1\%$	38			
1-Butanol	<i>n</i> -Hexane $\rightarrow$ butanol	$-2.19 \pm 1\%$	36	Butanol $\rightarrow$ water	$2.23 \pm 1.8\%$	36
	<i>n</i> -Heptane $\rightarrow$ butanol	$-2.18 \pm 1\%$	36			
$\Delta H^\circ$ , kcal/mol						
Methanol	Hydrocarbon $\rightarrow$ methanol	$-5.81$ to $-5.62$	39 <sup>a,b</sup>	Methanol $\rightarrow$ water	$-1.756 \pm 0.010$	40
					$-1.733 \pm 0.014$	41
					$-1.754 \pm 0.007$	42
Ethanol	Hydrocarbon $\rightarrow$ ethanol Heptane $\rightarrow$ ethanol	$-5.74$ to $-5.55$	39 <sup>a</sup>	Ethanol $\rightarrow$ water	$-2.380 \pm 0.010$	40
		$-5.67 \pm 1\%$			37	$-2.42 \pm 0.10$
						$-2.415 \pm 0.020$
					$-2.433 \pm 0.012$	42
1-Propanol	Hydrocarbon $\rightarrow$ propanol Heptane $\rightarrow$ propanol	$-5.67$ to $-5.48$	39 <sup>a</sup>	Propanol $\rightarrow$ water	$-2.20 \pm 0.10$	43
		$-5.60 \pm 1\%$			38	$-2.422 \pm 0.019$
						$-2.419 \pm 0.007$
1-Butanol	Hydrocarbon $\rightarrow$ butanol	$-5.60$ to $-5.41$	39 <sup>a</sup>	Butanol $\rightarrow$ water	$-2.15 \pm 0.10$	43
					$-2.217 \pm 0.018$	41
					$-2.249 \pm 0.010$	42

<sup>a</sup> Estimated from data at 30 and 45°, assuming the variation of  $\Delta H^\circ$  with  $T$  is linear.<sup>38</sup> The hydrocarbon solvents on which the data are based are *n*-hexane, *n*-heptane, and *n*-nonane. <sup>b</sup> Estimated from a graph of  $\Delta H^\circ$  vs.  $n$ , the number of carbon atoms, using data for  $n = 2-4$ .

of alcohol from hydrocarbon to aqueous solution have been calculated. Experimental values of the parameters for this process may be obtained by combining data for the solution of alcohols in hydrocarbon solvents with those for the solution of alcohols in water. The most recently available data at 25° are listed in Table III.<sup>35</sup> In those cases where the same measurement has been performed by different workers,<sup>36-43</sup> the results are in fairly good agreement. Also, the specific choice of hydrocarbon solvent seems to be unimportant.

The observed thermodynamic parameters for the overall solution process are compared with those calculated theoretically in Table IV and in Figure 3.<sup>44</sup> Considering the simplicity of the model and the fact that no adjustable parameters were used, the agreement between theory and experiment can be considered fairly good. The value of  $z_u = 5$ , while not rigorously defined, was chosen only on the basis of physical and geometrical considerations and was not treated as an adjustable parameter for fitting the experimental data. Except for methanol, the maximum deviation between experimental and theoretical values for  $\Delta G^\circ$  is less than 0.2 kcal/mol, while that for  $\Delta H^\circ$  is about 0.4 kcal/mol. It should be mentioned that the parent model for aqueous solutions of the hydrocarbons gave rather poor results

for methane.<sup>1</sup> Presumably, the simple model for hydrocarbon solutions is inadequate for very small solutes.

The temperature dependence of the calculated thermodynamic parameters is shown in Figure 4. Ethanol is used as a representative example, since complete

(35) Complete data are available only for  $\Delta G^\circ$  and  $\Delta H^\circ$ . The observed  $\Delta S^\circ$  values (reported in Table IV) were calculated from them.

(36) G. J. Pierotti, C. H. Deal, and E. C. Derr, *Ind. Eng. Chem.*, **51**, 95 (1959); American Documentation Institute, Document No. 5782 (1959).

(37) H. C. Van Ness, C. A. Soczek, and N. K. Kochar, *J. Chem. Eng. Data*, **12**, 346 (1967).

(38) H. C. Van Ness, C. A. Soczek, G. L. Peloquin, and R. L. Machado, *ibid.*, **12**, 217 (1967).

(39) C. G. Savani, D. R. Winterhalter, and H. C. Van Ness, *ibid.*, **10**, 168 (1965).

(40) G. L. Bertrand, F. J. Millero, C. Wu, and L. G. Hepler, *J. Phys. Chem.*, **70**, 699 (1966).

(41) D. M. Alexander and D. J. T. Hill, *Austr. J. Chem.*, **22**, 347 (1969).

(42) E. M. Arnett, W. B. Kover, and J. V. Carter, *J. Amer. Chem. Soc.*, **91**, 4028 (1969).

(43) R. Aveyard and R. W. Mitchell, *Trans. Faraday Soc.*, **64**, 1757 (1968).

(44) The use of ranges in presenting the observed thermodynamic parameters reflects the uncertainties in the experimental data as well as discrepancies among the data reported by various authors.

**Table IV:** Comparison of Observed and Calculated Thermodynamic Parameters for the Transfer of One Mole of Alcohol from Hydrocarbon to Aqueous Solution at 25<sup>o</sup>a

Alcohol	Observed			Calculated		
	$\Delta G^\circ$	$\Delta H^\circ$	$\Delta S^\circ$	$\Delta G^\circ$	$\Delta H^\circ$	$\Delta S^\circ$
Methanol	-2.44 to -2.37	-7.58 to -7.34	-17.5 to -16.5	-3.18	-8.03	-16.3
Ethanol	-1.68 to -1.58	-8.26 to -7.87	-22.4 to -20.4	-1.85	-7.76	-19.8
1-Propanol	-0.91 to -0.74	-8.11 to -7.58	-24.8 to -22.4	-0.83	-7.37	-21.9
1-Butanol	-0.02 to +0.11	-7.86 to -7.46	-26.8 to -24.9	+0.16	-7.04	-24.2

<sup>a</sup>  $\Delta G^\circ$  and  $\Delta H^\circ$  are in kcal/mol.  $\Delta S^\circ$  is in cal/deg mol.

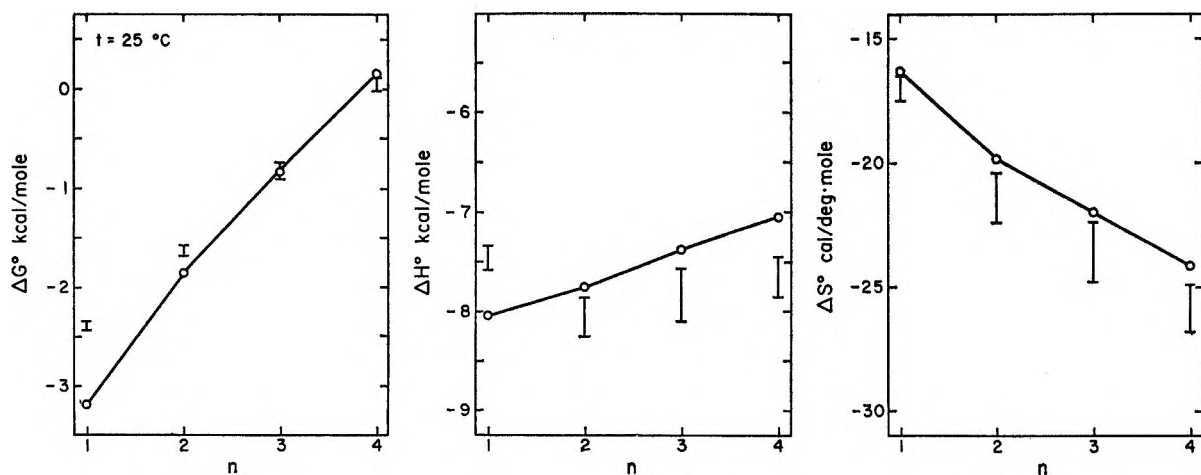


Figure 3. Comparison of experimental and calculated thermodynamic parameters for the transfer of one mole of alcohol from dilute hydrocarbon solvent to dilute aqueous solution at 25°.  $n$  is the number of carbon atoms in the chain. The open circles and the line drawn through them represent the calculated values. The experimental values<sup>36-43</sup> are shown by the symbol I, with the vertical bar indicating the range of the values observed.

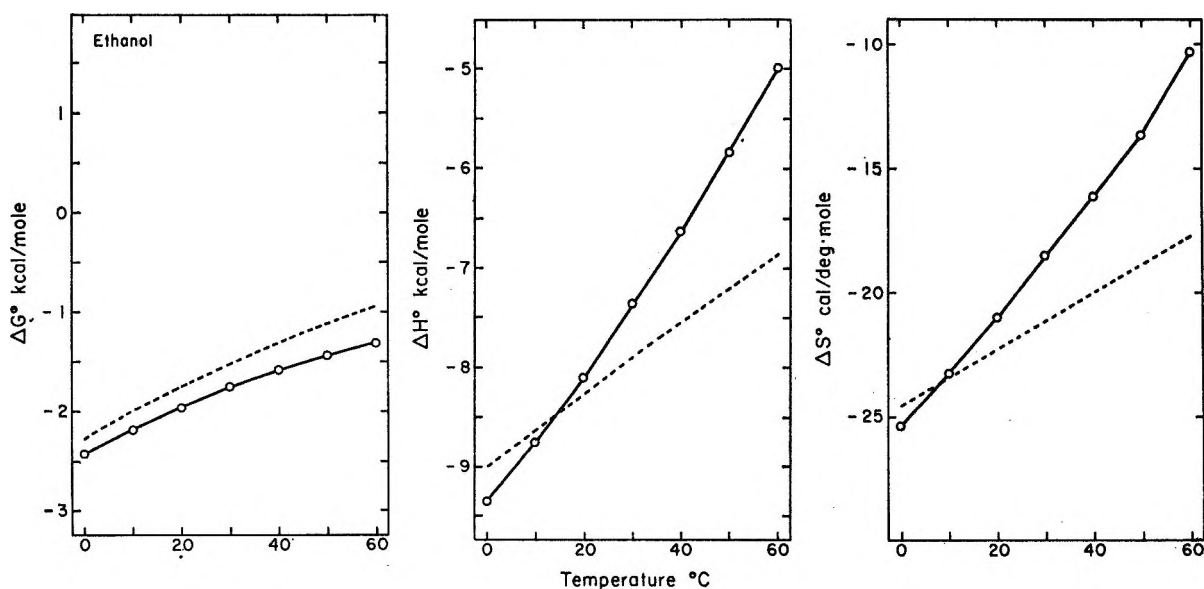


Figure 4. The temperature dependence of the experimental and calculated thermodynamic parameters for the transfer of one mole of ethanol from dilute hydrocarbon solvent to dilute aqueous solution. The open circles and the line through them represent the calculated values. The dotted line represents the observed values.<sup>36-37,41</sup> For some temperature ranges, the experimental values were obtained by extrapolation of those reported in the references.

experimental data on the temperature dependence is not available for most of the alcohols. Again, reasonable agreement between theory and experiment is obtained. The excessive temperature dependence of

$\Delta H^\circ$  and  $\Delta S^\circ$  is found in the parent hydrocarbon model as well,<sup>1</sup> and probably can be attributed to shortcomings of the hydrocarbon model rather than the present theory.

At 25°, the mole fractions of the various OH species were found to be  $x_u^{\text{OH}} = 0.216$  to  $0.248$ ,  $x_1^{\text{OH}} = 0.149$  to  $0.133$ ,  $x_2^{\text{OH}} = 0.205$  to  $0.210$ , and  $x_3^{\text{OH}} = 0.431$  to  $0.409$ . The ranges shown indicate the variation between methanol and butanol.

Since the OH group is assumed to be similar to a water molecule in the present model, it is of interest to compare some of its properties with those of liquid water. Of particular significance is the degree of hydrogen bonding of the OH group. As can be seen from Table V, a larger fraction of the hydrogen bonds of

**Table V:** Fraction of Hydrogen Bonds Unbroken at 25°<sup>a</sup>

OH groups	
Methanol	0.617
Ethanol	0.606
Propanol	0.598
Butanol	0.593
Bulk water	0.447
Water in contact with hydrocarbon	0.575

$$^a \text{ Calculated as } \frac{1}{n_{\text{H}}} \sum_{i=1}^{n_{\text{H}}} ix_i.$$

the OH group remain unbroken than for either bulk water or cage water. The most probable reason for this is the larger spacings between energy levels for the OH group (Figure 1), although undoubtedly the assignment of weighting factors is important as well.

In Table VI, it is shown that the total increase in hydrogen bonding caused by the addition of 1 mol of alcohol to water is approximately the same as that

**Table VI:** Excess Hydrogen Bond Formation Resulting from the Addition of One Mole of Solute to Water at 25°<sup>a</sup>

Methanol	6.59	Methane	6.62
Ethanol	8.10	Ethane	8.15
Propanol	9.11	Propane	9.17
Butanol	10.1	Butane	10.2

<sup>a</sup> Calculated as  $y \left( \sum_{i=1}^4 ix_i^{\text{e}} - \sum_{i=1}^4 ix_i^{\text{c}} \right) + \sum_{i=1}^3 ix_i^{\text{OH}}$  for the alcohols and  $Y^{\text{c}} \left( \sum_{i=1}^4 ix_i^{\text{e}} - \sum_{i=1}^4 ix_i^{\text{c}} \right)$  for the hydrocarbons, where  $Y^{\text{c}}$  is the number of water molecules in contact with the hydrocarbon.<sup>1</sup>

caused when 1 mol of the corresponding hydrocarbon is added. Indeed, the  $\Delta S^{\circ}$  values for the two processes, which originate mostly from ordering effects of hydrogen bond formation, differ only by about 1 entropy unit. However, this similarity does not extend to the effect of the solute on the structure of water since the number of water molecules in contact with the hydrocarbon chain of an alcohol is somewhat smaller than the number in contact with the corresponding normal hydrocarbon. Therefore, it is the contribution from the hydrogen bond of the OH group which produces the aforementioned agreement in the total degree of hydrogen bonding.

In applications of the model to the thermodynamics of protein functional groups, it is necessary to evaluate the contribution of the OH group alone. However, the thermodynamic parameters cannot be separated rigorously into additive contributions due to the OH group and the hydrocarbon chain, since (i) the statistical weights which appear in the partition function for the OH group depend on the size of the alcohol considered, and (ii) some water molecules ( $y_{\text{ROH}}$ ) are in contact with both the OH group and the alkyl chain. Thus, the proposed model must be modified in applications to proteins, which are now in progress. For example, the dependence on molecular size becomes negligible since the OH group is attached, essentially, to an infinite mass for the evaluation of  $f_v$ , with corresponding changes in  $f_t$  and  $f_r$ .

A very rough estimate of the OH group contribution to the thermodynamic properties of small alcohols can be obtained by subtracting the contributions of the alkyl chain, as obtained from theory,<sup>1,2</sup> from the calculated values for the alcohols (Table IV). In this manner, one obtains, at 25°,  $\Delta G^{\circ}_{\text{OH}} = -5.1$  to  $-4.7$  kcal/mol,  $\Delta H^{\circ}_{\text{OH}} = -7.1$  kcal/mol, and  $\Delta S^{\circ}_{\text{OH}} = -7.0$  to  $-8.5$  cal/deg mol. Although these numbers serve only as approximate guidelines, it is evident that the favorable free energy of transfer of the OH group from hydrocarbon to water is, as expected, the result of a favorable enthalpy change. The excess entropy of transfer is negative due to the restrictions on the OH group introduced by hydrogen bond formation in aqueous solution.

The model presented here can be extended to the treatment of other polar groups, such as primary amino groups, with minor changes.

*Acknowledgment.* This work was supported in part by Grant No. 8410 of the National Science Foundation.

# The Viscous Flow and Glass Transition Temperature of Some Hydrocarbons

by Gerald L. Faerber, Sung Wan Kim, and Henry Eyring\*

Department of Chemistry, University of Utah, Salt Lake City, Utah 84112 (Received January 14, 1970)

The significant structure theory of liquids has been extended to the supercooled region and to the prediction of glass transition temperatures. The constants  $A$  and  $B$  fitted from Barlow's<sup>3</sup> experimental data of viscosities and densities of alkylbenzenes are in good agreement with those calculated from significant structure theory. In calculating  $B$  we used the same constant  $a' = 0.0085$  for all substances. The  $a'$  value is larger than the parameter  $a$  in significant structure theory since the activation energy for flow, involving  $a'$ , should be equal to or greater than the energy, involving  $a$ , required by a molecule to deny a neighboring vacancy to the other neighbors. We used significant structure theory to treat the viscosity in the non-Arrhenius region. The theory also automatically predicts the occurrence of a temperature,  $T_k$ , near the melting point, at which  $\log \eta$  plotted against  $(1000/T)^3$  shows a break. If the fact that the solid-like microstructure should shrink near the melting point, due to a shift to more dense conformers, is taken into account, this effect should become more conspicuous. The glass transition temperature,  $T_g$ , can be calculated from the viscosity equation by defining it as  $\eta_g \approx 10^{13}$  P. Alternatively,  $T_g$  can be calculated from a viscosity equation derived from significant structure theory by expressing it as a ratio of viscosities at two temperatures. The free volume fractions obtained in this work are smaller than the WLF "iso-free volume fraction" of 0.025. The average value found is 0.013, which is closer to the values of Barlow, *et al.* In fact there is not an exact iso-free volume fraction. The glass point is well characterized as the point where the viscosity reaches about  $10^{13}$  P. This is a more reproducible criterion than specifying the ratio of free volume to total volume at the glass transition. The exciting result is that significant structure theory yields both the thermodynamic and transport properties of liquids down to the glassy region. The theory connects the disappearance of entropy upon supercooling with the disappearance of fluidity in a single all-embracing theory.

## Introduction

Liquids that do not crystallize readily exhibit a so-called "glass transition." When many liquids such as hydrocarbons and amorphous polymers are slowly cooled, they become extremely viscous and brittle below a certain temperature. The glass transition temperature is conventionally defined as the temperature at which the specific heat or the thermal expansion coefficient of the liquid shows an abrupt change.<sup>1</sup> It corresponds to a change in slope of a plot of specific volume *vs.* temperature. The glassy state is a form of matter which maintains the structure, energy, and volume of a liquid, but for which the changes in energy and volume with temperature are similar in magnitude to those of a crystalline solid. From X-ray data it is found that there is no essential change in structure at the glass transition.<sup>2</sup>

Alternatively, the glass transition has been described as the temperature where the liquid viscosity reaches  $10^{13}$  P.<sup>1,3,4</sup> It was first shown by Tamann that a steep change in properties occurs around a temperature  $T_g$  for which the viscosity,  $\eta$ , was  $10^{13}$  P.<sup>5</sup> Subsequent experiments with other glass-forming melts have verified that this criterion of congelation is quite general and appears to be of wide physical significance.<sup>6-10</sup> Many current workers hold to the isoviscous criterion of the glass transition.<sup>11-14</sup> We shall use this definition of  $T_g$  in this paper.

Many authors<sup>1,7,15-21</sup> have explained that the glass transition of liquids is an apparent second-order transi-

tion which is accompanied by some peculiarities in viscoelastic behavior. This theory in terms of thermodynamics and structure stresses the role of configurational energy and entropy in the liquid. The glass transition

\* To whom correspondence should be addressed.

- (1) W. Kauzman, *Chem. Rev.*, **43**, 219 (1948).
- (2) S. Urnes, "X-Ray Diffraction Studies of Glass," Vol. 1, J. D. MacKenzie, Ed., Butterworths, London, 1960, pp 10-37.
- (3) A. J. Barlow, J. Lamb, and A. J. Matheson, *Proc. Roy. Soc., Ser. A*, **292**, 322 (1966).
- (4) G. D. Jones, "Glass," Wiley, New York, N. Y., 1956.
- (5) G. Tamann and W. Hesse, *Z. Anorg. Allgem. Chem.*, **156**, 245 (1926).
- (6) A. R. Ubbelohde, "Melting and Crystal Structure," Oxford University Press, London, 1965, Chapter 15.
- (7) M. Gordon, "High Polymers," Iliffe Books, Ltd., London, 1963, p 52.
- (8) J. D. Ferry, "Viscoelastic Properties of Polymers," Wiley, New York, N. Y., 1961, p 261.
- (9) E. Jenchel, *Z. Anorg. Allgem. Chem.*, **216**, 367 (1934).
- (10) J. D. Ferry and G. S. Parks, *Physics*, **6**, 360 (1935).
- (11) A. A. Miller, *J. Polym. Sci., A*, **2**, 1095 (1964).
- (12) A. A. Miller, *ibid.*, **A-2**, **6**, 249, 1161 (1968).
- (13) D. B. Davies and A. J. Matheson, *J. Chem. Phys.*, **45**, 1000 (1966).
- (14) M. R. Carpenter, D. B. Davies, and A. J. Matheson, *ibid.*, **46**, 2451 (1967).
- (15) H. Mark and A. V. Tobolsky, "Physical Chemistry of High Polymeric Systems," 2nd ed, Interscience, New York, N. Y., 1950, Chapter 10.
- (16) E. A. DiMarzio and J. H. Gibbs, *J. Chem. Phys.*, **28**, 807 (1958).
- (17) J. H. Gibbs and E. A. DiMarzio, *ibid.*, **28**, 373 (1958).

is taken as the point where the number of possible conformations of the amorphous phase decreases sharply. This stress on the decrease of entropy at  $T_g$  is currently being examined.<sup>22</sup> Others have argued that this thermodynamic approach is not valid since there is not a true equilibrium at the glass point.<sup>7,8,23,24</sup> Recently, a potential energy barrier description of the glass transition has been published.<sup>25</sup>

An iso-free volume criterion for the glass transition temperature has been proposed by several authors.<sup>26-29</sup> The relative amount of free volume decreases sharply with decreasing temperature above  $T_g$  and is assumed to be constant at  $T_g$ . Williams, Landel, and Ferry<sup>27</sup> have proposed a constant free volume fraction of 0.025 at the glass transition. However, it has been pointed out that the free volume has both a pressure and temperature dependence.<sup>11,30</sup> It is interesting that Cohen and Turnbull have since improved their free volume model by dividing displacements into "gas-like" and "solid-like" categories in accord with significant structure theory.<sup>31</sup>

The viscosity of liquids at temperatures above their melting points are quite well described by an Arrhenius type equation,  $\ln \eta = A + E/RT$ . Where  $A$  is a constant,  $R$  is the gas constant,  $T$  is the absolute temperature, and  $E$  is the activation energy for viscous flow.<sup>32</sup> However, this equation is usually inapplicable to liquids of high viscosity or to highly supercooled liquids. Another approach to liquid viscosity is based on the concept of free volume and Doolittle<sup>33</sup> developed an empirical free volume equation,  $\log \eta = A + B(V_0/V_f)$ , which accurately represents many viscosity data in the non-Arrhenius temperature region. Here  $V_0$  is the limiting specific volume of the liquid at low temperatures,  $V_f$  is the free volume, and  $A$  and  $B$  are constants. For most liquids it is found experimentally that density varies linearly with temperature. Barlow, Lamb, and Matheson<sup>3</sup> combined this variation with the Doolittle equation to derive an equation previously found empirically by Fulcher<sup>34</sup> and by Tamann and Hesse,<sup>5</sup>  $\log \eta = A' + B'/(T - T_0)$ , where  $A'$ ,  $B'$ , and  $T_0$  are constants. The temperature  $T_0$  is a second-order transition temperature, and is the fundamental reference temperature for all molecular transport and relaxation processes in the liquid. Ree and Jhon have recently derived the WLF equation using significant structure theory.<sup>35</sup> Barlow, *et al.*,<sup>3</sup> measured the viscosities and densities of a number of aromatic hydrocarbons from room temperature down to temperatures in the highly supercooled region. They found that the modified free volume equation gave an excellent description of the viscosity of several liquids over the whole non-Arrhenius temperature range. However, for other liquids it was necessary to apply this equation in two separate temperature regions with two different sets of the constants  $A'$ ,  $B'$ , and  $T_0$ . The discontinuity in viscous behavior appeared at a temperature,  $T_k$  which

lies above  $T_g$  and usually slightly below the melting point. They also obtained experimental  $T_g$  values by differential thermal analysis taking the average of at least three observations, which were estimated to be accurate to  $\pm 2^\circ$ .<sup>14</sup>

Much work<sup>3,11-14,20,30,36,37</sup> on the glass transition is limited to empirical fitting of data by using the Doolittle or modified Tamann-Hesse equations. We shall examine the alkylbenzenes studied by Barlow, *et al.*,<sup>3</sup> using the significant structure theory of liquids. We will calculate an  $A$  and  $B$  and the viscosity as well as the temperature at which the glass transition will take place. Our values will be compared with experimental results.<sup>3,14</sup> The free volume fractions fitted to the Barlow, *et al.*, experimental data will be compared with those calculated from significant structure theory.

Not only is there agreement between the theoretical and experimental glass transition temperatures as calculated from viscosity data but the fact that significant structure theory also gives the thermodynamic properties of liquids means that it connects the disappearance of entropy upon supercooling with the disappearance of fluidity in a single all-embracing theory.

### Viscosity Theory

The reaction coordinates of viscous flow and diffusion are of interest. A condensed phase is in some ways like a giant molecule with many isomeric structures corresponding to arrangements that give minima in the potential energy. As is seen from significant structure theory a fraction,  $(V - V_s)/V$ , of the degrees of freedom will be simulating gas-like motion at any instant.

(18) J. H. Gibbs, "Nature of the Glass Transition and the Vitreous State," Vol. 1, J. D. MacKenzie, Ed., Butterworths, London, 1960, pp 152-187.

(19) G. Adam and J. H. Gibbs, *J. Chem. Phys.*, **43**, 139 (1965).

(20) O. G. Lewis, *ibid.*, **43**, 2693 (1965).

(21) M. Goldstein, *ibid.*, **39**, 3369 (1963).

(22) C. A. Angell, *ibid.*, **46**, 4673 (1967); *J. Phys. Chem.*, **70**, 2793 (1966).

(23) F. W. Billmeyer, Jr., "Textbook of Polymer Science," Interscience, New York, N. Y., 1966, Chapter 6.

(24) P. J. Flory, *Ric. Sci. Suppl.*, **3** (1955).

(25) M. Goldstein, *J. Chem. Phys.*, **51**, 3728 (1969).

(26) T. G. Fox, Jr., and P. J. Flory, *J. Appl. Phys.*, **21**, 581 (1950); *J. Phys. Chem.*, **55**, 221 (1951); *J. Polym. Sci.*, **14**, 315 (1954).

(27) M. F. Williams, R. F. Landel, and J. D. Ferry, *J. Amer. Chem. Soc.*, **77**, 3701 (1955).

(28) D. Turnbull and M. H. Cohen, *J. Chem. Phys.*, **34**, 120 (1961)

(29) F. Beuche, "Physical Properties of Polymers," Interscience, New York, N. Y., 1962, Chapter 4.

(30) A. J. Matheson, *J. Chem. Phys.*, **44**, 695 (1966).

(31) D. Turnbull and M. H. Cohen, *ibid.*, **52**, 3038 (1970).

(32) E. N. da C. Andrade, *Nature*, **125**, 309 (1930).

(33) A. K. Doolittle, *J. Appl. Phys.*, **22**, 1471 (1951); A. K. Doolittle and D. B. Doolittle, *ibid.*, **28**, 901 (1957).

(34) G. S. Fulcher, *J. Amer. Ceram. Soc.*, **8**, 339 (1925).

(35) T. Ree and M. S. Jhon, *J. Korean Chem. Soc.*, **14**, 45 (1970).

(36) C. A. Angell, *J. Phys. Chem.*, **68**, 1917 (1964).

(37) C. A. Angell, L. J. Pollard, and W. Strauss, *J. Chem. Phys.*, **43**, 2899 (1965).

These degrees of freedom which momentarily simulate gas-like diffusion and viscosity will immediately thereafter show "solid-like" behavior. Here  $V$  is the molal volume of the liquid while for simple molecules like argon,  $V_s$  is the molal volume of the solid. The remaining fraction  $V_s/V$  of the degrees of freedom are at any instant undergoing oscillational motions as in a solid and are using the degeneracies associated with the fluidized vacancies to relax the local solid-like stresses in a way to be described next.

If a potential energy surface is plotted in a space of as many independent coordinates as are required to fix the potential energy of the solid-like system in a liquid, then a reaction coordinate is the continuous path between two minima on this surface lying normal to contour lines and passing through a saddle point. As is true for reactions in general, the passage from one minimum to the next will involve a displacement in multidimensional space. Because of the complexity of this motion which will vary with the shapes and sizes of the molecules and with the forces between them, it is convenient to plot a section through the potential surface in which distance along the reaction coordinate is plotted as abscissa while the energy of the system is plotted as ordinate. In discussing this motion it will be convenient further to fasten attention on one of the molecules which undergoes maximum displacement with respect to its neighbors. This motion ordinarily involves a change of the nearest neighbors on one side of a molecule or on one side of a flowing segment if it is a high polymer. Since for simple molecules viscosity and self-diffusion have the same activation energies it follows that the mode of relaxation is characteristic of the system and not of the nature of the stresses which simply bias the motion in a direction to relieve the stress. A pure shear results from a composite of such motions. In general the simplest possible motions which will relieve a stress will be heavily favored at low stresses, because of the lower free energies of activation involved. This is no longer true at sufficiently high stresses when turbulent flow rather than laminar flow becomes the stable steady state.

The simple episodes we have so far described in which a molecule shifts from one minimum to the next requires a discussion of the relaxation processes by which the stresses built up by such a shift are in turn relaxed. The point is that such an episode is not an isolated event. Such uncoordinated fluctuations are going on all the time in all possible directions but always with a statistically greater probability in those directions which relax the internal and the externally imposed stresses. For simple molecules deactivation of one fluctuation by the others apparently occurs so that about 4 out of 10 of the excursions a molecule makes to a new minimum are stabilized in this new position. For more complicated molecules this transmission coefficient apparently approaches unity.

The significant structure theory of liquids has implicit in it a general theory of transport properties.<sup>38</sup> There are the solid-like and gas-like degrees of freedom in the liquid which must be taken into account in the calculation of viscosity. Earlier papers<sup>39,40</sup> give the derivation of the viscosity equation from significant structure theory. If a fraction,  $x_s$ , of the shear plane is covered by solid-like molecules and the remaining fraction,  $x_g$ , by gas-like molecules, then the viscosity  $\eta$ , which is the ratio of shear stress,  $f$ , to the rate of strain,  $\dot{\gamma}$ , is

$$\begin{aligned}\eta &= \frac{f}{\dot{\gamma}} = (x_s f_s + x_g f_g) / \dot{\gamma} \\ &= x_s \eta_s + x_g \eta_g \\ &= \frac{V_s}{V} \eta_s + \frac{V - V_s}{V} \eta_g\end{aligned}\quad (1)$$

The viscosity equation derived by Eyring and coworkers can be written in an alternative form. We use the equation for the rigid sphere system<sup>40</sup>

$$\eta = \frac{(\pi m k T)^{1/2} N l_f}{2(V - V_s) \kappa} \exp\left(\frac{\epsilon_0^\ddagger}{RT}\right) + \frac{V - V_s}{V} \left(\frac{5}{16d^2}\right) \left(\frac{m k T}{\pi}\right)^{1/2}\quad (2)$$

here  $m$  and  $d$  are the molecular mass and diameter, respectively. The free distance between nearest neighbors is denoted by  $l_f$ ,  $\kappa$  is a constant transmission coefficient, and  $\epsilon_0^\ddagger$  is the activation energy required for jumping which is written as

$$\epsilon_0^\ddagger = \frac{a' E_s V_s}{(V - V_s)}\quad (3)$$

$E_s$  and  $V_s$  have the usual meanings in significant structure theory; however,  $a'$  must be called a kinetic parameter rather than necessarily being equal to  $a$ , a thermodynamic parameter, since the activation energy for flow,  $a' E_s V_s / (V - V_s)$  should be equal to or greater than the energy,  $a E_s V_s / (V - V_s)$ , which is necessary for a molecule to preempt a neighboring vacancy.  $l_f$  is expressed as<sup>41</sup>

$$l_f = 2 \left[ \left( \frac{2V_s}{N} \right)^{1/3} - \sigma \right]$$

where the collision diameter  $\sigma$  is related to  $\sigma \simeq (b/4N)^{1/3} \simeq (V_c/12N)^{1/3}$ ;  $b$  is the van der Waals constant and  $V_c$  is the critical molar volume. The contribution of the gas-like viscosity term  $\eta_g$  is at most 0.2% of the total viscosity, which is well within the experimental

(38) H. Eyring and M. S. Jhon, "Significant Liquid Structures," Wiley, New York, N. Y., 1969, Chapter 5.

(39) R. Marchi and H. Eyring, *J. Chem. Educ.*, **40**, 526 (1963).

(40) T. S. Ree, T. Ree, and H. Eyring, *J. Phys. Chem.*, **68**, 3262 (1964).

(41) M. S. Jhon, W. L. Klotz, and H. Eyring, *J. Chem. Phys.*, **51**, 3692 (1969).

**Table I:**  $T_g$  Calculated Without Varying Parameters from Eq 5 ( $a' = 0.0085$ ; Free Volume Fraction = 0.0130;  $V_s = (0.9870)V_g$ ;  $A$  and  $B$  Calculated from Thermodynamic Data)

Compd	A	B	$E_s$ (cal/mol) <sup>a</sup>	$V_o$ (cc/mol)	$V_s$ (cc/mol)	$T_g$	
						Calcd, °K	Exptl, °K
Toluene	-5.601	43.07	10,070	320	87.65	98	113
Ethylbenzene	-5.473	50.02	11,695	360	101.51	113	111
<i>n</i> -Propylbenzene	-5.388	53.45	12,497	440	117.85	122	122
Isopropylbenzene	-5.385	50.89	11,897	440	118.14	116	125
<i>n</i> -Butylbenzene	-5.295	60.87	14,232 <sup>b</sup>	500 <sup>d</sup>	132.90	138	125
<i>sec</i> -Butylbenzene	-5.295	59.87	13,998 <sup>c</sup>	500 <sup>d</sup>	133.07	136	127

<sup>a</sup> Values from reference 42 unless specified otherwise. <sup>b</sup> Calculated from reference 43. <sup>c</sup> Estimated from relative changes in homologous series. <sup>d</sup> Calculated according to reference 44.

**Table II:**  $A$  and  $B$  Calculated from Thermodynamic Data ( $T_g$  from Eq 5)

Compd	A	B	$V_s$ (cc/mol)	Free volume fraction	$T_g$	
					Calcd, °K	Exptl, °K
Toluene	-5.600	43.07	87.79	0.0114	113	113
Ethylbenzene	-5.473	50.02	101.48	0.0133	111	111
<i>n</i> -Propylbenzene	-5.388	53.45	117.85	0.0130	122	122
Isopropylbenzene	-5.374	50.89	118.25	0.0121	125	125
<i>n</i> -Butylbenzene	-5.302	60.87	132.75	0.0141	125	125
<i>sec</i> -Butylbenzene	-5.295	59.87	132.93	0.0140	127	127

error in the measurements considered here and so can be neglected.

The expression for  $\eta$  is given as

$$\eta = \eta_s \frac{V_s}{V} = \frac{(\pi mkT)^{1/2} N l_f}{2(V - V_s) \kappa} \exp\left(\frac{\epsilon_0 \mp}{RT}\right) \quad (4)$$

Taking the logarithm, eq 4 becomes

$$\ln\left(\frac{\eta(V - V_s)}{T^{1/2}}\right) = \ln\left[\frac{(\pi mk)^{1/2} N l_f}{2\kappa}\right] + \left[\frac{a' E_s V_s}{(V - V_s) RT}\right]$$

$$\ln\left[\frac{\eta(V - V_s)}{T^{1/2}}\right] = A + B \left[\frac{V_s}{(V - V_s) T}\right] \quad (5)$$

where

$$A = \ln\left[\frac{(\pi mk)^{1/2} N l_f}{2\kappa}\right] \quad (6)$$

and

$$B = \frac{a' E_s}{R} \quad (7)$$

Equation 5 can be used to calculate the viscosity at any given temperature, and by using  $\eta_g = 10^{13}$  P a value of  $T_g$  can also be calculated. Beuche<sup>29</sup> points out in the study of the variation of viscosity with temperature it is customary to express the results as ratios of viscosities at two temperatures. This approach has been taken using the Doolittle equation and familiar WLF equation. Following this idea the glass transition temperatures can be obtained by the viscosity

equation written as an expression of the ratio of viscosities at two temperatures. From eq 5 it is given by

$$\ln \frac{\eta_g}{\eta} = V_s \times B \left[ \frac{1}{(V_g - V_s) T_g} - \frac{1}{(V - V_s) T} \right] + \ln \left[ \frac{V - V_s}{V_g - V_s} \sqrt{\frac{T_g}{T}} \right] \quad (8)$$

where  $\eta_g$  and  $V_g$  are the viscosity and the molar volume at the glass transition, respectively, and  $T_g$  is the glass transition temperature.

### Calculations

The gas-like contribution to the viscosity was first calculated and found to be no more than 0.2% of the total viscosity. The experimental error in viscosity measurements was 0.5 to 1%<sup>3</sup> and in  $T_g$  measurements it was 1.8%.<sup>14</sup> Therefore we are justified in neglecting the gas-like term in eq 2. Ideally  $V_s$  values from crystallographic data would be used. However since they are not available for the alkyl benzenes, we took a different approach. A plot of the liquid volume *vs.* temperature is linear down to the supercooled region.<sup>3,42</sup>  $V_g$  was obtained by extrapolating a plot of volume *vs.* temperature down to the experimental glass point and reading the value of  $V_g$  from the ordinate scale.  $V_s$  was then obtained from  $V_s = (\text{iso-free volume fraction}) V_g$ , where we have used 0.013 as the free volume fraction at the glass point.

(42) N. N. Greenwood and R. L. Martin, *Proc. Roy. Soc., Ser. A*, 215, 46 (1952).

Table III:  $A$  and  $B$  Fitted from Viscosity Data ( $T_g$  from Eq 5)

Compd	$A$	$B$	$V_a$ (cc/mol)	Free volume fraction	Barlow, <i>et al.</i> <sup>a</sup> free volume	$T_g$	
						Calcd, °K	Exptl, °K
Toluene	-5.742	44.054	87.77	0.0116	0.010	113	113
Ethylbenzene	-5.593	46.280	101.57	0.0124	0.010	111	111
<i>n</i> -Propylbenzene	-6.210	56.090	117.81	0.0133	0.016	122	122
Isopropylbenzene	-7.669	60.950	118.08	0.0135	0.024	125	125
<i>n</i> -Butylbenzene	-6.303	67.258	132.59	0.0153	0.019	125	125
<i>sec</i> -Butylbenzene	-5.846	55.110	133.11	0.0127	0.024	127	127

<sup>a</sup> See Ref. 3.Table IV:  $T_g$  Calculated Without Varying Parameters from Eq 8 ( $a' = 0.0085$ ; Free Volume Fraction = 0.0132;  $V_a = (0.9868)V_g$ ;  $A$  and  $B$  Calculated from Thermodynamic Data)

Compd	$A$	$B$	$E_a$ (cal/mol) <sup>a</sup>	$V_o$ (cc/mol)	$V_g$ (cc/mol)	$T_g$	
						Calcd, °K	Exptl, °K
Toluene	-5.601	43.07	10,070	320	87.63	97	113
Ethylbenzene	-5.473	50.02	11,695	360	101.49	112	111
<i>n</i> -Propylbenzene	-5.388	53.45	12,497	440	117.82	125	122
Isopropylbenzene	-5.385	50.89	11,897	440	118.12	118	125
<i>n</i> -Butylbenzene	-5.295	60.87	14,232 <sup>b</sup>	500 <sup>d</sup>	132.87	138	125
<i>sec</i> -Butylbenzene	-5.295	59.87	13,998 <sup>c</sup>	500 <sup>d</sup>	133.04	139	127

<sup>a</sup> Values from reference 42 unless specified otherwise. <sup>b</sup> Calculated from reference 43. <sup>c</sup> Estimated from relative changes in homologous series. <sup>d</sup> Calculated according to reference 44.Table V:  $A$  and  $B$  Calculated from Thermodynamic Data ( $T_g$  from Eq 8)

Compd	$A$	$B$	$V_a$ (cc/mol)	Free volume fraction	$T_g$	
					Calcd, °K	Exptl, °K
Toluene	-5.600	43.07	87.79	0.0114	113	113
Ethylbenzene	-5.473	50.02	101.48	0.0133	111	111
<i>n</i> -Propylbenzene	-5.388	53.45	117.80	0.0134	122	122
Isopropylbenzene	-5.374	50.89	118.23	0.0123	125	125
<i>n</i> -Butylbenzene	-5.302	60.87	132.68	0.0146	125	125
<i>sec</i> -Butylbenzene	-5.295	59.87	132.87	0.0145	127	127

Table VI:  $A$  and  $B$  Fitted from Viscosity Data ( $T_g$  from Eq 8)

Compd	$A$	$B$	$V_a$ (cc/mol)	Free volume fraction	Barlow, <i>et al.</i> <sup>a</sup> free volume	$T_g$	
						Calcd, °K	Exptl, °K
Toluene	-5.742	44.054	87.77	0.0116	0.010	113	113
Ethylbenzene	-5.593	46.280	101.57	0.0124	0.010	111	111
<i>n</i> -Propylbenzene	-6.210	56.090	117.74	0.0139	0.016	122	122
Isopropylbenzene	-7.669	60.950	118.00	0.0142	0.024	125	125
<i>n</i> -Butylbenzene	-6.303	67.258	132.52	0.0158	0.019	125	125
<i>sec</i> -Butylbenzene	-5.846	55.110	132.99	0.0136	0.024	127	127

The constants  $A$  and  $B$  were calculated from equations 6 and 7 directly. Rossini's data<sup>43</sup> were used where available for the heats of fusion and vaporization. For *n*-butylbenzene the heat of vaporization was obtained from ref 44. No literature value for the heat of vaporization of *sec*-butylbenzene was available, so it was estimated from relative changes in the homologous

series of alkylbenzenes. In the calculation of  $B$  a constant value of the dimensionless number  $a' = 0.0085$

(43) F. D. Rossini, *et al.*, "Selected Values of Physical and Thermodynamic Properties of Hydrocarbons and Related Compounds," Carnegie Press, Pittsburgh, Pa., 1953.(44) J. F. Messerly, S. S. Todd, and H. L. Finke, *J. Phys. Chem.*, **69**, 4304 (1965).

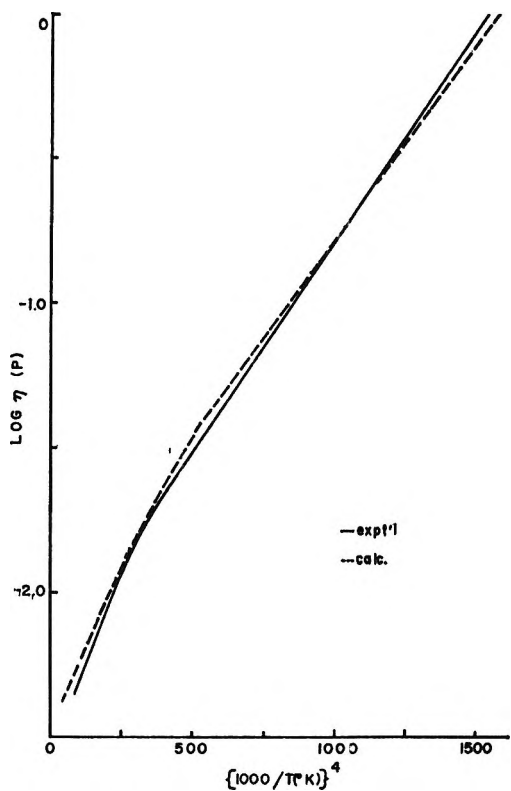


Figure 1. Logarithm of the viscosity of toluene plotted against  $(1000/T)^4$ .

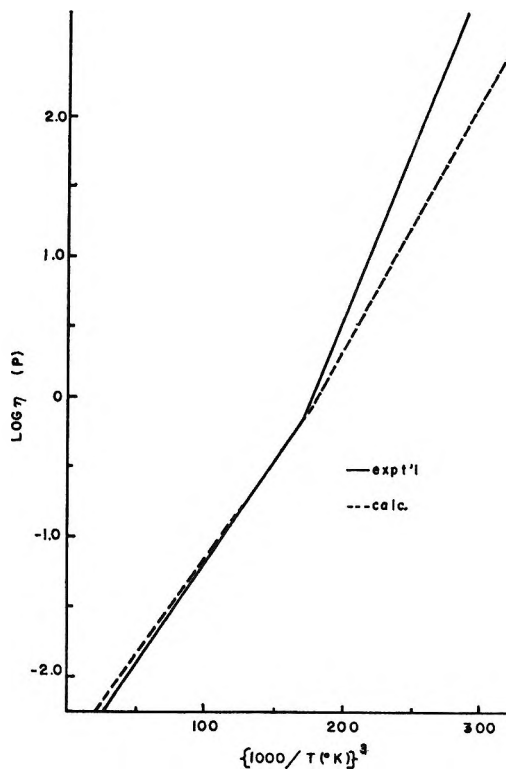


Figure 3. Logarithm of the viscosity of *n*-propylbenzene plotted against  $(1000/T)^3$ .

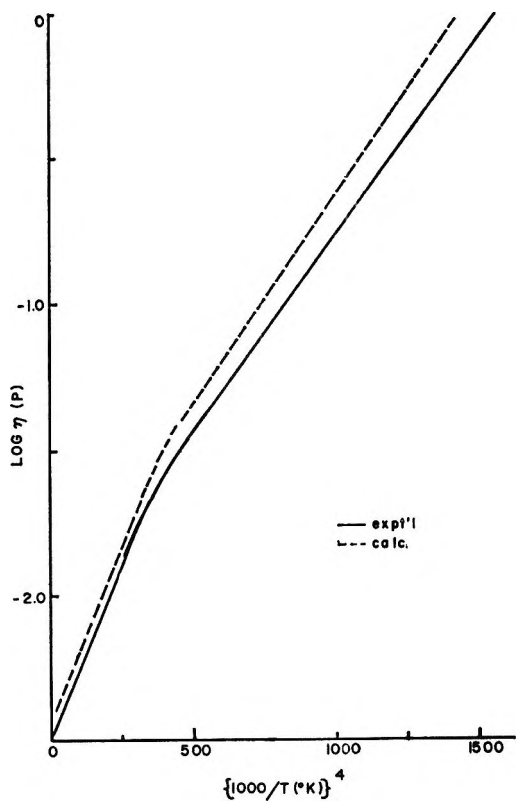


Figure 2. Logarithm of the viscosity of ethylbenzene plotted against  $(1000/T)^4$ .

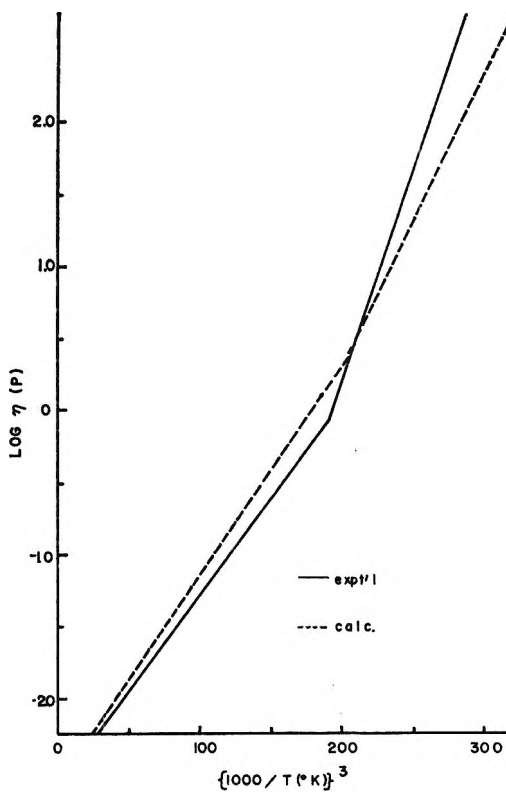


Figure 4. Logarithm of the viscosity of isopropylbenzene plotted against  $(1000/T)^3$ .

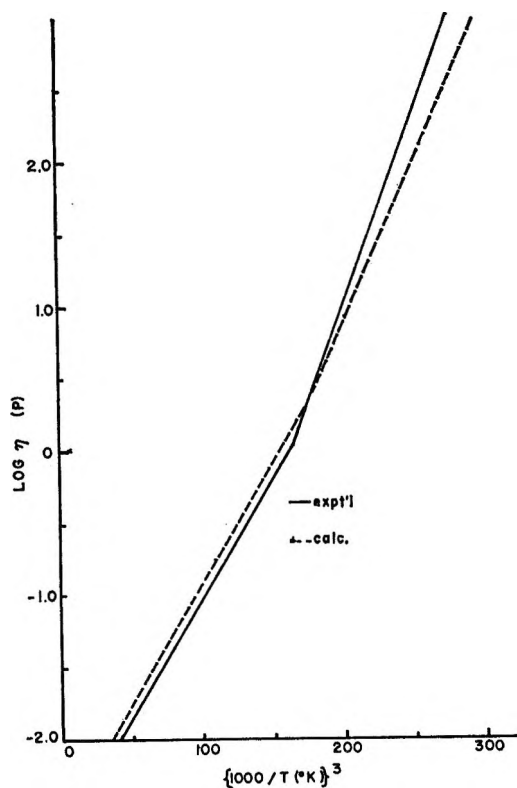


Figure 5. Logarithm of the viscosity of *n*-butylbenzene plotted against  $(1000/T)^3$ .

was used for all substances. This is larger than the parameter  $a = 0.0052$  which is found theoretically and experimentally for the thermodynamic and transport properties of simple spherical molecules like argon. Where critical volumes were not available, they were calculated by the method of Moritz.<sup>45</sup> Using these calculated values of  $A$  and  $B$  and  $\eta_g = 10^{13}$  and  $V = V_g$  in eq 5, we solved for  $T_g$ . The results are tabulated in Table I. Closer correlation of the predicted  $T_g$  values with those experimentally determined can be obtained by a slight variation in the free volume fraction. These results are shown in Table II.

It is of some interest to compare the calculated  $A$  and  $B$  values with those fitted in a manner similar to Barlow, *et al.* For this purpose  $A$  and  $B$  were fitted from experimental viscosity data using eq 5. These values are listed in Table III as well as the free volume fraction and resulting  $V_s$  values needed to obtain  $T_g(\text{calcd}) = T_g(\text{exptl})$ .

$T_g$  values can also be obtained from eq 8 using the calculated  $A$  and  $B$  and by substituting sets of  $T$ ,  $V$ , and  $\eta$  data. The value of  $V$  at a given temperature is obtained in the usual manner by  $V_t = V_0(1 + \alpha(T - T_0))$ . Following the procedure just described for calculating the data in Tables I to III, we used eq 8 and obtained the following results (Tables IV–VI). It is seen that both equations give essentially the same results.

The viscosity was also calculated at several temperatures using the values of  $A$ ,  $B$ , and  $V_s$  from Table I and

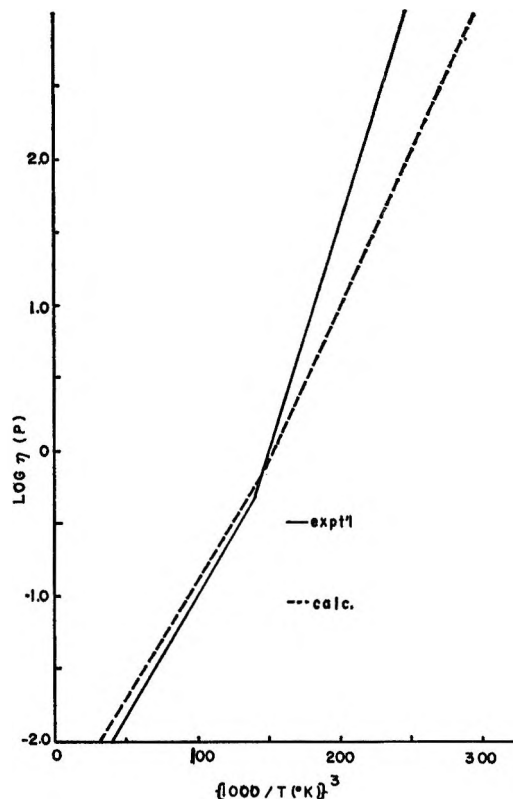


Figure 6. Logarithm of the viscosity of *sec*-butylbenzene plotted against  $(1000/T)^3$ .

calculated  $V$  values in eq 5. The results are in good agreement with the experimental values of Barlow, *et al.* However, the interesting result is that our theory also automatically gives the break,  $T_k$ , found experimentally. In addition, our  $T_k$  values are at the most 4° lower than the experimental values (see Table VII). The correlation may be seen in Figures 1–6

Table VII: Comparison of  $T_k$  Values

Compd	Matheson's $T_k(\text{exptl})$ , °K	$T_k(\text{calcd})$ , °K	Devia- tion, °K	Mp. °K
<i>n</i> -Propylbenzene	176	176	0	174
Isopropylbenzene	171	171	0	177
<i>n</i> -Butylbenzene	181	178	-3	185
<i>sec</i> -Butylbenzene	191	187	-4	198

where the data are plotted in the usual way<sup>3,46,47</sup> according to  $\ln \eta$  vs.  $(1000/T)^n$  where  $n = 3$  or  $4$ . It is easy to see why our theory gives the break at  $T_k$  when one examines the analytical expression for the slope  $(d\eta/dT)$  from equation 4. It is a two-term expression

(45) P. Moritz, *Periodica Polytech.*, **7**, 27 (1963).

(46) T. A. Litovitz, *J. Chem. Phys.*, **20**, 1088 (1952).

(47) A. J. Barlow and J. Lamb, *Proc. Roy. Soc., Ser. A*, **253**, 52 (1959).

Table VIII: Comparison of  $A$  and  $B$  Values

Compd	$A$			$B$		
	Above $T_k$	Below $T_k$	Calcd	Above $T_k$	Below $T_k$	Calcd
Toluene	-5.742		-5.600	44.05		43.07
Ethylbenzene	-5.593		-5.473	46.28		50.02
<i>p</i> -Propylbenzene	-6.211	-5.565	-5.388	56.09	48.86	53.45
Isopropylbenzene	-7.669	-5.508	-5.374	60.95	42.80	50.89
<i>n</i> -Butylbenzene	-6.303	-5.421	-5.302	67.26	56.38	60.89
<i>sec</i> -Butylbenzene	-5.846	-5.467	-5.295	55.11	47.50	59.87

and the contribution of one term is about 5% at low temperatures and rises to over 17% at higher temperatures thus giving the inflection in the  $\log \eta$  vs.  $(1000/T)^2$  curve near the melting point.

### Discussion

The significant structure model for viscous flow which also yields the thermodynamic properties of liquids gives a very satisfactory account of the glass transition phenomena. The constants  $A$  and  $B$  fitted from the Barlow's experimental data of viscosities and densities are in good agreement with those calculated from significant structure theory. In calculating  $B$  we used the dimensionless number  $a' = 0.0085$  for all substances. The  $a'$  value is larger than the parameter  $a$  in significant structure theory since the activation energy for flow, involving  $a'$ , should be equal to or greater than the energy, involving  $a$ , required by a molecule to deny a neighboring vacancy to the other neighbors.

The increase in the glass transition temperatures with increased asymmetry is in harmony with the idea that it is easier to form a glass as asymmetrization increases the entropy of the amorphous phase so that the amorphization energy at the melting temperature is reduced.<sup>28</sup>

The values of  $V_s$  used in our calculations appear reasonable. Since the melting points of these compounds are very low (174–198°K), very little crystallographic work has been done. The only available data are for toluene using powder crystallography and it gives a value of  $V_s = 87.48$  cc/mol at 93°K.<sup>45</sup> Our value at the melting point (178°K) is  $V_s = 87.65$  cc/mol.

The empirically fitted values of  $A$  and  $B$  above  $T_k$  which fit the viscosity data are quite different from those below  $T_k$  (see Table VIII). This fact is in accord with the results of Barlow, *et al.* Thus  $T_k$  is an important temperature. The discontinuity in viscous behavior has been attributed by Barlow, *et al.*,<sup>3</sup> to the fact that below  $T_k$  the molecular aggregate constitutes the unit of flow, while above  $T_k$  the molecules flow as single units, or to restriction of the rotation of the molecules in the liquid.<sup>13,14</sup> According to significant structure theory, transitions in the solid-like structure like that occurring at  $T_k$  are to be expected because of the well known polymorphism of solids. In particular, there is the tendency of the microstructure in liquids to be made up of the more dense conformers below the

melting point. Such a change in  $V_s$  changes both  $V - V_s$  and  $E_s$  and therefore  $A$  and  $B$ . Such changes in  $V_s$  necessarily alter the viscosity dependence on the volume,  $V$ . The "free volume" ( $V - V_s$ ) plays the important role in the viscous flow and thus reflects any change in the solid-like structure. Significant structure theory is quite successful in predicting the inflection point  $T_k$ . This inflection point should be more conspicuous if we take into account the more compact conformers. Thus we expect a value of  $T_k$  in the immediate neighborhood of the melting point as is frequently observed. The viscosity values from eq 5 using calculated  $A$ ,  $B$ , and  $V_s$  values from Table II are also in satisfactory agreement with experiment. Better viscosity values in the lower region are obtainable by varying the free volume fraction slightly.

Data in Tables II, III, IV, and V suggest that  $T_g$  is not simply an "iso-free volume" state with  $V - V_s/V = 0.025$  at the glass transition temperature as discussed by Fox and Flory.<sup>26</sup> The free volume fractions obtained in this work are smaller than the WLF "iso-free volume fraction" of 0.025. The average value found is 0.0130 which is more in harmony with that of Barlow, *et al.*, (0.017). Barlow used  $V_0$ , the volume at 0°K, instead of the  $V_s$  of significant structure theory. He suggests that  $T_g$  is primarily an iso-viscous condition and not an "iso-free volume" condition.<sup>3,13,14</sup> The variation in free volume fraction in Tables II and V is understandable when we consider shapes of the molecules involved. Toluene molecules can fit more closely together than the bulkier *sec*-butylbenzene molecules.

It is interesting to compare the  $T_g$  values predicted by eq 5 and 8 (Tables I and IV). The straightforward calculation (using  $\eta = 10^{13}$  and  $V_g$  values in eq 5) gives better results than the more laborious method of using experimental  $T$ ,  $V$ , and  $\eta$  values in eq 8. Therefore  $T_g$  can be calculated even when low-temperature viscosity data are not available. Significant structure theory will be helpful in predicting unknown glass transition temperatures for other hydrocarbons. Since the same model serves to explain both thermodynamic and transport properties, significant structure theory serves also as a point of departure for explaining why with the disappearance of fluidity most of the entropy of melting

(48) S. G. Biswas and S. C. Sirkar, *Indian J. Phys.*, **31**, 141 (1957).

also disappears.<sup>18,22,25,41</sup> In many cases the entropy of melting can be expressed approximately as  $\Delta s = k \ln(1 + n_h e^{-\epsilon_k/kT})$  where  $n_h$  is the number of vacancies available to a molecule each time it has the energy  $\epsilon_k$  required to exclude competitors. The fluidity is proportional to  $n_h e^{-\epsilon_k/kT}$  (the fluidity  $\phi = 1/\eta$ ). As the term  $(\eta_h e^{-\epsilon_k/kT})$  approaches zero this contribution to the entropy of melting disappears at the same time as the

fluidity goes to zero. A more careful comparison of this situation will be reserved to a later date.

*Acknowledgment.* We are very grateful to the National Science Foundation (GP-6494X2) and the U. S. Army (Contract DA ARO-D-31-1240 G 1110) for support of this work. We also express our thanks to Dr. Shirl Breitling for his helpful suggestions.

## Mutual and Tracer Diffusion Coefficients and Frictional Coefficients for the Systems Benzene-Chlorobenzene, Benzene-*n*-Hexane, and Benzene-*n*-Heptane at 25°

by Kenneth R. Harris, Claudio K. N. Pua, and Peter J. Dunlop\*

*Department of Physical and Inorganic Chemistry, University of Adelaide, Adelaide, South Australia 5001*  
(Received April 16, 1970)

Mutual and tracer diffusion coefficients and frictional coefficients,  $R_{ik}$ , of mixtures of benzene with *n*-hexane, *n*-heptane, and chlorobenzene have been determined as a function of composition at 25°. A new Tiselius cell which does not require greasing is described for the optical measurement of mutual diffusion coefficients of organic liquids. Evidence is presented that the isotope effect predicted by Eppstein is smaller than experimental error for <sup>14</sup>C-labeled benzene and that calibration of diaphragm cells with aqueous electrolyte and nonelectrolyte solutions yields identical results. It is found that the product of the tracer diffusion coefficient of benzene and the solvent viscosity is a linear function of solvent molar volume for *n*-alkanes in accord with the empirical relation of Hammond and Stokes. The frictional coefficient function  $R_{10}^2/(R_{03}R_{12})$  is shown to be equal to unity when  $G^E \simeq 0$  and less than unity when  $G^E > 0$ .

Isothermal diffusion in a ternary system may be described either in terms of a set of four experimental diffusion coefficients<sup>1-5</sup> or in terms of a set of three frictional coefficients<sup>1,6-11</sup> which may be calculated from the four diffusion coefficients and the dependence on concentration of the two independent chemical potentials of the system. The three frictional coefficients of a ternary system are independent, but the four diffusion coefficients are related by the Onsager Reciprocal Relation (ORR).<sup>12,13</sup> The purpose of this paper is firstly to summarize briefly the relationships (some of which have been previously reported) which exist between the ternary diffusion coefficients<sup>14-16</sup> and between the diffusion and frictional coefficients for the special case in which one of the components is present in *tracer* amounts in mixtures of the other two, and secondly to report diffusion data which test the relations discussed.

### Theory

For a ternary system consisting of components 0, 1, and 2, it has now been well established that isothermal transport in such a system may be described in terms of the equations<sup>2</sup>

\* To whom correspondence should be addressed at Department of Chemistry, Simon Fraser University, Burnaby 2, British Columbia, Canada.

- (1) L. Onsager, *Ann. N. Y. Acad. Sci.*, **46**, 241 (1945).
- (2) R. L. Baldwin, P. J. Dunlop, and L. J. Gosting, *J. Amer. Chem. Soc.*, **77**, 5235 (1955).
- (3) L. S. Darken and R. W. Gurry, "Physical Chemistry of Metals," McGraw-Hill, New York, N. Y., 1953, p 438.
- (4) O. Lamm, *J. Phys. Chem.*, **61**, 948 (1957).
- (5) J. S. Kirkaldy, *Can. J. Phys.*, **35**, 435 (1957).
- (6) O. Lamm, *Acta Chem. Scand.*, **11**, 362 (1957).
- (7) A. Klemm, *Z. Naturforsch.*, **8a**, 397 (1953).
- (8) R. W. Laity, *J. Phys. Chem.*, **63**, 80 (1959).
- (9) R. J. Bearman, *ibid.*, **65**, 1961 (1961).

$$J_1^V = -D_{21}^V(\partial C_1/\partial z)_{T,P,t} - D_{12}^V(\partial C_2/\partial z)_{T,P,t} \quad (1a)$$

$$J_2^V = -D_{21}^V(\partial C_1/\partial z)_{T,P,t} - D_{22}^V(\partial C_2/\partial z)_{T,P,t} \quad (1b)$$

where  $J_1^V$  and  $J_2^V$  are flows in units of moles (or grams) of each component crossing unit area in unit time,  $D_{11}$ ,  $D_{12}$ ,  $D_{21}$ , and  $D_{22}$  are the ternary diffusion coefficients, and  $(\partial C_1/\partial z)_{T,P,t}$  and  $(\partial C_2/\partial z)_{T,P,t}$  are gradients of the concentrations,  $C_1$  and  $C_2$  in moles (or grams) per unit volume, in the direction of transport. The superscript  $V$  indicates that the flows and the diffusion coefficients are for the volume frame of reference. This frame is convenient because, in the absence of "volume-changes-on-mixing," it is identical with the experimental or cell frame of reference. However, we assume such volume changes to be negligible and immediately drop the superscript  $V$  from all flows and diffusion coefficients. Inspection of equations 1a and 1b indicates that

$$D_{12} \longrightarrow 0 \text{ as } C_1 \longrightarrow 0 \quad (2a)$$

$$D_{21} \longrightarrow 0 \text{ as } C_2 \longrightarrow 0 \quad (2b)$$

Now for the ternary system (0, 1, 2): (a) as  $C_1 \rightarrow 0$ , (i)  $D_{12} \rightarrow 0$ ; (ii)  $D_{21}$  remains finite (but may be zero); (iii)  $D_{11}$  becomes the tracer diffusion coefficient for component 1,  $D_{T1}$ , in mixtures of 0 and 2; (iv)  $D_{22}$  becomes the mutual diffusion coefficient for mixtures of 0 and 2. (b) As  $C_2 \rightarrow 0$ , (i)  $D_{21} \rightarrow 0$ ; (ii)  $D_{12}$  remains finite (but may be zero); (iii)  $D_{22}$  becomes the tracer diffusion coefficient for component 2,  $D_{T2}$ , mixtures of 0 and 1; (iv)  $D_{11}$  becomes the mutual diffusion coefficient for mixtures of 0 and 1. (c) When, for case b above, the properties of components 2 and 1 become chemically identical yet remain distinguishable (isotopes), a particularly simple relationship<sup>14-17</sup> exists among the three nonzero coefficients

$$D = D_{T2} + D_{12} \quad (3)$$

where  $D$  is the mutual diffusion coefficient for components 0 and 1 (*i.e.*,  $D_{11}$  as  $C_2 \rightarrow 0$ ). This relation has been derived by Albright and Mills<sup>15</sup> by considering a special case of diffusion in such a system, and by Dunlop<sup>14</sup> from the ORR (microscopic reversibility). A relation similar to relation 3 may be written for another ternary system (0, 1, 3) consisting of the same components 0 and 1 as before, and 3 a tracer isotope of 0, *i.e.*

$$D = D_{T3} + D_{03} \quad (4)$$

where  $D$  is the mutual diffusion coefficient of components 0 and 1,  $D_{T3}$  is the tracer coefficient of component 3 in mixtures of 0 and 1, and  $D_{03}$  is the single cross-term diffusion coefficient for the system.

It is now possible to relate the binary diffusion coefficient for the system (0, 1) to the two tracer diffusion coefficients  $D_{T2}$  and  $D_{T3}$  associated with this binary system but measured in the ternary systems (0, 1, 2) and (0, 1, 3), respectively. The result is achieved by

multiplying eq 3 by  $x_0$  and eq 4 by  $x_1$ , and adding the result to yield

$$D = (x_0 D_{T2} + x_1 D_{T3}) + (x_0 D_{12} + x_1 D_{03}) \quad (5)$$

where  $x_0$  and  $x_1$  are mole fractions of components 0 and 1, respectively ( $x_2 = x_3 \simeq 0$ ).

Diffusion in a ternary system may also be described by the set of frictional coefficients defined by the equations<sup>1,6-11</sup>

$$-(\partial \mu_1/\partial z)_{T,P,t} = R_{10}C_0(v_1 - v_0) + R_{12}C_2(v_1 - v_2) \quad (6a)$$

$$-(\partial \mu_2/\partial z)_{T,P,t} = R_{21}C_1(v_2 - v_1) + R_{20}C_0(v_2 - v_0) \quad (6b)$$

$$R_{12} = R_{21}$$

where  $\mu_1$  and  $\mu_2$  are the chemical potentials of components 1 and 2, respectively,  $R_{10}$ ,  $R_{12}$ ,  $R_{21}$ , and  $R_{20}$  are the frictional coefficients,  $(\partial \mu_1/\partial z)_{T,P,t}$  and  $(\partial \mu_2/\partial z)_{T,P,t}$  are the chemical potential gradients, and  $v_0$ ,  $v_1$ , and  $v_2$  are the diffusion velocities of the components. The frictional coefficients are independent of the frame of reference and are inversely proportional to the frequency of molecular interchange.<sup>1</sup>

Now for the two special systems (0, 1, 2) and (0, 1, 3) discussed above, it may be shown<sup>15</sup> that (a) for the system 0, 1, and 2 (trace isotope of 1)

$$R_{10} = R_{20} = (C_1 \bar{V}_0 \mu_{11}/D) \quad (7a)$$

$$R_{12} = R_{21} = -[(C_0 \bar{V}_0 \mu_{11}/D) - RT/(C_1 D_{T2})] \quad (7b)$$

where

$$\mu_{11} = (\partial \mu_1/\partial C_1)_{T,P} \quad (7c)$$

and  $\bar{V}_0$  is the partial molar volume of component 0.

(b) For the system 0, 1, and 3 (trace isotope of 0)

$$R_{01} = R_{31} = (C_0 \bar{V}_1 \mu_{00}/D) \quad (8a)$$

$$R_{03} = R_{30} = -[(C_1 \bar{V}_1 \mu_{00}/D) - RT/(C_0 D_{T3})] \quad (8b)$$

where

$$\mu_{00} = (\partial \mu_0/\partial C_0)_{T,P} \quad (8c)$$

and  $\bar{V}_1$  is the partial molar volume of component 1.

$$\bar{V}_1 \mu_{11} = \bar{V}_0 \mu_{00} \quad (8d)$$

Equations 7 and 8 may be used to calculate  $R_{10}$  ( $= R_{01}$ ),  $R_{12}$  ( $= R_{21}$ ), and  $R_{03}$  ( $= R_{30}$ ) from the experimental diffusion coefficients  $D$ ,  $D_{T2}$ , and  $D_{T3}$  and the necessary thermodynamic data.

(10) S. Ljunggren, *Trans. Roy. Inst. Technol., Stockholm*, **172**, 1 (1961).

(11) P. J. Dunlop, *J. Phys. Chem.*, **68**, 26 (1964).

(12) L. Onsager, *Phys. Rev.*, **37**, 405 (1931); **38**, 2265 (1931).

(13) J. G. Kirkwood, R. L. Baldwin, P. J. Dunlop, L. J. Gosting, and G. Kegeles, *J. Chem. Phys.*, **33**, 1505 (1960).

(14) P. J. Dunlop, *J. Phys. Chem.*, **69**, 1693 (1965).

(15) J. G. Albright and R. Mills, *ibid.*, **69**, 3120 (1965).

(16) P. F. Curran, A. E. Taylor, and A. K. Solomon, *Biophys. J.*, **7**, 879 (1967).

(17) Curran, Taylor, and Solomon have shown that eq 23 of ref 14 may be simplified to eq 3.

It is also of interest to solve eq 7 and 8 for  $D$ ,  $D_{T_2}$ , and  $D_{T_3}$  to obtain

$$D = (C_1 \bar{V}_{0\mu_{11}}/R_{10}) = (C_0 \bar{V}_{1\mu_{00}}/R_{01}) \quad (9a)$$

$$D_{T_2} = RT/(C_0 R_{10} + C_1 R_{12}) \quad (9b)$$

$$D_{T_3} = RT/(C_0 R_{03} + C_1 R_{10}) \quad (9c)$$

Equations 5 and 9 may then be combined to yield the useful expression<sup>18</sup>

$$D = (x_0 D_{T_2} + x_1 D_{T_3}) \left( \frac{\partial \ln a_1}{\partial \ln x_1} \right)_{T,P} \times \left[ \frac{x_0 R_{10}}{x_0 R_{10} + x_1 R_{12}} + \frac{x_1 R_{10}}{x_1 R_{10} + x_0 R_{03}} \right]^{-1} \quad (10)$$

which reduces to the relation

$$D = (x_0 D_{T_2} + x_1 D_{T_3}) \left[ \frac{\partial \ln a_1}{\partial \ln x_1} \right]_{T,P} \quad (11)$$

if<sup>19</sup>

$$R_{10}^2 = R_{12} R_{03} \quad (12)$$

For ideal solutions in which the derivative of the logarithm of the activity,  $a_1$ , with respect to  $x$ , is independent of mole fraction, eq 11 becomes

$$D = (x_0 D_{T_2} + x_1 D_{T_3}) \quad (13)$$

Thus it follows that if 0 and 1 form an ideal solution and if eq 12 is valid, then (see eq 5)

$$(x_0 D_{12} + x_1 D_{03}) = 0 \quad (14)$$

Equations 5, 10, and 13 are quite similar to *modifications*<sup>20,21</sup> of a relation proposed by Kincaid, *et al.*,<sup>22</sup> and Hartley and Crank.<sup>23</sup> Bearman<sup>9</sup> has shown that for regular solutions (with no volume change on mixing)

$$(R_{03}/R_{10}) = (\bar{V}_0/\bar{V}_1) \quad (15a)$$

$$(R_{12}/R_{10}) = (\bar{V}_1/\bar{V}_0) \quad (15b)$$

$$(D_{T_3}/D_{T_2}) = (\bar{V}_1/\bar{V}_0) \quad (15c)$$

and thus, as that author indicated, eq 15a and 15b ensure the validity of eq 11.

The experimental results in the next section were obtained to investigate the relations outlined above.

## Experimental Section

(a) *Materials.* The purification of the benzene, cyclohexane, *n*-hexane, *n*-heptane, and *n*-octane has been previously described.<sup>24</sup> The chlorobenzene was similarly treated. Densities, determined by pycnometry<sup>25</sup> at 25°, and purities, estimated by gas chromatography (column: squalane on Silocel), are given in Table I.

Uniformly labeled <sup>14</sup>C-benzene, cyclohexane, and chlorobenzene were obtained from the Radiochemical Centre, Amersham, England, and <sup>14</sup>C-labeled alkanes

Table I

	—Density (25°, g/cm <sup>3</sup> )—		Mol % impurity	Mol wt
	This work	Literature		
Benzene	0.87368	0.87369 <sup>a</sup>	<0.001	78.115
Chlorobenzene	1.10110	1.10110 <sup>b</sup> 1.10130 <sup>c</sup>	0.02	112.56
Cyclohexane	0.73389	0.73389 <sup>a</sup>	0.005	84.163
<i>n</i> -Hexane	0.65479	0.65479 <sup>a</sup>	<0.001	86.179
<i>n</i> -Heptane	0.67949	0.67949 <sup>a</sup>	<0.001	100.21
<i>n</i> -Octane	0.69854	0.69846 <sup>a</sup>	0.005	114.23

Precision  $\pm 10^{-6}$  g/cm<sup>3</sup>

<sup>a</sup> Reference 43. <sup>b</sup> R. E. Gibson and O. H. Loeffler, *J. Amer. Chem. Soc.*, **61**, 2515 (1939). <sup>c</sup> W. M. Rećko and K. W. Sadowska, *Bull. Acad. Pol. Sci., Ser. Chim.*, **17**, 307 (1969).

from the International Chemical and Nuclear Corporation, California, U. S. A. The estimated radio-purity was 99%, the impurity in the cyclohexane being benzene.

(b) *Density Data.* Densities determined for the systems are published elsewhere.<sup>26</sup> They may be represented by equations of the form

$$\rho(25^\circ, \text{g/cm}^3) = 0.87368 + \sum_i a_i c^i \quad (16)$$

( $c$ , mol/dm<sup>3</sup>), from which partial molar volumes may be calculated using the equations given by Ellerton, *et al.*<sup>25,27</sup> The coefficients,  $a_i$ , are given in Table II.

(c) *Activity Data.* All the details of the vapor pressure measurements of the systems have been published

Table II: Least-Squares Constants for Equation 16

	Benzene-chlorobenzene	Benzene- <i>n</i> -hexane	Benzene- <i>n</i> -heptane
$10^2 \times a_1$	2.31529	-3.04340	-3.12768
$10^4 \times a_2$	0.0982	2.3941	4.3678
$10^6 \times a_3$		-1.3561	-2.2443
$10^6 \times a_4$		1.3461	2.2757
$10^6 \times \sigma^2$	2.1	1.9	2.2

<sup>a</sup>  $\sigma$  is the standard deviation.

- (18) T. Lofin and E. McLaughlin, *J. Phys. Chem.*, **73**, 186 (1969).  
 (19) H. J. V. Tyrrell, *J. Chem. Soc.*, 1599 (1963).  
 (20) L. S. Darken, *Trans. A.I.M.E. (Met.)*, **175**, 184 (1948).  
 (21) P. C. Carman and L. H. Stein, *Trans. Faraday Soc.*, **52**, 619 (1956).  
 (22) J. F. Kincaid, H. Eyring, and J. Stern, *Chem. Rev.*, **28**, 301 (1941).  
 (23) G. S. Hartley and J. Crank, *Trans. Faraday Soc.*, **45**, 801 (1949).  
 (24) T. N. Bell, E. L. Cussler, K. R. Harris, C. N. Pepela, and P. J. Dunlop, *J. Phys. Chem.*, **72**, 4693 (1968).  
 (25) H. D. Ellerton, G. Reinfelds, D. E. Mulcahy, and P. J. Dunlop, *ibid.*, **68**, 398 (1964).  
 (26) K. R. Harris and P. J. Dunlop, *J. Chem. Thermodynamics*, in press.  
 (27) Equation 6a of ref 25 may be more simply written as  $\bar{V}_1 = [\Phi_1 - C(\partial\Phi_1/\partial C)][1000 + C^2(\partial\Phi_1/\partial C)]^{-1}$ .

elsewhere.<sup>26</sup> The excess Gibbs free energy function, calculated from these, may be represented by

$$\frac{G^E}{RT} (25^\circ) = \frac{\alpha x_0 x_1}{1 - k(x_1 - x_0)} \quad (17)$$

Thus

$$\left[ \frac{\partial \ln a_1}{\partial \ln N_1} \right]_{T,P} = 1 - \frac{2\alpha(1-k)x_0 x_1}{[1 - k(x_1 - x_0)]^2} \quad (18)$$

$\alpha$  and  $k$  for each system are given in Table III.

Table III: Constants for Equation 17

	Benzene-chlorobenzene	Benzene- <i>n</i> -hexane	Benzene- <i>n</i> -heptane
$\alpha$	0.0565 ± 0.0032	0.6218 ± 0.0008	0.5667 ± 0.0008
$k$	-0.500	-0.200	-0.268

(d) *Tracer Diffusion Data.* Magnetically stirred Stokes diaphragm cells<sup>28</sup> were used, both upper and lower compartment stoppers being similar to the lower one designed by Albright and Mills.<sup>16</sup> The metal valve in the top stopper had a capped capillary set in it. Ordinary stoppers were found to allow evaporation. The ratio of the diaphragm volume to the mean compartment volume was less than 0.02 as suggested by Gordon.<sup>29</sup> The rule of Robinsor, *et al.*,<sup>30</sup> was used to estimate the diffusion time.

The cells were periodically calibrated by allowing 0.5 *M*<sup>31</sup> KCl or 1 *M* urea solutions to diffuse into water.<sup>32</sup> The cell "constants" were linear in time within ±0.1%. Integral diffusion coefficients were taken from published tables<sup>33</sup> for KCl and computed from the data of Gosting and Akeley<sup>34</sup> for urea. Density data<sup>35</sup> for H<sub>2</sub>O-KCl were fitted to the equation

$$n(25^\circ, \text{g/cm}^3) = 0.997048 + 4.73157 \times 10^{-2}c - 1.9873 \times 10^{-3}c^2 + 4.594 \times 10^{-4}c^3 \quad (19)$$

$$c < 1.2 \text{ mol/dm}^3$$

with a standard deviation of  $8 \times 10^{-6}$  g/cm<sup>3</sup>. For H<sub>2</sub>O-urea the data of Gucker, *et al.*,<sup>36</sup> were used. KCl solutions were diluted to about 0.03 *M* and analyzed conductometrically as has been described earlier,<sup>32</sup> use being made of the recent conductance equation of Fuoss and Hsia.<sup>37</sup> Urea solutions were analyzed by allowing them to diffuse into water and measuring the refractive index increment with a Gouy diffusimeter. The technique has been previously described.<sup>32,38</sup>

Radioactive solutions were prepared by adding 20 to 50  $\mu$ l of active material to a portion of inactive stock solution. Two diffusion techniques were employed. One was the usual method whereby a linear gradient is allowed to form in the diaphragm before diffusion begins. The other made use of the boundary conditions of Barnes and of Mills, *et al.*,<sup>39</sup> the particular condition

being that there was initially no active material in the diaphragm. The two techniques yielded identical results. The diffusion period was taken to be from the time the upper compartment was initially half-filled to that moment when the lower was opened to sample its contents, the upper solution having been withdrawn with a pipet. This was about 2-3 min longer than the stirring period of 1-4 days.

Radioactive solutions were analyzed by liquid scintillation counting. The scintillator solution was a mixture of 3 g/dm<sup>3</sup> of diphenyloxazole and 0.3 g/dm<sup>3</sup> of 1,4 bis(2-(5-phenyloxazoly))benzene in xylene. The electronic equipment consisted of the following components: an ECKO N664A counter, an EMI 9514S photomultiplier tube, a Fluke 412B high-voltage supply (0 to 2100V dc 0-30 mA, resolution 5 mV), and a Philips PW4280 single-channel pulse amplitude analyzer, a PW4230 scaler (resolution 10<sup>-6</sup> sec), a 10-kHz PW4261 crystal oscillator timer, and an automatic printout. Drift was less than 0.1% over 8 hr. Solutions were diluted to give about the same counting rate ( $2 \times 10^5$  counts/min). Each was counted for long enough to give more than 10<sup>6</sup> counts, thus reducing statistical fluctuations to less than 0.1%. The background correction was of the order of 0.2%. Top and bottom solutions were counted in triplicate in vials which could be reproducibly mounted in the counter. Due to differences in transparency it was necessary to calculate concentration ratios for each vial. Generally, the technique used was similar to that of Mills.<sup>40</sup>

Results for the three systems studied are given in Table IV. Superscript 0 denotes benzene and 1 the other component. Thus  $D_{T_3}$  is the tracer coefficient of benzene and  $D_{T_2}$  is that of chlorobenzene, *n*-hexane, and *n*-heptane, respectively.  ${}^0D_{T_3}$  was also measured for benzene + *n*-octane as part of this study. The estimated error, found by summing contributions due to

(28) R. H. Stokes, *J. Amer. Chem. Soc.*, **72**, 763 (1950).

(29) A. R. Gordon, *Ann. N. Y. Acad. Sci.*, **46**, 285 (1945).

(30) R. L. Robinson, Jr., W. C. Edmister, and F. A. L. Dullien, *J. Phys. Chem.*, **69**, 258 (1965).

(31)  $M \equiv \text{mol/dm}^3$ .

(32) E. L. Cussler and P. J. Dunlop, *J. Phys. Chem.*, **70**, 1880 (1966).

(33) L. A. Woolf and J. F. Tilley, *ibid.*, **71**, 1962 (1967).

(34) L. J. Gosting and D. F. Akeley, *J. Amer. Chem. Soc.*, **74**, 2058 (1952).

(35) (a) G. Jones and S. K. Talley, *ibid.*, **55**, 624, 4124 (1933); (b) W. Geffcken and D. Price, *Z. Phys. Chem.*, **B26**, 81 (1934); (c) A. Kruis, *ibid.*, **B34**, 1 (1936).

(36) F. T. Gucker, F. W. Gage, and C. E. Moser, *J. Amer. Chem. Soc.*, **60**, 2582 (1938).

(37) R. M. Fuoss and K.-L. Hsia, *Proc. Nat. Acad. Sci.*, **57**, 1550 (1967).

(38) H. D. Ellerton, G. Reinfelds, D. E. Mulcahy, and P. J. Dunlop, *J. Phys. Chem.*, **68**, 403 (1964).

(39) (a) C. Barnes, *J. Appl. Phys.*, **5**, 4 (1934); (b) R. Mills, L. A. Woolf, and R. O. Watts, *Trans. Am. Inst. Chem. Eng. J.*, **14**, 671 (1968).

(40) R. Mills, *J. Phys. Chem.*, **67**, 600 (1963).

uncertainties in the cell constant, concentrations, diffusion time, and compartment volumes, is  $\pm 0.5\%$ . The self-diffusion coefficient of benzene is an average of 9 runs and has the value  $(2.210 \pm 0.002) \times 10^{-9} \text{ m}^2 \text{ sec}^{-1}$  with a maximum deviation of  $0.4\%$ . The data may be represented by equations of the form

$$D = \sum_i b_i x_i^i \quad (20)$$

where the  $b_i$  were calculated by the method of least squares and are given in Table V together with the average deviations,  $\tau$ .

Table IV: Tracer Diffusion Coefficients at  $25^\circ\text{a}$

(1) Benzene(0,3) + Chlorobenzene(1,2)

$x_1$	$D_{T_1}$	$x_1$	$D_{T_1}$
0.0	2.210	0.0	2.084
0.0984	2.159	0.0985	2.047
0.4986	2.025	0.4996	1.911
0.8927	1.883	0.9000	1.792
1.0000	1.848	1.0000	1.758

(2) Benzene(0,3) + *n*-Hexane(1,2)

$x_1$	$D_{T_1}$	$x_1$	$D_{T_1}$
0.0	2.210	0.0	2.294
0.14683	2.710		
0.24824	3.036		
0.37566	3.430		
0.49506	3.713	0.50005	3.543
0.62476	4.019		
0.62525	4.012		
0.74780	4.246		
0.87447	4.527		
1.0	4.747	1.0	4.263

(3) Benzene(0,3) + *n*-Heptane(1,2)

$x_1$	$D_{T_1}$	$x_1$	$D_{T_1}$
0.0	2.210	0.0	2.070
0.12538	2.590	0.0	2.060
0.12890	2.588	0.0	2.053
0.24411	2.870	0.12385	2.363
0.24888	2.884	0.24671	2.564
0.38574	3.149	0.37349	2.727
0.50039	3.300	0.50039	2.871
0.61981	3.423	0.62011	2.958
0.75396	3.576	0.75112	2.995
0.87982	3.727	0.87982	3.023
1.0	3.871	1.0	3.016

<sup>a</sup> The  $D_{T_1}$  have the units  $10^{-9} \text{ m}^2/\text{sec}$ .

Hammond and Stokes<sup>41</sup> found that the product<sup>42</sup>  ${}^0D_{T_3}\eta_1$  was a linear function of the solvent molar volume,  $V_1^0$ , for carbon tetrachloride in different series of organic compounds. ( $\eta_1$  is the solvent viscosity.) It may be seen from Figure 1 and Table VI<sup>43</sup> that this is also the case for benzene in *n*-hexane, *n*-heptane, and *n*-octane at  $25^\circ$ .

Values of the self-diffusion coefficients of benzene and *n*-hexane are compared with literature values in

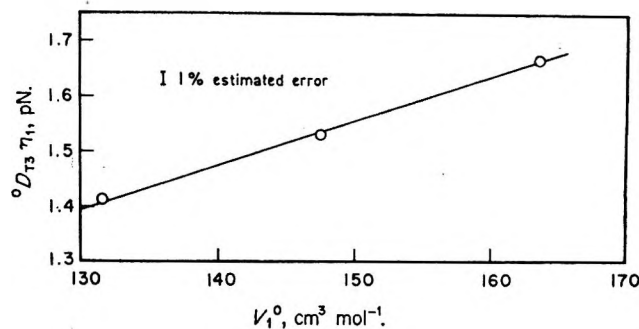


Figure 1. Graph of the product ( ${}^0D_{T_3}\eta_1$ ) vs. the molar volume of the solvent,  $V_1^0$ .  ${}^0D_{T_3}$  is the uncorrected limiting tracer diffusion coefficient of benzene, and  $\eta_1$  is the viscosity of the solvent. The three points are for the solvents *n*-hexane, *n*-heptane, and *n*-octane.

Table VII<sup>44-47</sup> all being obtained by the diaphragm cell technique. For further comparison, limiting coefficients for the system benzene + cyclohexane at  $25^\circ$  were also measured. It may be seen that the values obtained fall about 1 to 3% below those of Mills, but are in reasonable agreement with those of Lyons and coworkers and of Kamal and McLaughlin. A measurement of the self-diffusion coefficient of unpurified benzene ( $\rho$  ( $25^\circ$ ,  $\text{g}/\text{cm}^3$ ) = 0.87356) yielded the same value as for the purer material.

Eppstein<sup>48</sup> has recently sought to explain deviations between limiting tracer diffusion coefficients obtained by Mills and coworkers and limiting mutual coefficients obtained by extrapolation. These should be equal, as may be shown by substituting eq 2a into 3; thus

$${}^1D = {}^1D_{T_2} \quad (21)$$

Mills's results in some cases are in excellent agreement, but in others are up to 1% higher than the limiting mutual coefficients. However, Eppstein brings all these results into good correspondence by making the substitution

$$(D_{T_i})_{\text{true}} = \frac{1}{1.020} \left( \frac{M_k}{M_i} \right)^{1/2} (D_{T_k})_{\text{observed}} \quad (22)$$

where  $M_k$  and  $M_i$  are the molecular weights of the labeled and unlabeled species. The factor 1.020 cor-

(41) B. R. Hammond and R. H. Stokes, *Trans. Faraday Soc.*, **51**, 1641 (1955).

(42)  ${}^iD_{T_k}$  is defined in ref 14 to be the value of  $D_{T_k}$  in the limit  $C_i \rightarrow 0$ , ( $i = 0, 1; k = 2, 3$ ). Thus  $D_{S_0} \equiv {}^1D_{T_3}$  is the self-diffusion coefficient of component 0 and  ${}^0D_{T_3}$  is the coefficient of a trace of 3 in pure 1.

(43) F. D. Rossini, *et al.*, "Selected Values of the Physical and Thermodynamic Properties of Hydrocarbons," Carnegie Press, Pittsburgh, Pa, 1953. A.P.I. Research Project 44.

(44) R. Mills, *J. Phys. Chem.*, **69**, 3116 (1965).

(45) I. Kamal and E. McLaughlin, *Trans. Faraday Soc.*, **62**, 1762 (1966).

(46) J. C. Shieh and P. A. Lyons, *J. Phys. Chem.*, **73**, 3259 (1969).

(47) M. V. Kulkarni, G. F. Allen, and P. A. Lyons, *ibid.*, **69**, 2491 (1965).

(48) L. B. Eppstein, *ibid.*, **73**, 269 (1969).

**Table V:** Least-Squares Constants for Equation 20

	$b_0$	$b_1$	$b_2$	$b_3$	$b_4$	$\tau^a$
(a) Benzene + Chlorobenzene						
$D$	2.1180	-0.2494				0.008
$D_{T_2}$	2.0832	-0.3630	0.0401			0.002
$D_{T_3}$	2.2100	-0.3563				0.004
(b) Benzene + <i>n</i> -Hexane <sup>b</sup>						
$D$	2.3118	-0.8349	4.7480	-1.4664		0.008
$D_{T_2}$						
$D_{T_3}$	2.2100	3.6826	-1.4649	0.3124		0.010
(c) Benzene + <i>n</i> -Heptane						
$D$	2.1304	-1.4958	7.2650	-5.9750	1.9391	0.003
$D_{T_2}$	2.0635	2.5225	-2.0876	0.5189		0.006
$D_{T_3}$	2.2100	3.3909	-3.1467	1.4143		0.007

<sup>a</sup> The units of  $D$  are  $10^{-9}$  m<sup>2</sup> sec<sup>-1</sup>;  $\tau$  is the average deviation. <sup>b</sup> The three experimental points for  $D_{T_2}$  in Table IV were not least-squared.

**Table VI:** Limiting Tracer Diffusion Coefficients,  ${}^0D_{T_3}$ , of Benzene in *n*-Alkanes at 25°<sup>a</sup>

Solvent	$10^6 {}^0D_{T_3}$ , m <sup>2</sup> /sec	$10^3 \eta$ , Ns/m <sup>2</sup>	${}^0D_{T_3} \eta$ , pN	$V_1^0$ , cm <sup>3</sup> /mol
<i>n</i> -Hexane	4.747	0.2976	1.413	131.6
<i>n</i> -Heptane	3.871	0.3955	1.531	147.5
<i>n</i> -Octane	3.246	0.5136	1.667	163.5

<sup>a</sup> Viscosities were taken from reference 43 and have been adjusted to be relative to the 1958 N.B.S. standard for water,  $\eta(\text{H}_2\text{O}, 20^\circ) = 1.002 \times 10^{-3}$  Ns/m<sup>2</sup>.

rects for an assumed systematic error due to the use of electrolyte (KCl) solutions for all calibrations. Our work, see Figure 2, shows no difference between calibrations performed with nonelectrolyte (urea) and electrolyte (KCl) solutions within an experimental error of  $\pm 0.1\%$ .

The isotope effect, also postulated by McLaughlin,<sup>49</sup> was examined by measuring the self-diffusion coefficients of benzene with labeled samples of different number average molecular weight (*viz.* 81, 84, and 88). (<sup>14</sup>C benzene is obtained in a uniformly labeled form, being prepared from a mixture of <sup>12</sup>CO<sub>2</sub> and <sup>14</sup>CO<sub>2</sub> *via* acetylene as an intermediate. Thus it contains molecules with a distribution of labeled atoms.) Measurements made with all these samples fell within the range 2.203 to 2.218 units, with an average value of 2.210 quoted above. Eppstein's relation would predict a maximum disparity of  $\sqrt{88/81}$  or about 4% in this case. It would also predict a difference of 8% between the limiting conductances of <sup>6</sup>Li<sup>-</sup> and <sup>7</sup>Li<sup>+</sup> which are directly proportional to the limiting ionic diffusion coefficients. Kunze and Fuoss<sup>50</sup> have found only 0.35% difference. Thus it would seem that equation 22 is invalid.

We would further comment that it is sometimes difficult to extrapolate mutual diffusion coefficients, particularly when they are strongly concentration de-

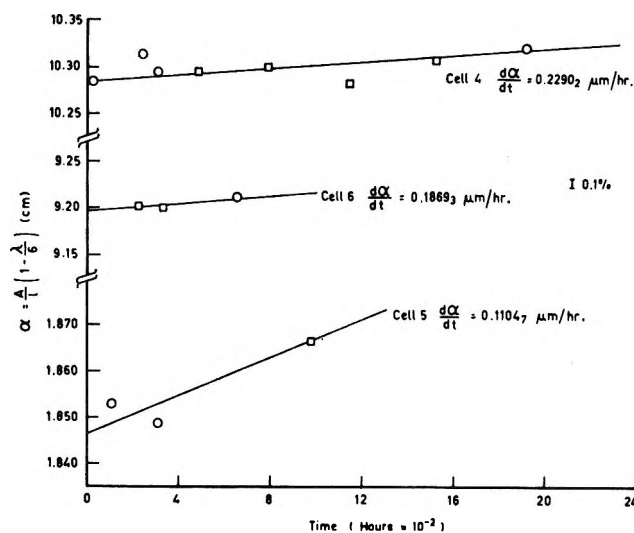


Figure 2. Graphs of the cell constants<sup>39</sup> vs. time for the three diaphragm cells used in this study: O, using 1 M urea; □, using 0.5 M KCl.

pendent. The limiting value depends very much on the form of the equation used to fit the data or on the judgement of the person drawing the graph. Similar behaviour has been noted in conductance work, even though such results are available at very low concentrations.

(e) *Mutual Diffusion Data.* The mutual diffusion coefficient of each system was obtained as a function of composition from measurements made with a Goüy diffusimeter. The optical system and general technique used have been previously described,<sup>38</sup> as has the general method of calculation of the results.<sup>51</sup> The reader is referred to the latter paper for definitions of the quantities given below.

(49) E. McLaughlin, *Physica*, **26**, 650 (1960).

(50) R. W. Kunze and R. M. Fuoss, *J. Phys. Chem.*, **66**, 930 (1962).

(51) D. F. Akeley and L. J. Gosting, *J. Amer. Chem. Soc.*, **75**, 5685 (1953).

Table VII:<sup>a</sup> Comparison of Literature Tracer Diffusion Coefficients with Those Obtained in This Work

	This work	Mills	Lyons	McLaughlin	References
$D_{S0}$ , benzene	2.210	$2.247 \pm 0.007^b$		$2.12 \pm 0.04$	40, 44, 45
$D_{S1}$ , benzene	$4.263^c$		$4.131 \pm 0.047$		46
$D_{S1}$ , cyclohexane	1.440	$1.475 \pm 0.004$	1.443	$1.41 \pm 0.03$	44, 47, 45
$^0D_{T3}$ , benzene in cyclohexane	1.835	$1.892 \pm 0.006^d$		$1.89^e$	44, 45
$^1D_{T2}$ , cyclohexane in benzene	2.084	$2.104 \pm 0.006$		$2.07^e$	44, 45

<sup>a</sup>  $D$  values,  $10^{-9}$  m<sup>2</sup>/sec. <sup>b</sup> Mills (private communique) recently remeasured the self-diffusion coefficient of benzene at 25° and obtained a value of  $(2.205 \pm 0.004) \times 10^{-9}$  m<sup>2</sup>/sec. <sup>c</sup> D. C. Douglass and D. W. McCall, *J. Phys. Chem.*, **62**, 1102 (1958), using the spin-echo technique, obtained a value of 4.21 for  $D_{S1}$ . <sup>d</sup> Average of two values given in this paper. <sup>e</sup> Extrapolated values.

The procedure differed from that of earlier work in that a new design of Tiselius diffusion cell was used. The cells previously used for work on aqueous solutions consisted of three parts, a center section containing the diffusion channel and upper reservoir and lower connector sections which may be slid to and fro to facilitate filling, allow boundary formation, and to isolate the cell during diffusion. For work with organic solutions it has been the practice to grease the flanges between the sections with an inner band of benzene-washed Fisher "Nonaq" polysaccharide grease and an outer band of petroleum grease. Thus the hydrocarbon soluble grease is separated from the contents of the cell and the water-soluble grease from the bath water. However, inconsistent results were obtained using this method and were attributed to the slight solubility of Nonaq in hydrocarbons. Indeed it was found that  $\delta''$  corrections (the fringe displacements used to calculate the fractional part of  $J$ ), taken during siphoning *without* a gradient in the cell were neither constant nor reproducible. Bonner<sup>52</sup> has shown Nonaq to be soluble in *n*-octane at 23° to the extent of half a fringe (cell path length,  $a = 1$  cm,  $\lambda = 546$  nm), but he was able to correct his thermal diffusion measurements for this factor. An experiment with the new cell used in this study ( $a = 3.1$  cm,  $\lambda = 546$  nm) in which a boundary was formed between Nonaq saturated benzene and pure benzene yielded a constant  $\delta''$  correction corresponding to 0.6 of a fringe.

The new cell used ( $a$  and  $b$  dimensions, 3.0975 and 305.31 cm, respectively) was a quartz, one-piece, fixed section cell (Figure 3) manufactured by Hellma GmbH, Baden-Müllheim, Germany. The lower connector had the dimensions of the diffusion channel while the reservoirs at the top were separated from the center section by tapered holes in midchannel. In use, the cell was filled to this point with the denser solution and a Teflon plug inserted in the hole above the diffusion channel. The reservoirs were then filled with the two solutions to such a relative height that, when the cell was opened after the initial  $\delta$  correction photographs had been taken, no movement of solution took place due to the existence of

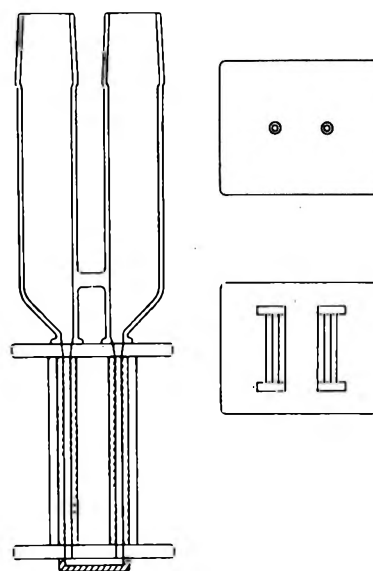


Figure 3. Diagram of the one-piece quartz Tiselius cell used for measuring all the mutual diffusion coefficients. Sections of the top and bottom of the optical channel are shown at the right.

the density gradient across the boundary. If the height difference was made purposely large to shift the boundary down, mixing occurred in the reservoir due to the pulsing of solution through the hole as the plug was removed. The boundary was sharpened by siphoning using the capillary technique<sup>53</sup> and experiments carried out in the usual manner except that the cell was not "closed" during the diffusion period. Movement of air in the laboratory at this time was not found to affect the process as judged by fringe deviations measured for photographs taken at such times. This is not the case for small gradients.<sup>54</sup> The solutions in the reservoirs were also gently stirred before removal of the plug and shortly after the boundary sharpening had begun. The

(52) F. J. Bonner, *Arkiv Kemi*, **27**, 97 (1967).

(53) D. S. Kahn and A. Polson, *J. Phys. Colloid Chem.*, **51**, 816 (1947).

(54) C. N. Pepela, B. J. Steel, and P. J. Dunlop, *J. Amer. Chem. Soc.*, in press.

**Table VIII:** Mutual Diffusion Coefficients for Water + Sucrose and Benzene + Biphenyl at 25°

Experiment	32	42	81	82	75
System	Sucrose	Sucrose	Sucrose	Sucrose	Biphenyl
$\bar{c}_1$ (mol/dm <sup>3</sup> )	0.014630	0.017445	0.014604	0.011682	0.042861
$D$ (10 <sup>-9</sup> m <sup>2</sup> /sec)	0.5203	0.5193	0.5191	0.5201	1.567
$D$ (literature)	0.5189	0.5182	0.5189	0.5197	1.549
$\Delta n/\Delta c_1$ (cm <sup>3</sup> /mol)	48.99	48.93	48.85	48.48	18.33
$\Delta n/\Delta c_1$ (literature)	48.97	48.97	48.97	48.97	18.25
$10^4 \times Q$	3.5	3.0	1.0	2.0	3.0
$\Delta c_1$	0.029259	0.034990	0.029209	0.023364	0.085722
$J$	81.30	97.12	80.93	64.25	89.13
$\Delta t$ (sec)	12.49	15.78	18.15	20.81	25.95

**Table IX:** Mutual Diffusion Coefficients of Benzene + Chlorobenzene at 25°

Experiment	B- $\phi$ C12	74	73	75	72
$\bar{c}_1$ (mol/dm <sup>3</sup> )	0.31790	2.6985	5.2020	7.5730	9.4689
$\bar{x}_1^a$	0.02854	0.24996	0.49847	0.75000	0.96340
$D$ (10 <sup>-9</sup> m <sup>2</sup> /sec)	2.110	2.063	1.987	1.925	1.884
$\Delta n/\Delta c_1$ (cm <sup>3</sup> /mol)	2.450	2.478	2.468	2.488	2.502
$10^4 \times Q$	0.0	5.1	5.6	0.0	2.9
$\Delta c_1$	0.6358	0.6608	0.6349	0.6330	0.6267
$J$	88.35	92.89	88.88	89.34	88.90 <sup>b</sup>
$\Delta t$ (sec)	11.84	12.24	9.17	9.54	4.99

<sup>a</sup>  $\bar{x}_1$  is the mole fraction of chlorobenzene corresponding to the mean concentration,  $\bar{c}_1$ . <sup>b</sup>  $J$  was obtained by extrapolation.

procedure described above was derived from experiments with colored solutions.

The total number of fringes,  $J$ , was estimated by plotting the fringe displacements,  $Y_j$ , against the fringe number,  $j$ , and extrapolating the curve to zero  $Y_j$ . For the minima this yields  $J = 0.75$ . It was important to resolve the highest numbered fringes for this measurement by manipulating the cell mask<sup>55</sup> and adjusting the plate exposure, while avoiding the fine structure noticed by Longworth<sup>56</sup> which is due to the "slits" formed by the mask and boundary edges. The fractional part of  $J$  was also obtained from the  $\delta''$  correction and the two methods yielded values differing by 0.15 of a fringe or less, the first giving consistently the higher value, the second being that preferred for calculation.

The cell was tested by performing diffusion experiments with the systems water-sucrose and benzene-biphenyl. (The biphenyl<sup>57</sup> and sucrose<sup>58</sup> samples have been previously described.) The results are given in Table VIII. The values for the sucrose runs are all within 0.3% of those calculated from the measurements of Akeley and Gosting<sup>51</sup> but the benzene-biphenyl value is 1.2% higher than that calculated from the data of Sandquist and Lyons.<sup>59</sup> Tests with more concentrated sucrose solutions ( $\bar{c} = 0.25$  and  $0.5 M$ ) were unsuccessful,  $\delta''$  and the fringe deviations being inconsistent and time dependent. This is probably due to the higher viscosity of these solutions which could well prevent complete washing of the cell above the boundary.

Notwithstanding the precautions described above, it was found that in some experiments with the organic systems either  $\delta''$  or both  $\delta''$  and the fringe deviations were time dependent. In the first case  $J$  was then estimated by the extrapolation procedure described above and in two examples (experiments 50, 39 and 42, 46) the coefficients so calculated agreed within 0.5% with those obtained from normal experiments. Hence such points are included in Tables IX, X, and XI. The overall precision is therefore estimated to be  $\pm 0.5\%$ . It may also be noted that the areas under the fringe deviation graphs are generally positive and the refractive index increments show greater scatter than has been noted in earlier work on aqueous systems. This is not understood at present but we do not believe it to be due to the volatility of the components or to the concentration dependence of the diffusion coefficients. It is intended to test in the future an improved cell with a flowing junction boundary of the type used for Bryngdahl diffusion in this laboratory<sup>54</sup> and with better washing of the portion of the cell above the boundary.

The measured diffusion coefficients may be expressed by equations of the form of (20) and the coefficients are also given in Table V.

(55) L. J. Gosting and L. Onsager, *J. Amer. Chem. Soc.*, **74**, 6066 (1952).

(56) L. G. Longworth, *ibid.*, **69**, 2510 (1947).

(57) K. R. Harris and P. J. Dunlop, *J. Phys. Chem.*, **71**, 483 (1967).

(58) H. D. Ellerton and P. J. Dunlop, *ibid.*, **71**, 1538 (1967).

(59) C. L. Sandquist and P. A. Lyons, *J. Amer. Chem. Soc.*, **76**, 4641 (1954).

Table X: Mutual Diffusion Coefficients of Benzene + *n*-Hexane at 25°

Experiment	58	54	65	61	66	57	62	69	67	68	55
$\bar{c}_1$ (mol/dm <sup>3</sup> )	0.05641	0.10482	1.3220	2.4902	3.5491	4.5163	4.5150	5.3772	6.1800	6.9911	7.5531
$\bar{x}_1$	0.00506	0.00942	0.12545	0.24997	0.37481	0.50111	0.50093	0.62464	0.74998	0.88817	0.99144
$D$ (10 <sup>-9</sup> m <sup>2</sup> /sec)	2.314	2.298	2.279	2.371	2.606	2.884	2.905	3.281	3.744	4.290	4.720
$\Delta n/\Delta c_1$ (cm <sup>3</sup> /mol)	-18.46	-18.23	-17.19	-15.54	-16.17	-15.55	-16.07	-15.79	-16.03	-15.40	-14.97
10 <sup>4</sup> × $Q$	3.6	4.9	3.2	4.6	6.7	-1.3	2.3	1.7	2.6	2.3	-2.3
$\Delta c_1$	-0.1128	-0.2097	-0.0874	-0.0984	-0.1051	-0.1397	-0.1337	-0.1086	-0.1109	-0.1335	-0.0903
$J$	118.15	216.63	85.25 <sup>a</sup>	86.75 <sup>a</sup>	96.40 <sup>a</sup>	119.75 <sup>a</sup>	121.85 <sup>a</sup>	97.25 <sup>a</sup>	100.82	116.68	76.66
$\Delta t$ (sec)	71.74 <sup>b</sup>	17.08	13.18	17.23	13.49	9.45	12.03	6.70	6.10	11.18	13.02

<sup>a</sup>  $J$  was obtained by extrapolation. <sup>b</sup> This is probably in error by 60 sec.

Table XI: Mutual Diffusion Coefficients of Benzene + *n*-Heptane at 25°

Experiment	50	39	51	38	52	46	53	48	47	43
$\bar{c}_1$ (mol/dm)	0.04970	0.05498	1.1842	1.1900	2.2846	2.2916	3.2542	4.4492	5.6572	6.6847
$\bar{x}_1$	0.00446	0.00493	0.11405	0.11466	0.23674	0.23761	0.36102	0.54803	0.75667	0.97732
$D$ (10 <sup>-9</sup> m <sup>2</sup> /sec)	2.126	2.121	2.043	2.050	2.105	2.113	2.293	2.682	3.206	3.799
$\Delta n/\Delta c_1$ (cm <sup>3</sup> /mol)	-19.30	-19.20	-18.72	-19.20	-18.14	-18.36	-18.00	-17.62	-16.65	-14.58
10 <sup>4</sup> × $Q$	3.9	5.3	4.0	3.5	3.7	5.9	3.7	1.6	-0.6	0.0
$\Delta c_1$	-0.09939	-0.1099	-0.1192	-0.1105	-0.1199	-0.1163	-0.0966	-0.1055	-0.1200	-0.1924
$J$	108.80 <sup>a</sup>	119.76	126.60 <sup>a</sup>	120.50 <sup>a</sup>	123.35 <sup>a</sup>	121.15	98.65	105.46	113.32	159.17
$\Delta t$ (sec)	25.91	19.61	21.05	26.26	13.19	23.46	10.90	13.89	15.08	12.81

<sup>a</sup>  $J$  obtained by extrapolation.

**Table XII:** Limiting Diffusion Coefficients ( $10^{-9} \text{ m}^2/\text{sec}$ )

(0,3)-(1,2)	$z_1 = 0$			$z_1 = 1$		
	${}^1D$	$D_{T_3}$	$\gamma^a$	${}^2D$	${}^2D_{T_1}$	$\gamma^a$
Benzene + chlorobenzene	2.118	2.083	1.7%	1.869	1.848	1.1%
Benzene + <i>n</i> -hexane	2.312	2.294	-0.8%	4.758	4.740	0.4%
Benzene + <i>n</i> -heptane	2.130	2.064	3.2%	3.864	3.869	-0.1%

$^a \gamma = 100(D - D_{T_i})/D.$

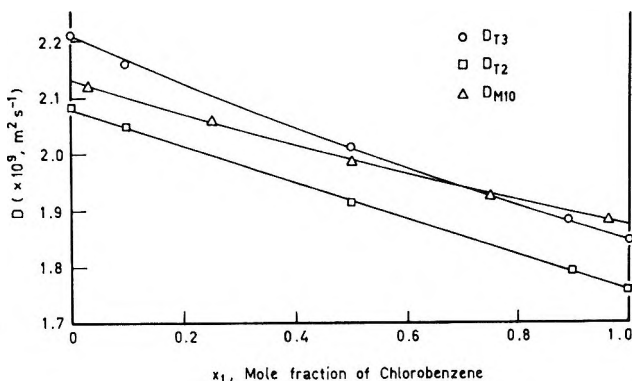


**Figure 4.** Graphs of  $D_{T_2}$ ,  $D_{T_3}$ , and  $D$  vs. concentration for the system benzene + chlorobenzene.

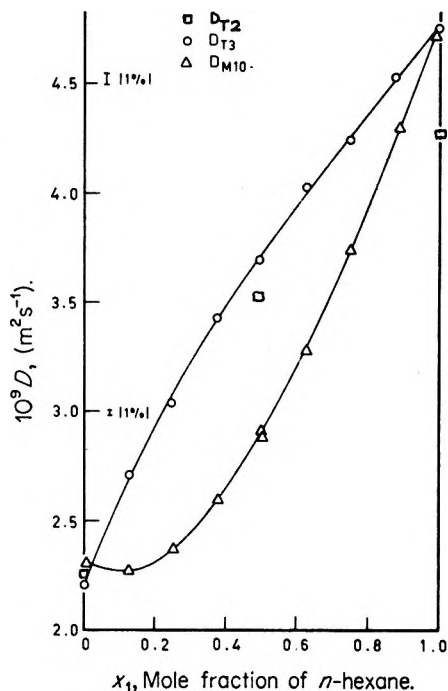


**Figure 5.** Graphs of  $D_{T_2}$ ,  $D_{T_3}$ , and  $D$  vs. concentration for the system benzene + *n*-hexane.

**Discussion**

The tracer and mutual diffusion coefficients are plotted vs. mole fractions in Figures 4-6. The limiting diffusion coefficients are given in Table XII. These were calculated from equation 20. The maximum combined error in the two coefficients is 1%. The agreement is good for the limiting mutual and tracer coefficients of benzene but the other limiting tracer

values tend to be lower than the corresponding mutual ones. In the calculations below, the tracer values have been adjusted by the increments necessary to obtain agreement, since we believe the above differences are due to radioactive impurities in the labeled samples.

The frictional coefficients,  $R_{11}$ ,  $R_{03}$ , and  $R_{12}$  are given in Table XIII for each system together with the ratio

**Table XIII:** Frictional Coefficients and Tests of Equation 12

(a) Benzene(0,3) + Chlorobenzene(1,2)

$z_1$	$C_1$ (mol/dm <sup>3</sup> )	$R_{10}$	$R_{03}$ ( $10^8 \text{ J.m.s./mol}^2$ )	$R_{12}$	$R_{10}^2 / (R_{03}R_{12})$
0.0	0.0	1.059	1.008		
0.1	1.1025	1.049	1.038	1.49	0.71
0.2	2.1742	1.072	1.071	1.35	0.79
0.3	3.2163	1.105	1.104	1.30	0.85
0.4	4.2301	1.143	1.137	1.28	0.90
0.5	5.2169	1.181	1.169	1.290	0.92
0.6	6.1778	1.219	1.20	1.308	0.95
0.7	7.1138	1.257	1.23	1.333	0.96
0.8	8.0259	1.295	1.26	1.363	0.97
0.9	8.9152	1.334	1.30	1.394	0.98
1.0	9.7824	1.372		1.429	

(b) Benzene(0,3) + *n*-Hexane(1,2)

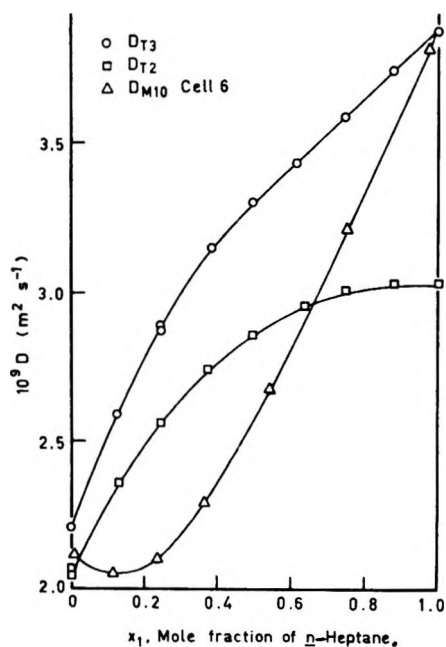
$z_1$	$C_1$	$R_{10}$	$R_{03}$	$R_{12}$	$R_{10}^2 / (R_{03}R_{12})$
0.0	0.0	0.970	1.007		
0.1	1.0662	0.847	0.918		
0.2	2.0383	0.763	0.867		
0.3	2.9292	0.711	0.839		
0.4	3.7496	0.684	0.823		
0.5	4.5081	0.674	0.813	0.878	0.64
0.6	5.2123	0.672	0.81		
0.7	5.8683	0.675	0.80		
0.8	6.4817	0.680	0.80		
0.9	7.0569	0.687	0.80		
1.0	7.5982	0.694	...	0.762	...

(c) Benzene(0,3) + *n*-Heptane(1,2)

$z_1$	$C_1$	$R_{10}$	$R_{03}$	$R_{12}$	$R_{10}^2 / (R_{03}R_{12})$
0.0	0.0	1.053	1.017		
0.1	1.0475	0.941	0.954	1.78	0.56
0.2	1.9715	0.876	0.930	1.47	0.56
0.3	2.7944	0.848	0.929	1.33	0.58
0.4	3.5330	0.844	0.941	1.23	0.61
0.5	4.2001	0.855	0.960	1.180	0.65
0.6	4.8077	0.874	0.98	1.154	0.67
0.7	5.3629	0.896	1.01	1.149	0.69
0.8	5.8731	0.919	1.03	1.157	0.71
0.9	6.3442	0.940	1.06	1.176	0.71
1.0	6.7810	0.958		1.200	

Table XIV: Values of the Quantity  $(x_0D_{12} + x_0D_{03}) \times 10^9 = \Delta$ 

(a) Nearly Ideal Systems								
$x_1$	Benzene(0) + Chlorobenzene(1)		$n$ -Dodecane(0) + $n$ -Hexane(1)			$n$ -Dodecane(0) + $n$ -Octane(1)		
	$\frac{\partial \ln f_0}{\partial \ln x_0}$	$\Delta(25^\circ)$	$\frac{\partial \ln f_0}{\partial \ln x_0}$	$\Delta(25^\circ)$	$\Delta(35^\circ)$	$\frac{\partial \ln f_0}{\partial \ln x_0}$	$\Delta(25^\circ)$	$\Delta(60^\circ)$
0.1	-0.035	0.000	0.007	0.000	0.086	0.003	0.008	0.034
0.2	-0.040	0.000	0.013	0.017	0.092	0.006	0.031	0.058
0.3	-0.035	-0.001	0.017	0.043	0.075	0.007	0.059	0.074
0.4	-0.028	-0.002	0.019	0.068	0.065	0.008	0.080	0.082
0.5	-0.021	-0.003	0.020	0.087	0.068	0.009	0.091	0.083
0.6	-0.015	-0.004	0.019	0.094	0.079	0.008	0.087	0.077
0.7	-0.010	-0.005	0.017	0.089	0.082	0.007	0.071	0.066
0.8	-0.006	-0.004	0.013	0.070	0.068	0.006	0.046	0.048
0.9	-0.003	-0.003	0.007	0.039	0.036	0.003	0.018	0.026
	Error in $\Delta \pm 0.03$		Error in $\Delta \pm 0.06$			Error in $\Delta \pm 0.10$		
(b) Nonideal Systems (25°)								
$x_1$	Benzene(0) + $n$ -Hexane(0)		Benzene(0) + $n$ -Heptane(1)		Benzene(0) + Cyclohexane(1)			
	$\frac{\partial \ln f_0}{\partial \ln x_0}$	$\Delta$	$\frac{\partial \ln f_0}{\partial \ln x_0}$	$\Delta$	$\frac{\partial \ln f_0}{\partial \ln x_0}$	$\Delta$		
0.1	-0.081		-0.195	-0.330	-0.110	-0.165		
0.2	-0.280		-0.285	-0.521	-0.183	-0.279		
0.3	-0.322		-0.310	-0.603	-0.226	-0.345		
0.4	-0.324		-0.298	-0.601	-0.248	-0.372		
0.5	-0.298	-0.774	-0.263	-0.540	-0.249	-0.365		
0.6	-0.254		-0.216	-0.440	-0.233	-0.331		
0.7	-0.199		-0.163	-0.321	-0.200	-0.277		
0.8	-0.136		-0.108	-0.200	-0.151	-0.205		
0.9	-0.067		-0.053	-0.089	-0.084	-0.114		
	Error in $\Delta \pm 0.03$		Error in $\Delta \pm 0.03$		Error in $\Delta \pm 0.03$			

Figure 6. Graphs of  $D_{T_2}$ ,  $D_{T_3}$ , and  $D$  vs. concentration for the system benzene- $n$ -heptane.

$R_{10}^2/(R_{03}R_{12})$  (see equation 12). The estimated error in  $R_{10}$  is about 1.5% due to an uncertainty of 1% in the activity term and 0.5% in  $D$ . The errors in  $R_{03}$  and  $R_{12}$  depend on composition and are greatest as

$D \rightarrow D_{T_3}$  ( $x_1 \rightarrow 1$ ) and  $D \rightarrow D_{T_2}$  ( $x_0 \rightarrow 1$ ), respectively. If it is assumed that the relative errors in  $R_{10}$  and  $D_{T_3}$  are both equal to  $\epsilon$  and that the diffusion coefficients are approximately equal in magnitude, then the maximum relative error in  $R_{03}$  is given by<sup>19</sup>

$$\left(\frac{\delta R_{03}}{R_{03}}\right)^2 = \epsilon^2 \left(\frac{1 + x_1^2}{x_0^2}\right) \quad (23)$$

and takes the values  $\epsilon (= 1.5\%)$  at  $x_1 = 0$ ,  $\sqrt{5}\epsilon$  at  $x_1 = 0.5$ , and  $\sqrt{181}\epsilon$  at  $x_1 = 0.9$ . The tabulated values are calculated from the smoothed functions of eq 20.

The quantity  $\Delta$  (see eq 5) defined by

$$\Delta = (x_0D_{12} + x_1D_{T_3}) \times 10^9 \quad (24)$$

is given in Table XIV for the three systems studied and also for the systems benzene-cyclohexane,<sup>44</sup>  $n$ -dodecane- $n$ -hexane,<sup>47</sup> and  $n$ -dodecane- $n$ -octane.<sup>60</sup> For the nearly ideal systems where the excess Gibbs free energy is small,  $\Delta$  is zero within experimental error, and eq 13 holds. It is of interest to note that kinetic theory<sup>61</sup> for gaseous mixtures yields the approximate relations

(60) A. L. van Geet and A. W. Adamson, *J. Phys. Chem.*, **68**, 238 (1964).

(61) C. F. Curtiss and J. O. Hirschfelder, *J. Chem. Phys.*, **17**, 550, 1076 (1949).

$$\frac{1}{D_{T_3}} = \frac{x_0}{D_{S_0}} + \frac{x_1}{D}$$

$$\frac{1}{D_{T_2}} = \frac{x_1}{D_{S_1}} + \frac{x_0}{D} \quad (25)$$

where the  $D_{S_i}$  are self-diffusion coefficients and  $D$  is assumed to be constant. (For real gas mixtures  $D$  may vary by approximately 5% over the whole concentration range; for the liquid systems studied in this work  $D$  varies markedly with concentration.) The condition that eq 13 and 25 hold has been given by McCarthy and Mason<sup>62</sup> as

$$D^2 = D_{S_0}D_{S_1} \quad (26)$$

which they show by example is only true for mixtures of very similar gases (e.g.  $H_2$ - $D_2$ ), for which systems one would expect  $\Delta$  to be very close to zero.

For the two systems in Table XIV which show positive excess Gibbs energies, use of the Darken relation,<sup>20</sup> equation 11, to predict mutual diffusion coefficients from corresponding values of  $D_{T_2}$  and  $D_{T_3}$  yields values which are much too low. For example, when  $x_0 = x_1$

= 0.5 the value of  $D$  computed for the system benzene-cyclohexane is  $1.624 \times 10^{-9}$  (25% low) and the value computed for the system benzene-*n*-heptane is  $2.271 \times 10^{-9}$  (26% low). These results are presumably due to the fact that eq 12 does not hold for these two systems. Indeed the data in Table XIII show that the ratio  $R_{10}^2/(R_{03}R_{12})$  is considerably less than unity for systems having positive excess Gibbs energies.

One would expect the quantity  $R_{10}^2/(R_{03}R_{12})$  to be greater than unity for systems having negative excess Gibbs energies and hence diffusion coefficients predicted by eq 11 to be too great, although this has yet to be tested. Some of the aqueous systems studied by Mills, Albright, and coworkers fall into this class but, as yet, the tracer diffusion coefficients of water in these systems remain undetermined.

*Acknowledgment.* It is a pleasure to thank Dr. R. Mills of the National University, Canberra, for helpful discussions concerning counting techniques. This work was supported in part by a grant from the Australian Research Grants Committee.

(62) K. P. McCarthy and E. A. Mason, *Phys. Fluids*, **3**, 908 (1960).

## Membrane Osmometry of Aqueous Micellar Solutions of

### Pure Nonionic and Ionic Surfactants

by D. Attwood,\* P. H. Elworthy, and S. B. Kayne

*School of Pharmaceutical Sciences, University of Strathclyde, Glasgow, C.1., United Kingdom (Received May 14, 1970)*

Membrane osmometry has been used to determine the number-average micellar molecular weights,  $M_n$ , of the nonionic surfactants *n*-dodecyl hexaoxyethylene monoether ( $C_{12}n_6$ ) and *n*-hexadecyl nonaoxyethylene monoether ( $C_{16}n_9$ ) at a series of temperatures and of the ionic surfactant *N*-cetyltrimethylammonium bromide (CTAB). Osmotic pressure measurements on systems permeating the osmometer membrane have been corrected using the partition coefficient of the micelles between the membrane and the solution, as determined from diffusion and dialysis measurements.  $M_n$  values for  $C_{12}n_6$  at all temperatures studied were within the limits of error of the corresponding weight-average values,  $M_w$ , determined by light scattering, with a mean  $M_w/M_n$  ratio over the temperature range of 1.00 ( $\pm 0.13$ ). Osmometer measurements on  $C_{16}n_9$  indicated a threshold temperature  $T_h$  similar to that reported from light scattering. At temperatures below  $T_h$ , the  $M_w/M_n$  ratio was 1.10 ( $\pm 0.14$ ). An  $M_n$  of  $10.5 \times 10^4$  was determined for CTAB in 0.025 *N* KBr at 30°, which is within the limits of error of the light-scattering value.

#### Introduction

Although several determinations of the number-average micellar molecular weight,  $M_n$ , of aqueous surfactant systems have been reported, these have mainly been restricted to surfactants of a sufficiently small micellar size ( $M_n < 20,000$ ) to be studied by vapor

pressure osmometry. It is only recently that the technique of membrane osmometry has been applied to a study of micellar systems. In a previous paper<sup>1</sup> we

\* To whom correspondence should be addressed.

(1) D. Attwood, P. H. Elworthy, and S. B. Kayne, *J. Pharm. Pharmacol.*, **21**, 619 (1969).

reported on the use of this technique in the measurement of  $M_n$  of the nonionic surfactant Cetomacrogol 1000 in aqueous solution. Comparison with the weight-average micellar molecular weight,  $M_w$ , from light-scattering determinations indicated a discrepancy of less than 5% between the two average values, which is well within the limits of error of the light-scattering technique. Membrane osmometry has also been used by Coll in a study of the degree of micellization of an ionic surfactant<sup>2</sup> and of several commercial nonionic surfactants.<sup>3</sup>

This present investigation reports on the further application of this technique to the study of pure ionic and nonionic surfactants and comments on the polydispersity of micellar size in these systems.

### Experimental Section

**Materials.** *n*-Hexadecyl nonaoxyethylene monoether ( $C_{16}n_9$ ) was prepared by the Williamson ether synthesis as described previously,<sup>4</sup> recrystallized from anhydrous ether, and chromatographed on neutral alumina using a 25:24:1 acetone:benzene:methanol solvent system. The sample had an ethylene oxide content, as determined by the method of Siggia, *et al.*,<sup>5</sup> of 62.07% in agreement with the theoretical value (62.05%) and a melting point of 44° compared with reported values of 43° and 45.7°.<sup>7</sup>

*n*-Dodecyl hexaoxyethylene monoether ( $C_{12}n_6$ ) was synthesized and chromatographed in a similar manner to that described above. The sample had an ethylene oxide content of 58.64% in agreement with the theoretical value (58.65%). The melting point (24.9°) and refractive index ( $n_D^{40}$  1.4479) are both in agreement with published values (25.2° and 1.4483, respectively).<sup>8</sup>

*N*-Cetyltrimethylammonium bromide (CTAB) was prepared by reacting equimolar quantities of trimethylamine and cetyl bromide in ethanolic solution for seven days at -3°. Extraction with diethyl ether and recrystallization from absolute ethanol yielded a product with a melting point of 237-239° in agreement with literature values (237-243°).<sup>9</sup>

A commercial sample (B.D.H.) of polyoxyethylene glycol 6000 (P.E.G. 6000) was ion-exchanged in methanol on a mixed bed resin ("Biodeminrolit"). An ethylene oxide determination indicated 135 ethylene oxide units per molecule.

**Membrane Osmometry.** Measurements were made on a Hewlett-Packard 503 high-speed membrane osmometer with variable temperature control. B.19 cellulose acetate membranes (Schleicher and Schuell) were used which were found to retain the micelles of most of the surfactants studied, but which were freely permeable to monomers. It was therefore necessary to achieve, as far as was possible, an equal concentration of monomers on each side of the osmometer membrane, in order to reduce to a minimum the contributions to the osmotic pressure from the monomeric species. Errors

arising from possible inequality of monomer concentration in the sample and solvent compartments are not, however, likely to be excessive because of the low critical micelle concentrations (cmc's) of the surfactants used in this investigation. With the nonionic surfactants, osmotic pressure measurements were made against solutions with a concentration,  $c'$ , several times the critical micelle concentration and therefore containing approximately the same concentration of monomers as the test solution.

With the ionic surfactant, measurements were made in the presence of 0.025 *N* KBr and in order to establish conditions of Donnan equilibrium each solution was dialyzed against 0.025 *N* KBr for 2 days. The dialyses were carried out in specially constructed cells using the osmometer membranes as the dialysis barriers, rather than in the osmometer itself. Osmotic pressure readings on the dialyzed solutions were then taken with the dialysates in the solvent compartment of the osmometer and equilibrium readings were obtained within 10 min for all solutions. In this way several solutions could be dialyzed simultaneously and also for each concentration sufficient dialyzed solution was available to enable duplicate measurements to be readily made without the lengthy equilibration periods in the osmometer which would otherwise be required to establish Donnan equilibrium. Any changes in the surfactant concentrations resulting from dialysis will be negligible since the cmc is very low.

For all systems studied, graphs of osmotic pressure *vs.* time were obtained in duplicate for each concentration of surfactant solution. For solutions in which the micellar species were shown to be held by the membrane, equilibrium values of osmotic pressure, reproducible to  $\pm 0.02$  cm of solvent, were obtained. In cases where membrane permeability to the micelles was demonstrated, an extrapolation procedure was employed (see below) and the reproducibility of the extrapolated osmotic pressure was estimated to be  $\pm 0.1$  cm of solvent. The limits of error of the  $M_n$  value for non-permeating micellar systems were estimated as  $\pm 3\%$ .

**Measurement of the Membrane Partition Coefficient.** The partition coefficient  $\gamma$  of the micelles between the membrane and the solution was determined by a comparison of the diffusion and dialysis coefficients of the

(2) H. Coll, *J. Phys. Chem.*, **74**, 520 (1970).

(3) H. Coll, *J. Amer. Oil Chem. Soc.*, **46**, 593 (1969).

(4) P. H. Elworthy and C. B. Macfarlane, *J. Chem. Soc.*, 537 (1962).

(5) S. Siggia, A. C. Starke, J. J. Garis, and C. R. Stahl, *Anal. Chem.*, **30**, 115 (1958).

(6) B. A. Mulley in "Nonionic Surfactants," M. J. Schick, Ed., Marcel Dekker, New York, N. Y., 1967, p 428.

(7) J. E. Carless, R. A. Challis, and B. A. Mulley, *J. Colloid Sci.*, **19**, 201 (1964).

(8) J. M. Corkill, J. F. Goodman, and R. H. Ottewill, *Trans. Faraday Soc.*, **57**, 1627 (1961).

(9) R. S. Shelton, M. G. Van Campen, C. H. Tilford, H. C. Lang, L. Nisonger, F. J. Bandelin, and H. L. Rubenkoenig, *J. Amer. Chem. Soc.*, **68**, 753 (1946).

micelles<sup>10</sup> and was used as a measure of the permeability of the membrane to the micellar species. The diffusion measurements were carried out using the porous plate technique.<sup>11</sup> The two halves of the diffusion cell were separated initially by a 16- $\mu$  Sartorius filter which was completely permeable ( $\gamma = 1$ ) to the ions of the calibrating solute (potassium chloride) and to the micelles of the surfactant under investigation. Stirring of the cell was effected by its eccentric motion as proposed by Hartley and Runnicles.<sup>12</sup> The concentrations of KCl and of the surfactant in the two cell compartments after diffusion were determined by conductivity and refractive index measurements, respectively, and the rate constants for the diffusion of KCl, ( $K_{p\text{KCl}}$ ), and surfactant, ( $K_p$ ), were calculated from

$$K_p = (2.303/t) \log c_0/(c_1 - c_2) \quad (1)$$

where  $c_0$  is the initial concentration of solution, and  $c_1$  and  $c_2$  are the solute concentrations in the sample and solvent compartments, respectively, after diffusion for a time,  $t$ . The Sartorius filter was replaced by the osmometer membrane, and dialysis measurements were carried out in a similar manner. The partition coefficient was calculated, assuming the membrane to be completely permeable to KCl, from

$$(K_{p\text{KCl}}/K_p)_{\text{Sartorius}} = \gamma(K_{p\text{KCl}}/K_p)_{\text{membrane}} \quad (2)$$

The value of  $\gamma$  calculated from eq 2 is a weight-average rather than a number-average value and this may give rise to error in the  $M_n$  values determined for the permeating systems, although this error will not be excessive unless there is a significant polydispersity of micellar size. Since it was not practical to use the same membrane in the osmometer as that used in the determination of  $\gamma$ , possible variations of permeability throughout a batch of membranes were investigated. Repeated determinations of  $K_p$  for a solution of given concentration using a series of different membranes yielded a reproducibility to within  $\pm 2.7\%$  which indicates a reasonable degree of uniformity of the membranes. In systems where a dependence of  $\gamma$  on surfactant concentration was evident, the required values of  $\gamma$  were interpolated from graphs of  $\gamma$  vs. concentration.

**Light Scattering.** The construction and calibration of the light-scattering apparatus have been described previously.<sup>13</sup> Temperature control was to  $\pm 0.1^\circ$  and measurements were made at a wavelength of 4358 Å. The surfactant solutions were clarified by ultrafiltration through 0.22- $\mu$  Millipore filters and the concentration of each solution after filtration was determined using a Hilger-Rayleigh interference refractometer. Symmetrical scattering envelopes were obtained for all solutions and  $M_w$  was calculated from the intercept of plots of  $K(c - \text{cmc})/\Delta R_{90}$  against  $(c - \text{cmc})$  where  $c$  is concentration of surfactant in g/ml,  $\Delta R_{90}$  is the scattering at  $90^\circ$  to the incident beam in excess of that from a

solution at the cmc, and  $K$  is the usual optical constant. For systems in which the light-scattering graphs showed a pronounced upward curvature at low concentrations,  $M_w$  was calculated from the horizontal portion of the graph as suggested previously.<sup>13</sup>

**Vapor Pressure Osmometry.** Measurements were carried out using a Hewlett-Packard 302 vapor pressure osmometer calibrated with aqueous sucrose solutions of known activity.  $M_n$  was calculated from the intercept of plots of  $\Delta R/c$  against  $c$  where  $\Delta R$  is the measured resistance difference in ohms.

## Results and Discussion

**Treatment of Osmotic Pressure Data.** Previous studies on Cetomacrogol 1000 have shown that in cases where the micelles are completely retained by the membrane, *i.e.*, where  $\gamma$  approaches zero ( $\gamma = 0.003$  for Cetomacrogol), the osmotic pressure reaches an equilibrium value after about 10 min and remains constant for several hours. The attainment of an osmotic pressure (constant for 1–2 hr) was consequently taken as the criterion for membrane impermeability. For such systems, the measured osmotic pressure,  $\pi$ , between a sample solution of concentration  $c$  g/l. and a solvent of concentration  $c'$  g/l. is given by<sup>2</sup>

$$\pi = RT(c - c')/M_n +$$

$$BRT[(c - c')^2 + 2(c - c')(c' - \text{cmc})] \quad (3)$$

where  $B$  is the second virial coefficient and  $RT$  has the usual meaning. Hence, plots of  $\pi/(c - c')$  against  $(c - c')$  were extrapolated to  $c = c'$  and  $M_n$  was calculated from the intercept which is given by

$$(\pi/c - c')_{c=c'} = RT/M_n + 2RTB(c' - \text{cmc}) \quad (4)$$

Values of  $8.7 \times 10^{-5}$  mol/l. and  $7.2 \times 10^{-5}$  mol/l. are quoted<sup>8</sup> for the cmc's of  $\text{C}_{12}\text{n}_6$  at 25 and  $35^\circ$ , respectively, values for the intermediate temperatures were obtained by interpolation. Cmc values for  $\text{C}_{16}\text{n}_9$  have not been reported for the temperature range involved in this investigation and calculations were carried out using the value of  $2.1 \times 10^{-6}$  mol/l. quoted<sup>14</sup> for  $25^\circ$ . The cmc of CTAB in 0.025  $N$  KBr at  $30^\circ$  is reported as being too low for accurate determination by light scattering.<sup>15</sup> Since in all the systems studied the correction term  $2RTB(c' - \text{cmc})$  had a negligible effect on the value of  $M_n$ , accurate values of the cmc's and the second virial coefficients are not essential.

(10) J. L. Gardon and S. G. Mason, *J. Polym. Sci.*, **26**, 255 (1957).

(11) R. H. Stokes, *J. Amer. Chem. Soc.*, **72**, 763 (1950).

(12) G. S. Hartley and D. F. Runnicles, *Proc. Roy. Soc., Ser. A*, **168**, 401 (1938).

(13) D. Attwood, *J. Phys. Chem.*, **72**, 339 (1968).

(14) P. H. Elworthy and C. B. Macfarlane, *J. Pharm. Pharmacol.*, **14**, 100T (1962).

(15) H. J. L. Trap and J. J. Hermans, *Proc. Kon. Ned. Akad. Wetensch.*, **58B**, 97 (1955).

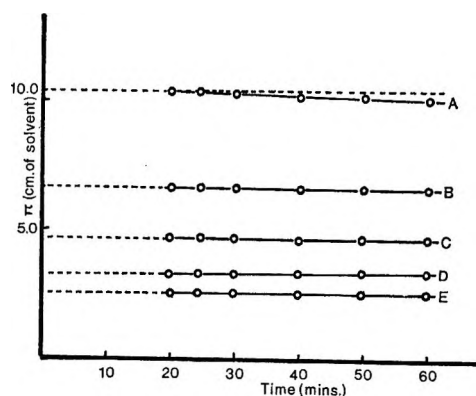


Figure 1. Change of osmotic pressure with time for  $C_{12}n_6$  (concentration = 43.90 g/l.) as a function of temperature, showing membrane permeability at 25°: A, 25°; B, 27.5°; C, 30°; D, 32.5°; E, 36°.

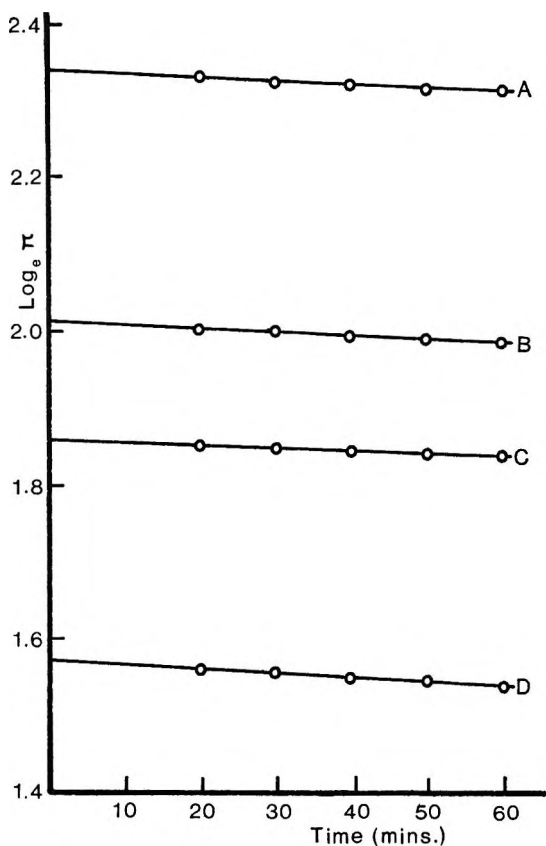


Figure 2. Decrease of  $\ln$  (osmotic pressure) with time for aqueous  $C_{12}n_6$  solutions at 25°: A, 58.46 g/l.; B, 43.90 g/l.; C, 38.12 g/l.; D, 20.72 g/l.

In systems where osmotic pressure failed to attain an equilibrium value, the data were plotted as graphs of  $\ln \pi$  against time and extrapolated to zero time to yield an apparent initial osmotic pressure,  $\pi_a$ . The true osmotic pressure,  $\pi_t$  was calculated using an equation derived by Gardon and Mason.<sup>10</sup>

$$\pi_t = \pi_a / [1 + K_p/K_s] \times [1 - \gamma - (K_p k \rho \bar{V}_p / K_s RT)] \quad (5)$$

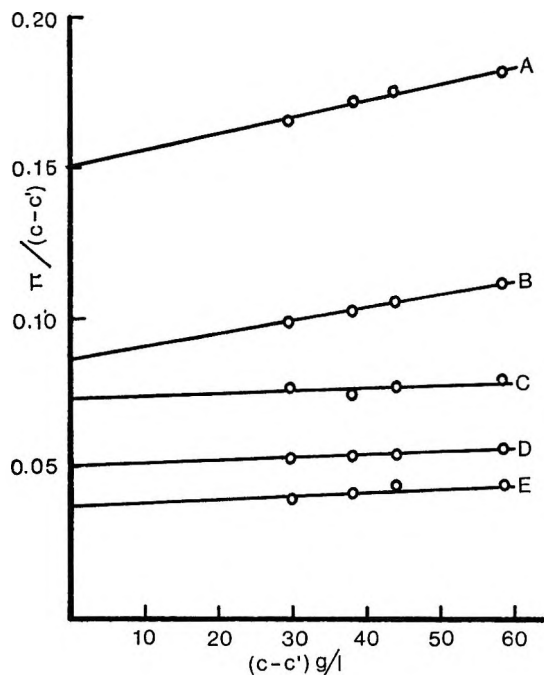


Figure 3. Variation of reduced osmotic pressure with concentration for  $C_{12}n_6$  at A, 25°; B, 27.5°; C, 30°; D, 32.5°; E, 36°.

$K_p$  and  $K_s$  are the rate constants for solute and solvent diffusion, respectively;  $\rho$  is the density of the manometer liquid;  $\bar{V}_p$  is the effective molar volume of the solute and  $k$  is an instrumental constant. Since  $K_s \gg K_p$  for all systems investigated here, eq 5 reduces to

$$\pi_t = \pi_a / (1 - \gamma) \quad (6)$$

Plots of  $\pi_t / (c - c')$  against  $(c - c')$  were extrapolated to  $c = c'$  and  $M_n$  calculated as described above.

As a test of the applicability of this treatment of the osmotic pressure data for permeating solutes, the method was applied in the determination of  $M_n$  of P.E.G. 6000. A mean value of 0.10 was determined for  $\gamma$  and an  $M_n$  of  $6.91 \times 10^3$  obtained, in reasonable agreement with the values obtained by vapor pressure osmometry ( $6.12 \times 10^3$ ) and by estimation of the ethylene oxide content ( $5.96 \times 10^3$ ).

*n*-Dodecyl Hexaoxyethylene Monoether ( $C_{12}n_6$ ). As seen from Figure 1, a constant osmotic pressure was not attained at 25° suggesting membrane permeation by the micellar species. This was in contrast to the results at higher temperatures where complete impermeability was demonstrated. Similar graphs were obtained for all other concentrations studied. The data at 25° were treated according to the method of Gardon and Mason. Values of  $\pi_a$  extrapolated from the linear plots of  $\ln \pi$  vs. time (Figure 2) were corrected using the partition coefficients given in Table I. Values of  $\pi$  were small, indicating only slight permeation of the membrane. The  $M_n$  values obtained by extrapolation of plots of  $\pi / (c - c')$  vs.  $(c - c')$  (Figure 3) are given in

**Table I:** Osmotic Pressure Data for  $C_{12}n_6$  in  $H_2O$  at  $25^\circ$ 

Concentration, g/l.	Partition coefficient, $\gamma$	Apparent osmotic pressure $\pi_a$ , cm of solvent	Corrected osmotic pressure $\pi_c$ , cm of solvent
58.46	0.022	10.35	10.58
43.90	0.020	7.47	7.62
38.12	0.020	6.40	6.53
29.72	0.016	4.82	4.90

**Table II:** Number-Average Micellar Weights and Second Virial Coefficients for  $C_{12}n_6$ ,  $C_{16}n_9$ , and CTAB

Surfactant	Temperature, $^\circ C$	$M_n \times 10^{-4}$	$B \times 10^4$ , ml-mol $g^{-1}$
$C_{12}n_6$	25	1.69	0.22
	27.5	2.47	0.14
	30	3.43	0.03
	32.5	4.89	0.03
	36	6.65	0.03
$C_{16}n_9$	35	1.39	1.25
	45	1.61	0.95
	50	4.88	0.01
	53.5	7.66	0.09
	CTAB in 0.025 N KBr	30	1.05

Table II and compared graphically in Figure 4 with  $M_n$  values from light scattering, including literature values.<sup>16</sup> At all temperatures, the osmotic micellar weights fall within the limits of error ( $\pm 10\%$ )<sup>17</sup> of those

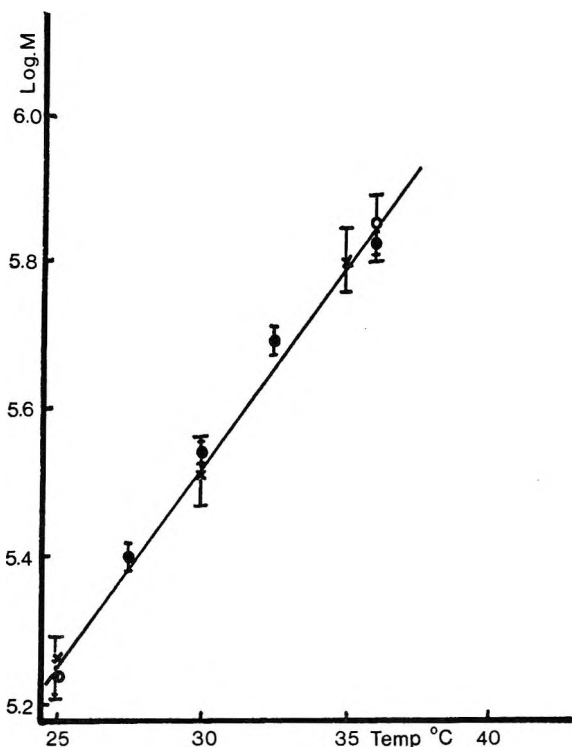


Figure 4. Log (micellar weight) against temperature for  $C_{12}n_6$ : ●,  $M_n$  by osmometry; ○,  $M_w$  by light scattering; ×,  $M_w$  results of Balmбра, *et al.*,<sup>16</sup> by light scattering.

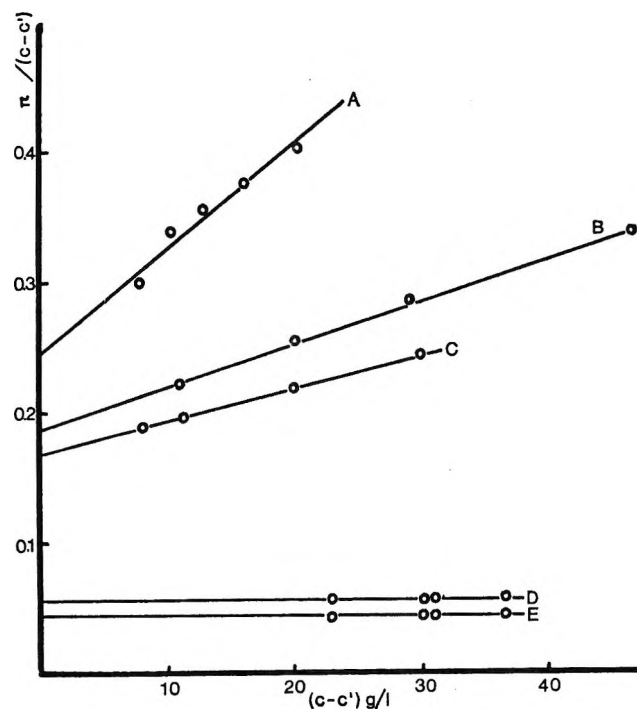


Figure 5. Variation of reduced osmotic pressure with concentration: A, CTAB in 0.025 N KBr at  $30^\circ$ ; B,  $C_{16}n_9$  at  $35^\circ$ ; C,  $45^\circ$ ; D,  $50^\circ$ ; E,  $53.5^\circ$ .

determined by light scattering. The mean  $M_w/M_n$  ratio over the temperature range studied is  $1.00 (\pm 0.13)$ , indicating that the micelles are monodisperse or have a very narrow range of sizes.

*n*-Hexadecyl Nonaoxyethylene Monoether ( $C_{16}n_9$ ). At all temperatures studied, equilibrium values of osmotic pressure were attained, indicating impermeability of the membrane to the micellar species.  $M_n$  values calculated from plots of  $\pi/(c - c')$  vs.  $(c - c')$  (Figure 5), are compared with weight-average values determined by light scattering and with literature values of  $M_w$ ,<sup>18</sup> in the form of a plot of  $\log M$  against temperature (Figure 6). The osmotic measurements indicate an abrupt change of slope of the plot in approximately the same temperature region as was reported from the light-scattering study of this compound. Below this threshold temperature,  $T_h$ , the  $M_n$  values were lower than the corresponding  $M_w$  values but within the combined limits of error of the two techniques. The mean  $M_w/M_n$  ratio was  $1.10 (\pm 0.14)$  for this temperature region. The results obtained at temperatures exceeding  $T_h$  are anomalous, the  $M_n$  values being 20–30% higher than the values from light scattering. This is probably attributable to the very pronounced temperature dependence of the micellar weight in this region; a dif-

(16) R. R. Balmбра, J. S. Clunie, J. M. Corkill, and J. F. Goodman, *Trans. Faraday Soc.*, **58**, 1661 (1962).

(17) J. N. Phillips and K. J. Mysels, *J. Phys. Chem.*, **59**, 325 (1955).

(18) P. H. Elworthy and C. McDonald, *Kolloid-Z. Z. Polym.*, **195**, 16 (1964).

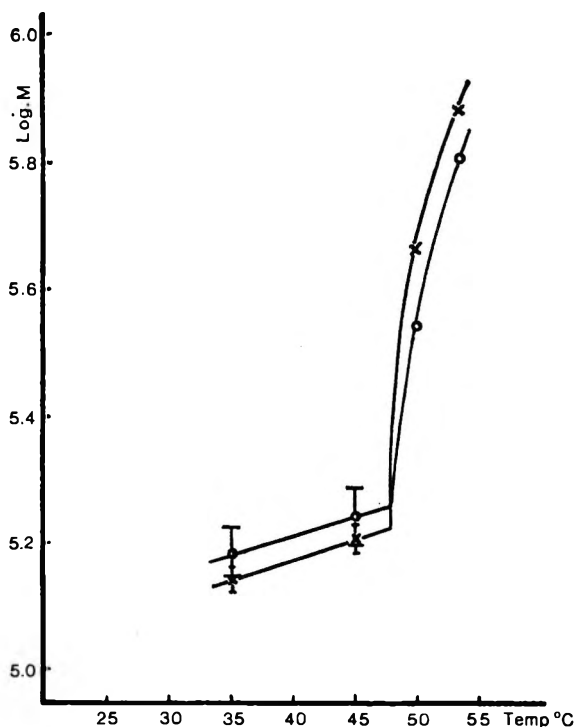


Figure 6. Log (micellar weight) against temperature for  $C_{16}n_3$ :  $\times$ ,  $M_n$  by osmometry;  $\bullet$ ,  $M_w$  by light scattering;  $\circ$ ,  $M_w$  results of Elworthy and McDonald<sup>18</sup> by light scattering. Limits of error are uncertain for measurements at temperatures  $>45^\circ$ .

ference of approximately  $1^\circ$  in the temperatures of measurement of  $M_w$  and  $M_n$  would account for the observed discrepancy in these values. Errors in  $M_n$  may also arise due to nonideality, since solutions of a high concentration were required to produce osmotic pressures of a reasonable magnitude because of the high micellar weights involved at these temperatures. Table II indicates a decrease in the values of  $B$  with increase of temperature which is particularly pronounced as the threshold temperature is exceeded. This is in agreement with the light-scattering results of Elworthy and McDonald,<sup>18</sup> although these workers reported negative values of  $B$  above  $T_h$  which were not detected here.

*N-Cetyltrimethylammonium Bromide (CTAB)*. Osmotic pressure measurements were made at  $30^\circ$  and for each concentration, equilibrium values were rapidly attained showing that Donnan equilibrium conditions had been established. The reduced osmotic pressure *vs.* concentration graph (Figure 5) extrapolated to an  $M_n$  value of  $10.5 \times 10^4$  which is within the limits of error of the quoted<sup>15</sup>  $M_w$  of  $9.84 \times 10^4$ , both values referring to CTAB in  $0.025 N$  KBr. Hence there is no evidence of any significant polydispersity of micellar size in this system.

*Acknowledgment.* The authors wish to thank the Science Research Council for the award of a Research Studentship to S. B. K.

# Linear Enthalpy-Spectral Shift Correlations

## for 2,2,2-Trifluoroethanol

by A. D. Sherry and K. F. Purcell\*

Department of Chemistry, Kansas State University, Manhattan, Kansas 66502 (Received January 22, 1970)

A new calorimeter design is presented and calorimetric enthalpy data are reported for the acid-base interaction of 2,2,2-trifluoroethanol with a variety of Lewis bases. The following correlations are found:  $\Delta H(\pm 0.13) = 0.0121\Delta\nu + 2.70$  and  $\Delta H(\pm 0.26) = 0.98\Delta + 2.30$ . These correlations are compared with the similar data for phenol and 1,1,1,3,3,3-hexafluoro-2-propanol to reveal the relative abilities of the phenyl, trifluoroethyl, and hexafluoroisopropyl substituents to withdraw electron density from OH and to characterize their role in hydrogen bond formation. Other correlations such as  $\Delta H$  vs.  $\Delta H$  are instrumental in this regard as they give meaning to the  $\Delta H$  vs.  $\Delta\nu$  correlations. All correlations can be interpreted within the framework of the Lippincott-Schroeder model of hydrogen bond formation. The data adhere nicely to a double-scale enthalpy ( $E$  and  $C$ ) relation; in addition, a single-scale enthalpy relation ( $\Delta H = \alpha\beta_B$ ) is established which reveals substituent inductive effects and, in the cases of phenol and di-*t*-butylcarbinol, resonance and steric effects, respectively.

### Introduction

Linear enthalpy-spectroscopic shift relationships have been reported for phenol<sup>1</sup> and 1,1,1,3,3,3-hexafluoro-2-propanol (HFIP).<sup>2</sup> Comparison of the slopes and intercepts of the linear  $\Delta H$  vs.  $\Delta\nu$  and  $\Delta$  relations suggested that enhanced alcohol acidity leads to increased slope and intercept. Comparison<sup>3</sup> of the spectroscopic data for phenol and 2,2,2-trifluoroethanol (TFE) indicated that phenyl and trifluoroethyl are very similar in their roles in the control of the OH group upon formation of a hydrogen bond. To test these early conclusions, as well as to obtain more information about the factors involved in formation of a hydrogen bond, a calorimetric determination of the enthalpies of hydrogen bond formation between TFE and various donors was undertaken.

In this report, we present a much less expensive calorimeter design than has been used previously<sup>2</sup> and report calorimetric data for the reaction of TFE with various oxygen and nitrogen donors.

### Experimental Section

**Chemicals.** Fisher Analytical Reagent Grade ethyl acetate, acetone, and pyridine were freshly distilled before use from BaO; bp: ethyl acetate, 76.0°; acetone, 55.0°; pyridine, 114.6°. Fisher Analytical Reagent Grade dimethyl sulfoxide and dimethylacetamide were stored over barium oxide for several days and purified by vacuum distillation. Fisher Analytical Reagent Grade acetonitrile was distilled twice from P<sub>2</sub>O<sub>5</sub> and once from BaO, bp 81.2°. Baker ethyl ether was stored 2 days over CaH<sub>2</sub> and freshly distilled from CaH<sub>2</sub>, bp 33.0°. Eastman White Label triethylamine was distilled once from acetic anhydride and once from barium oxide, bp 88.2°. Mallinckrodt Analytical Reagent carbon tetrachloride and Fisher Certified ACS

hexane were thoroughly dried over Linde 4A molecular sieves. Mallinckrodt Analytical Reagent potassium chloride was dried at 130° for 1 week before use and Baker Analytical Reagent sulfuric acid was used without further purification. 2,2,2-Trifluoroethanol was purchased from Columbia Organics and purified by distillation through a 52-theoretical plate spinning band column, bp 73.5–74.0°.

**Calorimetry.** The major calorimeter components are outlined in the block diagram shown in Figure 1. The component box contains two constant-voltage power supplies; one powers the calorimeter calibration heater (located in the Dewar) and the other powers the thermistor bridge. The calibration heater power supply output was found to be constant at 10.66 V over a period of 1 year. The details of the wiring are presented in Figure 2. The use of the constant-voltage source eliminates the need for a standard resistor and a potentiometer. A Heath (Model EUW-20A) recorder is used in our system with the recorder slide wire connected in parallel with the thermistor bridge. This change in bridge design eliminates the more expensive thermistor bridge and recorder used before.<sup>2</sup>

The calorimeter vessel is a standard 265-ml silvered Dewar flask. A Teflon cap is used as a cover for the Dewar flask and supports the heater, thermistor, and sample injection device. The calorimeter heater is made by coiling no. 36 manganin wire (ca. 120 ohms) and placing it inside an nmr tube with mineral oil.

\* To whom correspondence should be addressed.

(1) T. D. Epley and R. S. Drago, *J. Amer. Chem. Soc.*, **89**, 5770 (1967).

(2) K. F. Purcell, J. A. Stikeleather, and S. D. Brunk, *ibid.*, **91**, 4019 (1969).

(3) K. F. Purcell and S. T. Wilson, *J. Mol. Spectrosc.*, **24**, 468 (1967).

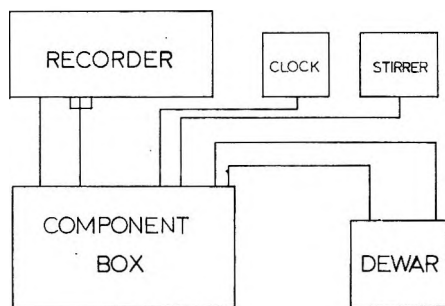


Figure 1. Box diagram of calorimeter system.

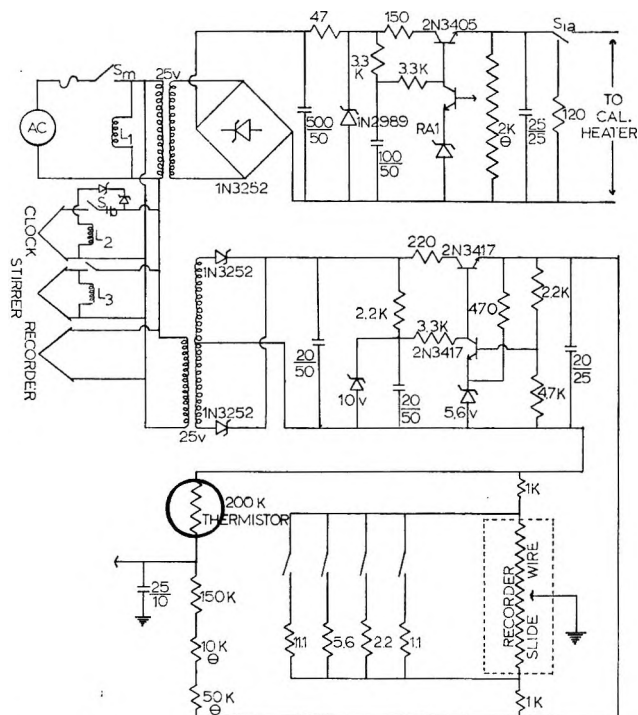


Figure 2. Wiring diagram of calorimeter.

The resistance of the heater (after aging in an oven) is periodically checked for resistance change. The temperature-sensing element is a Fenwal No. GA 52P2 thermistor with a resistance of 200 K. The thermistor is also placed inside an nmr tube containing a few drops of mineral oil to establish good thermal contact of the thermistor bead with the nmr tube wall. The nmr tube provides a stationary support for the thermistor while assuring that the thermistor is located near the vertical center of the calorimeter fluid. We found that the thin-walled nmr tube did not appreciably affect the sensitivity of the thermistor. The stirrer is similar to that used before<sup>2</sup> and the clock, purchased from Precision Scientific Co. (No. 69230), is accurate to  $\pm 0.1$  sec. A 100- $\mu$ l gas-tight Hamilton syringe (No. 1710-NC) is used to introduce all liquid samples into the reaction flask. The Chaney adaptor is set to deliver a calibrated weight of TFE which is known to within 0.5%. Solid samples are added to the reaction flask by means of glass bulbs blown from 8-mm Pyrex tubing. The general procedure used in the acid-base reaction

measurements was to inject TFE into a 200-ml solution of a base which was prepared by accurately weighing the base into a 200-ml volumetric flask and filling to the mark with solvent. The solutions were emptied into a Dewar flask and allowed to come to thermal equilibrium under stirring. At this point, the recorder pen traces a linear base line, which slopes slightly in the exothermic direction due to the heat of stirring (we found it unnecessary to use a base-line compensator). The calibration heater and clock are simultaneously activated with one switch ( $S_1$  of Figure 2). In this way, the calorimeter and its contents were calibrated before and after each of several additions of TFE to the same base solution. The techniques are the same as were used in the earlier study of hexafluoroisopropanol.<sup>2</sup>

**Infrared Spectral Measurements.** The infrared spectra in the OH region were obtained with a Perkin-Elmer 457 grating infrared spectrophotometer. The experimental procedures were similar to those used in the previous study<sup>3</sup> except a 2.5 $\times$  expanded scale was used and no solvent was placed in the reference beam. Using this technique, we were able to reproduce the reported shifts<sup>3</sup> within  $\pm 10$   $\text{cm}^{-1}$ .

**Least-Squares Treatment of Data.** The statistical analyses of the enthalpy and spectroscopic data given in this report were performed on the IBM 360/50 machine at this university. The programs are local, and in addition to calculating the least-squares slopes and intercepts, output the standard error of estimate at the 95% confidence level, the standard error in slope, and the standard error in intercept. (The equations for these quantities were taken from L. G. Parratt, "Probability and Experimental Errors in Science," John Wiley and Sons, Inc., New York, N. Y., 1961, p 127 ff.)

## Results

To test the accuracy of the calorimeter system and the associated techniques, the heat of solution of KCl in water and the partial molal heats of solution of  $\text{H}_2\text{SO}_4$  in water were determined. The results are shown in Tables I<sup>4</sup> and II.<sup>5</sup> The heats of solution of TFE in

Table I: Heat of Solution of KCl<sup>a</sup>

Wt of KCl, g	Vol of H <sub>2</sub> O, ml	Q, cal	$\Delta H$ , kcal/mo
0.2038	200	11.402	4.16
0.1179	200	6.583	4.17
0.1123	200	6.303	4.17
0.1614	200	8.928	4.13
0.2006	200	11.486	4.26
			$\bar{A}_v = 4.19$
			Std error = 0.05

<sup>a</sup> Literature value ( $\Delta H = 4.185 \pm 0.001$ ), ref 4.

(4) G. Sompsen, J. Coops, and M. W. Tolk, *Recl. Trav. Chim.*, **32**, 321 (1963).

(5) National Bureau of Standards Circular No. 500, U. S. Government Printing Office, Washington, D. C., Part 1, 1961, p 41.

**Table II:** Heat of Dilution of Sulfuric Acid in Water

Wt of H <sub>2</sub> SO <sub>4</sub> , g	Moles of H <sub>2</sub> O/moles of H <sub>2</sub> SO <sub>4</sub>		-ΔH <sub>f</sub> <sup>a</sup> , kcal/mol		-ΔH <sub>dil</sub> , kcal/mol	
	Initial	Final	Initial	Final	Lit. <sup>a</sup>	This work
0.8662	6.456	2754.1	208.69	213.54	4.85	4.97
0.5579	6.456	4273.3	208.69	213.96	5.27	5.39
0.3690	4.141	5199.2	206.99	214.16	7.17	7.27
0.5121	4.141	3747.3	206.99	213.82	6.83	6.72
0.3489	2.906	4789.3	205.51	214.09	8.58	8.52
0.3532	2.906	4731.3	205.51	214.07	8.56	8.63
0.5929	1.426	2490.5	202.58	213.45	10.82	10.51
0.4000	1.426	3690.6	202.58	213.82	11.24	11.00

<sup>a</sup> Reference 5.

Std error = 0.16

**Table III:** Hydrogen-Bond Data for TFE

Donor	-ΔH, kcal/mol	K <sup>-1</sup> , mol/l. (24 ± 1°)	Δν <sup>-1</sup> , cm (±10 cm <sup>-1</sup> )	Δ, ppm <sup>a</sup>
1. Acetonitrile	4.35 ± 0.2	0.1809 ± 0.0040	130	2.16
2. Ethyl acetate	4.45 ± 0.2	0.1441 ± 0.0008	150	...
3. Acetone	5.05 ± 0.2	0.1366 ± 0.0008	201	2.62
4. Diethyl ether	5.10 ± 0.2	0.1928 ± 0.0010	232	3.30
5. N,N-Dimethylformamide	6.10 ± 0.2	0.0244 ± 0.0007	262	...
6. Dimethyl sulfoxide	6.25 ± 0.2	0.0071 ± 0.0005	303	...
7. N,N-Dimethylacetamide	6.37 ± 0.2	0.0142 ± 0.0006	283	3.79
8. Hexamethylphosphoramide	7.67 ± 0.2	0.0032 ± 0.0004	405 <sup>c</sup>	...
9. Pyridine <sup>b</sup>	7.82 ± 0.2	0.0170 ± 0.0027	428	5.52
10. 2,4,6-Trimethylpyridine <sup>b</sup>	8.80 ± 0.2	0.0095 ± 0.0006	503 <sup>c</sup>	...
11. Triethylamine <sup>b</sup>	8.82 ± 0.2	0.0140 ± 0.0005	513	6.74

<sup>a</sup> Reference 3. <sup>b</sup> Using hexane as solvent. <sup>c</sup> This work.

CCl<sub>4</sub> and hexane were determined as a function of alcohol concentration. These values were found to be constant (5.16 ± 0.01 kcal mol<sup>-1</sup> and 6.08 ± 0.03 kcal mol<sup>-1</sup>, respectively) over a concentration range of 0.003 to 0.018 M in TFE. Above this concentration, the heat of solution tends to decrease due to alcohol association.

The workup of the raw calorimetric data into ΔH's for the acid-base reactions was performed in the manner used in the hexafluoroisopropanol report.<sup>2</sup> The results are presented in Table III. The *precision* estimates on K<sup>-1</sup> are those which result from the sharpness of fit criterion while those on ΔH are, by the same criterion, much less than 0.1. We have chosen to report ±0.2 limits on the latter as more realistic estimates of the *accuracy* since the standard errors for the calibration tests are 0.05 for KCl and 0.16 for H<sub>2</sub>SO<sub>4</sub>. The value for H<sub>2</sub>SO<sub>4</sub> is larger probably because of greater handling of those solutions, errors in measuring (pycnometrically) the H<sub>2</sub>SO<sub>4</sub> concentrations, and errors in interpolating NBS literature values from smoothed curves.

### Discussion

As shown in Figures 3 and 4, the enthalpy data for 2,2,2-trifluoroethanol (TFE) generate linear relations

with the frequency shifts and the chemical shifts. The equations for these lines, with the standard error of estimate at the 95% confidence level, are

$$\Delta H_T (\pm 0.1) = 0.0121 (\pm 0.0005) \times \Delta \nu_T + 2.7 (\pm 0.2) \quad (1)$$

$$\Delta H_T (\pm 0.3) = 0.98 (\pm 0.06) \Delta_T + 2.3 (\pm 0.3) \quad (2)$$

It is apparent that curvature in ΔH vs. Δν and vs. Δ is called for below ΔH ~ 3 kcal.

It was predicted, from consideration of linear Δ<sub>TFE</sub> vs. Δ<sub>PhOH</sub> and Δ<sub>νTFE</sub> vs. Δ<sub>νPhOH</sub> relationships, in an earlier paper<sup>3</sup> in this series that the bond "making and breaking" processes for TFE and phenol are quite similar. It might be expected, then, that the ΔH vs. Δν relationships for these two alcohols would be closely the same. This expectation seemed to be reinforced when data for 1,1,1,3,3,3-hexafluoro-2-propanol (HFIP) became available<sup>2</sup> and a much different ΔH vs. Δν relationship was found for this alcohol than had been reported for phenol. The corresponding ΔH vs. Δν equation for phenol (calculated from data in ref 1) is

$$\Delta H_P (\pm 0.3) = 0.0111 (\pm 0.0007) \times \Delta \nu_P + 2.8 (\pm 0.3) \quad (3)$$

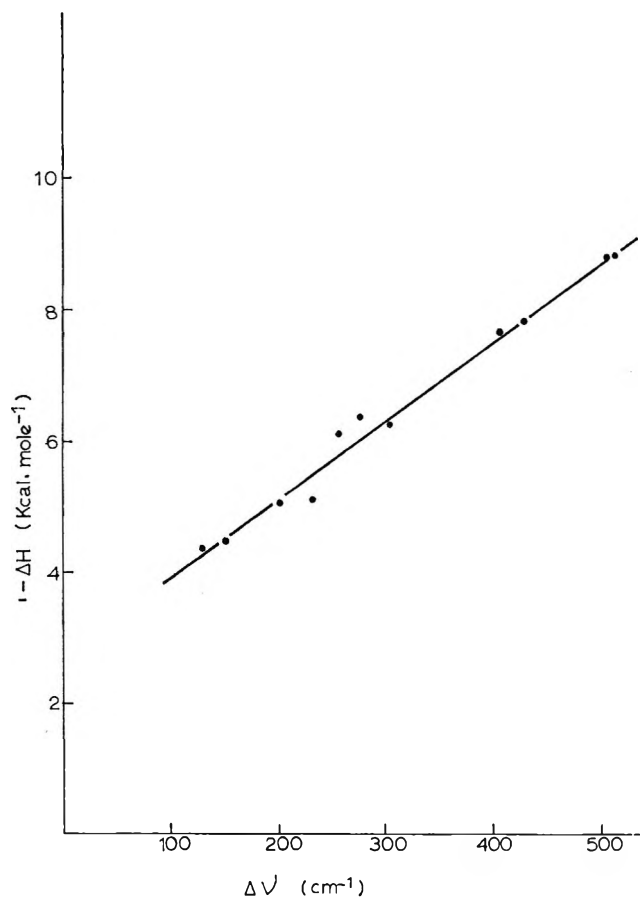


Figure 3. Enthalpy vs. frequency shift for TFE.

Comparing eq 1 and 3 we see that they are not greatly different. The intercepts of these relations are obviously indistinguishable.

The standard errors in the slopes of eq 1 and 3 are 4% (0.0005) and 6% (0.0007), respectively, so it appears that the 9% larger slope for the TFE relation is also barely significant. Nevertheless, the expectation<sup>2</sup> of a correlation of slope with acidity is not borne out since the slope of the HFIP relation, *cf.* (10), is intermediate but indistinguishable from those of phenol and TFE. In order to clarify the lack of correlation between acidity and  $\Delta H$ ,  $\Delta\nu$  slope we find it expedient to compare enthalpies with enthalpies and frequency shifts with frequency shifts. In doing this, we seek to establish quantitative relationships between experimental data for different acids which may then be related to the role of the substituent in the OH hydrogen bond reaction. It will be shown that  $\Delta H$  vs.  $\Delta\nu$  plots are not the most suitable relationships to use in achieving this goal.

As was done earlier,<sup>2,6</sup> we will assume a model<sup>7</sup> by which the energy of adduct formation may be partitioned into three terms

$$\Delta H = E_{\text{HB}} + \delta E_{\text{OH}} + V_{\text{OB}}$$

where  $E_{\text{HB}}$  = exothermic HB bond formation plus exothermic lowering of OB coulombic repulsions as a result

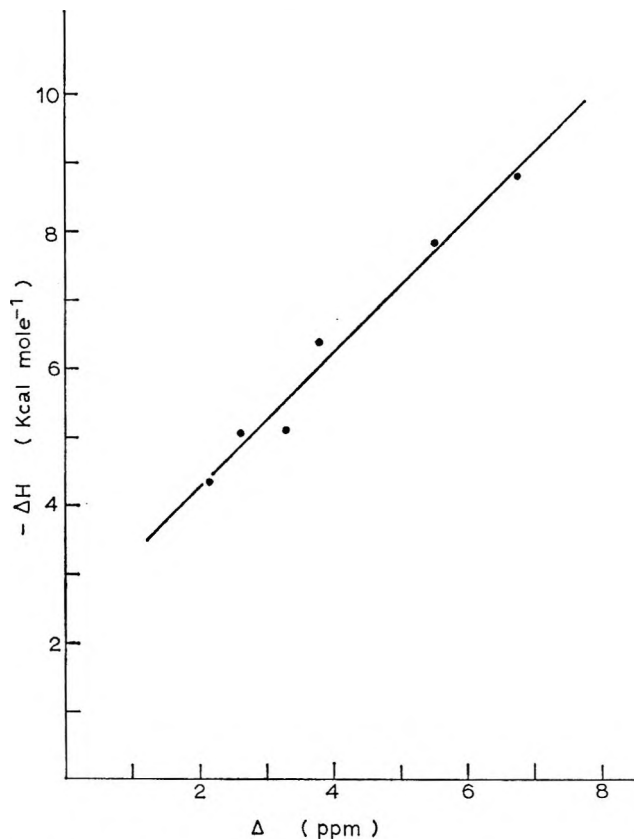


Figure 4. Enthalpy vs. chemical shift for TFE.

of B to OH charge transfer,  $\delta E_{\text{OH}}$  = endothermic OH bond breaking, and  $V_{\text{OB}}$  = endothermic OB van der Waals repulsions.

The role of  $(\delta E_{\text{OH}} + V_{\text{OB}})$  (endothermic terms) is to moderate the donor-acceptor interaction. To make comparisons of alcohols, we can adopt the procedure<sup>2</sup> used in comparing HFIP and PhOH or use the following equivalent technique. The two procedures are not of equal complexity, however.

*Slopes of the Linear Relationships.* To compare TFE with phenol we plot the enthalpies of these two acids vs. the enthalpies of a third reference acid (HFIP). The following equations are found in which unsigned values of the experimental quantities are used, as they are throughout this report.

$$\Delta H_T (\pm 0.1) = 0.86 (\pm 0.03) \times \Delta H_{\text{ref}} - 0.9 (\pm 0.3) \quad (4)$$

$$\Delta H_P (\pm 0.2) = 0.85 (\pm 0.04) \times \Delta H_{\text{ref}} - 0.6 (\pm 0.3) \quad (5)$$

With  $\Delta H$  as the measure of alcohol acidity, TFE and PhOH are seen to be quite similar acids. There is <2% difference in the slopes of (4) and (5) and the

(6) K. F. Purcell and R. S. Drago, *J. Amer. Chem. Soc.*, **89**, 2874 (1967).

(7) E. R. Lippincott and R. Schroeder, *J. Chem. Phys.*, **23**, 1099 (1955).

intercept difference is experimentally, but not statistically, significant. That is, the corresponding  $\Delta H$ 's for PhOH are consistently about 0.2 kcal/mol larger than those for TFE. (The negative intercepts mean HFIP is a stronger acid than either TFE or PhOH). For a unit change in  $\Delta H_{ref}$ , over the range of donor strength covered by our data, the change in  $\Delta H_P$ , 0.85, is indistinguishable from the change in  $\Delta H_{TFE}$ , 0.86. This implies that  $(\delta E_{OH} + V_{OB})$  moderates  $E_{HB}$  equally well for TFE and phenol. That is,  $\delta[E_{HB}^P - E_{HB}^T] = [(\delta E_{OH}^P + V_{OB}^P) - (\delta E_{OH}^T + V_{OB}^T)]$  where all quantities are treated as positive. To compare frequency shifts and chemical shifts, we have made direct plots and have found

$$\Delta\nu_T (\pm 11) = 0.79 (\pm 0.04) \Delta\nu_{ref} - 36 (\pm 16) \quad (6)$$

$$\Delta\nu_P (\pm 8) = 0.89 (\pm 0.03) \Delta\nu_{ref} - 41 (\pm 11) \quad (7)$$

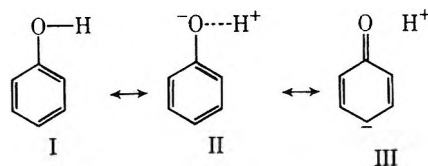
$$\Delta\tau (\pm 0.1) = 0.73 (\pm 0.02) \Delta\tau_{ref} + 0.1 (\pm 0.1) \quad (8)$$

$$\Delta\rho (\pm 0.2) = 0.74 (\pm 0.04) \Delta\rho_{ref} + 0.5 (\pm 0.2) \quad (9)$$

The slopes of the frequency shift relations show that for a given change in  $\Delta\nu_{ref}$ , the  $\Delta\nu$  change will be clearly larger for phenol than TFE. Thus, we find the slopes of eq 1 and 3 to be internally consistent with (4)–(7). Knowing that the changes in  $\Delta H$  with donor strength for these two acids are nearly the same while  $\Delta\nu$  changes more rapidly for phenol than TFE, we can understand why the  $\Delta H$  vs.  $\Delta\nu$  plot for phenol gives a smaller slope than the corresponding plot for TFE. For the slopes of the  $\Delta H$  vs.  $\Delta\nu$  plots to be equal, the ratio of the  $\Delta H$ ,  $\Delta H_r$  slope to that of  $\Delta\nu$ ,  $\Delta\nu_r$  must be the same for both acids; alternately, the ratio of their  $\Delta H$ ,  $\Delta H_r$  slopes must equal that of the  $\Delta\nu$ ,  $\Delta\nu_r$  slopes. The experimental slopes of the  $\Delta H$  vs.  $\Delta\nu$  plots are 0.0121 and 0.0111 for TFE and phenol, respectively. Thus, the  $\Delta H$ 's and  $\Delta\nu$ 's when used as indices of acid strength disagree, quantitatively, on the relative acidities of TFE and phenol (they are not of the same sensitivity to changes in donor strength). As discussed in the earlier report,<sup>3</sup> this difference in  $\Delta\nu$ 's, when converted to  $\delta E_{OH}$ 's, may not stand in disagreement with the  $\Delta H$ 's on relative acidities. In other words, in deriving the  $\delta E_{OH}$ 's from the  $\Delta\nu$ 's, the mechanical anharmonicities are such that the  $\delta E_{OH}$ 's for phenol and TFE interacting with a common donor are essentially equal, in agreement with the  $\Delta H$ 's and  $\Delta$ 's. The slopes of the two chemical shift equations are equal (0.73 vs. 0.74); a plot of  $\Delta H$  vs.  $\Delta$  for these two acids should give very similar slopes. Experimentally, these slopes are found to be 0.98 for TFE and 0.96 for phenol.  $\Delta H$  and  $\Delta$  appear to be compatible indices of acidity.

To interpret these conclusions, we compare the trifluoroethyl and phenyl substituents with regard to their effect upon the OH group. As deduced from the intercepts (see later) in (4) and (5), we expect very similar ground-state acid dipoles for phenol and trifluoro-

ethanol. This means the ground state electronegativity of phenyl, due to the "sp<sup>2</sup>" character of C–O carbon atom of phenol and to the  $\pi$  system of the phenyl group which can act in a resonance capacity as indicated by structures I, II, and III, is very much like that of the trifluoroethyl group, which arises from an "sp<sup>3</sup>" carbon carrying a CF<sub>3</sub> substituent.



As the acid–base interaction increases with increasing donor strength, charge-transfer effects become more important for the two alcohols and the amount of charge transferred from the base to the acid will depend upon the ability of the substituent to synergistically withdraw charge from the OH group. Consequently, the substituent should play a synergic role in the hydrogen bonding process. Such a role of the substituent is analogous to the phenomenon of "variable" acid reorganization energies<sup>8</sup> which play a major part in adduct reactions of more conventional Lewis acids. Without data to examine, we *might* expect that phenyl, acting through both its  $\sigma$  and  $\pi$  systems, could perhaps relieve (*cf.* III) charge built up on the oxygen (*cf.* II) more easily than could trifluoroethyl, acting through its  $\sigma$  system. Consequent to this, we could predict greater OH bond breaking ( $\delta E_{OH}$ ) and HB bond making ( $E_{HB}$ ) for phenol. Furthermore, the expected greater ability of phenyl to remove charge density should also make the change in  $V_{OB}$  with donor strength somewhat less important for phenol than TFE. We would therefore be led to expect greater moderation of  $E_{HB}$  by  $(\delta E_{OH} + V_{OB})$  in TFE than in phenol reactions. The initial presumption of relative substituent effects would be clearly in error, however, since the enthalpy data show the relative dynamic leveling effects of  $(\delta E_{OH} + V_{OB})$  on  $E_{HB}$  to be quite similar for phenyl and trifluoroethyl.

The average ratio of enthalpies,  $\Delta H_{TFE}/\Delta H_P$ , is 0.96 ( $\pm 0.04$ )<sup>9</sup> as compared to the ratio of frequency shifts and chemical shifts of 0.93 ( $\pm 0.09$ ) and 0.95 ( $\pm 0.02$ ), respectively.<sup>10</sup> That all three values are  $< 1$  is consistent with the slightly reduced acidity of TFE. The errors associated with these least-squares slopes make it difficult to single out frequency shifts, as before, as

(8) D. G. Brown, R. S. Drago, and T. F. Bolles, *J. Amer. Chem. Soc.*, **90**, 5706 (1968).

(9) To calculate this ratio, a least-squares analysis was performed on a line constrained to pass through the origin of the  $\Delta H_T$  vs.  $\Delta H_P$  plot. If this constraint is not applied, the least-squares analysis shows the intercept of this plot is small (*cf.* eq 12); thus the  $\Delta H$  ratio includes a systematic variation arising from this small intercept but the error limits ( $\pm 0.04$ ) include this variation and show that the variation is of no real consequence for our purposes. Similar comments apply to the other enthalpy ratios.

(10) K. F. Purcell, J. A. Stikeleather, and S. D. Brunk, *J. Mol. Spectrosc.*, **32**, 202 (1969).

more markedly varying with substituent. However, that trend is still evident and is even more so in a comparison of HFIP with TFE.

If we change the OH substituent from trifluoroethyl to hexafluoroisopropyl we would expect to find differences which might be related, barring steric effects, only to the difference in ground state and "synergic" electronegativities of the two groups. The  $\Delta H$  vs.  $\Delta\nu$  and vs.  $\Delta$  relationships for HFIP with various oxygen and nitrogen donors have been reported.<sup>2</sup>

$$\Delta H_H (\pm 0.2) = 0.0114 (\pm 0.0008) \times \Delta\nu_H + 3.6 (\pm 0.3) \quad (10)$$

$$\Delta H_H (\pm 0.3) = 0.86 (\pm 0.05) \times \Delta_H + 3.6 (\pm 0.3) \quad (11)$$

The larger intercepts for the HFIP relations indicate a greater dipole-dipole attraction between HFIP and a weak base than between TFE and the same base. This is as expected, since the hexafluoroisopropyl group is considered to be more electron withdrawing than the trifluoroethyl group. Thus, for the series HFIP, TFE, phenol, the intercepts of the  $\Delta H$ ,  $\Delta\nu$  relations parallel the order of acid strengths as measured by  $\Delta H$ 's,  $\Delta\nu$ 's, and  $\Delta$ 's. To compare the acidities of the two aliphatic alcohols we have plotted enthalpies, frequency shifts, and chemical shifts of these alcohols vs. the same measure of hydrogen bond interaction for phenol as a reference acid. These equations are

$$\Delta H_T (\pm 0.2) = 0.98 (\pm 0.04) \times \Delta H_{\text{ref}} - 0.1 (\pm 0.3) \quad (12)$$

$$\Delta H_H (\pm 0.2) = 1.16 (\pm 0.05) \times \Delta H_{\text{ref}} + 0.8 (\pm 0.4) \quad (13)$$

$$\Delta\nu_T (\pm 16) = 0.90 (\pm 0.05) \Delta\nu_{\text{ref}} - 4 (\pm 16) \quad (14)$$

$$\Delta\nu_H (\pm 9) = 1.11 (\pm 0.04) \Delta\nu_{\text{ref}} + 48 (\pm 10) \quad (15)$$

$$\Delta_T (\pm 0.1) = 0.97 (\pm 0.03) \Delta_{\text{ref}} - 0.3 (\pm 0.1) \quad (16)$$

$$\Delta_H (\pm 0.3) = 1.33 (\pm 0.07) \Delta_{\text{ref}} - 0.5 (\pm 0.3) \quad (17)$$

Equations 12 and 13 indicate that for a unit change in  $\Delta H_{\text{ref}}$ , the change in  $\Delta H_{\text{HFIP}}$  (1.16) is greater than the change in  $\Delta H_{\text{TFE}}$  (0.98). Thus,  $(\delta E_{\text{OH}} + V_{\text{OB}})$  moderates  $E_{\text{HB}}$  greater for TFE than HFIP. Due to the greater electronegativity of the hexafluoroisopropyl group, we would again expect this group to be able to remove excess charge from the oxygen better than the trifluoroethyl group. This synergic effect would increase both the  $\delta E_{\text{OH}}$  and  $E_{\text{HB}}$  terms and reduce the importance of the  $V_{\text{OB}}$  term for HFIP relative to TFE. The enhanced moderation of  $E_{\text{HB}}$  by  $(\delta E_{\text{OH}} + V_{\text{OB}})$  for TFE, as is evident from a comparison of (12) and (13), can be related to the greater importance of van der Waals repulsions with that acid.

Similarly, in eq 14 and 15, we find a larger change in  $\Delta\nu_{\text{HFIP}}$  than in  $\Delta\nu_{\text{TFE}}$  for a given change in  $\Delta\nu_{\text{ref}}$ . Com-

paring the slopes of (12)–(15) we expect to find more closely similar slopes for the HFIP and TFE  $\Delta H$  vs.  $\Delta\nu$  relationships than for those of TFE and PhOH. That is, the ratio 1.16/0.98 is slightly less than 1.11/0.90 (the numbers are of the slopes of eq 12–15) and the  $\Delta H$  vs.  $\Delta\nu$  slope for HFIP is slightly less than that for TFE.

Comparing the chemical shifts (eq 16 and 17), we see that for a given change in  $\Delta_{\text{ref}}$ , the change in  $\Delta_{\text{HFIP}}$  will be larger than that of  $\Delta_{\text{TFE}}$ . The ratio of the slopes of the chemical shift equations for these acids is larger than the ratios of the slopes of the enthalpy equations. Thus, as in the  $\Delta H$  vs.  $\Delta\nu$  plots, we would predict a slightly smaller slope from a  $\Delta H_{\text{HFIP}}$  vs.  $\Delta_{\text{HFIP}}$  plot than from the corresponding TFE plot. Experimentally we find the slopes to be 0.98 for TFE and 0.86 for HFIP.

The average ratio<sup>9</sup> of enthalpies  $\Delta H_{\text{HFIP}}/\Delta H_{\text{TFE}}$ , is found to be 1.35 ( $\pm 0.06$ ) which can be compared to the ratio of frequency shifts and chemical shifts of 1.46 ( $\pm 0.06$ ) and 1.32 ( $\pm 0.04$ ), respectively.<sup>10</sup> As in the TFE-phenol comparison, the three ratios generally agree on the relative acidities of HFIP and TFE but we note that the  $\Delta\nu$  ratios are consistently different from the other two which agree closely.

*Intercepts of the Linear Relations.* In analyzing  $\Delta H$  vs.  $\Delta\nu$  (and  $\Delta$ ) plots for a given acid, we have already advanced<sup>2,10</sup> a reason for the curvature as  $\Delta H$  and  $\Delta\nu$  (and  $\Delta$ ) increase from zero. The argument is based on the Lippincott-Schroeder model<sup>7</sup> and reveals the importance of van der Waals repulsions in the hydrogen bond energy. A similar analysis may be applied to a  $\Delta H_{\text{HFIP}}$  vs.  $\Delta H_{\text{TFE}}$  plot (or any other pair from the set HFIP, TFE, phenol), from which it is also concluded that van der Waals repulsions appear to be more important to  $\Delta H_{\text{HFIP}}$  than to  $\Delta H_{\text{TFE}}$ . This conclusion seems to be at odds with that given above from consideration of slopes. The apparent discrepancy results, however, from a subtle change in reference from which the moderation effect is measured.

In analyzing a plot such as  $\Delta H$  vs.  $\Delta H$  we note that as the  $\Delta H$ 's increase from zero, those of one acid are larger than those of the other, but that the disparity (ratio) gradually decreases with increasing acid-base interaction. The slope of the full curve decreases, with increasing interaction, to the constant value of the linear region. The Lippincott-Schroeder model suggests that the data in the region below the linear one arise from O-H...B attraction before appreciable charge transfer sets in; *i.e.*, the attraction is of a much more dipolar nature than covalent. Convincing evidence for this concept is provided by recent *ab initio* calculations on H<sub>2</sub>O linear dimers.<sup>11</sup> Another *ab initio* calculation<sup>12</sup> shows, *via* charge-density plots, the importance of  $R$  in ROH in assisting hydrogen bond forma-

(11) K. Morokuma and J. R. Winick, *J. Chem. Phys.*, **52**, 1301 (1970).

(12) P. A. Kollman and L. C. Allen, *ibid.*, **51**, 3286 (1969).

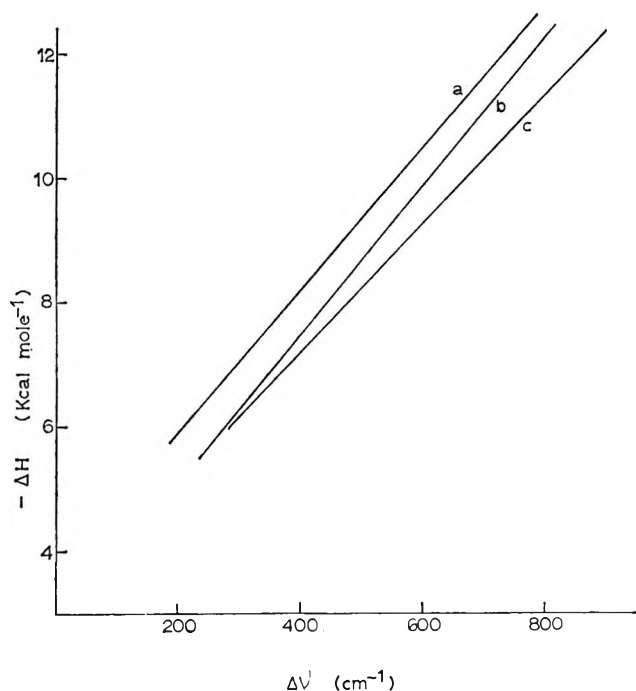


Figure 5. Enthalpy vs. frequency shift relations for: a, HFIP; b, TFE; c, phenol.

tion. According to the Lippincott-Schroeder model, a range of acid-base interaction is soon reached which is characterized by a more sharply increasing OH distance as  $R_{OB}$  is decreased and this is reflected in more sharply increasing  $\Delta H$  and  $\Delta\nu$ . This region corresponds to markedly enhanced charge transfer which is accompanied by increased  $O \cdots B$  repulsions (see also ref 11). In considering the full  $\Delta H$  vs.  $\Delta\nu$  curve we are, in effect, comparing these two regions for two different acids and, also, comparing their relative sharpnesses of transition from one region to the next. The fact that a plot of HFIP (ordinate) vs. TFE or PhOH (abscissa) has an intercept on the ordinate axis indicates that the greater electrostatic interaction for HFIP with very weak donors is not matched by a proportionately greater covalent interaction on passing from the weak donor region to the "strong" donor region, but since the slope  $> 1$ , still shows that the covalent energy, like the dipolar, is greater for HFIP. It is in this latter sense that van der Waals repulsions were claimed<sup>2</sup> to be greater in HFIP than in PhOH. This failure of the covalent contribution to maintain the acidity position, for strong donors, of HFIP over TFE or PhOH is borne out by the  $E_a$  and  $C_a$  numbers for these alcohols.<sup>13</sup> The  $E_a$  of HFIP is approximately 38% larger than that of TFE while the  $C_a$  is only 14% larger. Similarly, the  $E_a$ ,  $C_a$  values for PhOH and TFE are such as to be consistent with a small intercept and a slope  $\approx 1$  for a plot of

	$E_a$	$C_a$	$C/E$
HFIP	5.5	0.50	0.091
PhOH	4.4	0.41	0.093
TFE	4.0	0.44	0.11

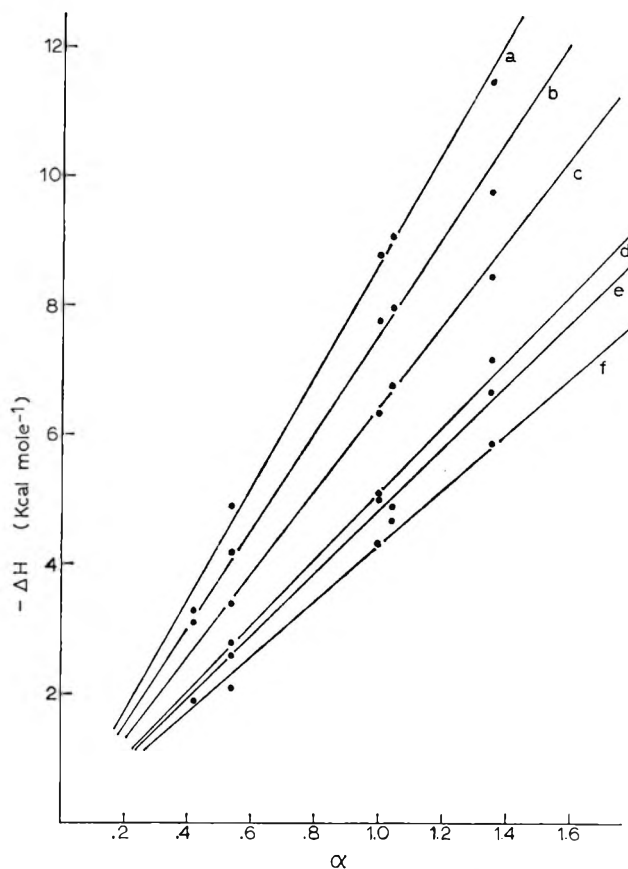


Figure 6. Enthalpy vs. hydrogen bonding constant ( $\alpha$ ) for the following bases: a, triethylamine; b, pyridine; c, *N,N*-dimethylacetamide; d, diethyl ether; e, acetone; f, acetonitrile.

$\Delta H_F$  vs.  $\Delta H_T$ . The greater the disparity in electrostatic and covalent energy contributions, the greater will be the intercept of the  $\Delta H$  vs.  $\Delta H$  plot. It is in this way that we are led to associate the intercept with relative "dipolar" acidity.

In summary, by comparing slopes and intercepts of  $\Delta H$  vs.  $\Delta\nu$  plots for these three acids (Figure 5), we find that the intercepts nicely follow the trend in hydrogen bond acidities,  $TFE \approx PhOH < HFIP$ . The trend in slopes seems confusing as they are in the relative order  $TFE \approx HFIP \approx PhOH$ . The important point is that the  $\Delta H$ ,  $\Delta\nu$  slopes do not necessarily reflect the order of acidities whereas those of the  $\Delta H$ ,  $\Delta H$  and  $\Delta\nu$ ,  $\Delta\nu$  plots do. Thus the slopes and intercepts of the latter plots agree on the acidity order  $HFIP > PhOH \sim TFE$ . The slopes of these plots, in turn, determine the slopes of the  $\Delta H$ ,  $\Delta\nu$  plots for each acid.

*Single-Scale Enthalpy Relationship.* We have found that the  $\Delta H$  ratios discussed earlier can be combined

(13) R. S. Drago and B. B. Wayland, *J. Amer. Chem. Soc.*, **87**, 3571 (1965). The fluoro acid  $E$  and  $C$  parameters in this paper have been calculated from our data by R. S. Drago's group. This was done to incorporate these acids into the general  $E$ ,  $C$  correlation for which they have extensive data. The standard errors of estimate of  $\Delta H$  calculated by  $-\Delta H = E_A E_B + C_A C_B$  are 0.2 for HFIP and 0.2 for TFE.

**Table IV:** The Calculated (from  $\Delta H = \alpha\beta_B$ ) and Measured Enthalpies of Hydrogen Bond Formation

	—HFIP $\alpha$ —		—PhOH $\alpha$ —		—TFE $\alpha = 1.00$ —		— <i>t</i> -BuOH $\alpha$ —		—DTBC $\alpha$ —	
	Calcd	Exptl <sup>a</sup>	Calcd	Exptl <sup>b</sup>	Calcd	Exptl <sup>c</sup>	Calcd	Exptl <sup>d</sup>	Calcd	Exptl <sup>e</sup>
Acetonitrile	5.9	5.9	4.5	4.7	4.3	4.4	2.3	2.1	1.8	...
Acetone	6.6	6.7	5.1	4.9	4.9	5.1	2.6	2.6	2.1	1.9
(C <sub>2</sub> H <sub>5</sub> ) <sub>2</sub> O	6.9	7.2	5.4	...	5.1	5.1	2.8	2.8	2.2	1.9
DMA	8.8	8.5	6.7	6.8	6.5	6.4	3.5	3.4	2.7	3.1
Pyridine	10.3	9.8	7.9	8.0	7.6	7.8	4.1	4.2	3.2	3.3
(C <sub>2</sub> H <sub>5</sub> ) <sub>3</sub> N	11.8	11.5	9.1	9.1	8.7	8.8	4.7	4.9	3.7	...
Std error of estimate	0.3		0.1		0.1		0.1		0.3	

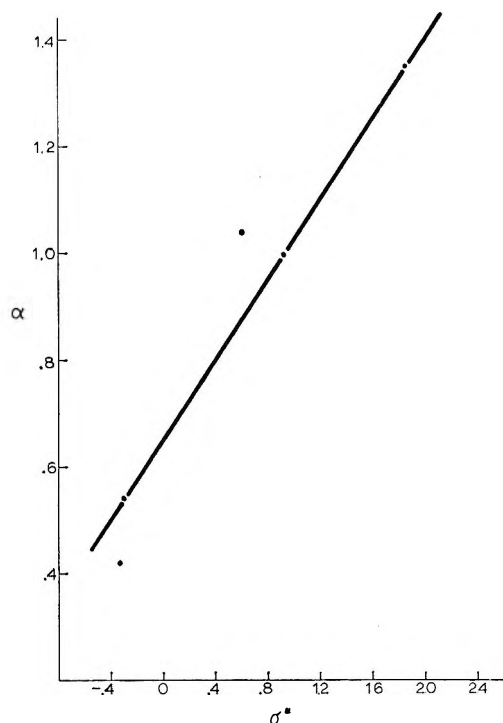
<sup>a</sup> Reference 2. <sup>b</sup> Reference 1. <sup>c</sup> This work. <sup>d</sup> Reference 15. Note: These enthalpies are not experimentally determined values but were determined using the equation  $-\Delta H = E_a E_b + C_a C_b$ . <sup>e</sup> Reference 11. There is a larger error (than the usual  $\pm 0.2$  kcal mol<sup>-1</sup>) associated with these experimental enthalpies and hence with the value of  $\alpha$ , due to small hydrogen bond enthalpies.

with those for di-*tert*-butylcarbinol<sup>14</sup> and *tert*-butyl alcohol<sup>15</sup> ( $\Delta H_{t\text{-BuOH}}/\Delta H_{\text{TFE}} = 0.54 (\pm 0.03)$  and  $\Delta H_{\text{DTBC}}/\Delta H_{\text{TFE}} = 0.42 (\pm 0.07)$ ) to establish a single-scale enthalpy relationship ( $\Delta H = \alpha_A \beta_B$ ) for hydrogen bonding acids. Taking TFE as the reference acid,  $\alpha_A = \Delta H_A/\Delta H_{\text{TFE}}$  and  $\beta_B = \Delta H_{\text{TFE}}$  with donor B. The  $\alpha_A$ 's are: HFIP = 1.35, phenol = 1.04, TFE = 1.00, *tert*-butyl alcohol = 0.54, and DTBC = 0.42. A plot of  $\Delta H$  vs.  $\alpha$  for the five alcohols and a series of six bases is shown in Figure 6. Good linearity is found with the slopes ( $\beta_B$ ) of the lines changing with the strength of the base. Tables IV and V present a summary of calculated and experimental values of  $\Delta H$ ,  $\alpha_A$ , and  $\beta_B$ . The standard error of estimate of all acids with all bases is 0.08 kcal/mol.

**Table V:** Calculated and Experimental Values of  $\beta_B$ 

Base, B	— $\beta_B$ , kcal/mol—		Std error
	Calcd	Exptl	
CH <sub>3</sub> CN	4.34	4.35	$\pm 0.24$
(CH <sub>3</sub> ) <sub>2</sub> CO	4.87	5.05	$\pm 0.20$
(C <sub>2</sub> H <sub>5</sub> ) <sub>2</sub> O	5.14	5.10	$\pm 0.14$
CH <sub>3</sub> C(O)N(CH <sub>3</sub> ) <sub>2</sub>	6.48	6.37	$\pm 0.16$
C <sub>6</sub> H <sub>5</sub> N	7.61	7.82	$\pm 0.24$
(C <sub>2</sub> H <sub>5</sub> ) <sub>3</sub> N	8.73	8.82	$\pm 0.24$

Taft polar substituent constants,  $\sigma^*$ , have been reported for trifluoroethyl (+0.92), *tert*-butyl (-0.30), and phenyl (+0.60).  $\sigma^*$  values can also be calculated<sup>16</sup> with accuracy for hexafluoroisopropyl (+1.84) and di-*tert*-butylmethyl (-0.33). As a check on the accuracy of the  $\sigma^*$  of HFIP, a plot of  $pK_a$  vs.  $\sigma^*$  for various acids of known  $\sigma^*$  has been made from which we estimate a value of 1.84. Figure 7 shows a plot of  $\alpha$  vs.  $\sigma^*$  for the five acids. This plot gives a straight line through the *tert*-butyl, trifluoroethyl, and hexafluoroisopropyl points with the points for phenol and di-*tert*-butylcarbinol falling off the line. Since  $\sigma^*$  includes only the polar or inductive effect of a substituent while  $\alpha$  should include polar, steric, and resonance effects, the

**Figure 7.** Hydrogen bonding constant ( $\alpha$ ) vs. Taft substituent parameters ( $\sigma^*$ ).

deviations of points for phenyl and di-*tert*-butylmethyl are not surprising. The deviation of 0.16 for phenyl reflects the  $\pi$  resonance enhancement of the acidity of the OH group. The deviation of 0.10 for di-*tert*-butylmethyl suggests a steric effect in hydrogen bond formation for di-*tert*-butylcarbinol. This conclusion is tentative because of a possible large error in the  $\Delta H$ 's for this acid.<sup>17</sup>

(14) P. Rider, Ph.D. Thesis, Kansas State University, 1969.

(15) R. S. Drago, N. O'Brien, and G. C. Vogel, submitted for publication in *J. Amer. Chem. Soc.*

(16) J. Leffler and E. Grunwald, "Rates and Equilibria of Organic Reactions," John Wiley and Sons, New York, N. Y., 1963, p 224.

(17) A discussion similar to all the above could be given if  $\Delta\nu$ 's had been used in place of  $\Delta H$ 's. However, the correlations are not as good as when the latter are used. A major discrepancy is that di-*tert*-butylmethyl falls above the  $\alpha$  vs.  $\sigma^*$  line.

The single-scale equation is not only useful for predicting enthalpies of hydrogen bonding interactions but also for identifying the operation of resonance and steric factors in hydrogen bond reactions.

*Intramolecular Hydrogen Bonding.* A possible complication arises with the fluoroalcohols discussed in this report because of intramolecular hydrogen bonding. As discussed in the earlier report on hexafluoroisopropanol,<sup>2,10</sup> the effect of such intramolecular bonding would be principally to increase the intercepts of the  $\Delta H$  vs.  $\Delta\nu$  relations for TFE and HFIP. This state of affairs would not alter the interpretation of the slopes of these correlations.

If the intramolecular bonding enthalpy is as large as  $\sim 3$  kcal, as has been suggested,<sup>18</sup> drastic changes in the intercepts of the fluoroalcohol plots of  $\Delta H$  vs.  $\Delta\nu$  and in the  $\Delta H$  ratios ( $\alpha$  values) would result. In particular, TFE would be *twice* as strong a hydrogen bonding acid as phenol toward weak donors and the agreement between  $\Delta H$ 's,  $\Delta\nu$ 's, and  $\Delta$ 's with regard to the acidity order would be destroyed; furthermore, the effect of such a large enthalpy correction would render the  $\alpha$  values (and the single-scale enthalpy equation) statis-

tically meaningless. These consequences cannot, however, be cited as evidence to preclude the existence of large enthalpy corrections to the acid-base enthalpies. Rather, an accurate and highly reliable technique to determine the intramolecular enthalpy is required to settle this question. Tentative and indirect evidence that the intramolecular enthalpy should be *much* less than 3 kcal comes from the linear  $\sigma^*$ ,  $pK_a$  relationship, mentioned above, which is obeyed by both TFE and HFIP. An intramolecular enthalpy as large as 3 kcal would result in TFE and HFIP deviations from the  $\sigma^*$ ,  $pK_a$  correlation of *several*  $pK_a$  units. None of our conclusions would be materially affected by an intramolecular enthalpy of about 1 kcal or less.

*Acknowledgment.* Acknowledgment is made to the donors of the Petroleum Research Fund administered by the American Chemical Society for partial support of this research. We also express our appreciation to the Bureau of General Research, Kansas State University, and wish to thank Dr. Maarten van Swaay for his assistance in the building of the calorimeter.

(18) P. J. Kruger and H. D. Metee, *Can. J. Chem.*, **42**, 340 (1964).

## Dielectric Behavior of the System Benzyl Chloride-Benzene<sup>1a</sup>

by E. M. Turner, W. W. Ehrhardt, G. Leone, and W. E. Vaughan<sup>1b</sup>

*Department of Chemistry, University of Wisconsin, Madison, Wisconsin (Received February 27, 1970)*

Measurements of the dielectric permittivity and loss at 20, 30, and 40° at various wavelengths in the microwave region are reported for mixtures containing benzyl chloride and benzene. These data are fitted to a microscopic molecular model due to Budó. The model parameters are interpreted in terms of molecular and liquid structure. Existing theories of the internal electric field are used to correct for the effect of long-range dipole-dipole forces. In contrast to the results of a similar study on anisole-benzene mixtures, it is found that the dielectric behavior of the benzyl chloride-benzene mixtures, as analyzed above, is consistent with the hypothesis that the group dipole moment components in benzyl chloride are independent of its concentration in the mixture.

### Introduction

A model calculation due to Budó, based on the rotational Brownian motion of a molecule containing a freely rotating polar group, gave the following relation between the Laplace transform of the negative time derivative of the molecular dipolar autocorrelation function,  $\gamma$ , and the parameters of the model,  $C_1$ ,  $\tau_1$ , and  $\tau_2$ .<sup>2</sup> To the extent that the molecular dipole moment

$$\mathcal{L}_{i\omega}(-\dot{\gamma}) = [C_1/(1 + i\omega\tau_1)] + [(1 - C_1)/(1 + i\omega\tau_2)] \quad (1)$$

components along ( $\mu_1$ ) and perpendicular ( $\mu_2$ ) to the group rotation axis are independent of the molecular conformation,  $C_1$  should be constant since the Budó model predicts that

$$C_1/(1 - C_1) = \mu_1^2/\mu_2^2 \quad (2)$$

The effects of long-range dipole-dipole forces may be

- (1) (a) This work was supported by the National Science Foundation; (b) to whom correspondence should be addressed.  
(2) A. Budó, *Phys. Z.*, **39**, 706 (1938).

**Table I:** Dielectric Permittivity and Loss of Benzyl Chloride-Benzene Mixtures<sup>a</sup>

Wavelength, cm	20°		30°		40°	
	$\epsilon'$	$\epsilon''$	$\epsilon'$	$\epsilon''$	$\epsilon'$	$\epsilon''$
$X_{\text{benzyl chloride}} = 0.25$						
0.219	2.446	0.171	2.158	0.197	2.505	0.249
1.260	2.753	0.392	2.771	0.392	2.762	0.387
1.401	2.793	0.416	2.818	0.424	2.806	0.410
1.700	2.921	0.473	2.920	0.477	2.884	0.447
1.948	2.924	0.446	2.938	0.444	2.944	0.438
2.618	3.022	0.469	2.999	0.434	3.003	0.422
2.905	3.057	0.445	3.075	0.431	3.049	0.397
7.50	3.421	0.406	3.498	0.384	3.294	0.267
15.00	3.477	0.208	3.461	0.195	3.394	0.127
14990	3.577	—	3.500	—	3.448	—
$X_{\text{benzyl chloride}} = 0.50$						
0.219	2.600	0.318	2.630	0.312	2.581	0.334
1.260	3.127	0.732	3.164	0.736	3.179	0.739
1.401	3.217	0.779	3.166	0.753	3.264	0.787
1.700	3.328	0.769	3.363	0.831	3.394	0.837
1.948	3.389	0.854	3.415	0.821	3.434	0.811
2.618	3.565	0.870	3.574	0.844	3.615	0.840
2.905	3.676	0.875	3.678	0.842	3.719	0.839
7.50	4.397	0.662	4.375	0.620	4.387	0.574
15.00	4.470	0.530	4.514	0.494	4.361	0.373
14990	4.787	—	4.664	—	4.585	—
$X_{\text{benzyl chloride}} = 0.75$						
0.219	2.785	0.419	2.706	0.370	2.759	0.431
1.260	3.362	0.997	3.415	1.022	3.420	1.027
1.401	3.474	1.059	3.506	1.059	3.554	1.066
1.700	3.669	1.135	3.711	1.140	3.734	1.137
1.948	3.779	1.167	3.833	1.171	3.855	1.159
2.618	4.113	1.221	4.167	1.194	4.183	1.164
2.905	4.173	1.231	4.216	1.218	4.217	1.171
14990	5.848	—	5.659	—	5.501	—
$X_{\text{benzyl chloride}} = 1.00$						
0.219	2.817	0.507	2.826	0.477	2.815	0.470
1.260	3.610	1.202	3.655	1.298	3.736	1.270
1.401	3.689	1.264	3.752	1.294	3.830	1.310
1.700	3.879	1.380	3.939	1.374	4.015	1.389
1.948	4.076	1.497	4.104	1.639	4.192	1.431
2.618	4.362	1.534	4.445	1.535	4.457	1.500
2.905	4.564	1.559	4.593	1.553	4.631	1.522
14990	7.095	—	6.822	—	6.618	—

<sup>a</sup> Reported permittivities have probable errors of  $\pm 1\%$  except at 2-mm and 7.5- and 15-cm wavelengths where the errors are  $\pm 3\%$ . Losses are accurate to  $\pm 1.5\%$  except at 2 mm and 7.5 and 15 cm, where the accuracy is  $\pm 5\%$ .

accounted for in the Onsager approximation<sup>3</sup> to give an expression relating the autocorrelation function to the complex dielectric permittivity. Equations 3<sup>4,5</sup> and 4<sup>6</sup> are two such relations which differ only slightly in their predictions of the frequency dependence of the complex dielectric permittivity for most autocorrelation functions.

$$\mathcal{L}_{\omega}(-\gamma) = \epsilon_0(\epsilon^* - \epsilon_\infty)(2\epsilon^* + \epsilon_\infty) / \epsilon^*(\epsilon_0 - \epsilon_\infty)(2\epsilon_0 + \epsilon_\infty) \quad (3)$$

$$\mathcal{L}_{\omega}(-\gamma) = 3\epsilon_0(\epsilon^* - \epsilon_\infty) / (\epsilon_0 - \epsilon_\infty)(\epsilon^* + 2\epsilon_0) \quad (4)$$

When the scheme above was used to interpret the dielectric behavior of anisole and solutions of anisole in

nonpolar solvents, values of  $C_1$  were found which ranged from 0.75 to 0.20.<sup>7-13</sup> In order to see whether eq 1 and 3 (or 1 and 4) can be used to describe the dielectric behavior of a molecule with a shape similar to that of

(3) L. Onsager, *J. Amer. Chem. Soc.*, **58**, 1486 (1936).

(4) D. D. Klug, D. E. Kranbuehl, and W. E. Vaughan, *J. Chem. Phys.*, **50**, 3904 (1969).

(5) H. C. Bolton, *ibid.*, **16**, 486 (1948).

(6) R. H. Cole, *ibid.*, **42**, 637 (1965).

(7) D. E. Kranbuehl, D. D. Klug, and W. E. Vaughan, *ibid.*, **50**, 5266 (1969).

(8) S. K. Garg and C. P. Smyth, *ibid.*, **46**, 373 (1967).

(9) W. E. Vaughan, S. B. W. Roeder, and T. Provder, *ibid.*, **39**, 701 (1963).

**Table II:** Dielectric Dispersion Parameters and Viscosities for Benzyl Chloride-Benzene Mixtures<sup>a</sup>

Temp, °C	Mole fraction of benzyl chloride	Eq 3			Eq 4			$\epsilon_{\infty}$	$\eta$
		$\tau_1(\pm 1.5)$	$\tau_2(\pm 0.5)$	$C_1$	$\tau_1(\pm 1.5)$	$\tau_2(\pm 0.5)$	$C_1$		
20	1.00	29.7	4.6	0.62	26.6	4.8	0.64	2.74	1.396
	0.75	26.4	5.6	0.59	24.8	6.0	0.55	2.72	1.151
	0.50	23.6	4.2	0.60	22.1	4.2	0.60	2.52	0.965
	0.25	20.9	4.3	0.57	20.3	4.3	0.57	2.40	0.798
30	1.00	26.1	4.9	0.62	23.7	5.2	0.59	2.74	1.196
	0.75	21.7	4.7	0.60	20.1	4.9	0.57	2.65	0.987
	0.50	20.1	4.0	0.62	18.7	4.0	0.62	2.54	0.834
	0.25	13.2	1.0	0.73	12.8	1.0	0.73	2.34	0.683
40	1.00	23.7	4.3	0.66	21.5	4.3	0.60	2.71	1.038
	0.75	17.1	3.3	0.67	15.1	3.0	0.70	2.63	0.855
	0.50	17.4	3.2	0.62	16.3	3.2	0.62	2.47	0.726
	0.25	12.9	0.9	0.69	12.6	0.9	0.69	2.30	0.601

<sup>a</sup>  $\tau_1$  and  $\tau_2$  in psec ( $10^{-12}$  sec).  $\eta$  in centipoises.

anisole, we determined the complex dielectric permittivity of benzyl chloride-benzene mixtures as a function of wavelength, composition, and temperature.

### Experimental Section

**Purification of Materials.** Benzyl chloride was obtained from the Fisher Scientific Co. and was fractionally distilled and stored over anhydrous calcium sulfate. Benzene was obtained from laboratory stock and was stored over anhydrous calcium sulfate.

**Dielectric Measurements.** Static dielectric permittivities were determined by the heterodyne beat techniques at a frequency of 2 MHz.<sup>14</sup> Measurements of dielectric permittivity and loss at 7.5- and 15-cm wavelengths were made by the "breadth-of-the-minimum" technique, using a coaxial transmission line.<sup>14</sup> Centimeter wavelength measurements were made using a waveguide transmission line coupled to an automated detection system.<sup>14,15</sup> Measurements at 2-mm wavelength were made using a free-space oblique incidence interferometer.<sup>14</sup> Values of the permittivity and loss for each composition, wavelength, and temperature are shown in Table I.

**Viscosity Measurements.** The macroscopic shear viscosity of each mixture was determined at 20, 30, and 40° using an Ostwald viscometer. The raw data were reduced using the equation

$$\eta = A\rho t - B\rho/t \quad (5)$$

where  $\eta$  is the coefficient of viscosity,  $t$  is the time of flow, and  $\rho$  is the density. The constant  $B$  was computed from the viscometer dimensions and the constant  $A$  was determined by calibration with water.<sup>16</sup> The values of the viscosity are shown in Table II.

### Discussion

**Dipole Moments.** The dipole moment of benzyl chloride may be calculated from the low-frequency

dielectric permittivity ( $\epsilon_0$ ) using the Onsager equation for mixtures.<sup>3</sup>

$$\sum_i \theta_i \frac{\epsilon_0 - \epsilon_{\infty i}}{2\epsilon_0 + \epsilon_{\infty i}} = \sum_i \frac{\epsilon_0(\epsilon_{\infty i} + 2)^2 4\pi N_i}{3(2\epsilon_0 + \epsilon_{\infty i})^2 3kT} \mu_i^2 \quad (6)$$

$N_i$  is the number density and  $\theta_i$  the volume fraction of the  $i$ th species. The limiting permittivity at high frequency may be approximated by  $n^2D$  or (for benzyl chloride) it may be found from the fit of the frequency dependent dielectric measurements on pure benzyl chloride to eq 3 or 4. This latter procedure allows for atomic polarization and leads to a smaller value for the dipole moment. The values of  $\epsilon_{\infty}$  found using eq 3 differ by less than 0.005 from those found using eq 4. Dipole moments of benzyl chloride calculated by the two methods are shown in Table III. The values using  $n^2D$  are in good agreement with those calculated the same way and reported previously (1.75 to 1.89).<sup>17</sup> The fact that the dipole moments do not vary appreciably with concentration or temperature supports the use of the Onsager model.

**Dielectric Dispersion Parameters.** The results of fitting the experimental data by computer using a least-squares criterion to eq 1 and 3 (or 1 and 4) are shown in

(10) W. E. Vaughan and C. P. Smyth, *J. Phys. Chem.*, **65**, 98 (1961).

(11) E. Forest and C. P. Smyth, *ibid.*, **69**, 1302 (1965).

(12) E. L. Grubb and C. P. Smyth, *J. Amer. Chem. Soc.*, **83**, 4873 (1961).

(13) D. B. Farmer, A. Holt, and S. Walker, *J. Chem. Phys.*, **44**, 4116 (1966).

(14) N. Hill, W. E. Vaughan, A. H. Price, and M. Davies, "Dielectric Properties and Molecular Behaviour," Van Nostrand-Reinhold Co., London, 1969.

(15) J. D. Cutnell, D. E. Kranbuehl, E. M. Turner, and W. E. Vaughan, *Rev. Sci. Instrum.*, **40**, 908 (1969).

(16) F. Daniels, *et al.*, "Experimental Physical Chemistry," 7th ed, McGraw-Hill Book Co., New York, N. Y., 1970.

(17) A. L. McClellan, "Tables of Experimental Dipole Moments," W. H. Freeman and Co., San Francisco, Calif., 1963.

**Table III:** Dipole Moment of Benzyl Chloride

Mole fraction of benzyl chloride	Temp, °C	Dipole moment using	
		$\epsilon_{\infty}$	$n^2_D$
0.25	20	1.67	1.83
	30	1.66	1.82
	40	1.67	1.84
0.50	20	1.61	1.78
	30	1.60	1.78
	40	1.62	1.80
0.75	20	1.58	1.75
	30	1.56	1.75
	40	1.56	1.75
1.00	20	1.60	1.78
	30	1.58	1.77
	40	1.58	1.77

Table II. The  $\tau_1$  values are of the magnitude expected for dielectric relaxation by overall molecular rotational diffusion as a survey of relaxation times for rigid molecules with similar molecular volumes and solution viscosities shows.<sup>18</sup> The  $\tau_1$  values decrease with dilution and with increasing temperature paralleling decreases in the viscosity. Although no specific connection between the molecular relaxation time and the macroscopic shear viscosity has been established, it is found generally that the relaxation time increases with viscosity, but the change in viscosity is larger than the change in relaxation time. A detailed empirical analysis has been given by Higasi.<sup>19</sup> In the case considered here, the relation between  $\tau_1$  and  $\eta$  is nearly proportional (a least-squares plot of  $\ln \tau_1$  vs.  $\ln \eta$  has a slope of 0.93), which is characteristic of the limit of large unsymmetrical solute molecules in a solvent whose molecules are relatively small. When symmetrical molecules are dissolved in a solvent whose molecular size exceeds that of the solute,  $\tau_1$  becomes insensitive to changes in  $\eta$ . (Use of a model involving rotational diffusion would be unphysical in this case although the same functional form for eq 1 might result.)

The dielectric dispersion parameters reported here are consistent with parameters found from dilute solution data for benzyl chloride in benzene. At 20°, Purcell, Fish, and Smyth<sup>20</sup> found  $\tau_1 = 23.7$  and  $\tau_2 = 2.3$  by a cut-and-try method involving drawing chords through the data points on a normalized Debye semicircle until a consistent set is obtained.<sup>21</sup> A graphical method based on the Debye equation gave  $\tau_1 = 18.7$  and  $\tau_2 = 2.9$ . We fitted the data of Purcell, Fish, and Smyth and found  $\tau_1 = 20.2$ ,  $\tau_2 = 2.6$ , and  $C_1 = 0.57$ . Klages and Knobloch report  $\tau_1 = 14.0$ ,  $\tau_2 = 1.4$ , and  $C_1 = 0.70$ .<sup>22</sup>

The  $\tau_2$  values show considerable scatter, indicating uncertainty resulting from lack of measurements in the millimeter wavelength region and from the smaller term involving  $\tau_2$  in eq 1. The values are similar to relaxa-

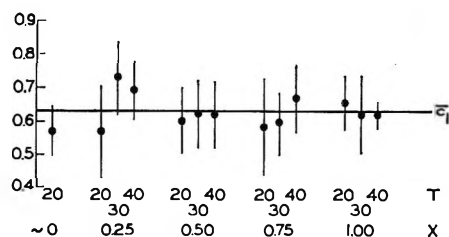


Figure 1. Scatter diagram of  $C_1$  values derived from eq 3. The horizontal line indicates the average value of  $C_1$  and the vertical lines show the range between the 95% confidence limits.

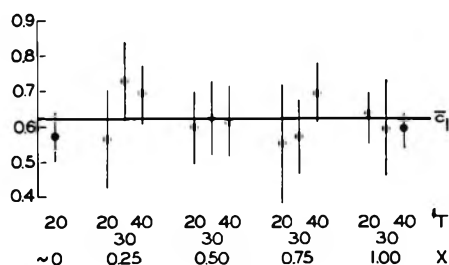


Figure 2. Scatter diagram of  $C_1$  values derived from eq 4.

tion times for processes, in which internal rotation is involved, reported in the literature.<sup>18</sup> The inertial correction, which might contribute to uncertainty in the  $\tau_2$  values *via* contribution to the millimeter wavelength measurements, has been neglected in the analysis.

A major aim of this work is to test the hypothesis that  $C_1$  is constant as the model employed predicts. The nonlinear least-squares subroutine employed to fit the experimental values of the dielectric permittivity and loss to the model predictions furnishes 95% confidence limits on the parameters as part of the output. An indication of the fluctuation of  $C_1$  about its average value is given by Figures 1 and 2. Based on the confidence intervals the variation of  $C_1$  observed seems reasonable and there is no reason to doubt the hypothesis. It is apparent that eq 3 and 4 cannot be distinguished by these data. The same information may be interpreted in terms of the Student's  $t$  statistic.<sup>23</sup> For the  $C_1$  values resulting from eq 3, the value of  $t$  is 0.73 for ten degrees of freedom. A larger (absolute) value of  $t$  (greater scatter of  $C_1$  about the average value) would be expected in 48% of similar experiments.

(18) See, for example, the tables of dielectric constants, dipole moments, and dielectric relaxation times included in the "Digest of Literature on Dielectrics," published yearly by the National Academy of Sciences.

(19) K. Higasi, Monograph No. 13 of the Research Institute of Applied Electricity, Hokkaido University, Sapporo, 1965.

(20) W. P. Purcell, K. Fish, and C. P. Smyth, *J. Amer. Chem. Soc.*, **82**, 6299 (1960).

(21) K. Bergmann, D. M. Roberti, and C. P. Smyth, *J. Phys. Chem.*, **64**, 665 (1960).

(22) G. Klages and P. Knobloch, *Z. Naturforsch.*, **20A**, 580 (1965).

(23) P. G. Hoel, "Introduction to Mathematical Statistics," John Wiley and Sons, Inc., New York, N. Y., 1954, p 231.

For the  $C_1$  values resulting from eq 4, the value of  $t$  is 1.11 for ten degrees of freedom. A larger value of  $t$  would be expected in 28% of similar experiments. In either case, there is statistical support for the hypothesis that  $C_1$  is constant and the conclusion that the molecular dipole moment components are independent of temperature and concentration seems well founded. On the other hand, an attempt to compute  $C_1$  *a priori* from bond moments derived from other molecules is unsuccessful. Based on a dipole moment of 2.20 D for *p*-bis(chloromethyl)benzene,<sup>17,20</sup> the component of the moment of the chloromethyl group perpendicular to the rotation axis would be 1.56 D. Using this group moment component in combination with our average dipole moment for the benzyl chloride molecule of 1.79 D leads to  $C_1 = 1 - (1.56/1.79)^2 = 0.24$  which is in very poor agreement with the experimental result. Discrepancies of this type are frequent and they have been discussed by Klages and Knobloch,<sup>22</sup> who conclude that interactions with the  $\pi$ -electron system of the aromatic ring are very significant and might account for the differences in the perpendicular group dipole moment found in different compounds. In order to

account for the  $C_1$  value reported here, the perpendicular component of the chloromethyl group in benzyl chloride would have to be 1.04 D.

The extent to which the experimental data fit the predictions of eq 1 and 3 (or 1 and 4) may be seen from the back calculations furnished as part of the computer output. The differences usually lie within the estimated probable errors of measurement (see Table I) with an occasional discrepancy of several times the estimated error. The quality of the fit may be evaluated also by the typical Cole-Cole plot shown in Figure 3.

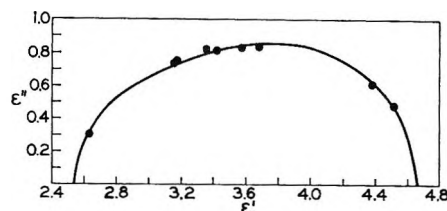


Figure 3. Cole-Cole locus for equimolar benzyl chloride-benzene mixture at 30°. The solid line is back calculated from the dispersion parameters for eq 3 shown in Table II.

## NOTES

### Behavior of Structure-Making and Structure-Breaking Solutes Near Temperature of Maximum Density of Water

by T. S. Sarma and J. C. Ahluwalia

Department of Chemistry, Indian Institute of Technology, Kanpur, U. P., India (Received June 2, 1969)

The occurrence of maximum density of water at 3.98° has been attributed to the balancing of the two opposing effects, namely, the increase in volume resulting from the thermal expansion and the decrease in volume resulting from the breakdown of water structure<sup>1</sup> as the temperature is increased. The structure-breaking and structure-making effects of solutes<sup>2</sup> may be described in terms of the shift of equilibrium  $(\text{H}_2\text{O})_b = (\text{H}_2\text{O})_d$ , where  $(\text{H}_2\text{O})_b$  represents the bulky ice-like hydrogen-bonded clusters of water molecules and  $(\text{H}_2\text{O})_d$  represents denser, nonhydrogen

bonded water molecules. The structure-breaking solutes like simple electrolytes<sup>2</sup> which shift the above equilibrium to the denser form are expected to lower the temperature of maximum density (TMD) whereas the structure-making solutes like tetraalkylammonium halides which shift the equilibrium towards bulky form by forming Frank-Evans<sup>3</sup> icebergs around the ions are expected to increase TMD.

The studies<sup>4-6</sup> on the effects of simple electrolytes on TMD reveal that TMD is lowered and the lowering is proportional to the concentration of the particular solute which is known as the Despretz rule.<sup>7</sup> The effect of nonelectrolytes (except for monomeric alco-

(1) W. K. Röntgen, *Ann. Phys. Chim. (Wied)*, **45**, 91 (1892); J. L. Kavanau, "Water and Solute-Water Interactions," Holden-Day, San Francisco, Calif., 1964.

(2) H. S. Frank and W. Y. Wen, *Discuss. Faraday Soc.*, **24**, 133 (1957).

(3) H. S. Frank and M. W. Evans, *J. Chem. Phys.*, **13**, 507 (1945).

(4) R. Wright, *J. Chem. Soc.*, **115**, 119 (1919).

(5) E. W. Washburn, Ed., "International Critical Tables," Vol. III, McGraw-Hill, New York, N. Y., 1933, p 107.

(6) N. G. Wilson and R. Wright, *J. Phys. Chem.*, **35**, 624 (1931).

(7) M. C. Despretz, *Ann. Chim. Phys.*, **70**, 49 (1839).

Table I: Integral Heats of Solution of Bu<sub>4</sub>NBr, Pr<sub>4</sub>Ni, and NaBPh<sub>4</sub> in Water at 3, 5, and 15°

Temperature, 3.0°				Temperature, 5.0°				Temperature, 15.0°			
Salt	$m \times 10^2$	$\sqrt{m} \times 10^2$	$\Delta H_s, \text{ cal mol}^{-1}$	Salt	$m \times 10^2$	$\sqrt{m} \times 10^2$	$\Delta H_s, \text{ cal mol}^{-1}$	Salt	$m \times 10^2$	$\sqrt{m} \times 10^2$	$\Delta H_s, \text{ cal mol}^{-1}$
Bu <sub>4</sub> NBr	0.27	1.64	-6180	Bu <sub>4</sub> NBr	0.45	2.12	-5702	Bu <sub>4</sub> NBr	0.59	2.43	-3977
	0.42	2.05	-6228		0.46	2.14	-5772		0.65	2.55	-3904
	0.58	2.40	-6214		0.82	2.86	-5714		0.75	2.70	-3850
$\Delta H_s^\circ = -6204 \pm 35 \text{ cal mol}^{-1}$			$\Delta H_s^\circ = -5780 \pm 25 \text{ cal mol}^{-1}$			$\Delta H_s^\circ = -3920 \pm 45 \text{ cal mol}^{-1}$					
Pr <sub>4</sub> Ni	3.11	5.57	253	Pr <sub>4</sub> Ni	0.93	3.05	527				
	4.01	6.33	271		0.93	3.05	513				
	4.73	6.86	268		1.03	3.21	487				
$\Delta H_s^\circ = 264 \pm 15 \text{ cal mol}^{-1}$			$\Delta H_s^\circ = 507 \pm 16 \text{ cal mol}^{-1}$								
NaBPh <sub>4</sub>	0.29	1.70	-8377		2.00	4.47	514				
	0.52	2.28	-8297		4.12	6.42	489				
	0.71	2.66	-8366		4.87	6.97	524				
$\Delta H_s^\circ = -8345 \pm 40 \text{ cal mol}^{-1}$											

hols) on TMD has been shown by Wada and Umeda<sup>8</sup> to result in lowering of TMD at all concentrations. The monomeric alcohols, on the other hand, were observed to cause slight increase in TMD only in very dilute solutions. They further observed that the lowering of TMD was not proportional to concentration.

Very recently Darnell and Greyson,<sup>9</sup> who studied the effect of structure-making solutes such as tetraalkylammonium halides on TMD, observed that these solutes resulted in the lowering of TMD. Furthermore, the lowering of TMD was larger, the larger the alkyl group R of R<sub>4</sub>N<sup>+</sup> salts. This led these authors to conclude that tetraalkylammonium halides which are structure makers at room temperature behave as structure breakers in the neighborhood of TMD. Since the change in TMD is a resultant effect of ideal mixing and solute-solvent interactions<sup>8,10</sup> it does not seem justifiable to make inferences about solute-solvent interactions from the changes in TMD without considering the ideal mixing contribution. On the other hand, the changes in the heat capacities of solutes in water can give directly the influence of solutes on water structure.<sup>11</sup> Therefore, we undertook the work of investigation of the changes in partial molal heat capacity in aqueous solutions of highly structure making salts Bu<sub>4</sub>NBr, Pr<sub>4</sub>Ni, and NaBPh<sub>4</sub> from room temperature to TMD to see if the behavior of these salts as structure makers is really reversed at or near TMD as suggested by Darnell and Greyson.<sup>9</sup>

### Experimental Section

The submarine calorimeter and operational procedure used for the measurements of heats of solution have been described previously.<sup>11</sup> The temperature control

of the thermostat was maintained to  $\pm 0.002^\circ$  for measurements at 25° and to  $\pm 0.008^\circ$  at lower temperatures (3, 5, and 15°). The calorimeter was calibrated by measuring the heats of solution of KCl in water and tris(hydroxymethyl)aminomethane in 0.1 N HCl at 25°. The values obtained were in good agreement (within 0.2%) with those reported by Gunn.<sup>12</sup>

Tetraalkylammonium halide salts Bu<sub>4</sub>NBr and Pr<sub>4</sub>Ni were obtained from Distillation Products Industries. These were recrystallized twice by the methods reported in the literature<sup>13,14</sup> and dried *in vacuo* at 60–80° and kept in a desiccator before use. NaBPh<sub>4</sub> was procured from Fisher Scientific Co. (assay 99.7%) and was used as such. The sample bulbs were filled with the salts and then kept in an oven (Pr<sub>4</sub>Ni at 100° and Bu<sub>4</sub>NBr at 80°) and dried to constant weight and sealed. The water used was conductivity water obtained by passing distilled water through a Barnstead mixed bed ion-exchange resin column.

### Results and Discussion

Integral heats of solution  $\Delta H_s^\circ$  of Bu<sub>4</sub>NBr and Pr<sub>4</sub>Ni<sup>15</sup> at 25 and 35° and that of NaBPh<sub>4</sub><sup>11</sup> in water at 5, 15,

(8) G. Wada and S. Umeda, *Bull. Chem. Soc. Jap.*, **35**, 646, 1797 (1962).

(9) A. J. Darnell and J. Greyson, *J. Phys. Chem.*, **72**, 3021 (1968).

(10) F. Franks and B. Watson, *Trans. Faraday Soc.*, **63**, 329 (1967).

(11) S. Subramanian and J. C. Ahluwalia, *J. Phys. Chem.*, **72**, 2525 (1968).

(12) S. R. Gunn, *ibid.*, **69**, 2902 (1965).

(13) D. F. Evans, C. Zawoyski, and R. L. Kay, *ibid.*, **69**, 3878 (1965).

(14) A. K. R. Unni, L. Elias, and H. I. Schiff, *ibid.*, **67**, 1216 (1963).

(15) T. S. Sarma, R. K. Mohanty, and J. C. Ahluwalia, *Trans. Faraday Soc.*, **65**, 2333 (1969).

**Table II:**  $\Delta H_s^\circ$  (cal mol<sup>-1</sup>) of Bu<sub>4</sub>NBr, Pr<sub>4</sub>NI, and NaBPh<sub>4</sub> in Water from 3 to 35°

Solute	Temp. °C				
	3	5	15	25	35
Bu <sub>4</sub> NBr	-6204 ± 35	-5780 ± 25	-3920 ± 45	-2050 ± 15 <sup>a</sup>	-260 ± 15 <sup>a</sup>
Pr <sub>4</sub> NI	264 ± 15	507 ± 16	...	2767 ± 20 <sup>a</sup>	3955 ± 20 <sup>a</sup>
NaBPh <sub>4</sub>	-8345 ± 40	-8000 ± 16 <sup>b</sup>	-6380 ± 15 <sup>b</sup>	-4805 ± 15 <sup>b</sup>	-3110 ± 20 <sup>b</sup>

<sup>a</sup> See ref 15. <sup>b</sup> See ref 11.

25, and 35° have already been reported from our laboratory.

In this work we have extended the determinations of integral heats of solution  $\Delta H_s$  of Bu<sub>4</sub>NBr to 15, 5, and 3°, of Pr<sub>4</sub>NI to 5 and 3° and that of NaBPh<sub>4</sub> to 3°. The measurements were made in the low concentration range of 0.3 to 5 × 10<sup>-3</sup> *m*. The values of integral heats of solution at different concentrations are given in Table I.  $\Delta H_s^\circ$  values at 5° were obtained by extrapolating to infinite dilution  $\Delta H_s$  values against square root of molality using Debye-Hückel limiting slope as a guide line. Because of low number of runs at 3°, and the fact that the experimental error in these runs at such low concentrations was more than the Debye-Hückel dilution correction, the values of  $\Delta H_s^\circ$  at 3° were obtained by averaging out  $\Delta H_s$  values. The values of  $\Delta H_s^\circ$  along with their estimated uncertainties are given in Table I.

$\Delta H_s^\circ$  values of Bu<sub>4</sub>NBr, Pr<sub>4</sub>NI, and NaBPh<sub>4</sub> at temperatures varying from 3 to 35° are given in Table II.

Heat capacity changes  $\Delta C_p^\circ$  in aqueous solutions of Bu<sub>4</sub>NBr, Pr<sub>4</sub>NI, and NaBPh<sub>4</sub> at temperatures varying from 4 to 30° as derived from  $\Delta H_s^\circ$  values given in Table II are shown in Table III.

**Table III:**  $\Delta C_p^\circ$  (cal mol<sup>-1</sup> deg<sup>-1</sup>) of Bu<sub>4</sub>NBr, Pr<sub>4</sub>NI, and NaBPh<sub>4</sub> from 4 to 30°

Solute	Temp. °C				
	4	10	15	20	30
Bu <sub>4</sub> NBr	212 ± 20	186 ± 7	...	187 ± 6	179 ± 3 <sup>a</sup>
Pr <sub>4</sub> NI	121 ± 4	...	113 ± 3	...	119 ± 4 <sup>a</sup>
NaBPh <sub>4</sub>	173 ± 20	162 ± 3 <sup>b</sup>	..	158 ± 3 <sup>b</sup>	170 ± 4 <sup>b</sup>

<sup>a</sup> See ref 15. <sup>b</sup> See ref 11.

$\Delta H_s^\circ$  values at 3 and 5° and therefore  $\Delta C_p^\circ$  values at 4° have a larger uncertainty than the values reported for higher temperatures due to lack of better temperature control and slow dissolution of salts at lower temperatures. However, we will see that the uncertainty in  $\Delta C_p^\circ$  values at 4° hardly makes any difference in the interpretation of the results and conclusions drawn therefrom.

It may be seen from Table III that the  $\Delta C_p^\circ$  of aqueous solutions of Bu<sub>4</sub>NBr, Pr<sub>4</sub>NI, and NaBPh<sub>4</sub> at

30° are all positive and very large in magnitude (in fact the highest of those reported in the literature), indicating that these solutes are very strong structure makers at this temperature. It is clear from Table III that as the temperature is decreased from 30 to 4° no appreciable changes in  $\Delta C_p^\circ$  values are observed. The maximum change observed in  $\Delta C_p^\circ$  values between room temperature and TMD is only 17%. In other words, structure-making capacity of these salts at TMD differs slightly from that at room temperature. If these solutes were to behave as structure breakers at TMD then  $\Delta C_p^\circ$  values would have been negative rather than positive. Furthermore, the relative order of structure-making ability of Bu<sub>4</sub>N<sup>+</sup> > Pr<sub>4</sub>N<sup>+</sup> at room temperature is also preserved at TMD as shown by  $\Delta C_p^\circ$  values in Table III.<sup>16</sup> Because of the small changes in  $\Delta C_p^\circ$  values at different temperatures and large uncertainty in  $\Delta C_p^\circ$  values at 4° it has not been possible to establish clear decreasing or increasing trends in  $\Delta C_p^\circ$  values as the temperature is decreased from 30 to 4°.

Darnell and Greyson<sup>9</sup> have observed that the tetraalkylammonium salts which are structure makers at room temperature lower the TMD and attribute the lowering of TMD to nonmanifestation of room temperature structure-making propensities of the quaternary ammonium halides in the neighborhood of TMD. These authors have attributed such a behavior to the increase in cluster size<sup>17</sup> at low temperatures which makes available less free water for structure making due to incompatibility of the R<sub>4</sub>N<sup>+</sup> ions and water solvent.

This is in discord with what can be concluded from our results of  $\Delta C_p^\circ$ , which indicate that manifestation of room temperature structure-making propensities of quaternary ammonium halides are retained even in the neighborhood of TMD.

We believe that it is not the TMD results of Darnell and Greyson<sup>9</sup> which are in conflict with our  $\Delta C_p^\circ$  values but it is their interpretation of TMD results which is not tenable on the basis of our  $\Delta C_p^\circ$  values. The change  $\Delta T$  in TMD has been represented by Franks

(16) It has been recently shown from our laboratory (see ref 15) that for bromide and iodide salts of R<sub>4</sub>N<sup>+</sup>, where R is C<sub>2</sub>H<sub>5</sub> or a larger alkyl group, the influence of anions in modifying water structure is not significant.

(17) G. Nemethy and H. A. Scheraga, *J. Chem. Phys.*, **36**, 3382 (1962).

and Watson<sup>10</sup> in the empirical expression

$$\Delta T = -\frac{xV_2^0\alpha_2}{2(1-x)\alpha_1V_1^*} - \frac{\partial\Delta V_z^M/\partial T}{2(1-x)V_1^*\alpha_1} \quad (1)$$

where  $x$  is the mole fraction of the solute,  $\alpha_1$  and  $\alpha_2$  are the thermal coefficients of solute and solvent, respectively,  $\Delta V_z^M$  is the excess volume of mixing,  $V_2^0$  is the molar volume of the solute and  $V_1^*$  is the molar volume of water at TMD.

The first term ( $-xV_2^0\alpha_2/2(1-x)\alpha_1V_1^*$ ) is known as the Despretz slope and represents the contribution  $\Delta T_{id}$  from ideal mixing which is always negative. The second term  $-\partial\Delta V_z^M/\partial T/2(1-x)V_1^*\alpha_1$  represent the contribution ( $\Delta T_{st}$ ) of structural changes in water brought about by solutes which is found to be negative for electrolytes and positive for nonelectrolytes such as monohydric alcohols, and amines.<sup>10</sup> The negative contribution of  $\Delta T_{st}$  resulting from positive excess expansibilities  $\partial\Delta V_z^M/\partial T$  of aqueous solutions of electrolytes is associated with their water structure-breaking propensities. The positive  $\Delta T_{st}$  contribution resulting from negative excess expansibilities  $\partial\Delta V_z^M/\partial T$  of aqueous solutions of monohydric alcohols and amines is associated with their water structure-making propensities which is found to increase<sup>10</sup> with the number of carbon atoms and with the degree of complexity of the alkyl group.

On this basis one would, therefore, expect tetraalkylammonium halide salts (with the exception of  $\text{Me}_4\text{N}^+$  salts) which are now established as strong water structure makers at room temperature from various studies<sup>15</sup> and also at temperatures near TMD from this work, to result in large enough positive  $\Delta T_{st}$  contribution to overcome the negative  $\Delta T_{id}$  contribution. Furthermore, positive  $\Delta T_{st}$  contribution should increase as the size of the alkyl group in tetraalkylammonium halide salts is increased in accordance with the corresponding increase in structure-making propensities of tetraalkylammonium halides.<sup>15</sup> On the contrary, Darnell and Greyson observed large negative changes in  $\Delta T$  which became more and more negative with the increase in the size of the alkyl group R in  $\text{R}_4\text{N}^+$  halide salts.

This is not surprising if one examines the expansibility data of aqueous solutions of  $\text{R}_4\text{N}^+$  halide salts by Franks and Smith,<sup>18</sup> Millero and Drost-Hansen,<sup>19</sup> and by Ram Gopal and Siddiqi.<sup>20</sup> All these workers have obtained positive values of excess expansibilities  $\partial\Delta V_z^M/\partial T$  which are found to increase with the increase in the size of the alkyl group and the temperature. Therefore, aqueous solutions of  $\text{R}_4\text{N}^+$  halide salts will give rise to negative  $\Delta T_{st}$  contribution (second term in eq 1) which when combined with negative  $\Delta T_{id}$  contribution (first term in eq 1) results in large negative values of  $\Delta T$  or in other words tetraalkylammonium halide salts lower the TMD of water as in the case of electrolytes. Furthermore, the lowering of TMD will be greater the larger the size of the alkyl group in  $\text{R}_4\text{N}^+$  salts due to more and

more negative contributions of  $\Delta T_{st}$ . Thus the above analysis explains why the tetraalkylammonium halide salts, while retaining the water structure-making propensities at temperatures near TMD (as shown by our  $\Delta C_p^0$  values), lower TMD of water. However, one may raise the question why it is that structure maker nonelectrolytes (monohydric alcohols and amines) gave negative values of excess expansibilities or positive values of  $\Delta T_{st}$ , while structure-maker tetraalkylammonium halides give positive values of excess expansibilities or the negative values of  $\Delta T_{st}$ . This difference in behavior toward the effect on TMD between these two classes of water structure-maker solutes is also exhibited in the nmr chemical shifts of water protons. For monohydric alcohols EtOH, *n*-BuOH, and *t*-BuOH up to 10 mole per cent at 0° the chemical shifts of the water protons moves downfield in accordance with the structure promotion concept<sup>21,22</sup> while the nmr chemical shifts of water protons in the presence of  $\text{R}_4\text{N}$  halides<sup>23</sup> and long-chain alkyl salts<sup>21</sup> get shifted upfield. These observations qualitatively, at least, indicate that the structure of hydrophobic hydration may be different for different kinds of solutes even through there may be broad features of similarity. Thus, for example, heat capacity data, entropies of dilution, and similar studies bear evidence for increased structuredness of water around nonpolar solutes. It is possible that the hydration sheath around nonpolar groups is not definitely ice-I-like but rather resembles a Pauling-type clathrate cage or some other polymorphic modification of ice. The "thermal" melting of the "icebergs" would be accounted for by either of these structures while the positive excess expansibilities or lowering of TMD and upfield shifts of water protons might be accounted for on the basis of high packing density of hydrophobic hydration and greater electronic shield for the water protons around the nonpolar solutes. A similar suggestion has been made by Wicke,<sup>24</sup> who suggests the existence of nontetrahedral H bonds around the nonpolar parts of the solutes. These nontetrahedral H bonds will offer greater shielding for the water protons but give positive excess heat capacity and entropy loss due to ordering.

On the basis of the above discussion it is worthwhile to point out that one should be careful in deriving inferences regarding the nature of the solute-water

(18) F. Franks and H. T. Smith, *Trans. Faraday Soc.*, **83**, 2586 (1968).

(19) F. J. Millero and W. Drost-Hansen, *J. Phys. Chem.*, **72**, 1758 (1968).

(20) R. Gopal and M. A. Siddiqi, *ibid.*, **72**, 1814 (1968).

(21) J. Clifford and B. A. Pethica, *Trans. Faraday Soc.*, **61**, 182 (1965).

(22) D. N. Glew, H. D. Mak, and N. S. Rath, *Chem. Commun.*, 264 (1968).

(23) H. G. Hertz and M. D. Ziedler, *Ber. Bunsenges Phys. Chem.*, **68**, 821 (1964).

(24) E. Wicke, *Angew. Chem. Int. Ed. Engl.*, **5**, 106 (1966).

interactions from the results of the effect of solutes on the temperature of maximum density of water using Frank and Watson's relationship<sup>10</sup> (eq 1). The use of TMD results alone as a criterion for structure-making or structure-breaking effect of solutes on water can be misleading.

*Acknowledgment.* We thank Mr. R. K. Mohanty for measurements on heats of solution of Pr<sub>4</sub>NI at 5°.

## Direct Determination of Triplet ← Triplet Absorption Extinction Coefficients. II. Quinoline, Isoquinoline, and Quinoxaline

by Steven G. Hadley

Department of Chemistry,  
University of Utah, Salt Lake City, Utah 84112  
(Received May 11, 1970)

The characterization of the electronic absorption bands arising from the metastable triplet state has been a problem of interest for over 20 years.<sup>1</sup> The extinction coefficients of these bands have been a particularly elusive quantity due to the difficulty in measuring the concentration of triplets. Recently, this problem has been overcome through a new technique for measuring ground-state depletions by observing the singlet ← singlet absorption bands. This technique does not rely upon any assumptions that cannot be checked during the experiment. Further, it is not handicapped by triplet ← triplet absorption overlapping the singlet ← singlet bands or by photochemical decomposition. This technique has been described in a publication hereafter referred to as I.<sup>2</sup>

The triplet ← triplet absorption spectra of aromatic heterocycles have not been investigated to the same extent as those of aromatic hydrocarbons. Of the two ring aza-aromatics, triplet ← triplet absorption has been reported for quinoline and isoquinoline by Craig and Ross,<sup>3</sup> and for quinoxaline by Astier and Meyer,<sup>4</sup> and by Henry and Kasha.<sup>5</sup> To further characterize these electronic absorption bands for quinoline, isoquinoline, and quinoxaline, we wish to report measurement of their extinction coefficients and oscillator strengths.

Samples of isoquinoline and quinoxaline were obtained from Distillation Products Industries; quinoline was obtained from Matheson Coleman and Bell. The quinoline and isoquinoline were purified by vacuum distillation. Quinoxaline was purified by repeated vacuum sublimation. No impurities with concentrations greater than 1% were observed in any of these compounds after purification. The phosphorescent lifetimes were also measured and found to agree with those reported in the literature.

Solutions of these solutes were prepared using a solvent mixture of 30% *n*-butyl alcohol and 70% isopentane by volume. The solvents were spectrograde quality supplied by Matheson Coleman and Bell. When cooled to the temperature of boiling nitrogen this mixture formed a clear rigid glass in which the solute concentrations were typically 10<sup>-5</sup> to 10<sup>-4</sup> M. Further details of sample preparation are described in I.

The sample was contained in a metal dewar constructed from stainless steel with a copper sample compartment. The liquid nitrogen was in direct contact with the copper sample compartment during the experiments. Quartz windows were sealed to the sample compartment using Lo-Load Teflon-coated inconel seals purchased from the Advanced Products Co. No liquid nitrogen was in the light path. This dewar was placed in the cell compartment of a Cary 14 spectrophotometer where singlet ← singlet absorption spectra were determined.

The flash lamp used to pump the molecules into the triplet state was similar to the one used in I. The capacitor bank in the present work consisted of five 450-μF capacitors. To obtain reproducible light output the lamp was evacuated and then filled with air at a pressure of 2 Torr before each discharge. The capacitor bank was charged to 4.0 kV and the discharge was initiated by a high-voltage pulse. The 18,000 J was dissipated giving a light pulse of 100 μsec duration. Over 10<sup>16</sup> quanta were absorbed by the samples. Under these conditions the reproducibility of the light output was found to be ±3% over a series of ten flashes, as determined by measuring the initial optical density of the triplet ← triplet absorption of a rigid glass solution of naphthalene.

A McPherson Model 216.5 0.5-m monochromator was used with a 1P28A photomultiplier. The signals were displayed on a Tektronix 544 oscilloscope using a Type W preamplifier. The other details of the measurements are like those described in I, except no corrections for variations in flash lamp intensity were applied, as it was felt that these errors were small enough as to be unimportant.

The measured values of the extinction coefficient for the triplet ← triplet absorption,  $\epsilon_T$ , for quinoline, isoquinoline, and quinoxaline are given in Table I. The wavelength of the triplet ← triplet absorption maximum,  $\lambda_T$ , and the wavelength where the singlet depletion was determined,  $\lambda_S$ , are also given. The oscillator strength,  $f_T$ , for the triplet ← triplet bands was

(1) Much of the literature on triplet ← triplet absorption has been collected in S. P. McGlynn, T. Azumi, and M. Kinoshita, "Molecular Spectroscopy of the Triplet State", Prentice-Hall, Inc., Englewood Cliffs, N. J., 1969.

(2) S. G. Hadley and R. A. Keller, *J. Phys. Chem.*, **73**, 4351 (1969).

(3) D. P. Craig and I. G. Ross, *J. Chem. Soc.*, 1589 (1954).

(4) R. Astier and Y. Meyer, *J. Chim. Phys.*, **64**, 919 (1967).

(5) B. Henry and M. Kasha, *J. Chem. Phys.*, **47**, 3319 (1967).

**Table I:** Extinction Coefficients for Triplet  $\leftarrow$  Triplet Absorption

Molecule	$\epsilon_T \times 10^{-3}$ , l. mol <sup>-1</sup> cm <sup>-1</sup> a,b	$\lambda_T$ , nm <sup>c</sup>	$\lambda_S$ , nm <sup>d</sup>	$f_T^e$
Quinoline	7.1 $\pm$ 0.7	400.0	312.7	0.13
Isoquinoline	14.9 $\pm$ 1.0	419.0	320.2	0.11
Quinoxaline	8.1 $\pm$ 0.8	425.0	316.0	0.15
Naphthalene <sup>f</sup>	40. $\pm$ 6	414.0	310.9	0.14

<sup>a</sup> Computed from  $\log(I_0/I) = \epsilon_T C_T^0 d$ . <sup>b</sup> Estimated error. <sup>c</sup> Wavelength of maximum triplet  $\leftarrow$  triplet absorption. <sup>d</sup> Wavelength where ground-state depletion was measured. <sup>e</sup> Oscillator strength computed from  $f = 4.32 \times 10^{-9} \int_{\nu_1}^{\nu_2} \epsilon d\nu$ . <sup>f</sup> Reference 2.

determined from the integrated absorption spectrum. For comparison, the corresponding values for naphthalene are also included in Table I. The absorption spectra are shown in Figure 1.

For quinoline and isoquinoline no triplet  $\leftarrow$  triplet absorption was observed in the wavelength region where the singlet depletion was measured.<sup>6</sup> Equation 1 of paper I reduces to

$$OD(t) = \log [I(\infty)/I(t)] = d\epsilon_S C_T^0 \exp(-t/\tau_T) \quad (1)$$

where  $I(\infty)$  is the intensity of the transmitted light at a time long with respect to  $\tau_T$ , the lifetime of the triplet state.  $I(t)$  is the intensity of the transmitted beam at a time  $t$ .  $d$  is the sample path length. The initial concentration of triplets,  $C_T^0$ , was obtained using eq 1, as described in I. For quinoxaline, triplet  $\leftarrow$  triplet ab-

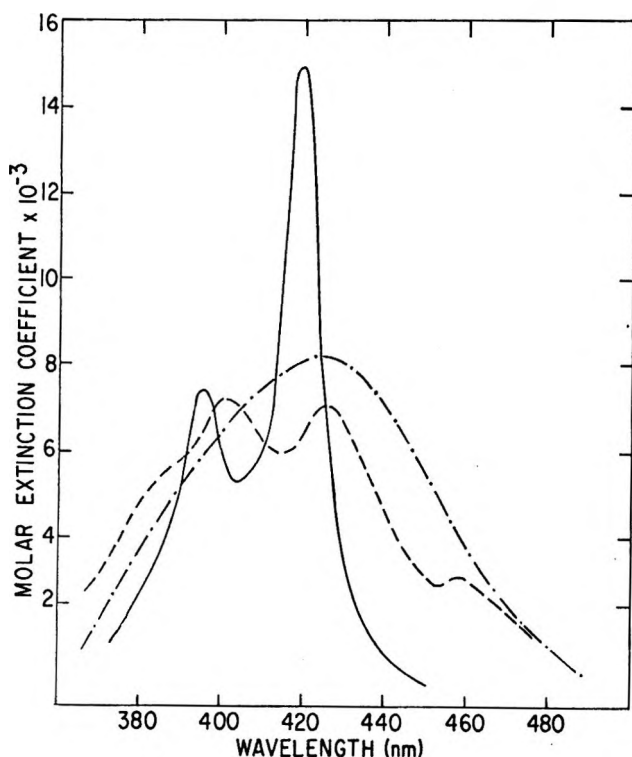


Figure 1. Triplet  $\leftarrow$  triplet absorption spectra: quinoline, -----; isoquinoline, ———; quinoxaline, -·-·-·.

sorption was observed at the wavelength region where the singlet depletion was measured. In this case values of  $C_T^0$  were calculated as described in I. For all cases  $\epsilon_T$  was calculated (using the value of the optical density of the triplet  $\leftarrow$  triplet absorption measured at wavelength  $\lambda_T$  and the value of  $C_T^0$  obtained above) from the Beer-Lambert law.

The rate of depopulation of the triplet state was always found to be the same as the rate of repopulation of the ground state. Typical ground-state depletions were 5%. No permanent photochemical changes were observed in any of these systems.

The extinction coefficients for triplet  $\leftarrow$  triplet absorption for quinoline and isoquinoline have not been previously reported. For quinoxaline a minimum value of  $\epsilon_T$  at 410.0 nm of 2500 l. mol<sup>-1</sup> cm<sup>-1</sup> has been reported by Astier and Meyer.<sup>4</sup> This is in agreement with the value reported in the present work. The values of  $\epsilon_T$  are large enough to suggest that these are allowed transitions. This is confirmed by the oscillator strength values, which are similar to those reported for naphthalene. The similarity in oscillator strength and transition energy indicates that these transitions may be of the same orbital type. For naphthalene these bands have been assigned as  ${}^3K_a \leftarrow {}^3L_a$ <sup>7</sup> (Platt's notation<sup>8</sup>). Thus, these transitions in quinoline, isoquinoline, and quinoxaline, can tentatively also be assigned as  ${}^3K_a \leftarrow {}^3L_a$ . Polarization data would be of considerable help in confirming this assignment.

*Acknowledgment.* The support of the Petroleum Research Fund (Grant No. 1432-G2) is gratefully acknowledged.

(6) In this wavelength region  $\epsilon_S > 10\epsilon_T$ .

(7) M. El-Sayed and T. Pavlopoulos, *J. Chem. Phys.*, **39**, 834 (1963).

(8) J. Platt, *ibid.*, **17**, 484 (1949).

### Chemiluminescence and Thermoluminescence from a $\gamma$ -Irradiated Silica-Alumina Gel

by Robert R. Hentz<sup>1a</sup> and S. B. Ziemecki

Department of Chemistry and the Radiation Laboratory,<sup>1b</sup>  
University of Notre Dame, Notre Dame, Indiana 46556  
(Received May 25, 1970)

The observation of luminescence, with concomitant bleaching of visible coloration, on exposure of a  $\gamma$ -irradiated silica gel to various vapors and gases (including H<sub>2</sub>, O<sub>2</sub>, N<sub>2</sub>, and He) was described to us recently by Rabe in a private communication and a preprint of

(1) (a) To whom correspondence should be addressed. (b) The Radiation Laboratory of the University of Notre Dame is operated under contract with the U. S. Atomic Energy Commission. This is AEC Document No. COO-38-734.

a paper.<sup>2</sup> The luminescence spectrum is reported to have a maximum at 450 nm and to be identical with the spectrum of thermoluminescence which has a glow peak at 55° and which accompanies bleaching of the visible coloration. We have studied such luminescence phenomena with a  $\gamma$ -irradiated silica-alumina gel.<sup>3</sup> Because our observations differ considerably from those of Rabe, it is worthwhile to publish a brief report of the results.

The visible coloration, a center of chemical activity, and a characteristic esr signal of a  $\gamma$ -irradiated silica-alumina gel have been identified with an Al positive-hole center.<sup>4</sup> Such properties of the irradiated gel are destroyed by contact with certain reagents and are unaffected by others. A correlation was noted between reactivity and ionization potential of a reagent. Therefore, neutralization of the Al positive-hole center by transfer of an electron from a reactive reagent was postulated as the mechanism. To determine whether such a process is accompanied by luminescence, the reactive reagents H<sub>2</sub>, NO, NO<sub>2</sub>, NH<sub>3</sub>, H<sub>2</sub>S, C<sub>2</sub>H<sub>4</sub>, and C<sub>3</sub>H<sub>8</sub> were used and O<sub>2</sub> was used as a representative unreactive reagent.

Properties of the silica-alumina gel and sources of reagents have been reported.<sup>4</sup> Procedures for treatment and  $\gamma$  irradiation of the gel, for reagent purification, and for exposure of irradiated gel to reagents have been described.<sup>4</sup> In all experiments, the gel received a dose in excess of that (10<sup>21</sup> eV g<sup>-1</sup>) required to attain the limiting yield of Al positive-hole centers.

For study of chemiluminescence, the gel was contained in a cylindrical Pyrex cell to which was attached a full-length inner 12/30 standard-taper joint with a breakoff tip formed in sealing the cell from the vacuum line above the taper. Cell depth (0.6 cm) was such that just two closely packed layers of the silica-alumina beads could be accommodated. Cell diameter (2.5 cm) matched that of the photomultiplier window with which optical contact was achieved with Dow-Corning Fluid 200. For determination of the luminescence spectrum, narrow band-pass filters (Optics Technology 227) were inserted between the cell and photomultiplier window. The photomultipliers used were an EMI 9601B with S-11 photocathode and an RCA 7102S with S-2 photocathode; partial overlap of their spectral ranges provides sensitivity from the uv to near-infrared. Photomultiplier output passed into a Victoreen VTE-1 electrometer and was displayed on a Sargent strip-chart recorder.

After an irradiation, the gel was kept in the side arm on the cell while the cylindrical cell was annealed with a flame. Then the cell, inserted in the apparatus for exposure to a reagent,<sup>4</sup> was mounted on an optical bench in a light-tight box and, after breaking the tip, the time dependence of luminescence intensity was recorded. For study of the temperature dependence of luminescence decay, the cell was placed in a large copper block

with only the front window protruding, and an extension of the block was inserted into a constant-temperature medium in a Dewar or into an oven.

For study of thermoluminescence, ~0.2 g of gel was placed in a cell made of 2.5-cm o.d. quartz tubing which was drawn down and sealed at one end, had a flat Suprasil window at the other end, and was equipped with a side arm for sealing after the standard treatment procedure. For luminescence measurement, the irradiated gel was situated in the cell's narrow end which was inserted in an oven controlled by a linear temperature programmer (Aerograph 326). Luminescence was conducted from the cell window *via* a quartz lightguide to the EMI 9601B photomultiplier which was cooled with a stream of air.

Exposure of the irradiated silica-alumina gel to H<sub>2</sub> produces a luminescence that is largely in the range 600–900 nm with a maximum near 750 nm. The absorption spectrum of the irradiated gel has a threshold near 700 nm and rises monotonically through a slight shoulder near 550 nm to a maximum at 360 nm.<sup>3</sup> Therefore, owing to the possibility of self-absorption, the observed luminescence spectrum may not correspond to the emission spectrum.

The luminescence yield (area under a decay curve) increases to a plateau with increase in pressure of H<sub>2</sub> in the system. All experiments were performed with a fixed H<sub>2</sub> pressure greater than that required (~40 Torr) for attainment of the plateau. Semilogarithmic plots of characteristic luminescence decay curves are presented in Figure 1. As shown in Figure 1, such curves can be represented reasonably well as a sum of two exponential decays. However, considerably greater complexity is indicated by study of the temperature dependence from which 0.03 eV was the largest phenomenological activation energy obtained by various treatments of the data.<sup>3</sup> Though the luminescence mechanism may be complex, shape of the decay curves obtained with different narrow band-pass filters was the same as that for the unfiltered luminescence. Besides indicating a negligible effect of self absorption, such a wavelength independence of luminescence decay suggests a single emission step the characteristics of which do not vary with time. That is, the elementary emission reaction is independent of the details of mechanism. Neutralization of an Al positive-hole center by an electron, donated by H<sub>2</sub> at the surface, is suggested as the elementary emission reaction by similarity of the decays (on exposure of irradiated gel to H<sub>2</sub>) of luminescence, visible coloration,<sup>3</sup> and the esr signal of the Al positive-hole center.<sup>3</sup>

(2) J. G. Rabe and K. Breittkreutz, *Z. Naturforsch.*, in press.

(3) S. B. Ziemecki, Ph.D. Thesis, University of Notre Dame, 1968.

(4) Cf. R. R. Hentz and D. K. Wickenden, *J. Phys. Chem.*, **73**, 817 (1969), and R. R. Hentz and D. K. Wickenden, *ibid.*, **73**, 1608 (1969), which include references to earlier papers in this series.

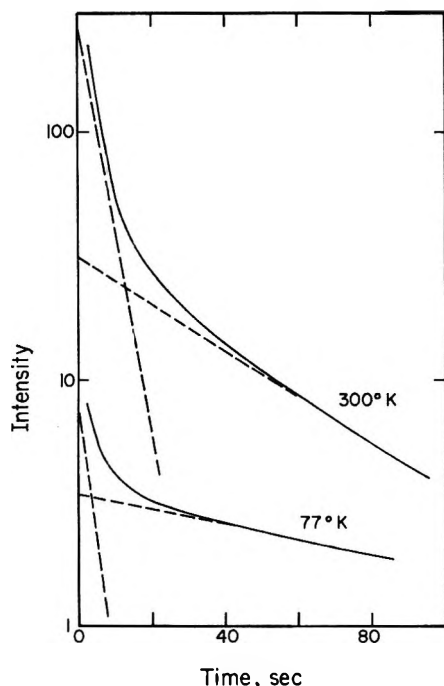


Figure 1. Semilogarithmic plots of characteristic luminescence decay curves obtained on exposure of a  $\gamma$ -irradiated silica-alumina gel to  $H_2$ .

Calculation from the overall sensitivity of the EMI 9601B photomultiplier and comparison with a scintillation standard<sup>3</sup> (Nuclear-Chicago Model 180050 for which  $G \approx 1$  photon/100 eV was assumed) both gave a luminescence yield of  $10^{11}$ – $10^{12}$  photons/g of gel (necessarily without any correction for self absorption). Comparison of such a result, though subject to considerable uncertainty, with the limiting yield of  $\sim 10^{18}$  Al positive hole centers/g<sup>4</sup> illustrates the small radiative efficiency of the neutralization reaction.

In addition to  $H_2$ , each of the other reagents reactive with Al positive-hole centers produced luminescence on contact with irradiated gel; only the unreactive reagent  $O_2$  did not. With each of the other reactive reagents, attainment of the limiting luminescence yield required a higher pressure (*e.g.*, 700 Torr in the case of  $NH_3$ ) than with  $H_2$ . Such behavior is related to the greater adsorption of such reagents on unirradiated gel. In one series of experiments,  $NH_3$  was added to irradiated gel at less than the saturation pressure and the luminescence yield was measured. After the  $NH_3$  was pumped

out,  $H_2$  at greater than its saturation pressure was admitted and the luminescence yield was measured. With increase in the pressure of  $NH_3$  from zero to 700 Torr, the  $NH_3$ -induced luminescence yield increases, the subsequent  $H_2$ -induced luminescence yield decreases, and the sum remains constant. Such results indicate that the elementary emission reaction is identical for each of the reactive reagents. In terms of the suggested mechanism, the elementary reaction in which an Al positive-hole center is neutralized by an electron is unaffected by the nature of the donor.

When irradiated silica-alumina gel is heated above  $100^\circ$ , thermoluminescence is observed concomitant with disappearance of the visible coloration and the esr signal of the Al positive-hole center. The thermoluminescence is largely in the range 400–650 nm with a maximum near 520 nm. Again, owing to the possibility of self-absorption, the observed spectrum may not correspond to the emission spectrum. However, the distinct difference between the thermoluminescence and chemiluminescence spectra does not appear attributable to an effect of self-absorption. Such a result suggests a difference either in the nature of the elementary emission reaction or in its energetics.

Glow curves show only one broad, slightly asymmetric peak in the temperature range  $30$ – $400^\circ$ ; the maximum corresponds to  $330^\circ$  with a heating rate of  $25^\circ/\text{min}$ . An activation energy of  $1.0 \pm 0.1$  eV<sup>5</sup> was determined by the initial-rise method.<sup>6</sup> After exposure of irradiated gel to greater than the saturation pressure of  $H_2$  and removal of the  $H_2$ , thermoluminescence is not observed. Such a result suggests that Al positive-hole centers are necessary for thermoluminescence. However, isothermal decay of thermoluminescence is exponential whereas isothermal decay of the visible coloration of irradiated gel is complex and includes an initial fast-decay component with a phenomenological activation energy of 0.2 eV.<sup>3</sup> Thus, there does not appear to be a simple relationship between the elementary emission reaction of thermoluminescence and the elementary reaction in which Al positive-hole centers disappear during thermal bleaching.

(5) S. Cohen, *Verres Refract.*, **20**, 336 (1967), has reported an activation energy of  $\sim 1$  eV for thermoluminescence from an irradiated high-purity vitreous silica doped with Al.

(6) J. J. Hill and P. Schwed, *J. Chem. Phys.*, **23**, 652 (1955).